



Full-Depth Precast Concrete Bridge Deck System: Phase II

Minnesota
Department of
Transportation

**RESEARCH
SERVICES**

Office of
Policy Analysis,
Research &
Innovation

Catherine French, Principal Investigator
Department of Civil Engineering
University of Minnesota

October 2012

Research Project
Final Report 2012-30

Your Destination... Our Priority



To request this document in an alternative format, please contact the Affirmative Action Office at 651-366-4723 or 1-800-657-3774 (Greater Minnesota); 711 or 1-800-627-3529 (Minnesota Relay). You may also send an e-mail to ADArequest.dot@state.mn.us.

(Please request at least one week in advance).

Technical Report Documentation Page

1. Report No. MN/RC 2012-30	2.	3. Recipients Accession No.	
4. Title and Subtitle Full-Depth Precast Concrete Bridge Deck System: Phase II		5. Report Date October 2012	
		6.	
7. Author(s) Max Halverson, Catherine French, and Carol Shield		8. Performing Organization Report No.	
9. Performing Organization Name and Address Department of Civil Engineering University of Minnesota 500 Pillsbury Drive SE Minneapolis, MN 55455		10. Project/Task/Work Unit No. CTS #2010017	
		11. Contract (C) or Grant (G) No. (C) 89261 (WO) 142	
12. Sponsoring Organization Name and Address Minnesota Department of Transportation Research Services 395 John Ireland Blvd., MS 330 St. Paul, MN 55155		13. Type of Report and Period Covered Final Report	
		14. Sponsoring Agency Code	
15. Supplementary Notes http://www.lrrb.org/pdf/201230.pdf			
16. Abstract (Limit: 250 words) <p>The Minnesota Department of Transportation (MnDOT) has developed a design for a precast composite slab-span system (PCSSS) to be used in accelerated bridge construction. The system consists of shallow inverted-tee precast beams placed between supports with cast-in-place (CIP) concrete placed on top, forming a composite slab-span system. Suitable for spans between 20 and 60 ft., the MnDOT PCSSS is useful for replacing a large number of aging conventional slab-span bridges throughout the United States highway system. The PCSSS has particular durability, constructability, and economical concerns that affect its value as a viable bridge design. To address these concerns, the performance of existing PCSSS bridges was evaluated and a review of a number of PCSSS design details was conducted. The field inspections demonstrated that design changes made to the PCSSS over its development have improved performance. A parametric design study was also conducted to investigate the effects of continuity design on the economy of the PCSSS. It was recommended that the PCSSS be designed as simply supported rather than as a continuous system.</p>			
17. Document Analysis/Descriptors Prestressed concrete bridges, Accelerated construction, Bridge construction, Bridge design, Restraint moment, Slabs, Bridge decks, Field studies		18. Availability Statement No restrictions. Document available from: National Technical Information Services, Alexandria, Virginia 22312	
19. Security Class (this report) Unclassified	20. Security Class (this page) Unclassified	21. No. of Pages 204	22. Price

Full-Depth Precast Concrete Bridge Deck System: Phase II

Final Report

Prepared by:

Max Halverson
Catherine French
Carol Shield

Department of Civil Engineering
University of Minnesota

October 2012

Published by:

Minnesota Department of Transportation
Research Services Section
395 John Ireland Boulevard, Mail Stop 330
St. Paul, Minnesota 55155

This report represents the results of research conducted by the authors and does not necessarily represent the views or policies of the Minnesota Department of Transportation or the University of Minnesota. This report does not contain a standard or specified technique.

The authors, the Minnesota Department of Transportation, and the University of Minnesota do not endorse products or manufacturers. Any trade or manufacturers' names that may appear herein do so solely because they are considered essential to this report.

Acknowledgements

The research presented in this report was the result of collaboration among many minds and hard work by many hands. Thank you to Phil Cici for his preliminary work on this project and for largely developing and implementing the procedure for the crack mapping surveys. Thank you as well to Paul Bergson and Rachel Gaulke for their assistance in coordinating field work and safety. Many graduate and undergraduate students were instrumental in the completion of the field work.

The Minnesota Department of Transportation (MnDOT) was integral to the success of this project. In addition to sponsoring the project, MnDOT provided many hours of technical advising and support which was greatly appreciated. In particular, thank you to Paul Pilarski for his thorough input on PCSSS design that greatly affected the outcome of the parametric design study. Also, thank you to the MnDOT bridge maintenance crews for their assistance with traffic control for the crack map surveys and core extractions.

Table of Contents

Chapter 1: Introduction	1
1.1 PCSSS Overview	1
1.2 Objectives	2
1.3 Organization.....	3
Chapter 2: Literature Review and Design History	4
2.1 PCSSS Literature Review	4
2.1.1 Instrumentation of the MnDOT Bridge No. 13004	5
2.1.2 Live-Load Distribution	6
2.1.3 Flange Thickness and Roughening	6
2.1.4 Transverse Reinforcement in Trough Region.....	7
2.1.5 Composite Action Stirrups.....	8
2.1.6 Restraint Moments	9
2.2 Current AASHTO LRFD 2010 Design Specifications.....	9
2.3 PCSSS Design History.....	11
2.3.1 Generation 1 (2005)	11
2.3.2 Generation 2 (2007)	12
2.3.3 Generation 3 (2009)	13
Chapter 3: Field Inspections	14
3.1 Crack Mapping Overview.....	14
3.1.1 Additional Field Observations	15
3.2 Core Examination Overview.....	15
3.2.1 Core Selection and Extraction	16
3.2.2 Examination Procedure	17
3.3 Observations from Field Inspections	18
3.3.1 Bridge No. 33532 – Conventional Slab Span on CR 60 over the Groundhouse River, Ogilvie, MN.....	18
3.3.2 Bridge No. 13004 – T.H. 8 over the Center Lake Channel, Center City, MN	19
3.3.3 Bridge No. 33005 – T.H. 65 over the Anne River, Mora, MN.....	20

3.3.4	Bridge No. 33008 – T.H. 65 over the Groundhouse River, Mora, MN	20
3.3.5	Bridge No. 49007 – T.H. 238 over the Swan River, Little Falls, MN	22
3.3.6	Bridge No. 49036 – T.H. 238 over Pike Creek, Little Falls, MN	23
3.4	Summary	23
Chapter 4: Monitoring of Instrumented Bridge		25
4.1	Instrumentation Overview	25
4.2	Reflective Cracking	25
4.3	Restraint Moment Cracking	26
4.4	Thermal Effects	27
4.5	Summary	27
Chapter 5: Review of Design Details and Methods.....		28
5.1	Shrinkage Restraint	28
5.1.1	Transverse Deck Reinforcement	28
5.1.2	Dowel Placement and Wrapping	30
5.1.3	Bearing Pads	31
5.2	Reflective Cracking	32
5.2.1	Flange Top Corner Chamfer	32
5.2.2	Longitudinal Joint Detailing	32
5.2.3	Flange Roughening	33
5.3	Composite Action Stirrups	34
5.4	Tolerances for PCSSS Beams	34
Chapter 6: Continuous System Economy		36
6.1	PCSSS Design Considerations	36
6.1.1	Restraint Moments	36
6.1.2	Thermal Gradient	37
6.1.3	Partial Continuity	38
6.2	Parametric Study	40
6.2.1	Part 1: Creep and Shrinkage Model	41
6.2.2	Part 2: Precast Age at Continuity	42
6.2.3	Part 3: Continuous System vs. Simple Span Economy	43

6.2.4	Recommendation	43
6.3	Corollary Studies	44
6.3.1	Simplified Continuity Connection	45
6.3.2	Longitudinal Deck Reinforcement.....	47
Chapter 7: Conclusions and Recommendations		49
7.1	Recommendations.....	50
References		53
Tables		55
Figures.....		73
Appendix A: Crack Mapping Procedure and Results		
Appendix B: Core Examination Records		
Appendix C: Center City Bridge Data		
Appendix D: Sample Calculations for PCSSS Design		

List of Tables

Table 2.1: Subassemblage specimen design details (French et al. 2011)	55
Table 2.2: Typical PCSSS details from the four design generations with changes from the previous generation in bold. Actual details may differ for particular bridges.	56
Table 2.3: Summary of design details for Bridge No. 13004 over the Center Lake Channel in Center City, MN.....	57
Table 2.4: Summary of design details for Bridge No. 33005 over the Ann River near Mora, MN	58
Table 2.5: Summary of design details for Bridge No. 33008 over the Groundhouse River near Mora, MN	59
Table 2.6: Summary of design details for Bridge No. 49007 over the Swan River near Little Falls, MN	60
Table 2.7: Summary of design details for Bridge No. 49036 over Pike Creek near Little Falls, MN	61
Table 3.1: Original crack width classification categories	62
Table 3.2: Refined crack width classification categories.....	62
Table 3.3: List of cores taken from in-field PCSSS bridges with coordinate locations and rationale.....	63
Table 3.4: Dates and bridge ages for each field bridge inspection	64
Table 3.5: Summary of the observed cracks from the core examinations	65
Table 3.6: Precasting data related to the in-field relative camber measurements of beams from Bridge No. 33008	66
Table 3.7: Beam age statistics for Bridge No. 33008 compared to the remaining field bridges ...	67
Table 4.1: Aspect ratios of the five inspected bridges	67
Table 5.1: Transverse deck reinforcement details compared to the recommendation by Frosh (2006).....	67
Table 5.2: Dowel details for the five inspected PCSSS bridges	68
Table 6.1: Span length configurations covering the range of feasible designs for the parametric study to investigate simple vs. continuous system designs. The highlighted configurations were used to compare creep and shrinkage models and precast beam ages for design	68
Table 6.2: Results of the parametric study comparing the AASHTO 2004 and AASHTO 2010 creep and shrinkage model for use in PCSSS design	69

Table 6.3: Results of the parametric study comparing 7-day and 14-day precast ages for use in PCSSS design	70
Table 6.4: Continuous system designs for comparison in the parametric study. More economical designs are highlighted.....	71
Table 6.5: Simply-supported designs for comparison in the parametric study. More economical designs are highlighted.....	71
Table 6.6: Redesigned prestressed beams for superimposed restraint moment with 4 No. 5 bars for positive moment connection (PMC) reinforcement	72
Table 6.7: Comparison of the governing Service I load combination, the approximate Service I load combination with $\gamma = 1.2$, and the design moment capacity of No. 7 bars at 4 in., all at the pier	72

List of Figures

Figure 1.1: Typical cross section of a PCSSS inverted-tee beam at midspan	73
Figure 1.2: Typical cross section of the PCSSS precast beam joint with transverse and drop-in cage reinforcement and continuity bars (only over pier).....	73
Figure 1.3: Photograph of Bridge No. 49036 during construction showing the drop-in cage reinforcement prior to placement of deck reinforcement and CIP concrete (MnDOT 2009).....	74
Figure 2.1: Conceptual layout of the Concept 1 laboratory bridge specimen and accompanying table with descriptions of each design change (Smith et al. 2008).....	75
Figure 2.2: Plan layout of Concept bridge 2 with details of each half-span indicated (French et al. 2011).....	76
Figure 2.3: Plan view of Stage 1 of bridge construction for Bridge No. 13004 showing the instrumented joints (Bell et al. 2006).....	76
Figure 2.4: Cross-sectional view of the instrumentation detail for the embedment VW strain gauges over each longitudinal joint (Bell et al. 2006)	77
Figure 2.5: Plan view of instrumentation detail for VW spot-weldable strain gauges on transverse (trough) hooks (Bell et al. 2006).....	77
Figure 2.6: Cross-sectional view of the instrumentation detail for locations with 3 VW spot-weldable strain gauges, typical at midspan (Bell et al. 2006).....	78
Figure 2.7: Precast flange surface (a) with voids from fabrication and (b) after patching preparation (French et al. 2011).....	78
Figure 2.8: Photograph of threaded transverse reinforcement mechanically anchored into the precast web and the non-hooked terminal end (French et al. 2011)	79
Figure 2.9: Restraint moments from the laboratory bridge specimen compared to PCA and P-method with creep and shrinkage models fitted to data (Smith et al. 2008).....	79
Figure 2.10: Typical PCSSS inverted-tee beam reinforcement at midspan from Generation 1	80
Figure 2.11: Typical PCSSS inverted-tee beam reinforcement at midspan from Generation 2	80
Figure 2.12: Typical PCSSS inverted-tee beam reinforcement at midspan from Generation 3	81
Figure 3.1: Crack map for Bridge No. 13004, Inspection No. 2, June 22 and 24, 2010 with core specimen locations indicated	82
Figure 3.2: Crack map for the north side of Bridge No. 33005, Inspection No. 3, August 9, 2011.....	83
Figure 3.3: Crack map for the south side of Bridge No. 33005, Inspection No. 3, August 9, 2011 with core specimen locations indicated	84

Figure 3.4: Crack map for Bridge No. 33008, Inspection No. 3, June 16 and August 10, 2011 with core specimen locations indicated	85
Figure 3.5: Crack map for the south side of Bridge No. 49007, Inspection No. 3, June 29, 2011 with core specimen locations indicated	86
Figure 3.6: Crack map for the north side of Bridge No. 49007, Inspection No. 3, June 29, 2011 with core specimen locations indicated	87
Figure 3.7: Crack map for Bridge No. 49036, Inspection No. 3, June 24, 2011 with core specimen locations indicated	88
Figure 3.8: Crack map for Bridge No. 33532 (conventional slab-span) from September 16, 2010.....	89
Figure 3.9: Efflorescence at a longitudinal joint underneath Bridge No. 49007	90
Figure 3.10: Terminology for the location and depth of cores	90
Figure 3.11: Definitions for core condition due to extraction; Intact: very few sections, easy to reassemble; Segmented: many sections, easy to reassemble; Broken: very many sections, difficult to reassemble.....	91
Figure 3.12: Examples of a physically identifiable longitudinal joint (left) and web corner (right)	91
Figure 3.13: Crack on the surface of Core 33008-1 labeled by a dotted red line	92
Figure 3.14: Orientation of core faces for locating cracks and reinforcement. The local faces (north, south, east and west) are associated with the longitudinal and transverse directions of the bridge, as shown. The azimuth for each core is the angle between true North and the local north face direction.	93
Figure 3.15: Crack on the pseudo-local south face of Core 33008-3 with a 1 in. offset to the west	94
Figure 3.16: The west face of Core 13004-1 showing that the core only captured one side of the joint	95
Figure 3.17: Core 33005-2 showing the precast web corner and 4¾ in. of CIP concrete above the precast web and less than 3 in. of cover.....	95
Figure 3.18: Uneven bearings of end-span precast beams at the north pier of Bridge No. 33005.....	96
Figure 3.19: Observed differential camber of the inverted-tee beams from Bridge No. 33008	97
Figure 3.20: Observed differential camber from the north span of Bridge No. 33008. Camber is measured relative to minimum observed camber in the span. Beam age at placement is shown for comparison.....	97

Figure 3.21: Observed differential camber from the south span of Bridge No. 33008. Camber is measured relative to the minimum camber in the span. Beam age at placement is shown for comparison.....	98
Figure 3.22: Cracked end-span beam at the north pier of Bridge No. 49007	99
Figure 4.1: Plan view of MnDOT Bridge No. 13004 in Center City, MN	100
Figure 4.2: Cross-sectional view of a typical precast longitudinal joint from Bridge No. 13004, taken at the pier	100
Figure 4.3: Naming convention for the instrumentation of Bridge No. 13004 (Smith et al. 2008)	101
Figure 4.4: Transverse strain data from concrete embedment gauges directly above longitudinal Joint 1 at midspan of the center span. Gauges CJ1-51-3 and CJ1-51-4 show increasing strain.....	102
Figure 4.5: Transverse strain data from concrete embedment gauges directly above longitudinal Joint 3 at midspan of the center span. Gauges CJ3-51-2 and CJ3-51-3 show increasing strain.....	102
Figure 4.6: Transverse strain data from concrete embedment gauges directly above longitudinal Joint 2 at midspan of the center span. Gauge CJ2-51-1 shows increasing strain.....	103
Figure 4.7: Longitudinal strain data from spot-weldable gauges on continuity and deck reinforcement along Joint 1 over the center of the pier cap. Data from gauge SJ1-31-1 (grey line) is shown for comparison	103
Figure 4.8: Crack map of Bridge 13004 showing a transverse crack at the pier over Joint 1 corresponding to the location of gauge SJ1-C3-2 from Figure 4.7.....	104
Figure 4.9: Longitudinal strain data from spot-weldable gauges on continuity and deck rebar over Joint 1 at the east side of the pier cap	104
Figure 4.10: Longitudinal strain data from spot-weldable gauges on continuity and deck rebar over Joint 3 at the west side of the pier cap	105
Figure 4.11: Temperature data at points 3 in and 9 in from the bridge surface at Joint 1 at midspan of the center span. A close-up of peak temperatures in 2008 shows daily temperature variations.....	106
Figure 5.1: Example dowel layouts for the five inspected PCSSS bridges and a recommended dowel layout.....	107
Figure 5.2: Skewed blackout regions from Bridge No. 33005 with dowels, all highlighted in red.	107
Figure 5.3: Crack map from inspection No. 2 of Bridge No. 33008 showing cracking in the region of precast beam blockouts	108

Figure 5.4: Construction photograph showing the placement of a mastic bond breaker on Bridge No. 08006.....	108
Figure 6.1: Deflections and restraint moments for simple beams made continuous: a.) positive and b.) negative restraint moments	109
Figure 6.2: Predicted time-dependent restraint moment for Bridge No. 13004 for various ages of the precast beams at the time of continuity, represented by t_{cont} (Smith et al. 2008).....	109
Figure 6.3: Typical time-dependent restraint moment (RM) for PCSSS design using the P-method with separate components shown. Precast beam age is 14 days at the time of continuity. The differences in moment at the piers (24 ft. and 48 ft.) are due to the effective diaphragm stiffness	110
Figure 6.4: Typical time-dependent and thermal gradient restraint moment envelopes (24-24-24 configuration). The 0.5TG is the factored thermal gradient restraint moment used in the Service III load combination.....	110
Figure 6.5: Service I and approximate Service I negative moment envelopes for a 24-24-24 bridge. The intersection between M_n Required and the service moment envelopes indicate the reinforcement cutoff locations.....	111
Figure 6.6: Service I and approximate Service I negative moment envelopes for a 20-30-20 bridge. The intersection between M_n Required and the service moment envelopes indicate the reinforcement cutoff locations.....	111
Figure 6.7: Service I and approximate Service I negative moment envelopes for a 34-34-34 bridge. The intersection between M_n Required and the service moment envelopes indicate the reinforcement cutoff locations.....	112
Figure 6.8: Service I and approximate Service I negative moment envelopes for a 45-62-45 bridge. The intersection between M_n Required and the service moment envelopes indicate the reinforcement cutoff locations.....	112

Executive Summary

The Minnesota Department of Transportation (MnDOT) developed a design for a precast composite slab span system (PCSSS) to be used in accelerated bridge construction. The system consists of shallow inverted-tee precast beams placed between supports with cast-in-place (CIP) concrete placed on top, forming a composite slab span system. Suitable for spans between 20 and 60 ft., the MnDOT PCSSS is useful for replacing a large number of aging conventional slab-span bridges throughout the United States highway system. Originally developed in 2005, the PCSSS had three distinct design generations in the 12 bridges that were constructed by MnDOT between 2005 and 2011. The objective of this investigation was to evaluate the field performance of a sample of the existing bridges through detailed crack mapping and core analysis and through continued monitoring of data obtained from one of the original PCSSS bridges (Bridge No. 13004) instrumented during construction in 2005. A parametric design study was also conducted to investigate the effects of continuity design on the economy of the PCSSS.

Five of the 12 PCSSS bridges, constructed between 2005 and 2011, were selected as the sample set to conduct detailed surveys of surface cracking and examinations of extracted core specimens to evaluate effects of the design changes. Surface cracking was recorded over three different inspections between the fall of 2009 and the summer of 2011. Each inspection was done using a systematic procedure of documenting crack locations and measuring crack widths. The result was a series of crack maps for each bridge, showing the surface cracking compared to major design features. Different line types were used to distinguish relative crack widths. Core specimens were taken from each of the five inspected bridges based on anticipated reflective crack locations. The cores were partial depth through the CIP concrete, taken over either the longitudinal joint between precast panels or over the precast web corner. Each core was examined under a digital microscope for cracking with particular attention paid to the regions above the longitudinal joints and web corners. The results of the core investigation were compared to the corresponding crack maps.

Overall, the field inspections indicated that the changes made between each design generation improved the performance of the PCSSS. Bridge No. 13004 in Center City, MN, from the first design generation showed many short, longitudinal cracks on the deck surface with very little transverse and map cracking. The longitudinal cracks were located primarily over the precast beam web, corresponding to what appeared to be insufficient consolidation of the CIP concrete around the stirrups projecting vertically from the section to facilitate composite action, which had little clearance above the precast webs. In the second generation, more clearance was provided under the stirrups projecting from the surface. Bridge Nos. 33005 and 33008 near Mora, MN, from the second generation did not show the short cracks over the webs from the first generation, but more transverse cracks and longer longitudinal cracks were observed.

Bridge No. 33008 showed significantly more longitudinal cracking than any of the other bridges. Significant longitudinal cracks were noted along several joints between the precast beams. Core specimens showed that these cracks were full-depth reflective cracks. The only other bridge to show reflective cracking from the core specimens was Bridge No. 13004, but these were not full-depth cracks. It was unclear from the design details of Bridge No. 33008 why it was in worse condition than the other bridges. This bridge also had noticeably different cambers between adjacent beams observed from the underside of the bridge, although it was unclear how this might be associated with the observed longitudinal cracking.

For the third design generation, the thickness of the precast beam flanges was decreased and the trough reinforcement spacing (consisting of trough hooks projecting horizontally from the beams across the joint, as well as a drop-in cage) was decreased from a maximum 10 in. center-to-center to 6 in. center-to-center to better control reflective cracking. The decreased spacing was accomplished by staggering the trough hooks from adjacent precast beams. Bridge Nos. 49007 and 49036 near Little Falls, MN, from the third generation did not exhibit longitudinal cracking over the precast beam joints, indicating that the design changes may have had a positive impact, though not conclusively. The most significant issue observed with the third generation was shrinkage cracking, indicated by longitudinal cracks located over the precast beam webs and more extensive transverse and map cracking. Generally, bridges with a larger length to width aspect ratio (i.e., L/W) had more transverse cracking, which could be related to more longitudinal shrinkage restraint.

In addition to the field inspections, strain data from the instrumentation of Bridge No. 13004 was analyzed to evaluate performance. The bridge was instrumented in 2005 to monitor reflective cracking and continuous system behavior. Six years of strain and temperature data showed a progression of reflective cracking in several locations and significant cracking due to thermally induced restraint moments. The reflective cracking from the strain data was confirmed by observed cracks in the core specimens near the locations of the strain gauges. While the width of the reflective cracks appeared to increase over time from the strain measurements, the measurements began to plateau by the end of the six-year monitoring period. Restraint moment cracking was indicated by strain gauges attached to continuity connection reinforcement. The measured restraint moment strains were large enough for fatigue to be of potential concern, although the strains were associated with environmental effects, which have a low number of cycles at once per day. Measured strains associated with both reflective cracking and restraint moments were primarily driven by seasonal and daily temperature variations, highlighting the important role of thermal effects in design.

Besides the detailed field investigations, a parametric study of PCSSS designs was conducted to determine whether there was an economic benefit of continuous system design. In particular, design implications of time-dependent and thermal gradient restraint moments and their effects on continuity were studied. Because the PCSSS is a simple-span system made continuous with a CIP deck, the effects of restraint moments must be considered in the design of continuous systems. The restraint moments are those that arise from continuity, or end restraint, over the piers due to beam creep, differential shrinkage between the CIP deck and beam, and thermal gradient. Restraint moments would not develop if PCSSS were built as a series of simple spans with no continuity provided between the spans.

Eight bridges covering the feasible range of span configurations were designed as both simple and continuous systems. Flexural design was performed for each case, resulting in optimized precast sections within practical design constraints. Primary design parameters were strand number, section depth, and precast concrete strength. These design parameters were compared between the continuous and simple-span designs for each configuration to evaluate economic benefit. Generally, continuous PCSSS designs were equally or less economical than simple-span designs. Spans less than 30 feet had a slight economic benefit with continuous design because large restraint moments did not develop. However, spans greater than 30 feet developed large restraint moments in continuous design, particularly due to thermal gradient effects. In addition, the restraint moments greatly reduced continuity, effectively negating the

benefit to live-load capacity. It was recommended that the PCSSS be designed as a simply-supported system for live load. Furthermore, because most continuous system designs were less economical than the corresponding simply-supported designs, it was concluded that designing the PCSSS as simply-supported while also including a continuity connection would be unconservative without accounting for restraint moments. A simple method was developed to account for restraint moments for this case without time-intensive calculations. Further recommendations related to the analysis of negative moments over PCSSS bridge piers were also provided.

A review of current design methods and details concluded that the current PCSSS design was generally sufficient, and recommendations for future PCSSS designs were provided. Items reviewed were related to shrinkage restraint, reflective crack control, composite action, and defining tolerances for the PCSSS. To try to better control top-surface deck cracking, recommendations included increasing the transverse reinforcement in the CIP deck to provide a gross reinforcement ratio, ρ_g , of 0.0063 with a spacing no greater than 9 in., based on the work of Frosch (2006). This would translate to increasing the current transverse deck reinforcement from No. 4 bars at 6 in. ($\rho_g=0.0056$) to No. 5 bars at 6 in. ($\rho_g=0.0086$) or No. 5 bars at an increased spacing of 8 in. ($\rho_g=0.0065$) to provide the needed volumetric ratio while maintaining the maximum spacing for surface crack control. The recommendations of NCHRP 10-71 for reinforcement in the trough are adopted to control reflective cracking. In addition, it was recommended that composite action stirrups need not be used if the required shear stress transferred between the CIP concrete deck and precast beam is less than 135 psi.

Chapter 1: Introduction

Many highway bridges in the United States are in need of replacement due to deterioration from aging infrastructure and increased traffic. Replacement projects are particularly detrimental to local traffic, with inconvenient and potentially hazardous detours. New accelerated construction methods incorporating precast elements are increasingly popular to reduce construction time, safety hazards, environmental impact, and quality control problems. In response to these demands, the Minnesota Department of Transportation (MnDOT) has developed a bridge concept termed the Precast Composite Slab Span System (PCSSS), which is based on the French Poutre Dalle system (Hagen et al. 2005). PCSSS bridges consist of adjacent inverted-tee precast beam elements that are made composite with a cast-in-place (CIP) concrete deck to form a composite slab-span system. PCSSS bridges are typically two or three spans, with spans ranging from 20 to 60 ft. in length, suited for replacing CIP slab-span bridges. First implemented in 2005, a total of twelve PCSSS bridges were constructed in Minnesota between 2005 and 2011.

Since its original implementation, the PCSSS underwent a number of design changes aimed at improving durability, economy, and constructability. Several PCSSS bridges were built following each set of design changes. These design changes were largely based on research at the University of Minnesota (UMN), which included investigation of the behavior of the PCSSS using laboratory bridge specimens and subassemblages, an instrumented bridge in the field, and numerical analyses of PCSSS elements. The focus of the study reported herein was to determine the effectiveness of the PCSSS design changes by evaluating the in-field performance of existing PCSSS bridges. The UMN research team also provided recommendations on design changes for PCSSS bridges. The results of this research contributed to a set of design practices established by MnDOT to be implemented for PCSSS bridges.

1.1 PCSSS Overview

As introduced above, the PCSSS uses inverted-tee elements topped with a CIP concrete deck to create a composite slab. The precast, prestressed inverted-tee elements incorporated in the MnDOT design are 6 ft. wide and 10 to 24 in. deep, where the depth depends on the span length and design loads. Figure 1.1 illustrates a typical PCSSS precast beam cross section at midspan. The inverted-tee web is 4 ft. wide and the flanges are each 1 ft. wide. Prestressing strands are placed in two rows at 2 and 4 in. from the bottom of the section, within the width of the web region. The number of strands in each precast section typically ranges between 16 and 50 (0.5 in. strands). The precast beams are placed adjacent to each other in the field, eliminating the need for formwork. There are typically 7 to 13 sections across the width of the bridge. The precast beams are joined transversely by overlapping trough hooks that extend from the precast webs, and through the transverse deck reinforcement. The overlapping trough hooks are assumed to transfer loads across the joints between the precast beams.

One of the potential areas of concern with the PCSSS is reflective cracking that may occur in the CIP concrete above the joint between adjacent precast beams. The discontinuity at the longitudinal joint between the beam flanges effectively acts as a pre-existing crack. As a result, the CIP concrete directly above the longitudinal joint experiences high stress concentrations like those seen at a crack tip. Reflective cracks are likely to initiate from this

stress concentration region and propagate vertically in the section. The PCSSS controls reflective cracking with drop-in reinforcement cages placed above the flanges in conjunction with the trough hooks. A cross section of this region, termed the trough region, which is filled with CIP concrete during the deck pour, is shown in Figure 1.2. Figure 1.3 shows a photograph of the construction of a PCSSS prior to CIP concrete placement, illustrating the layout of the reinforcement in the trough regions.

The precast elements are considered simply-supported beams prior to continuity with the CIP concrete. Because the precast beams provide shoring for the CIP concrete deck, the self-weight of the beams and CIP deck are supported by the precast beams alone. After continuity with the CIP deck is established, the system is considered a composite slab span. Composite action stirrups project through the top of the precast webs to engage the CIP deck, forming the composite slab span.

The CIP deck is typically 6 in. thick above the precast beam webs, extending down into the trough regions. Longitudinal deck reinforcement is designed for negative moment resistance and transverse deck reinforcement is designed for crack control. Typically 3 in. of clear cover is provided over the deck reinforcement. Two fabrication issues with the casting of the CIP deck cause concern for cracking in the CIP deck: (1) the precast beams have had some time to cure prior to placement of the CIP deck resulting in a restraint of the CIP deck shrinkage and (2) the CIP deck is shored by the precast during curing, thus it does not participate in carrying any of the gravity dead load.

MnDOT has been designing the PCSSS as a continuous system for live load. Negative moments are carried over the piers by longitudinal reinforcement in the CIP deck, while positive moments are carried by continuity reinforcement in the trough region. This reinforcement is also shown in Figure 1.2. Because the PCSSS consists of precast and CIP concrete, time-dependent effects due to differential creep and shrinkage cause flexural deformations. These deformations are restrained by the continuous connections at the bridge piers, leading to both positive and negative restraint moments over the course of time. Thermal gradients due to solar radiation also lead to restraint moments. Research by Miller et al. (2004) has shown that restraint moments contribute significant loads and must be considered in design.

Overall, the PCSSS has several benefits over conventional slab-span bridges and other alternative precast bridge systems. In addition to providing the majority of the structural capacity, the inverted-tee beams act as permanent formwork for placing reinforcement and the CIP deck. This feature eliminates the need for labor-intensive temporary formwork that is required for conventional slab-span construction. While voided slab and adjacent box girder systems serve a similar purpose as the PCSSS, the PCSSS has two distinct advantages. First, no post-tensioning is required to achieve transverse load sharing for the PCSSS. Transverse loads are transferred between the precast beams through the reinforcement extending from the inverted-tee webs. Second, the region above the inverted-tee flanges, termed the trough region, allows for the addition of drop in reinforcement cages to add additional crack control steel in the CIP concrete above the joints between adjacent beams.

1.2 Objectives

The research presented in this report had three primary objectives: evaluate the performance of existing PCSSS bridges, review the latest PCSSS design methods and details,

and recommend whether the PCSSS should be designed as a simply-supported or continuous system. Evaluation of the existing PCSSS bridges was accomplished through field inspections involving surveys of deck cracking and through inspections of cores taken from field bridges. Five existing PCSSS bridges were chosen for field inspections to encompass the range of PCSSS designs constructed between 2005 and 2009. The results of the field inspections were compared to determine the effect of the design changes on the observed performance. In addition to the field inspections, one of the bridges was monitored using previously installed strain gauge instrumentation. This instrumentation was configured to monitor reflective cracking and the continuity of the system under live loads. Reviewing the latest PCSSS design methods and details involved documenting recent changes to the PCSSS design as well as addressing specific design concerns from MnDOT. A parametric study was conducted to determine whether simply-supported or continuous system design should be used for the PCSSS. The study compared the economy of both simply-supported and continuous system designs for a number of sample PCSSS bridges.

1.3 Organization

Chapter 2 presents a literature review of previous PCSSS research, and an annotated summary of the history of PCSSS design, characterized by three distinct design generations between 2005 and 2009. Chapter 3 presents the field inspection of five PCSSS bridges by way of surface crack mapping and core examinations. Chapter 4 summarizes the monitoring of the instrumented PCSSS Bridge No. 13004 in Center City, MN. Chapter 5 provides commentary and recommendations for the significant PCSSS design changes that were implemented after 2009. Chapter 6 describes the parametric study comparing the economy of continuous system design to simple-span design for the PCSSS and provides recommendations for future design practices. Chapter 7 summarizes the results, conclusions, and recommendations from this report. Appendix A contains the surface crack maps from the field inspections and Appendix B contains the full set of core examination records. Appendix C shows strain data from the monitoring of Bridge No. 13004. Appendix D presents a set of sample calculations for the parametric study, particularly for determining restraint moments and continuity in PCSSS design.

Chapter 2: Literature Review and Design History

During the development of the MnDOT PCSSS, research was conducted to evaluate and improve system performance. An understanding of previous PCSSS research was necessary to form a comprehensive design history, to evaluate the behavior of existing in-field PCSSS bridges, and to make suggested design changes for future PCSSS bridges in Minnesota. The applicable provisions from AASHTO (2010) for PCSSS design were also reviewed, particularly as they pertain to the parametric design study in Chapter 6. Finally, the design history of the MnDOT PCSSS was compiled and organized according to three distinct design generations.

2.1 PCSSS Literature Review

Three publications were produced from the UMN research related to the PCSSS. An introduction to each project is given in this section, with the results and impact on specific design elements presented in the following sections.

Bell et al. (2006) documented the instrumentation of Bridge No. 13004 in Center City, MN, with vibrating wire (VW) gages which were intended to monitor reflective cracking and live load distribution and continuity. In addition, documentation of the PCSSS development history was provided. The literature review therein contained a summary of precast concrete bridge construction prior to development of the MnDOT PCSSS.

Smith et al. (2008) monitored data from Bridge No. 13004 and tested a large-scale laboratory specimen termed the Concept 1 bridge. The continuous, two-span laboratory Concept 1 bridge was load tested to investigate the effects of changing the beam flange thickness and the flange surface roughening, and to observe the development of restraint moments. The Concept 1 specimen had two beams per span for a total of four beams. Each beam incorporated several design modifications to determine the effect of each modification on the bridge behavior. Figure 2.1 shows the plan layout of the Concept 1 bridge with a summary of the design modifications for each beam. The laboratory bridge specimen was instrumented with VW gauges, linear variable differential transformers (LVDTs), and resistive strain gauges. A number of the resistive strain gauges were installed inside the precast beams to observe strains during fabrication.

French et al. (2011) expanded on the work done by Smith et al. (2008) as part of a study for the National Cooperative Highway Research Program (NCHRP). The research consisted of continued testing on the Concept 1 bridge followed by testing of a second large-scale specimen, the Concept 2 bridge. Both specimens were used to further investigate the effects of transverse reinforcement in the trough region and the effects of composite action stirrups. The Concept 2 bridge was a simply-supported, single-span specimen with two precast beams. Figure 2.2 shows a plan layout of the Concept 2 bridge and specifies design differences between the two half-spans. Seven subassembly specimens were also used in the study to investigate the effects of transverse reinforcement in the trough region. French et al. (2011) also included a design guide for the PCSSS and two design examples, one for a simply-supported bridge and the second for a continuous system. Proposed modifications to AASHTO (2010) based on this research were included with the design guide.

Prior to describing the behavior and recommendations for PCSSS obtained from the previous studies, a description of the instrumentation of the field bridge, MnDOT Bridge No.

13004, and the interpretation of the measurements is described in Section 2.1.1. This is followed by sections summarizing prior evaluations and recommendations for live-load distribution, flange thickness and roughening, transverse reinforcement in the trough regions for reflective crack control, composite action stirrups, and restraint moments.

2.1.1 Instrumentation of the MnDOT Bridge No. 13004

Bell et al. (2006) planned and installed instrumentation in MnDOT Bridge No. 13004. The bridge, built over the Center Lake Channel near Center City, MN, was one of the first PCSSS bridges constructed. The instrumentation was intended to monitor potential development of reflective cracking, continuity of live load over the bridge piers, and the effectiveness of the trough hooks in load transfer. To monitor these behaviors, concrete embedment and spot-weldable VW strain gauges were installed in the CIP concrete prior to the deck pour. In addition to strains, the VW gauges also recorded temperature data. The instrumentation was set to collect data every two hours indefinitely and could also be used to collect data on-demand during a truck test.

The instrumented region of Bridge No. 13004 covered three adjacent longitudinal joints on the east half of the bridge: Joints 1, 2 and 3 as shown in Figure 2.3. Fifteen concrete VW embedment gauges were installed transversely over each of these joints at midspan of the center span, as shown in Figure 2.4, to monitor potential reflective cracking (i.e., above the precast flanges and above the precast web corners). Twenty one (i.e., seven per joint) spot-weldable gauges were installed on trough hooks shown in Figure 2.5, in the vicinity of the concrete embedment gauges. These gauges were intended to measure the effectiveness of the transverse reinforcement at load-sharing during a truck test and also monitored the potential development of reflective cracks. Seventeen total spot-weldable gauges were installed on longitudinal reinforcement at six locations along Joint 1: three at the east abutment, three at midspan of the east span, two at both sides of the east pier, three at the center of the east pier, and four midspan of the center span. A section with three longitudinal spot-weldable gauges is shown in Figure 2.6. These gages were used to evaluate continuity and load distribution during a truck test. An additional thirteen spot-weldable gauges were installed at various locations over Joints 2 and 3 and over the precast beam webs at midspan of the center span.

Smith et al. (2008) investigated the behavior of the PCSSS using the instrumentation of Bridge No. 13004. Strain and temperature data from Bridge No. 13004 was collected over a period of 24 months after construction. The data indicated reflective cracks initiating at two of the three instrumented joints (i.e., Joints 1 and 3) and cracking at the bridge pier due to restraint moments. In all cases, strains fluctuated daily and correlated directly with the observed temperature. Because of this correlation, it was assumed that thermal gradients played a significant role in the performance of the bridge, both in reflective and restraint moment cracking.

In summary, strain information collected during the first two years of the bridge life indicated reflective cracking and Joints 1 and 3 and restraint moment cracking at the pier. The maximum daily strain fluctuations during the 24-month collection period measured by concrete vibrating wire gages in the transverse direction over the longitudinal joint were $160 \mu\epsilon$ at Joint 1 and $265 \mu\epsilon$ at Joint 3, which were high enough for cracks to initiate, with an assumed tensile-strain capacity of $150 \mu\epsilon$. At the east pier, the maximum daily longitudinal strain fluctuation measured on the positive moment reinforcement was $700 \mu\epsilon$, occurring directly over the pier cap

at Joint 1. These observed strains indicated that the positive restraint moments correlated with the daily temperature fluctuations and hence confirmed the contribution of the thermal gradient to positive restraint moment. These strains associated with restraint moment cracking were observed to increase over time. The magnitude of the strain fluctuation left it unclear whether the positive moment reinforcement would fracture because of fatigue in the future. Though the strain magnitudes were high due to environmental effects, the occurrences were much less frequent than strain changes due to vehicular loads, occurring only once daily associated with seasons of high solar radiation.

2.1.2 Live-Load Distribution

In order to design the PCSSS, the correct method to distribute live load among the precast beams needed to be determined. Design of the PCSSS bridges in Minnesota was based on the assumption that live load was distributed using the effective strip width method for slab spans. Bridge No. 13004 was used by Smith et al. (2008) for live load truck tests to evaluate the effectiveness of transverse reinforcement at load-sharing across the width of the bridge. The tandem rear axles, of the two trucks used, each averaged 18.7 kips per axle. Placing the truck load directly over the longitudinal joints at midspan produced transverse strains on the order of $30 \mu\epsilon$, which were minimal compared to the daily fluctuations due to solar radiation observed over the 24 month monitoring period. The results of the truck tests were compared to a finite element model of the bridge and the effective-width design assumption used in the original design. Both models were conservative compared to the strain data from the truck tests, confirming that the PCSSS bridge behaved like a slab span and that the effective strip width design method was appropriate.

The Concept 1 and Concept 2 laboratory bridges were also used to measure live-load distribution. Load tests were performed to determine the curvature and deflection behavior and to confirm the effective width and continuity assumptions used in the original PCSSS designs. The results of the service-level test of the laboratory bridge showed that both the load distribution and full-continuity assumptions were conservative. Although these tests were performed in a laboratory setting void of thermal gradients that often influence field behavior, the results were consistent with the truck test of Bridge No. 13004.

2.1.3 Flange Thickness and Roughening

Smith et al. (2008) used the Concept 1 bridge to determine the effect of reducing the precast flange thickness from $5\frac{1}{4}$ in. to 3 in. It was thought that thinner flanges would reduce tensile stresses over the longitudinal joint that cause reflective cracking, and that transverse load distribution would be improved. A 3 in. flange was assumed robust enough for transportation and construction loads. One span of the Concept 1 specimen had precast beams with 3 in. thick flanges without intentional roughening, while the other span had the original $5\frac{1}{4}$ in. thick flanges with intentional roughening. The Concept 1 bridge was initially subjected to one million cycles of fatigue loading. Minimal transverse strains were observed over the longitudinal joints of both spans. French et al. (2011) tested both Concept 1 and 2 bridge specimens under fatigue loads and to near ultimate and showed good durability for spans with 3 in. flanges. Overall, it was unclear whether the specimens with 3 in. flanges performed better than the original $5\frac{1}{2}$ in. flange design. In any case, good performance was observed for the 3 in. flange specimens and the thinner flanges permitted reinforcement to be placed lower in the trough region.

The use of smooth flanges simplified the fabrication process compared to the intentionally roughened flanges, because it was easier to remove the flange formwork from beneath the trough hooks protruding from the webs for the case of the smooth flanges. However, the effect on behavior of using smooth flanges rather than roughened flanges was difficult to determine from the Concept bridge specimens, which featured both types of surfaces. All of the subassemblage specimens from French et al. (2011) were fabricated with smooth flanges. For one specimen, voids on the flange surfaces due to “bug holes” from air bubbles were patched. These voids and the subsequent patching are shown in Figure 2.7. Voids occur on the top of the flange surface of PCSSS precast beams during fabrication because air bubbles get trapped during consolidation. The load testing of the patched specimen did not show significant differences in crack control from specimens with similar reinforcement without patching. All subassemblage specimens were prewetted and allowed to reach a “surface dry” condition prior to the placement of CIP concrete. Smooth flanges were recommended for PCSSS fabrication, although patching the voids was deemed unnecessary. The “roughness” created by the “bug holes” was thought to be advantageous; it was believed that full delamination between the CIP concrete and flange surface would be undesirable because it could promote cracking at the web-flange interface, bypassing the cage reinforcement.

2.1.4 Transverse Reinforcement in Trough Region

The transverse reinforcement in the trough region consists of the overlapping trough hooks that extend from the webs of the adjacent sections and stirrups from the cage that is placed within the trough. French et al. (2011) investigated the effects of transverse reinforcement in the trough region using the Concept 1 and Concept 2 specimens. The Concept 1 bridge had No. 6 trough hooks spaced at 12 in. with No. 5 cage stirrups adjacent to the trough hooks, the same reinforcement as used in Bridge No. 13004. Because the Concept 1 bridge had two spans with different flange thicknesses (i.e., 5-1/4 in. and 3 in.), the clearance between the trough hooks and flanges varied from 1-5/8 in. on one span to 3-1/8 in. on the other. It would have been desirable to have closer proximity to the bottom flange than 3-1/8 in. distance; however, the edge of the precasting bed that was used limited the depth of the trough hooks. The transverse reinforcement for the Concept 2 bridge was reduced from the Concept 1 design to No. 4 trough hooks spaced at 18 in. with No. 3 cage stirrups offset from the trough hooks by 9 in. (the overall transverse reinforcement spacing was 9 in. considering the cage and the trough hooks). One half-span of the Concept 2 bridge used the standard embedded hooked bars in the trough for transverse reinforcement, while the other half-span used threaded bars anchored mechanically into the precast web in the trough without a hooked end. The distance from the end of the anchored bars to the precast web face was shorter than the development length, so the bars were only expected to develop 80% of the full yield strength. Figure 2.8 shows the threaded bar and terminal end from the Concept 2 bridge. The threaded bars were investigated as a potential means to improve ease of fabrication by eliminating the bar protrusions from the web in the casting process. Straight threaded bars were used, as opposed to hooked bars, to avoid the expense of a more expensive coupler that would be needed to facilitate positioning a hooked bar in the correct orientation.

The large-scale specimens were tested for performance under fatigue loading, with loading up to transverse strains similar to those observed in Bridge No. 13004, and loading to near-ultimate capacity. Cyclic loads simulating traffic loads and environmental loads were applied to each bridge with stages of increased magnitude. After one million cycles, a crack was

intentionally introduced along the longitudinal joint in each bridge to determine the effect of a reflective crack on durability by investigating the stability of the behavior at intermittent intervals during the cyclic load tests. Each bridge exhibited good fatigue behavior over the range of fatigue loads, with minimal degradation to the longitudinal joint and good crack control by the trough reinforcement. Periodically throughout the fatigue tests, load transfer between the panels of each bridge was measured. Based on the observed correlations of longitudinal curvatures between the loaded and adjacent unloaded beams, each bridge was deemed sufficient at transferring loads. The similar reflective crack control behavior and load transfer between the two bridges suggested that the transverse reinforcement details from both bridges would be acceptable in PCSSS design.

The seven subassembly specimens were built to further investigate reflective crack control by various arrangements of transverse reinforcement. The reinforcement details for each subassembly are given in Table 2.1. Reinforcement ranged from using no cage reinforcement (only 18 in. spaced trough hooks), to cage reinforcement with 4.5 in. spacing. Each subassembly was subjected to cyclic loading at increasing intervals up to 200% of the cracking load. Overall, the specimens with larger area of reinforcement and spacing no further apart than 9 in. provided the best crack control.

Based on the results of the large-scale and subassembly specimens, French et al. (2011) recommended that the transverse reinforcement should satisfy the crack control recommendation by Frosch (2006), shown in Equation 2.1:

$$\rho_{cr} = 6 \frac{\sqrt{f'_c}}{f_y} \quad (2.1)$$

where f'_c is the precast concrete strength (psi), f_y is the reinforcement yield strength (psi) and ρ_{cr} is the ratio of all transverse reinforcement over the joint to the area of CIP concrete in the trough region. Transverse reinforcement, which consists of the combined cage stirrups and trough hooks, should be spaced no more than 9 in. apart, also as recommended by Frosch (2006). This could be accommodated by using 18 in. spacing of the trough hooks and 18 in. spacing of the cage stirrups, with the cage reinforcement staggered to obtain the 9 in. maximum spacing.

2.1.5 Composite Action Stirrups

At the conclusion of the fatigue load tests, both large-scale bridge specimens were loaded to the maximum possible load allowed by the laboratory actuators, which was above the predicted nominal capacity of the bridges. Longitudinal concrete embedment strain gauges through the thickness of the CIP deck and precast beam allowed for determination of slip between the precast section and CIP deck at near-ultimate capacity. Both bridges maintained composite action through the applied load range and showed no sign of imminent failure.

The Concept 2 bridge did not have any composite action stirrups, using only the roughened surfaces in contact with the CIP concrete to transfer shear. Naito et al. (2006) suggested that the minimum composite action stirrups required by AASHTO was overly conservative. Because the Concept 2 specimen had no composite action stirrups, this test showed that the PCSSS could transfer shear through the CIP-web interface without stirrups. The stress transferred across the interface at the maximum load was 135 psi, so it was recommended

that the PCSSS could be designed without composite action stirrups if the maximum factored shear at the interface was no larger than 135 psi.

2.1.6 Restraint Moments

Smith et al. (2008) investigated the development and modeling of restraint moments using the Concept 1 bridge prior to load testing. The precast beams were 7 days old when the CIP deck was poured, which was considered to be the earliest feasible age of the precast at CIP deck pour time. The restraint moments experienced by the bridge were measured over a period of 250 days using load cells at each simply-supported end of the specimen. Two methods were used to predict the restraint moments for comparison: the PCA method and the Peterman method (P-method). The PCA method, developed by Freyermuth (1969), used tabulated creep and shrinkage factors without accounting for shrinkage restraint by deck reinforcement. The P-method (Peterman and Ramirez 1998) used the AASHTO 2004 creep and shrinkage factors, and reduced the predicted deck concrete shrinkage based on the amount of deck reinforcement restraint. Figure 2.9 shows the measured restraint moments from Span 1 and 2 (lines i and ii, respectively) compared to restraint moment predicted by the PCA method (line iii) and P-method (lines v and vii). The P-method predicted different restraint moments for each span because each span had different designs and this method assumes a non-zero pier thickness, while the PCA method predicted only one restraint moment because the assumed pier support was assumed to have no length. From these results, the PCA method appeared to predict long-term positive restraint moments closely after 150 days, while the P-method over-predicted the results.

To evaluate the accuracy of each restraint moment analysis method, coefficients were fitted to the AASHTO 2004 and PCA creep and shrinkage models using measured strains from concrete test cylinders. The test cylinders were cast at the time the bridge was constructed and were allowed to creep and shrink under the same environmental conditions as the bridge. By using the cylinder test results to fit coefficients, the creep and shrinkage factors were better predicted by the AASHTO 2004 model. After fitting the creep and shrinkage coefficients, the PCA method predicted a negative restraint moment (line iv in Figure 2.9), while the P-method predicted a closer, yet still larger, positive restraint moment (lines vi and viii). The drastic change in the PCA method prediction indicated that the way creep and shrinkage affect restraint moments are better modeled by the P-method.

It was recommended that the P-method be used in future designs, or that the PCA method be modified to use a different creep and shrinkage model, such as AASHTO 2004, and to consider CIP concrete shrinkage restraint. In either case, the results showed that predicting restraint moments is highly dependent on the choice of model.

2.2 Current AASHTO LRFD 2010 Design Specifications

The parametric design study in Chapter 6 of this report was in compliance with specifications from the AASHTO LRFD Bridge Design Specification, 5th ed. (2010). In particular, provisions for prestress losses, creep and shrinkage, restraint moments, and thermal gradient effects were considered. Provisions for the creep and shrinkage model from AASHTO 3rd ed. (2004) were also considered.

Provisions for prestress losses are given in Section 5.9.5 of AASHTO (2010). Losses in pretensioned members are separated into those due to elastic shortening and those due to time-

dependent effects. Elastic shortening losses, Δf_{pES} , are derived from strain continuity between the strand and concrete at transfer. The time-dependent losses are given by both an approximate estimate (Section 5.9.5.3) and a refined estimate (Section 5.9.5.4). PCSSS precast beams do not meet dimensional requirements for the approximate estimate, so the refined estimate must be used. The refined estimate incorporates losses due to creep, shrinkage, and relaxation between transfer and deck placement and between deck placement and the end of design life. As such, the time-dependent losses are dependent on assumed creep and shrinkage models.

Creep and shrinkage provisions are given in Section 5.4.2.3 of AASHTO (2010). These models were updated for the 4th edition (2007) based on extensive research on high-strength concrete and the recommendations of ACI Committee 209. However, some studies found the creep and shrinkage models in AASHTO 2007 and 2010 predicted unconservative prestress losses for their applications and recommended using the model from AASHTO 2004 (Barr 2009, Youakim 2007). Part of the parametric study in Chapter 6 investigated the applicability of the creep and shrinkage models from both AASHTO 2004 and AASHTO 2010.

Section 5.14.1.4 of AASHTO (2010) contains provisions for considering restraint moments in bridges with precast, simply-supported elements made continuous. These provisions are largely the result of research by Miller et al. (2004) on continuous diaphragm connections between bulb-tee girders. Because the PCSSS consists of simply-supported precast beams made continuous with the CIP deck, the provisions for restraint moments apply. Continuity naturally enhances the span range for a given beam design. However, continuity requires evaluation and detailing for both the service and strength limit states. Restraint moments that develop as a result of continuity are the result of thermal gradient, beam creep and differential beam/deck shrinkage. The latter two restraint moment contributors are the result of time dependent effects. Section 5.14.1.4.4 allows positive time-dependent restraint moments to be neglected for the precast beam design if the precast beams are 90 days old at the time of CIP concrete deck placement. Aging the beams allows creep and shrinkage to occur prior to continuity, reducing the magnitude of positive restraint moments. In this case, a positive moment connection must be provided to resist $1.2M_{cr}$, where M_{cr} is the cracking moment. Negative restraint moments need to be considered for the purposes of deck design. Similarly, thermal gradient restraint moments exist in the system independent of beam age and therefore should still be considered in design irrespective of beam age. Research has shown that following the provisions in Section 5.14.1.4.4 without accounting for thermal effects can negatively affect the performance of continuity connections (Okiel 2011).

The design of positive moment connections to resist restraint moments and provide continuous action is covered in Section 5.14.1.4 of AASHTO (2010). Positive moment connections can be made using mild reinforcement or with anchored pretensioning strands, and must be able to resist the larger of the factored positive restraint moment and $0.6M_{cr}$. These restraint moment requirements satisfy continuity effects at the strength limit state but a separate check is required before assuming full continuity at the service limit states. The connection can only be considered fully effective at the service limit state if the diaphragm is engaged in compression under the load combination of permanent dead load, time-dependent restraint moment, thermal gradient, and 50% live load. If this condition is met, the superstructure can be designed as fully continuous under service loads. If this condition is not met, partial continuity must be considered. In either case, a complete positive moment connection satisfying the strength requirement must be provided.

Analysis of thermal gradients is specified by Section 4.6.6 of AASHTO (2010). Thermal gradient effects are separated into three components: axial expansion, flexural deformation, and internal stress. Axial expansion is the contribution of the temperature gradient to uniform axial strain. This axial strain only causes stress if the structure is axially restrained. Flexural deformation is the contribution of the temperature gradient to pure bending strain. The response of the structure is defined by a uniform curvature dependent on the thermal gradient profile through the section. Similar to axial expansion, flexural deformation only causes stress if the structure is rotationally restrained. In the case of the multiple span PCSSS, the continuity connection at the pier creates rotational restraint and the resulting moments are considered restraint moments. Internal stresses result from the necessary compatibility through the section that must be satisfied in the presence of axial expansion and flexural deformation. Internal stresses occur regardless of the system restraint.

2.3 PCSSS Design History

One of the primary goals of this report was to evaluate the effectiveness of design changes among the different generations of MnDOT PCSSS bridges using observations from previously constructed PCSSS bridges. In order to adequately evaluate the existing bridges, a comprehensive design history of the PCSSS was needed. From the introduction of the MnDOT PCSSS in 2005 through 2011, the MnDOT PCSSS underwent three major design revisions that characterize four distinct design generations. Five existing PCSSS bridges were chosen for field inspections covering the first three design generations, discussed further in Chapter 4. Design details for the fourth generation and recommendations for future design are discussed in part in Chapter 5. Table 2.2 contains a summary of the major design features for each generation with changes between successive generations emphasized. Design changes were primarily implemented to control reflective cracking, to control shrinkage cracking, and to improve constructability. The following design history summarizes the major characteristics of each design generation, mostly limited to those details that varied among generations. Each of the five field bridges is presented under the appropriate design generation with a further summary of details particular to each bridge.

2.3.1 Generation 1 (2005)

Generation 1 (Gen 1) was the original MnDOT PCSSS design developed in 2005. The MnDOT PCSSS design was based on the French Poutre Dalle system identified during the FHWA scanning tour in 2004 (Hagen et al. 2005). Figure 2.10 shows a typical midspan cross section for Gen 1 of the PCSSS design. The flanges of the inverted-tee beams were designed with a minimum thickness of 5¼ in. for adequate cover of the confining reinforcement. All of the corners of the precast beams were given a ¾ in. chamfer to reduce possible stress concentrations with the potential for crack generation. In order to increase shear transfer between the precast and CIP concrete, the tops of the flanges and the tops and sides of the webs were roughened during fabrication. The trough hooks were spaced at 12 in. in each beam, and for constructability, the trough hooks were offset by 2 in. in adjacent beams. The closely spaced trough hooks increased load transfer while accounting for construction tolerances and concrete placement. Composite action stirrups were spaced at 1 ft. to ensure the first PCSSS bridges would act as slab spans with full composite action. Clearance between the composite action stirrups and top of the precast web was not specified. Transverse deck reinforcement for crack control consisted of No. 5 bars spaced at 1 ft. Two bridges were built with the Gen 1 design:

MnDOT Bridge No. 13004 over the Center Lake channel in Center City, MN and MnDOT Bridge No. 04002 over the Tamarac River in Waskish Township, MN.

Bridge No. 13004 was instrumented by Bell et al. (2006) and was chosen to represent Gen 1 in the field inspections for this report. Table 2.3 contains a summary of the design details for Bridge No. 13004. Bridge No. 13004 was one of the wider MnDOT PCSSS bridges built (i.e., 72 ft. wide) and its aspect ratio was the smallest of any of the bridges inspected for this report. This bridge was constructed in two stages to permit continued traffic during construction. The anchorage dowels at the piers were placed between the precast panels along the middle 36 ft. At the abutments, three dowels were placed in each blockout. The configurations of dowels for all five field-inspected bridges are discussed further in Section 5.1.2.

2.3.2 Generation 2 (2007)

Generation 2 (Gen 2) was developed in 2007 following preliminary results of the study by Smith et al. (2008). Design changes for Gen 2 were intended to improve constructability and to address cracking due to insufficient CIP concrete consolidation under the composite action stirrups. Figure 2.11 shows a cross section of a typical Gen 2 inverted-tee beam at midspan. In Gen 1, a minimum clearance over the web for the composite action stirrups was not specified. This resulted in limited space for concrete placement around the composite action stirrups when the CIP topping was cast. It was suspected that observed surface cracks were originating at composite action stirrups due to incomplete consolidation. For Gen 2, a minimum projection of 2 in. was specified for the composite action stirrups. This reinforcement was also changed from a U-shape that surrounded the prestressing strand to a C-shape for ease of placement. Similarly, the confining reinforcement was changed from full hoops to separate J-bars. These two changes simplified fabrication of the precast beams because the reinforcement could be placed after prestressing strands were pulled. Three Gen 2 bridges were constructed: MnDOT Bridge No. 33005 over the Ann River and MnDOT Bridge No. 33008 over the Groundhouse River in Mora, MN, and the approach spans of MnDOT Bridge No. 06679 over the Root River in Sheldon Township, MN. Of the design changes made in Gen 2, it was expected that the clearance of the composite action stirrups would have the only visible effect on the field investigation.

Bridge No. 33005 was built on skewed supports, angled at 25°, and was chosen as one of the representative bridges for Gen 2. As shown by French et al. (2011), the skewed supports were not expected to affect the horizontal shear above the longitudinal joints of Bridge No. 30005. The anchorage dowels were placed in the blockouts at both the piers and abutments. During construction of Bridge No. 13004, the straight-line dowels at the piers caused complications because of the small 4 in. gap between the precast beam ends. By placing the dowels only in the blockouts, constructability was improved without a supposed loss of restraint. Four dowels were placed in each blockout at the piers and two dowels were placed in each blockout at the abutments. A full summary of the details for Bridge No. 33005 is given in Table 2.4.

Bridge No. 33008 was the second bridge chosen to represent Gen 2 in the field inspections. Table 2.5 contains the design details for Bridge No. 33008. Both Bridge Nos. 33005 and 33008 were built near Mora, MN at the same time. Bridge No. 33008 also had dowels in the blockouts at both the piers and abutments. However, each blockout had 3 dowels at the abutments and 6 dowels at the piers, which was assumed to increase the restraint at the

supports. This bridge has shown differences in camber between adjacent precast beams, which are discussed further in Chapters 3.

2.3.3 Generation 3 (2009)

Generation 3 (Gen 3) was developed in 2009, incorporating many design recommendations from the final report by Smith et al. (2008). Gen 3 saw significant changes to improve durability of the PCSSS system with attempts to reduce reflective and restrained shrinkage cracking. Figure 2.12 shows a cross section of a typical Gen 3 inverted-tee beam at midspan. During the construction of Gen 3 bridges, the precast beams were wetted prior to the CIP concrete placement. This prewetting was an attempt to reduce the shrinkage of the CIP concrete by preventing water from being absorbed from the CIP concrete into the precast concrete. The outer anchorage dowels at the piers and abutments were intended to be wrapped with polystyrene sleeves to reduce lateral restraint at the supports, although not all dowel wrapping was completed.

A major change was to reduce the inverted-tee flange thickness from 5 ¼ in. to 3 in. The reduced flange thickness allowed trough hooks to be placed lower in the cross section, intercepting potential reflective cracks sooner. The tops of the flanges were made smooth in fabrication instead of roughened to reduce the restraint between the CIP and precast concrete near the longitudinal joint, again to reduce reflective cracking and to aid in removal of the forms. To further improve reflective crack control, a wire mesh was to be placed over the longitudinal joints to intercept cracking. The drop-in cages were offset from the trough hooks so that the spacing between the cage ties and the trough hooks was 6 in. This was done to increase the chances of intercepting reflective cracking between the trough hooks and cage ties. Finally, the chamfers on the precast corners (i.e., both flange and web) were increased to further reduce potential stress concentrations. Three bridges were constructed with the Gen 3 design: MnDOT Bridge No. 49007 over the Swan River and MnDOT Bridge No. 49036 over Pike Creek, both in Little Falls, MN, and MnDOT Bridge No. 66044 over the Cannon River in Morrison Township, MN.

Bridge No. 49007 was one of the Gen 3 bridges selected for field inspection. Due to contractor error, only the dowels on the south pier were wrapped with polystyrene, potentially providing different restraint to the two ends. Also, wire mesh was not installed over the longitudinal joints on Bridge No. 49007. The wire mesh was complicated to install, needing to be wedged beneath the in-place trough hooks. Because the wire mesh was a precautionary addition, its omission was not a serious concern. Dowels were placed in the blockouts at the abutments and piers in sets of two and four, respectively.

Table 2.6 contains complete design details for Bridge No. 49007

Bridge No. 49036 was the second of the Gen 3 bridges selected for field inspection. Dowel wrapping was completed as specified for this bridge, although the wire mesh was still not used. Instead, perpendicular No. 3 bars were placed at 9 in. transversely and 6 in. longitudinally over the longitudinal joints. These bars were easier to place than the wire mesh, but they were held in place with ties to the trough hooks so it was labor intensive. Design details for Bridge No. 49036 are shown in Table 2.7.

Chapter 3: Field Inspections

Since the development of the MnDOT PCSSS in 2005, the bridge design was implemented in twelve bridges across Minnesota between 2005 and 2011. Over the course of the implementations, the PCSSS design underwent a number of modifications to improve performance in different design generations. To determine the effect of these design modifications on performance, a series of field inspections was done for five existing PCSSS bridges. The bridges under investigation represented the three distinct PCSSS design generations between 2005 and 2009. Results from the field inspections were compared among the various design generations in order to determine the effectiveness of the design changes.

Field inspections were conducted using two separate but related procedures: crack mapping and core examinations. First, observed cracks from the field inspections were systematically documented on crack maps for each bridge. Additional observations about the condition of each bridge were also recorded during the crack mapping inspections. Crack mapping was performed in three rounds between October 2009 and August 2011 to investigate changes in surface cracking over time. A total of 17 core specimens were extracted from the five inspected bridges in October 2010. The following sections explain the procedures for crack mapping and core examinations and present the results of the field inspections from each bridge.

3.1 Crack Mapping Overview

A method for documenting cracks was developed to obtain accurate and comparable records of surface cracking. As described below, the procedure involved an in-field method for locating cracks on the bridge surface, documenting the surface cracks on paper, and transcribing the paper records to electronic format. This procedure was originally developed by Phil Cici at the UMN in 2009 for the first set of inspections. The procedure was modified for the second and third sets of inspections to better characterize the cracking behavior by refining the crack width classifications.

Crack mapping inspections were conducted for five PCSSS bridges between October 2009 and August 2011. Three crack mapping inspections were performed for each bridge, except for Bridge No. 13004 which had two inspections due to scheduling conflicts with local road construction which prevented the third inspection of Bridge No. 13004 in August 2011. In addition to the five PCSSS bridges, crack mapping was also conducted for a conventional slab-span bridge of similar size and age. The conventional slab-span crack map was used as a “control” to evaluate the relative performance of the PCSSS to be used as a replacement system. Core specimens were not extracted from the slab-span bridge.

The procedure for locating and documenting the cracks entailed identifying cracks on the surface of the bridge and recording the following characteristics: crack length, crack width, and location with respect to the structural precast members. The crack mapping procedure and a full record of crack maps from each bridge is provided in Appendix A. For the first round of inspections the crack widths were characterized by four categories ranging from very small cracks to progressively larger cracks, given in Table 3.1. Based on the results of the first crack mapping inspections, it was determined that the crack width classification system needed to be refined. The original classification system grouped crack widths together in large ranges. For example, Class B cracks, of which a significant number were observed, spanned the range of

0.008 in. to 0.022 in. Even more dramatically, Class C cracks spanned the range of 0.023 in. to 0.20 in. Because these classification ranges differed by orders of magnitude, crack widths could be interpreted as more or less severe than in reality. Therefore, the original classification system was refined by splitting Classes A, B, and C into two ranges each. The refined classification scale is given in Table 3.2.

Crack maps for each PCSSS bridge from the most recent inspection are shown in Figure 3.1 through Figure 3.7. The crack map for the conventional slab-span bridge is shown in Figure 3.8.

3.1.1 Additional Field Observations

While the primary objective of crack mapping was to record the observed cracking of the PCSSS bridge decks, additional observations about the state of each bridge were also noted including issues such as the presence of efflorescence on the underside of the bridge and/or appearance of differential camber, if any. The additional observations were documented with the belief that they could be useful in the evaluation of the performance of the existing PCSSS bridges.

Each bridge showed, to some degree, an amount of efflorescence around the longitudinal joints on the underside of the precast beams. Figure 3.9 shows a typical region of efflorescence at a longitudinal joint. The efflorescence originated from the longitudinal joint and spread transversely along the underside of the precast section. The distance the efflorescence extended away from the joint varied for each bridge. When the efflorescence was first observed, the concern was whether it was caused by continued leakage through the joint. This would have been an indication of through-cracking between beams. If this were the case, it was assumed that the efflorescence would continue to extend away from the joint with time. To track the extent of the efflorescence, permanent marker was used to mark the observed efflorescence boundary, which was monitored at subsequent crack mapping inspections. These permanent markings can also be seen in Figure 3.9. As of August 2011, there was no indication that the efflorescence was spreading. It was believed that the efflorescence was initially caused by water from the CIP concrete pour that had gotten around the caulk in the joint under the pressure of the CIP concrete and stained the bottom surface.

Several observations were made of particular bridges concerning the condition of the precast beams. Specifically, issues of differential camber between beams of the same bridge, uneven bearing surfaces, and apparent flange cracking were observed. These observations are described further in Section 3.3 for specific bridges.

3.2 Core Examination Overview

Core samples were taken from the same five PCSSS bridges to investigate the possibility of reflective cracking. Target locations for taking the cores were over the longitudinal joint between adjacent flanges and over the vertical web-CIP interface. It was assumed that these regions would be most prone to reflective cracking. Through a process of examining the cores, cracks were located, documented and analyzed.

3.2.1 Core Selection and Extraction

Coring locations were chosen to maximize the potential for capturing reflective cracking. To this end, coring was restricted to the flange-flange longitudinal joint between precast panels and the web-CIP interface, which were believed to be most prone to reflective cracking in PCSSS bridges. Figure 3.10 shows a typical cross section of a longitudinal joint, with the coring locations indicated. Cores over a longitudinal joint were taken down to the top of the flanges, while those over a web-CIP interface were taken down to just past the web corner. Observations from the crack maps were used to determine several coring locations. The instrumentation in Bridge No. 13004 showed that initial reflective cracking tended to occur at alternating longitudinal joints, leaving the joint in between uncracked. Therefore, several cores were chosen on alternating joints, particularly if surface cracking was observed over one or more of the joints. Some core locations were also selected at joints adjacent to those with suspected cracking to confirm that the adjacent joint remained uncracked. Table 3.3 contains the nominal locations of all extracted cores relative to working points (WPs) in Figure 3.1 through Figure 3.7. These figures show the locations of the core specimens relative to major structural features and observed cracks from Inspection No. 3. The list in Table 3.3 also contains a rationale for choosing the location of each core specimen and served as a checklist of objectives for each core during examination.

A total of 17 cores were extracted from the inspected PCSSS bridges. The location of each core was measured on the surface of the bridge deck from the specified working point. Because of measuring errors and erection tolerances, the exact location of the core was not necessarily at the nominal location. Location errors were accounted for in the core examinations, described below. The depths of the cores were determined prior to extraction from bridge plans. However, the as-built depth varied because the exact thickness of the CIP deck was unknown. The location of reinforcement within the trough was used as a guide to determine the needed depth. As each core was extracted, the coring depth was adjusted depending on where reinforcement was intercepted. Because they were only partial depth, cores had to be extracted by prying them from the deck surface. Every attempt was made to extract cores in one piece, but in many cases cores had to be broken to remove them from reinforcement. Core holes were patched with ready-mix concrete.

Cores from Bridge Nos. 49007 and 49036 in Little Falls, MN were extracted by the local MnDOT coring crew with direction by UMN researchers. These cores were taken with a 4 in. bit on a truck-loaded coring drill. Cores over the longitudinal joints had to be extracted in two pieces because the drill bit was shallower than the full required core depth. Unfortunately, the locations of these 4 in. cores could not be verified by joint or web characteristics on the cores. Identification of these physical characteristics is described in more detail below.

Cores from Bridge Nos. 13004, 33005, and 33008 were extracted by American Engineering Testing with direction by UMN researchers. Because the cores from Bridge Nos. 49007 and 49036 did not necessarily capture the desired locations, some of the cores from Bridge Nos. 33005, and 33008 were taken with a 6 in. bit. The increased bit size made capturing the desired location more likely, but due to time constraints, the remaining cores were taken with a 4 in. bit. The coring drill for these extractions was deck mounted.

3.2.2 Examination Procedure

A summary of the results from the core examinations is given in Table 3.5. The core specimens were numbered by the bridge number followed by the core number from the corresponding crack maps. The condition of each core was evaluated according to the scale in Figure 3.11. As described in Section 3.2.1 and shown in Figure 3.10, cores were located either over the longitudinal joint or the web-CIP interface. In order to determine the accuracy of the core location relative to the nominal location, a measured offset was defined as the transverse distance between the center of the core and the intended location. The offset was determined for each core by measuring the transverse distance between the center of the core and either the longitudinal joint or the web corner. The longitudinal joints and web corners were physically identifiable on most cores; if the location of a core could not be physically identified, the exact location of the core was unknown and the data was less reliable. Examples of a physically identifiable joint and web corner are shown in Figure 3.12. Reinforcement intercepting the core was recorded to identify location and any possible effects on cracking.

Prior to being examined, the cores were prepped by rinsing with water, wiping them gently to remove any remaining sludge from the coring process, and patting them dry with paper towels. The drying concrete made cracks highly visible as water was retained in the cracks. The cores were reassembled if broken, and the general characteristics of the core were documented (e.g., core height, diameter, and number of sections). The cores were initially inspected by the naked eye before inspection with a microscope. Particular attention was paid to regions where cracking was expected such as the longitudinal joint. Any visible cracks were marked with a dotted red line, as shown in Figure 3.13. When the crack became too small to see clearly, a zPix 200 digital microscope was used to examine the cores more closely. This microscope had 26x – 130x digital magnification with an integrated camera.

A crack gage was used to measure the crack widths along the length of the crack both by the naked eye and with the microscope. As with the crack mapping, the refined classification scale in Table 3.2 was used to identify crack widths. The finer classification was beneficial for characterizing small changes in the width of the cracks, particularly as the widths fluctuated through the cores. The records from the core examinations can be found in Appendix B.

Identifying the orientation and location of cracks on the cores required defining a local coordinate system. Figure 3.14 contains a sketch of the typical orientation of the cores. Magnetic North was marked on the top of each core in the field. However, to facilitate the comparison among bridges, a pseudo local coordinate system was used based on the bridge longitudinal and transverse directions. The pseudo local “north” and “south” faces corresponded to the longitudinal direction and the pseudo local “east” and “west” faces corresponded to the transverse direction. The azimuth between true North and the pseudo local north face was both measured in the field and taken from the bridge plans. Depth through the core was measured from the top, increasing downward. Therefore, a crack starting at the top of the core started at a depth of 0 in. The locations of cracks on the face of the core were defined by the face on which the crack was located (pseudo local north, south, east, or west) and an offset distance in an orthogonal direction. For example, Figure 3.15 shows a crack on the south face of Core 33008-3 that is offset 1 in. to the west.

3.3 Observations from Field Inspections

The results of the crack mapping and core examinations were compiled for each PCSSS bridge for a complete account of the cracking behavior. Crack mapping provided a time-varying description of cracking that was comparable across design generations, recognizing that bridges from different design generations were constructed in different years. The core examinations provided further information about suspected reflective cracking from the crack maps. The following is a description of the results for each bridge from both parts of the investigation. Table 3.4 lists the inspection dates for each bridge and the age of the bridge at the time of inspection. The complete crack maps and core examinations can be found in Appendices A and B, respectively.

Several general observations were made from the results of the field inspections. Overall, cracks observed in Inspection No. 1 were wider than those observed in Inspections No. 2 and 3. The cracks observed during Inspection No. 1 were wider because Inspection No. 1 took place in the fall while Inspections No. 2 and 3 took place in the summer. The warmer temperatures during the summer inspections caused the bridge decks to expand, closing the surface cracks. This phenomenon was confirmed by the bridge maintenance crews. To some extent, the perception of wider cracks in Inspection No. 1 was compounded by the rougher crack width classification scale, which was refined for the later inspections. Smaller crack widths observed in summer due to warm temperatures made direct comparison with cracks widths observed in the fall difficult, although crack locations and relative widths could be compared.

The number of observed cracks generally increased between successive inspections of each bridge. More cracks may have been observed in the second and third inspections because more man-hours were used for these inspections. However, additional cracks located during Inspections No. 2 and 3 were mostly Classes A1 and A2, which were relatively small. In addition, bridge maintenance crews reported seeing cracks progressively increase from year to year on several bridges. It was assumed that all the major cracks were documented during all the bridge inspections.

Cracks recorded on the crack maps were separated into three types: longitudinal cracks, transverse cracks, and map cracking. Longitudinal cracks occurred along the precast beam joints and over the precast webs, particularly on end spans. It was assumed that longitudinal cracks aligned with the longitudinal joints were a result of a reflective through cracks. Longitudinal cracks distinctly over the precast webs may have been caused by restrained shrinkage due to the shallow CIP concrete relative to the CIP concrete over the trough region. Long transverse cracks typically formed over bridge piers and in the center spans. Transverse cracking was attributed to negative moments, both from live loads and restraint moments. Map cracking also occurred over the piers, which could have been the result of restrained shrinkage. Some longitudinal and map cracking continued to develop several years after construction, lending doubts to shrinkage as a cause.

3.3.1 Bridge No. 33532 – Conventional Slab Span on CR 60 over the Groundhouse River, Ogilvie, MN

Bridge No. 33532 was a conventional slab-span bridge built in 1995. The bridge consisted of three spans (24 ft., 30 ft., 24 ft.) designed continuous for live load, which was

inspected to compare with the five PCSSS bridges. One field inspection was performed on September 16, 2010 and the resulting crack map is shown in Figure 3.8.

Few surface cracks were observed on the bridge deck. Cracking was limited to transverse cracks directly over the pier and several long longitudinal cracks. The longitudinal cracks ran from the ends of the end spans to the piers, with one major crack across the center span. Map cracking was not observed, signifying that shrinkage restraint was not an issue. This was to be expected because the bridge was entirely CIP concrete with no excess restraint from precast elements. The slab was built integral with the substructure, but the substructure was also CIP concrete. The transverse cracks over the piers were most likely due to negative moments from live loads and did not extend past the pier cap. Most of the cracks on Bridge No. 33532 were Class A2 in width, and none exceeded Class B1. These cracks were not wider than those on the PCSSS bridges observed under similar conditions. It should be noted in the case of the slab-span bridge, that the system supports both its self-weight and live loads; whereas in the case of the PCSSS bridges, the CIP is only subjected to the live load stresses as the precast inverted-tee sections serve as stay-in-place formwork. The compressive stresses in the top of the slab-span system due to dead load stresses are likely to have an impact on the reduced cracking observed in the top surface away from the piers.

3.3.2 Bridge No. 13004 – T.H. 8 over the Center Lake Channel, Center City, MN

Bridge No. 13004 was a three-span bridge of a Gen 1 design, completed on November 2, 2005. The bridge was instrumented with strain gauges as discussed in Chapter 2. Research by Bell et al. (2006) and Smith et al. (2008) describes the instrumentation in detail, and Chapter 4 of this report summarizes observations from the instrumentation to date. The purpose of the strain gauge instrumentation was to investigate the possible development of reflective cracking and to investigate live load distribution and continuity.

Few cracks were observed on the deck surface above the longitudinal joints during crack mapping; longitudinal cracking was almost entirely over the precast webs. These longitudinal cracks were also fairly short. Sparse transverse cracking was observed over the piers and slight map cracking was observed sporadically on the bridge deck. Inspection No. 1 showed crack widths from Class A to Class D, where Class D cracks were wider than 0.20 in. The classification of cracks as Class D was suspect and as such was indicated on the crack map with a dashed line to convey uncertainty. The second inspection was conducted during the summer months, and there was no evidence of Class D cracks. Although the summer inspections led to narrower cracks due to the increased temperature of the deck, the Class D cracks should have still been distinguishable. Inspection No. 2 saw larger numbers of cracks, but the vast majority were Class A2. In general the surface cracking on Bridge No. 13004 was atypical of the group of PCSSS bridges inspected, as can be seen in the observations of the remaining four bridges.

Four cores were taken from Bridge No. 13004, all with 4 in. diameter. Core 13004-1 was taken over a longitudinal joint where the strain gauge instrumentation showed signs of reflective cracking. Reflective cracking was not observed on this core. However, Core 13004-1 only captured one side of the joint, as seen in Figure 3.16. The instrumentation indicated the crack originated on the side of the joint not captured by the core, so a reflective crack may have existed on the non-captured side. Core 13004-2 was taken from another longitudinal joint that showed cracking from the instrumentation. A reflective crack was observed on this core. The reflective crack was less than 0.002 in. wide (Class A1), and extended 1½ in. upwards from the joint.

Cores 13004-3 and 13004-4 were taken over the web-CIP interface. Core 13004-3 was taken from an end span, over a region that showed surface cracking over the interface. Core 13004-4 was taken next to Core 13004-1 to capture reflective cracking driven away from the joint and into the region of the web-CIP interface. Both of these cores showed only surface shrinkage cracking. All observed shrinkage cracks extended no further than ½ in. from the surface, and all were Class A1.

3.3.3 Bridge No. 33005 – T.H. 65 over the Anne River, Mora, MN

Bridge No. 33005 was a three-span skewed bridge of a Gen 2 design, completed on November 2, 2007. Transverse cracking occurred in the region over the skewed piers, with the individual cracks running perpendicular to the beams. The transverse cracks were Classes B and C from Inspection No. 1 and Class B2 from Inspection No. 2. Prior to Inspection No. 3, bridge maintenance crews sealed many of the large cracks on Bridge No. 33005. Because the sealant obscured the cracks, the width of the sealed cracks could not be measured. The locations of these cracks were recorded on the crack map with a dashed line to indicate uncertainty. Over the piers, transverse cracks were paired with significant map cracking. This crack behavior was more typical of the remaining bridges than the transverse cracking from Bridge No. 13004. The longitudinal cracks were observed over the precast webs, away from the longitudinal joints. These cracks were longer than the longitudinal cracks found on Bridge No. 13004.

Two core specimens were taken from Bridge No. 33005: Core 33005-2, a 4 in. diameter core, was taken at a surface crack over a web corner and Core 33005-1, a 6 in. diameter core, was taken at the adjacent longitudinal joint. Between the two cores, only one shrinkage crack was observed on Core 33005-2. This crack was ¼ in. deep and Class A1. No reflective cracking was observed in Core 33005-1 which was over the joint. In both cores, the clear cover over the deck reinforcement was less than the required 3 in. from the bridge plans. Reinforcement cover was only 1½ to 2 in. The thickness of the CIP concrete was less than required, as evinced by Core 33005-1. In this core, the precast web corner was visible, which indicated the total depth of the CIP concrete over the web was 4¾ in., seen in Figure 3.17. Although these cores were taken from the southbound shoulder where the surface may be sloped for runoff, the bridge plans specified a minimum CIP deck thickness of 6 in. The reduced clear cover was not expected to produce more cracking, but the deck reinforcement would be expected to have a greater risk of corrosion. The reduced deck thickness also meant that the total section height was reduced by about 10% from the intended height, changing the moment of inertia.

During Inspection No. 3, the bridge maintenance crew pointed out an issue with the placement of the precast panels on the bridge piers. The beams were visibly slanted on the bearings at the pier as shown in Figure 3.18. It was unclear how this had occurred or what impact it had on the behavior of the bridge.

3.3.4 Bridge No. 33008 – T.H. 65 over the Groundhouse River, Mora, MN

Bridge No. 33008 was a three-span bridge of a Gen 2 design, completed on November 2, 2007. Several large longitudinal cracks were observed over longitudinal joints, some extending over multiple spans. These cracks were categorized as Class C from Inspection No. 1 and Classes B1 and B2 from Inspection No. 2, the decreased width likely attributed to the summer conditions. Similarly to Bridge No. 33005, bridge maintenance crews sealed many visible cracks on the deck of Bridge No. 33008 prior to Inspection No. 3. Almost all the significant

longitudinal cracks were sealed, aside from a Class C1 crack along a joint over the southern pier. These sealed cracks were indicated on the crack maps with dashed lines. Longitudinal, transverse, and map cracking all increased significantly between the different inspections. Bridge No. 33008 was the only bridge of the five inspected PCSSS bridges that had significant surface cracking along the longitudinal joints.

Four cores were taken from Bridge No. 33008. All four were taken from midspan of the center span, from three adjacent longitudinal joints and an adjacent web-CIP interface. Core 33008-1, a 6 in. diameter core taken from the first longitudinal joint, had a full-depth reflective crack. The crack was widest (B1) at the top of the core and smallest (A1) at the bottom. Given that the surface crack followed the longitudinal joint, it was likely that the reflective crack propagated partially through the section before either continuing to the surface or promoting the development of a shrinkage crack. The two cracks (shrinkage and reflective) could have connected within the CIP concrete. In either case, neither the deck reinforcement nor the cage reinforcement prevented the propagation of cracking. The adjacent longitudinal joint was captured by Core 33008-2, a 4 in. diameter core. This core showed no reflective cracking, supporting the prediction that reflective cracks would occur on alternating longitudinal joints. The observed class A2 shrinkage crack only extended $\frac{1}{2}$ in. into the top of the core. Core 33008-3 was a 6 in. diameter core taken from the joint adjacent to Core 33008-2. There was a reflective crack observed in this core. The crack was not very wide, Class A1 for the entire length. The crack extended upwards from the joint $5\frac{3}{4}$ in. at the most. This depth and width was similar to the bottom of the crack observed on Core 33008-1, without the shrinkage crack extending from the top. Core 33008-4, a 4 in. diameter core, was taken from the web-CIP interface adjacent to Core 33008-3 because a large longitudinal crack was observed over this location. The core broke into a number of pieces during extraction, but a vertical crack was clearly visible, extending over 3 in. from the top of the core. The crack extended to the level of deck reinforcement where it was intercepted by a transverse bar. The crack may have extended beyond this, perhaps to the web corner, but this could not be confirmed because of the broken pieces. The crack was widest at the top, similar to the shrinkage portion of the crack of Core 33008-1. The cores from this bridge contained the most significant cracks, clearly exhibiting reflective cracking. The full-depth crack on Core 33008-1 was particularly concerning.

Inspection No. 2 also included a visual survey of the underside of the end spans of the bridge. During this survey, significant differences in camber among the precast beams of Bridge No. 33008 were observed; from the core extractions, the differential camber was clearly present at the time of construction. Figure 3.19 shows a photograph of the observed differential camber under the north end span. Figure 3.20 and Figure 3.21 show the observed camber profiles from the north and south end spans of Bridge No. 33008, respectively. The camber of each precast beam is shown relative to the minimum observed camber in the span. The underside of the center span was not observed because access was limited by the river. As seen in the profile plots, the camber of adjacent beams differed by as much as $\frac{7}{8}$ in., with a maximum difference between any two beams in one span of $1\frac{3}{4}$ in. Given the moderate span length and the initial camber data presented below, this variation in camber was a concern.

Cores 33008-2 and 33008-3 exhibited differential camber between the adjacent panels, confirming the observations from the field inspections. Because the CIP concrete from the core specimens showed these differences, it was assumed the differential camber of adjacent beams existed at the time of construction, prior to the deck placement. The observed differential

camber was not correlated with reflective cracking because the locations of surface longitudinal cracks did not correlate with the joints with the worst differential camber. A core from Bridge No. 13004 also showed some differential camber (3/8 in.), but camber differences were not readily observable in the field.

In order to determine a potential cause of the differential camber on Bridge No. 33008, the precasting records were examined for information regarding beam camber and ages. The precast beams for Bridge No. 33008 were fabricated by County Materials between July 6 and August 1, 2007. The camber of each beam was measured by the fabricator after prestressing release. The estimated camber at the time of placement was also calculated for each beam, to be compared with the observed cambers. The release camber measurements and estimated camber at placement are given in Table 3.6. The naming convention in Table 3.6 matches that of Figure 3.20 and Figure 3.21.

Overall, the release cambers of the beams in Bridge No. 33008 were similar to one another at around 1/2 in. Beams were fabricated in groups of three, but differential camber was observed among beams from the same group. All of the beams were released within 24 hours of casting, except for three beams from the north end span that cured over a weekend. Recent research has shown that longer curing times, especially over a weekend, could impact camber (O'Neill and French 2012). However, the weekend-cured beams were all for the north end span, so these beams were not associated with the differential camber that was also observed in the south end span. Also, Figure 3.20 shows that the weekend-cured beams, beams B2-5, B2-6, and B2-7, did not have the most significantly varying camber among the beams on the north end span.

The length of time that each beam was stored before being placed could have affected the development of camber. If adjacent beams had large age differences, the resulting camber prior to CIP concrete placement may have been different. The beams from Bridge No. 33008 had an average age at beam placement of 33.3 days, a maximum age of 57 days, and a minimum age of 20 days. While the range of beam ages was large and adjacent beams had different ages, the exact effect of beam age was unknown. To determine the effect, the ages of the beams from Bridge No. 33008 were compared with ages from the other inspected bridges, summarized in Table 3.7. The beam ages from Bridge No. 33008 were not significantly different than those of the other bridges, particularly Bridge No. 33005 from the same design generation. Bridge No. 13004 showed some differential camber from the core examinations, but it was not readily observable in the field and was not as severe as the differential camber on Bridge No. 33008. Because the beam ages of the other bridges were comparable, it was concluded that the differential camber was not a result of varying beam ages throughout Bridge No. 33008.

The cause of the differential camber problem of Bridge No. 33008 was not determinable from the precasting records. It was hypothesized that the problem could have been caused by inconsistent bunking of the individual beams. Differences in bunking can affect the development of camber in similar beams (O'Neill and French 2012).

3.3.5 Bridge No. 49007 – T.H. 238 over the Swan River, Little Falls, MN

Bridge No. 49007 was a three-span bridge of a Gen 3 design, completed on August 11, 2009. Inspection No. 1, conducted on October 14 and 19, 2009, showed light cracking throughout the bridge. Longitudinal cracks were observed on the end spans over the precast

webs, but none appeared along the longitudinal joints. Transverse cracks were observed over the piers and through the center span. All observed cracks were Class A. Inspection No. 2, conducted on June 14, 2010, and Inspection No. 3, conducted on June 29, 2011, showed increased numbers of cracks in both the longitudinal and transverse directions. However, the crack widths did not increase greatly, with only a few cracks growing to class B1. Map cracking also increased between each inspection. While map cracking and longitudinal cracking over the precast webs could be caused by shrinkage, the cracking was observed to continue for two years after construction.

During the third inspection, a survey of the underside of the bridge revealed a crack on one beam near the north pier, shown in Figure 3.22. The crack ran from the end of the beam flange about three feet longitudinally and one foot transversely to the edge of the pier cap. The crack appeared to run across the width of the one foot flange. It was speculated that the crack could have occurred during erection if the beam flange had been handled improperly.

The four cores from Bridge No. 49007 did not contain much information. First, none of the core locations could be confirmed because the joints and web-CIP interfaces were not apparent on the cores. Second, no significant vertical cracks were observed that may have been reflective. Core 49007-1 and Core 49007-2 were chosen because reflective cracking was more likely at midspan, but no surface cracking was observed. One class A2 shrinkage crack was observed on Core 49007-3, which extended 1 in. deep. Core 49007-3 was chosen because of the observed surface crack. Each core was 4 in. in diameter. Overall, these cores were not conclusive, in that reflective cracking could be present in the bridge, just not observed within the extracted cores.

3.3.6 Bridge No. 49036 – T.H. 238 over Pike Creek, Little Falls, MN

Bridge No. 49036 was a three-span bridge of a Gen 3 design, completed on August 11, 2009. Very little transverse cracking was observed during any of the inspections. Over the piers, map cracking was predominant. The map cracking extended across the center span as well. Longitudinal cracks were observed over the precast webs in both end spans and through the center span. None of the observed cracks were particularly wide, with a maximum of Class B1. As with the other inspected bridges, both the longitudinal and map cracking increased between each inspection.

Similarly to Bridge No. 49007, the 4 in. diameter cores from Bridge No. 49036 did not have significant cracks. The locations of these cores could not be confirmed. One shrinkage crack was observed, which was Class A1 with a depth of ½ in. As with Bridge No. 49007, without confirmation of the locations of the cores over the longitudinal joints, reflective cracking was not observed. Had the cores for Bridge Nos. 49007 and 49036 been 6 in. diameter cores, the location may have been confirmed. However, the 4 in. cores from the other bridges were all positively located.

3.4 Summary

Reflective cracking was observed on both Bridge Nos. 13004 and 33008. The cracking observed in Core 13004-2 from Bridge No. 13004 confirmed the presence of reflective cracking suspected from the strain gauge instrumentation. Even though the crack indicated in Joint 3 was not observed on Core 13004-1, it was likely present on the part of the joint that was not captured

in the extracted core. This cracking behavior of alternating longitudinal joints was expected, because stress relief from the cracking might preclude a reflective crack from forming on the adjacent joint. It should be noted that the more recent data measured from the instrumentation across the three longitudinal joints in Bridge No. 13004 indicated that a crack may have initiated in the trough in Joint 2, between Joints 1 and 3. The new crack in the trough region of Joint 2 appeared to initiate away from the longitudinal joint, and exhibited only small increases in strain during the course of the study as described in Chapter 4.

The only bridge with significant surface cracking along the longitudinal joints was Bridge No. 33008. The cracking on the cores from Bridge No. 33008 also exhibited the alternating joint reflective crack prediction. The full-depth crack on Core 33008-1 was concerning. Because the top portion of the through crack appeared to be related to shrinkage, it was possible that combined shrinkage and reflective cracking contributed to the through crack. With the exception of Cores 33008-1 and 33008-4, which saw what appeared to be deep shrinkage cracks, the observed shrinkage cracks were no more than 1 in. deep. It was encouraging that most of the observed shrinkage cracks did not extend to the deck reinforcement, which would have raised potential concerns of corrosion, although the reinforcement was epoxy-coated. The reason for the deeper shrinkage cracks on Bridge No. 33008 was unknown.

Chapter 4: Monitoring of Instrumented Bridge

The instrumentation of MnDOT Bridge No. 13004 in Center City, MN, was monitored for nearly six years, collecting strain and temperature data. Figure 4.1 shows a plan view of Bridge No. 13004, highlighting the instrumented region. One of the primary objectives during this project was to monitor the strain above the longitudinal joints between panel flanges to investigate potential reflective cracking. The flange and web corners were potential locations for initiation of reflective cracking, so transverse strains at these locations were of particular interest. In addition, growing longitudinal strains had been observed at the pier, indicating cracking due to restraint moment. Figure 4.2 shows a cross-sectional view of a typical longitudinal joint from Bridge No. 13004, taken from over the pier. The continuity reinforcement shown in Figure 4.2 was present over the bridge piers but not at midspan.

4.1 Instrumentation Overview

The instrumentation and data collection systems are described in detail in MnDOT Report 2006-37 (Bell et al. 2006) and MnDOT Report 2008-41 (Smith et al. 2008). Strain gauges were located at Joints 1, 2, and 3, in regions from the east abutment to midspan of the center span. Ninety-six vibrating wire (VW) strain gauges were used. Fifteen concrete embedment and seven spot-weldable strain gauges were oriented in the transverse direction at midspan of the center span in each of the three instrumented joints. Thirty spot-weldable strain gauges were oriented in the longitudinal direction throughout the remainder of the instrumented region. Figure 4.3 provides a description of the naming convention for the gauges throughout the bridge.

Strain data was collected for nearly six years, with measurements every two hours. The strains were processed to represent changes in mechanical strains from 10:00 AM on October 1, 2005 when the gauge readings were zeroed. This time was chosen because it was the first day readings were automatically taken at two hour intervals and the lowest thermal gradient through the section was observed at 10:00 AM. The mechanical strains were obtained by subtracting thermal strains from the total measured strain. Thermal strains for the concrete embedment gauges were calculated from the measured temperature data using the experimentally determined coefficient of thermal expansion ($\alpha_c = 5.67 \mu\epsilon/^\circ\text{F}$). The spot weldable gauges were not adjusted for thermal strains because the thermal expansion of the steel reinforcement and steel gauges was assumed to be equal. The strains presented also include creep and shrinkage strains. For all data given, compressive strains are negative and tensile strains are positive.

4.2 Reflective Cracking

The transverse concrete embedment and spot-weldable strain gauges at midspan of the center span indicated reflective cracking. Daily transverse strain fluctuations as large as $350 \mu\epsilon$ and $440 \mu\epsilon$ were seen from concrete embedment gauges in Joint 1 (CJ1-51-3, CJ1-51-4) and Joint 3 (CJ3-51-2, CJ1-51-2), respectively. This data can be seen in Figure 4.4 and Figure 4.5. These fluctuations occurred during the summer months and increased over time, initiating seven months after construction. Gauges on the adjacent trough hooks showed similarly increasing strains, suggesting that the reinforcement was adequately spanning the cracks. None of the concrete embedment gauges at the deck reinforcement level showed significant strain

fluctuations, indicating cracking had not propagated into the deck. The indication of cracking from the strain gauges over Joint 1 was confirmed by a core specimen, Core 13004-2, described in Section 3.3.2. Joint 2 did not see such large strain fluctuations as Joints 1 and 3, with strain increases initiating three years after construction with a maximum strain fluctuation of $200 \mu\epsilon$. These strains, shown in Figure 4.6, were only seen in gauge CJ2-51-1, which was 8 in. away from the longitudinal joint. A crack may have been forming at this location, but the smaller strain fluctuation compared to Joints 1 and 3 and no strain increases in the gauges on adjacent trough hooks suggested that significant reflective cracking had not occurred. Overall, strain data from the spot weldable gauges agreed with the concrete embedment data from their respective joints.

Observations from the field inspections were used to confirm strain gauge data. A core specimen was taken at both Joint 1 and Joint 3 to investigate potential reflective cracking. Reflective cracking was confirmed in the core from Joint 1. A reflective crack was not seen in the core from Joint 3; however, the core only captured the north side of the joint. The strain data in Figure 4.5 indicated that the crack formed on the south side of the joint, so it is possible that a reflective crack existed that was not captured by the core. Crack maps for Bridge No. 13004 did not show longitudinal cracks to correlate with any strains from transverse gauges at the deck reinforcement level.

4.3 Restraint Moment Cracking

Cracking due to restraint moments was indicated by longitudinal spot-weldable strain gauges on the continuity reinforcement over the piers. Spot-weldable strain gauges at the center of the pier cap over Joint 1 showed significant cracking, as shown in Figure 4.7. Gauge SJ1-C1-1, located at mid-depth of the cross section, showed maximum daily strain fluctuations of $750 \mu\epsilon$, with a maximum daily average strain of $1130 \mu\epsilon$. Therefore, the continuity reinforcement at this point saw a change in stress of 21.8 ksi. However, with a conservative estimate of 150 thermal cycles per year corresponding to 150 summer days, the contribution of this stress to fatigue compared to truck loads was minimal. Issues of fatigue were investigated following the parametric study, presented in Section 6.3.1.

There was most likely a significant crack at the bottom of the section over the pier caused by positive restraint moment. This restraint moment crack was a result of restrained thermal gradient effects, when the top of the bridge deck was heated by solar radiation. This, combined with time-dependent restraint moments from creep and shrinkage, caused increased strain at the bottom of the section at the piers. The overall strain at this location increased each summer since cracking appeared to initiate, but seemed to be reaching a plateau. This could be because the development of positive time-dependent restraint moments had slowed.

Crack maps showed transverse cracking at the pier over Joint 1, as shown in Figure 4.8. This cracking correlated with strains detected by gauge SJ1-C2-1, at the level of deck reinforcement, also shown in Figure 4.7. The strain behavior at this depth was different than that shown deeper in the trough; the deck experienced decreasing, more compressive strains during the summer with increasing, more tensile strains in the late winter. Thus there is no indication that the crack from the bottom of the section had propagated up to the deck reinforcement. Even though this is the only location along the pier that had a visible transverse crack, the crack was more likely caused by negative moment or shrinkage. Other inspected PCSSS bridges had exhibited extensive transverse cracking over the piers. Bridge No. 13004 may have exhibited

different behavior because of its very different aspect ratio relative to that of the other bridges, as seen in Table 4.1.

On the east side of the pier at Joint 1, gauge SJ1-31-1 also showed increased positive strains, with maximum daily fluctuations of 200 $\mu\epsilon$. As seen in Figure 4.9, these strains were not as large as those directly over the pier cap. However, there was likely a positive restraint moment crack at this location as well. Figure 4.10 also shows possible positive restraint moment cracking on the west side of the pier cap over Joint 3.

4.4 Thermal Effects

Figure 4.11 contains temperature data from two locations in Joint 1 at midspan of the center span. The data was collected from points 3 in. and 9 in. below the deck surface, at the locations of the concrete embedment gauges. Changes in temperature were generally consistent from year to year. As expected, the temperatures near the surface of the deck (3 in.) were higher than temperatures mid-depth in the cross section during the daytime hours. For example, daily fluctuations can be seen in the close-up plot in Figure 4.11 showing temperatures during the summer of 2008. Temperature changes near the surface were larger than temperature changes deeper in the section, indicating a thermal gradient through the section. Although the shape of the gradient (i.e. linear or nonlinear) cannot be determined from two points, the observed temperature behavior and its relation to observed strains support the consideration of thermal gradients in design.

The majority of the longitudinal spot-weldable strain gauges did not see large strains throughout the six year monitoring period, because they were intended to collect load transfer data during truck tests. However, these gauges show interesting strain behavior caused by thermal effects. During the summer months, gauges at both the bottom of the trough and at the deck reinforcement saw increasing negative strains. These compressive strains were attributed to restrained thermal expansion and restrained thermal gradient flexure. The deck reinforcement gauges saw both thermal expansion and an induced positive restraint moment due to thermal gradient in summer. The mid-depth gauges saw thermal expansion, but did not see much compressive contribution from the thermal gradient restraint moment because they were near the neutral axis.

4.5 Summary

Within one year after construction, reflective cracking at Joints 1 and 3 and restraint moment cracking at the east pier were identified. Over the past six years, the strains associated with these cracks steadily increased. Reflective cracking at midspan of the center span was confirmed by core specimens from the field inspections. The trend of the restraint moment strains over the pier at Joint 1 indicated that the growth of the crack could be reaching a plateau. While this was most likely because the time-dependent restraint moments may have neared full development, it was unclear how much further this crack would grow. The maximum strain range of 21.8 ksi experienced by the continuity steel was not concerning in terms of fatigue because of the low cycle count, conservatively estimated at 150 cycles per year.

Chapter 5: Review of Design Details and Methods

As a prelude to the MnDOT fourth generation PCSSS design, a comprehensive review of Generations 1-3 was completed. The review of these topics was intended to validate the current PCSSS design and to provide recommendations for further design changes. The design review was to incorporate literature review, field observations, and simple design calculations to provide opinions and recommendations, without extensive calculations such as a parametric study or finite element modeling. The methodology of the PCSSS design review varied depending on the particular topic, but generally involved evaluation of the current design practice and recommendation for how to proceed. A large part of the design review was documenting the changes leading up to the current design practices and the rationale for those changes. Commentary was provided about the effect of these design changes on behavior, constructability, and economy.

5.1 Shrinkage Restraint

The results of the PCSSS field inspections indicated that shrinkage was a primary cause for the observed deck cracking. As a result, design details related to shrinkage restraint and crack control were reviewed.

5.1.1 Transverse Deck Reinforcement

Transverse deck reinforcement in the PCSSS was designed for shrinkage crack control. Detailing for transverse deck reinforcement changed with the Gen 3 design. PCSSS bridges from Gen 1 and Gen 2 had No. 5 transverse bars spaced at 1 ft. over the entire bridge deck. Starting with Gen 3, No. 4 transverse bars were used, spaced at 6 in. In all cases, clear cover over the deck reinforcement was specified at 3 in., with the longitudinal reinforcement on top and the transverse reinforcement underneath.

Research by Frosch et al. (2006) on restrained shrinkage crack control concluded that a minimum reinforcement ratio and maximum bar spacing should be used in bridge decks to control shrinkage cracks. The minimum reinforcement ratio was given by:

$$\rho_g \geq 6 \frac{\sqrt{f'_c}}{f_y} \quad (6.1)$$

where ρ_g is the gross reinforcement ratio in the deck, f'_c is the specified 28-day deck concrete strength (psi), and f_y is the reinforcement yield strength (psi). This ratio was recommended to ensure reinforcement did not yield when cracks developed. The maximum reinforcement spacing was given by:

$$s \leq 9\alpha_r \left[2.5 - \frac{d_c}{2\alpha_r} \right] \leq 9\alpha_r \quad (6.2)$$

where s is the center-to-center spacing, α_r is a stress factor ($60,000/f_y$), and d_c is the clear cover (in.). For 60 ksi steel, the spacing should be no larger than 9 in. and smaller when the clear cover is more than 3 in. Table 5.1 shows the reinforcement ratios and spacings for the original (Gen 1 and 2) and revised (Gen 3) designs, as well as the values from the Frosch recommendation. The

recommended reinforcement ratio was calculated assuming a 4000 psi CIP concrete strength. The design gross reinforcement ratios were calculated using only the top 6 in. of CIP concrete for the deck thickness (i.e., the thickness over the precast webs). The Frosch recommended reinforcement ratio and spacing associated with these parameters were 9 in. and 0.0063, respectively. Transverse reinforcement from Gen 1 and Gen 2 designs did not meet either of the Frosch recommendations. The 6 in. spacing of the Gen 3 transverse reinforcement design does meet the Frosch recommendation for spacing. However, the reinforcement ratio is still lower than recommended, even with increased bar area.

Clear cover over the deck reinforcement is an important factor in crack control performance. In general, there is a trade off in specifying clear cover for crack control reinforcement: a smaller clear cover can better prevent shrinkage crack growth by locating the reinforcement closer to the surface to control the cracks but leaves the reinforcement more susceptible to corrosion. Incorporated into the Frosch recommendation is a suggested clear cover for deck reinforcement, apparent in Equation 6.2. For 60 ksi steel reinforcement, there is no benefit for a clear cover less than 3 in. A larger clear cover requires tighter spacing to provide good crack control. The current 3 in. of clear cover for the PCSSS is in agreement with the Frosch recommendation.

Longitudinal deck reinforcement also acts to control shrinkage cracking, but its primary function is to resist negative moments and transfer load across the piers. Over the piers there are No. 7 bars spaced at 4 in., while away from the piers two of every three bars is cutoff, leaving No. 7 bars spaced at 12 in. The longitudinal reinforcement does not meet the Frosch recommendation of 9 in. for maximum spacing away from the piers. However, minimal transverse cracking was observed in these regions on the five inspected bridges, indicating that transverse crack control was not a concern in these regions. The longitudinal reinforcement ratio, calculated similarly to the transverse reinforcement ratio, is 0.0250 over the piers and 0.0083 away from the piers. Clearly the longitudinal reinforcement meets the Frosch requirement for steel area to prevent yielding due to shrinkage.

It was difficult to determine the effect of changing the transverse reinforcement on surface cracking by looking at the crack maps. Several other sources of cracking were identified in the field inspections. Bridge No. 13004 from Gen 1 had many short, longitudinal cracks that were likely due to insufficient CIP concrete consolidation under low clearance composite action stirrups. In addition, this bridge had an aspect ratio (i.e., L/W) of 0.95 compared to the other four inspected bridges, which had aspect ratios ranging between 1.4 and 2.6. Bridges with a larger aspect ratio had more longitudinal restraint than transverse restraint, which would cause more transverse restrained shrinkage cracking. Bridge No. 33008, which had an aspect ratio most similar to Bridge No. 13004, exhibited many long reflective cracks, which is outside the scope of the Frosch recommendation, and may have affected the development of shrinkage cracks. Bridge No. 33005 was the only skewed bridge and had smaller surface cover than was specified in design, which may have resulted in fewer longitudinal cracks with smaller crack widths. Because the Gen 1 and 2 bridges had more dominant effects than restrained shrinkage causing surface cracking, the performance of the current transverse reinforcement design was only evaluated using the Gen 3 crack maps.

Based on the Frosch recommendation for crack control reinforcement and the development of cracks on the two inspected Gen 3 bridges, the current transverse reinforcement design is recommended to be changed for future PCSSS design. Bridge Nos. 49007 and 49036

from Gen 3 had similar surface cracking, with significant map cracks developing over the two years after construction. In the core samples taken, shrinkage cracks in the inspected PCSSS bridges extended less than 1 in. into the deck. Because significant shrinkage cracking was observed on the most recent PCSSS bridges, the transverse reinforcement design should be modified to ensure the best crack control performance. It is recommended that the transverse reinforcement be detailed in agreement with the recommendations of Frosch (Equations 6.1 and 6.2). One way of satisfying the Frosch recommendations would be to provide No. 5 bars at 6 in. spacing (as compared to the Gen 3 No. 4 bars at 6 in. spacing), providing a ρ_g of 0.0086. Alternatively, the reinforcement could be changed to No. 5 at 8 in. spacing, providing a ρ_g of 0.0065. This would require less steel than the No. 5 at 6 in. spacing while still staying within the Frosch recommendations.

5.1.2 Dowel Placement and Wrapping

The PCSSS superstructure and substructure are made integral with dowels embedded in the piers and abutments extending into the CIP deck. However, the restraint provided by the dowels can cause localized shrinkage cracking. This restraint must be balanced between preventing excessive displacement both transversely and longitudinally and reducing shrinkage cracks. Dowels also have the potential to create moment restraint at the pier, particularly if placed eccentrically from the centerline of the pier cap. The potential moment generated in the piers from the dowels is in addition to the moment created by the eccentric end reactions from each span. To address these issues, changes in the placement, number, size, and wrapping of the dowels have been made since the development of the PCSSS.

Table 5.2 lists the dowel details for the five inspected PCSSS bridges and Figure 5.1 shows example diagrams of the dowel layouts. Bridge No. 13004 (Gen 1) had dowels placed at the center of the pier cap in the 4 in. gap (typical) between the precast beam ends. These dowels extended over the central 36 ft. of the bridge (50% of the width). The dowels were not extended the full width of the bridge because they would have created large transverse shrinkage restraint. At the abutments, dowels were placed in the breakout regions along the full width of the bridge, because the approach slab was flush with the ends of the beams. The CIP concrete bonded directly to the dowels for full restraint. It was noted during construction that placement of the pier cap dowels proved difficult given the 4 in. spacing between precast beam ends. Therefore, dowels were moved to the breakout regions for the next design generation.

For Gen 2, Bridge Nos. 33005 and 33008 were detailed with dowels in each breakout at both the piers and abutments (Figure 5.1 (b) and (c)). At the piers for both bridges, dowels were placed in two rows on either side of the pier centerline, and dowels were placed in each breakout over the bridge width. Dowels for Bridge No. 33005 were placed in alignment with the skew of the substructure. The skew resulted in larger breakout regions with four dowels per breakout at the piers and abutments, shown in Figure 5.2. Bridge No. 33008 had six dowels in each breakout at the piers, a large concentration of dowels compared to the other four bridges. Surface cracking around some breakout regions of this bridge was observed during the field inspections. The cracking roughly outlined the blockouts, indicating a high level of restraint in the region. Figure 5.3 shows the observed cracking around the breakout regions of Bridge No. 33008. Cracking around breakout regions was not observed on the other inspected bridges. Because of the high level of restraint indicated, using more than four dowels per breakout is not recommended.

In the Gen 3 design, a number of dowels were wrapped with polystyrene sleeves to reduce restraint on the superstructure. Specifically, two-thirds of the blockouts in each outboard portion of the deck had wrapped dowels so that two-thirds of the total dowels were wrapped, leaving the center one-third of the total bridge width with unwrapped dowels. The polystyrene sleeves were intended to reduce the transverse restraint provided by the outside dowels by allowing some amount of movement. The dowels were expected to engage once the majority of the shrinkage had occurred in the superstructure. Similarly to the original dowel design from Bridge No. 13004, the polystyrene sleeves prevent excess transverse restraint. At the same time, the center dowels kept the superstructure integral with the substructure. Some evidence from the crack mapping inspection suggests that the polystyrene sleeves had some positive effect on alleviating shrinkage restraint. Due to a contractor error associated with Bridge No. 49007, only the dowels on the south pier were wrapped with polystyrene. Crack maps from all three inspections show that map cracks over the south pier were less extensive and had smaller crack widths. This suggests that the dowel wrapping allowed more movement (i.e., less transverse restraint) of the superstructure, preventing some amount of restrained shrinkage cracking. Bridge No. 49036 had the correct dowel wrapping in construction and showed less map cracking compared to Bridge No. 49007. Even though the two bridges were different lengths, the widths were comparable for lateral restraint.

Restricting dowels to the blockout regions facilitated construction with larger clearance and also allowed better consolidation of the CIP concrete in the narrow 4 in. gap between the ends of the precast webs. Evidence suggested that the polystyrene sleeves were effective in reducing transverse restraint while adding only minimal complexity to the construction. It is recommended for future PCSSS designs that dowels continue to be placed in the blockout regions with polystyrene wrapping. However, no more than four dowels should be placed in each blockout to avoid excessive restraint. A recent PCSSS bridge was detailed with three dowels on the pier centerline in each blockout, reducing the moment restraint created at the pier. Ideally, a single-line of dowels with polystyrene wrapping in each blockout along the centerline of the pier cap should be used (Figure 5.1 (d)).

5.1.3 Bearing Pads

The bearing pads at both the abutments and the piers of the PCSSS reduce some amount of longitudinal and transverse restraint to the superstructure. By providing separation between the superstructure and the pier caps, the bearing pads allow the superstructure to “float”, which reduces likelihood of developing stress from shrinkage restraint. Conversely, if the superstructure is in contact with the pier cap, the increased frictional restraint between the two concrete surfaces could cause stress due to restrained shrinkage and result in more cracking.

All PCSSS bridges from Gen 1 through Gen 3 had the same bearing pad design. At both the abutments and pier caps, a ½ in. elastomeric bearing pad was placed underneath the precast beam ends along the centerline of bearing. Polystyrene was also placed in the regions directly under the precast beams, excluding the area of the bearing pad. There was no polystyrene placed between the blockout regions or the ends of the beams. As a result, the CIP concrete came in contact with the tops of the abutment and pier caps. In conjunction with the embedded dowels, the contact of the CIP concrete provided restraint.

For the new PCSSS bridges to be built in 2011 (Gen 4), MnDOT proposed a new bearing design aimed at reducing lateral restraint of the superstructure. In the new design, the placement

of the elastomeric bearing pad was unchanged. However, polystyrene covered the entire surface of the abutments and pier caps, excluding the area of the bearing pad. The primary function of the extended polystyrene was to prevent contact between the CIP concrete and abutment or pier cap. Increasing the coverage of the polystyrene may improve the constructability because cut-out polystyrene would not need to be aligned with the blackout regions; only the elastomeric bearing pad would need to be aligned. It is recommended that this detail be used in future generations.

5.2 Reflective Cracking

Reflective cracking was a concern with the PCSSS from the beginning. The discontinuity at the longitudinal joint between the precast beam flanges effectively acts as a pre-existing crack. As a result, the region directly above the longitudinal joint experiences high stress concentrations as might be seen at a crack tip. Reflective cracks were observed to initiate in some cases from this stress concentration region. The PCSSS controls reflective cracking with the drop-in cage and trough hooks from the precast webs. In addition, several other design details have been considered over the PCSSS design history to control reflective cracking.

5.2.1 Flange Top Corner Chamfer

Since Gen 1, all PCSSS precast beams have had chamfered corners. Chamfered corners are particularly important at the web corners and the top flange corners because they reduce the likelihood of crack initiation at those regions of discontinuity. By reducing the severity of the discontinuity at the corner, and by increasing the surface area over which stresses develop in the CIP concrete at these points, the chamfer reduces the stress concentration.

Because the flange top corners are located at the high-stress region above the longitudinal joint, the detailing of the chamfer at this location is particularly important. Results from the U of M laboratory bridge and the core examinations from the in-field PCSSS bridges both showed that reflective cracking initiated at the flange corners. In particular, cracks initiated from the top of the corner chamfer, as opposed to directly over the longitudinal joint, which was filled with a bead of caulk. Originally, precast beams from Gen 1 had $\frac{3}{4}$ in. chamfers for all corners, including the flange top corner. As a result of the U of M laboratory study, the top edge chamfer was increased to 1 in. in the Gen 3 designs. The goal of increasing the chamfer was to further the effect of the chamfer in reducing stress concentrations at the longitudinal joint. The benefit from increasing the chamfer size does not come at a cost to constructability or economy. In addition, the increased chamfer of the flange top corner provides a larger area for a mastic bond breaker, described in the next section.

5.2.2 Longitudinal Joint Detailing

Because stress concentrations were expected in the CIP concrete directly above the longitudinal joint, a method for reducing this concentration was needed. The use of a mastic bond breaker above the longitudinal joint was thought to be an effective solution. A mastic bond breaker could be constructed by placing a strip of mastic along the longitudinal joint, covering the ends of the flanges and dipping into the chamfered region, as shown in Figure 5.4. The effect of the mastic bond breaker is to “blunt” the crack tip formed by the longitudinal joint. The mastic provides a degree of flexibility between the rigid CIP concrete and the joint opening. As

a result, it is expected that the bond breaker would dissipate the stress concentration at the longitudinal joint to some extent, reducing the likelihood of developing reflective cracks.

Methods for further controlling reflective cracks have also been considered, such as the wire mesh introduced in Gen 3. The wire mesh was placed directly over the longitudinal joint to intercept reflective cracks. As opposed to the mastic bond breaker, which reduces the likelihood of reflective cracking, the wire mesh was intended to control cracking. During the construction of Gen 3 bridges, the wire mesh proved complicated to install and was never implemented. On Bridge No. 49036, a series of small No. 3 bars was used in lieu of the mesh. These bars were placed at 9 in. transversely and 6 in. longitudinally over the longitudinal joints. The perpendicular bars were tied to the trough hooks, which was labor intensive. No performance difference was observed in the field inspections between Bridge No. 49036 and the other bridges with respect to the No. 3 bars over the joints.

In the recent construction of Bridge No. 08006 near Sleepy Eye, MN, the mastic bond breaker did not prove overly difficult to place. The mastic was placed under the trough hooks before the drop-in reinforcement cage was placed. Incidentally, the mastic was watertight, so the trough held water when prewetting was applied. To prevent weakening of the CIP concrete in the trough, the water was removed by puncturing the mastic at several points along each span for drainage. As long as measures are taken to remove water from the trough region after prewetting, the mastic bond breaker should provide an effective method for crack prevention, as opposed to crack control.

5.2.3 Flange Roughening

Some surfaces of the PCSSS precast beams were intentionally roughened to promote composite action with the CIP concrete. Originally, the top and sides of the web and the tops of the flanges were all roughened to achieve composite action. Roughening the tops of the flanges proved to be difficult in fabrication because the forms were difficult to remove from underneath the trough hooks with the surface roughened. It was also believed that a smoothed surface would better distribute stresses along the longitudinal joint, reducing the likelihood of large single reflective cracks. However, Smith et al. (2008) could not easily determine the benefit of the smooth flanges relative to reflective crack control. The flanges on the test specimen were reduced to 3 in., which probably had a larger effect on performance than the smooth flanges. In any case, smooth flanges facilitated removing forms during fabrication, so the Gen 3 flange surfaces were smoothed. In the other extreme, it was suggested that delamination between the CIP concrete and the top of the flange could occur if not enough roughness was provided. Delamination at the interface could drive a crack from the longitudinal joint to the web face, effectively missing the cage reinforcement which is placed to control potential reflective cracks above the longitudinal joint between the flanges. Therefore, it was thought that the flanges should have some degree of roughness to bond with the CIP concrete.

Results from previous PCSSS research have not shown delamination to be a problem with smooth flanges. French et al. (2011) tested a large-scale specimen and a number of subassembly specimens to specifically investigate the performance of the PCSSS at reflective crack control. All specimens were built with smooth flange surfaces. During fabrication of the smooth flanges, air bubbles trapped under the forms created shallow voids along the top flange surface, shown in Figure 2.7. These voids were also present on the smooth flanges of the Gen 3 bridges. It was suspected that the voids could provide some degree of roughening on the top of

the flange. For one of the subassemblage tests in the French et al. (2011) study, the voids were patched to determine their effect on reflective crack initiation. No significant difference in performance was observed between the patched and non-patched specimens. A clamping system was used for the subassemblages to prevent delamination between the flanges and CIP concrete and to better simulate the restrained boundary conditions along the width of the bridge. As such, the subassemblages could not be used to qualify the CIP-flange bond for smooth flanges.

From the results (French et al. 2011), it was concluded that the smooth flanges were sufficient for future PCSSS design. It is recommended that the shallow voids on the smooth flange surfaces not be patched. Patching is labor intensive with no apparent benefit in performance. In addition, the voids generally occur near the tips of the flanges where the mastic would cover the longitudinal joint. The precast beams should also be prewetted prior to CIP concrete placement. Aside from preventing excess shrinkage, the prewetting removes laitance from the smooth flange surface, improving the CIP-flange bond that is needed to prevent delamination. Laitance should also be removed before applying mastic, but this can be done by brushing, because wetting could be detrimental to the mastic bond. It is possible that water from prewetting could pond in the shallow voids, preventing CIP concrete consolidation within the voids. Prewetting of smooth flanges should be observed in the near-future to determine if ponding occurs often, especially with the use of mastic over the longitudinal joint. If ponding is an issue, the water should be blown out with equipment already used to clear debris off of the precast beams on-site.

5.3 Composite Action Stirrups

Full composite action between the CIP concrete deck and the precast beams is essential to forming the composite slab span system. To achieve composite action, the PCSSS beams were detailed with stirrups protruding from the top of the web. These stirrups, termed composite action stirrups, transferred shear from the beams to the CIP concrete. Originally, composite action stirrups were closely spaced at 1 ft. to ensure full composite action. However, the clearance of these stirrups over the top of the precast web was too small for sufficient CIP consolidation between the stirrups and the precast web surface. Field observations of Bridge No. 13004 showed cracking likely due to insufficient fill of the CIP concrete around the composite action stirrups. As a result, the clearance of the stirrups was increased to 2 in. over the web.

French et al. (2011) concluded that the bond between the roughened precast web and CIP concrete alone provided enough shear capacity to achieve full composite action. The Concept 2 bridge was based on the results of Naito and Deschenes (2006) that suggested the AASHTO requirements for horizontal shear reinforcement were overly conservative. With the precast web intentionally roughened, the Concept 2 bridge was observed to develop at least 135 psi of horizontal shear stress without the use of composite action stirrups. Therefore, it is recommended that the PCSSS not include composite action stirrups if the required shear transfer is less than 135 psi. Removing these stirrups simplifies fabrication.

5.4 Tolerances for PCSSS Beams

During the construction of Bridge No. 49007, inaccuracies in the precast beam lengths led to construction difficulties. The beams did not fit properly between the abutments and piers because a number of the beams were longer than expected. Methods of accounting for such tolerance errors were needed. With the advancement of the PCSSS, it is necessary to define

standard tolerances, specifically for the precast beams. As discussed above, inaccurate beam lengths pose other constructability problems. Tolerance issues have also been encountered with the alignment of trough hooks between precast beams. In NCHRP 10-71, one of the subassemblages was fabricated with misaligned trough hooks. A reasonable approach to defining tolerances for the PCSSS is to follow recommended tolerances for other precast elements, either from local fabricators or other accepted sources, such as the PCI Tolerance Manual MNL-135 (2000).

To account for possible beam length inaccuracies, as well as to increase the durability of the system, a 6 in. gap was added at each abutment between the ends of the precast beams and the approach slab for Gen 4 designs. The 6 in. gap is filled with CIP concrete from the deck pour. This detail better accommodates fabrication errors in beam lengths and protects the beam ends by separating them from the approach slab. Incorporating the bearing pad detail discussed in Section 3.3, the CIP concrete in the abutment gap is separated from the abutment by polystyrene. The result is a region of CIP concrete between the approach slab and the end of the precast beams, relatively unrestrained by the substructure. Evaluation of the performance of the 6 in. gap is ongoing. One concern is that while it is reinforced transversely and tied into the deck at the top of slab, there is no steel reinforcement tie to the relatively large surface of the beam end face. MnDOT has not quantified any recognizable tensile stress at this interface to initiate debonding. Therefore, no reinforcement into the back of beam web has been proposed at this time.

Chapter 6: Continuous System Economy

When originally conceived, MnDOT designed the PCSSS as a continuous system for live load, assuming that it would be the most economical method. For the continuous system design, time-dependent and thermal gradient restraint moment effects should be considered (AASHTO 2010). Accounting for restraint moment effects has been design-intensive and is highly variable depending on the method of analysis and assumed material properties. It was unclear how much benefit a continuous system design could provide versus simple-span design. As a result, a parametric study was conducted to evaluate the design economy of the PCSSS as a continuous system and to provide a recommendation for the design of future PCSSS bridges. The goal of the parametric study was to determine the most economical method of design for a feasible set of PCSSS bridge configurations. These configurations ranged between 20 and 60 ft. with both two and three spans. The results of the parametric study were used to recommend one of several design options: designing as a continuous system, as a simply-supported system, or as simply-supported system with an added continuity connection.

6.1 PCSSS Design Considerations

The parametric study was conducted to compare the design economy of a series of continuous and simple-span PCSSS designs. The PCSSS bridges for the parametric study were designed according to the AASHTO LRFD 2010. For the purposes of the study, “optimized” sections were not fully optimized in the analytical sense, but were subject to reasonable constraints such as whole strand number and whole inch beam depths. Only flexural design was performed because the precast beam design was primarily affected by flexural demands; shear capacity was not considered. Continuity connections at the piers for continuous system designs were also designed according to AASHTO 2010. All PCSSS designs were controlled by service limit states. In particular, the tensile stress limits in AASHTO Table 5.9.4.2.2-1 controlled the designs under the Service III load combination for tension cracking of prestressed members.

6.1.1 Restraint Moments

Restraint moments are caused by restrained deformations of bridges made continuous from simple-span precast beams. The continuity connections at the piers restrain the end rotations, causing moment to develop along the spans. Figure 6.1 shows the effect of both positive and negative restraint moment on a three-span system. Both the time-dependent effects of creep and shrinkage and the effect of thermal gradient can cause deformations that create restraint moments. AASHTO Section 5.14.1.4 contains provisions for simple-span beams made continuous, including consideration of restraint moment and continuity connection design. Positive restraint moments are critical in the design of PCSSS because they add to the stress of the Service III load combination.

Time-dependent restraint moments are caused by prestressing creep, dead-load creep, and differential shrinkage between the CIP deck and precast beams. Prestressing creep causes upward camber, creating positive restraint moment (Figure 6.1-a). Dead-load creep causes downward camber, creating negative restraint moment (Figure 6.1-b). Differential shrinkage is the effect of the CIP concrete shrinking more than the precast after continuity is made. This also causes downward camber and negative moment. The sum of these three effects results in the total time-dependent restraint moment.

The total restraint moment can be either positive or negative depending on the age of the precast beams at the time of continuity. Figure 6.2 shows the effect of the precast beam age on the development of time-dependent restraint moments (Smith et al. 2009). Older precast beams have had time to creep and shrink before continuity, so the effect of differential shrinkage dominates and negative restraint moment develops. Younger precast beams creep and shrink significantly after continuity, reducing the amount of differential shrinkage, so the effect of prestressing creep dominates and positive restraint moment develops. AASHTO 5.14.1.4.3 accounts for the effect of beam age by allowing restraint moment to be neglected in design if beams are aged at least 90 days. However, PCSSS fabricators do not typically store beams this long. Typically, PCSSS beams have been 14 days old at continuity, so positive restraint moments have been significant. For the parametric study, both 7-day and 14-day precast beams were considered, described in Section 6.2.2

The analytical model for calculating time-dependent restraint moments is left to the designer, depending on the particular application. Previous research by Smith et al. (2009) determined that time-dependent restraint moments for PCSSS were best modeled by the Peterman method (P-method) (Peterman and Ramirez 1998). The P-method predicts time-dependent restraint moments using the following equation:

$$M_{RM} = [M_p + (M_d)_{precast}][\Delta(1 - e^{-\phi_1})] - (M_d)_{CIP}(1 - e^{-\phi_2}) - M_s \frac{(1 - e^{-\phi_2})}{\phi_2} \quad (6.1)$$

where M_p is the prestressing moment, $(M_d)_{precast}$ is the precast dead load moment, $(M_d)_{CIP}$ is the CIP deck dead load moment, M_s is the differential shrinkage moment, ϕ_1 is the creep coefficient for loads at transfer, and ϕ_2 is the creep coefficient for loads at CIP concrete placement. The P-method accounts for the dead load creep of the precast and CIP concrete separately using their respective creep factors. The P-method also accounts for the restraining effect of the CIP deck reinforcement and precast beam on deck shrinkage. The nominal differential shrinkage moment is reduced by a factor η , with more reduction for a larger transformed area of steel. The sample calculations in Appendix D show a complete use of the P-method in PCSSS design. For the parametric study, the P-method was used to calculate time-dependent restraint moments, although the creep and shrinkage model needed to be determined, described in Section 6.2.1.

The moments used in Equation 6.1 are distributed moments calculated using the stiffness method with matrix analysis. To calculate the distributed moments, the P-method assumes the pier diaphragms act as short spans with a designated stiffness. This permits the consideration of cracked sections over the pier using a reduced diaphragm stiffness if the cracking moment is exceeded. Figure 6.3 shows a typical positive restraint moment distribution using the P-method for a three-span bridge with 14-day old beams, with the separate time-dependent components. The effect of the virtual pier spans is seen by the differences in restraint moment at the pier locations. As expected, the prestressing creep contributes to positive restraint moment, while dead load creep and differential shrinkage contribute to negative restraint moment.

6.1.2 Thermal Gradient

Thermal gradient effects contributed significantly to the parametric study designs. AASHTO Section 3.12.3 provides a simple definition for the thermal gradient profile, depending on the region of the United States. Zone 2, containing Minnesota, was used for the parametric

study. The thermal gradient profile is used in AASHTO Section 4.6.6 to calculate the response of the bridge. Three thermal gradient components are specified in this section: axial expansion, flexural deformation, and internal stress. Appendix D contains sample calculations showing the analysis of thermal gradient effects.

Axial expansion due to uniform temperature change causes compressive stress if the bridge is axially restrained. Axial expansion was considered in the parametric study designs. The PCSSS did not typically include detailing for full axial restraint, but it was a design possibility. Because the controlling limit state is tension from the Service III loading condition, compression from axial expansion could improve design performance. In order to achieve the best performance from the continuous designs, full axial restraint that caused axial compression was assumed for the parametric study. This assumption was chosen because it would indicate that either axial compression was necessary for better design economy, or that continuous design was less economical even with axial restraint.

Flexural deformation due to thermal gradient effects causes restraint moment similarly to time-dependent restraint moment. This thermal gradient restraint moment is positive if the thermal gradient is positive, caused by the spans deflecting upwards. Thermal gradient restraint moment from flexural deformation was given similar treatment as the time-dependent restraint moment. The stiffness method incorporating the diaphragm stiffness from the P-method was used to distribute the thermal gradient restraint moment. Thermal gradient restraint moment was significant compared to time-dependent restraint moments in the parametric study. Figure 6.4 shows typical restraint moments due to thermal gradient and time-dependent effects. In most load combinations, the thermal gradient is multiplied by a factor of 0.5 to reflect frequency of occurrence, but the magnitudes are still comparable.

The internal stress component is required to maintain compatibility for the case of nonlinear thermal gradients. Axial expansion and flexural deformation thermal strains are subtracted from the thermal strains caused by the non-linear thermal gradient. The non-linear thermal gradient induces non-linear thermal strains. These thermal strains are partially accounted for by uniform axial expansion and flexural deformation. The remaining strain must be a structural response caused by internal stress to keep strains linearly distributed through the cross section. In the case of positive thermal gradient, the internal stress component is compressive at the bottom of the section. Therefore, in the controlling limit state, internal stresses counteract the effect of flexural deformation.

When the total stress due to thermal gradient effects is calculated, compressive axial expansion stress and internal stresses oppose tensile stresses from restraint moments due to flexural deformation. If the system were not axially restrained, the stress due to thermal gradient would be more tensile, resulting in higher limit state stresses. By assuming axial expansion, the parametric study found the most economical designs subjected to thermal gradient. In the parametric study, the magnitude of compressive axial expansion and internal stresses were typically 70% of the magnitude of restraint moment stress.

6.1.3 Partial Continuity

The continuity connections of the PCSSS designs had to be effective in order to transfer load through the continuous system. The effectiveness of the continuity connections affected how much the live load moment envelope could be reduced by continuity action. For the

parametric study, the design and effectiveness of positive moment connections were particularly important for the Service III load combination. As described previously, the PCSSS incorporates longitudinal reinforcement across the piers at the bottom of the trough region to resist positive restraint moment. To be considered effective, the state of stress in the diaphragm had to be such that moment could be transferred over the piers, as required by AASHTO Section 5.14.1.4. Post-continuity loads, including time-dependent restraint moments, thermal gradient effects and live load, contributed to a loss of continuity effectiveness.

AASHTO Section 5.14.1.4.5 states that a diaphragm connection is only considered fully effective if the stress combination of post-continuity dead load, restraint moment, 50% live load, and 50% thermal gradient results in net compression on the bottom of the section at the pier. If there is net tension under this load combination, cracks at the pier are assumed to be open, and the full section is not engaged in continuity action. Partial continuity must be used to calculate live load moments in this case. This continuity check is a conservative requirement, because the positive moment reinforcement is still engaged when the diaphragm is cracked. However, the parametric study emulated true design, so methods were developed to accommodate this code provision.

In order to evaluate the continuity check from AASHTO Section 5.14.1.4.5, the appropriate live load stress needed to be used. With tensile restraint moment and thermal gradient stress, the live load stress needed be compressive to pass the continuity check. However, the maximum negative moment at the pier was not to be used to calculate this live load stress because it was not the critical case. The continuity check needed to pass for all possible live load configurations where continuity was needed. Of all the possible live load configurations, continuity action was most beneficial for reducing the positive live load moment for the truck near midspan of the center span. The truck position that created this maximum midspan moment put a negative moment at the bridge piers. This negative moment caused compressive stress at the bottom of the section at the pier, improving the continuity check. Because all other truck positions required less benefit from continuity, the compressive stress at the pier caused by the maximum midspan moment truck was used in the continuity check. This was only true because the center span length was always greater than or equal to the end spans. In the analysis, the maximum positive moment was found on the live load envelope, and the corresponding live load configuration was used to determine f_{LL} for the continuity check.

If 50% of the compressive stress caused by the truck position for maximum midspan moment was enough to satisfy the continuity check, then the connection was assumed to be fully continuous and the continuous live load envelope was used. In other words, if the critical live load added to the bridge was enough to overcome the restraint moment and thermal gradient already present at the piers, then the bridge was continuous. If the check was not satisfied, the connection was assumed to be partially continuous and the live load envelope was modified.

A linear approximation was used to evaluate partial continuity for ease of design. AASHTO suggests in the commentary that a percentage of the permanent and live loads be applied to a simple span. It was assumed that some of the live load is required to first close a potential positive moment crack at the pier to enable the generation of a compressive resultant force necessary for the development of the negative moment. This portion should cause zero tension at the bottom of the diaphragm, or enough to pass the continuity check. Then the remaining live load should be applied to the continuous span. In reality, calculating the effect of partial continuity is a non-linear problem that is not efficient for real world design.

The linear approximation described above was a rational and conservative simplification. The total compressive stress at the bottom of the diaphragm due to the maximum midspan moment associated with the truck was calculated, as opposed to 50% of that moment assumed for the continuity check. If this total stress was still not enough to pass the continuity check, then the system would not become continuous in the critical case, and the simply-supported live load envelope was used. If the total stress was enough to pass the continuity check, then the percentage of moment required to bring the tension at the bottom of the diaphragm to zero was calculated. This percentage of the simple-span envelope was then superimposed onto the remainder of the continuous envelope to get the final live load envelope. In the final designs, a system was termed “N% effective” if N% of the continuous live load envelope was used in the superposition. For example, if 65% of the total stress was required to pass the continuity check, then 65% of the simple-span moment envelope was superimposed on 35% of the continuous envelope. The resulting partially continuous live load envelope would be used in design, and the system would be 35% continuous. A sample calculation of this procedure is given in Appendix D of this report.

The result of this partial continuity analysis was a step function that penalized designs without fully effective connections. Connections were fully continuous if the continuity check passed with less than 50% of the live load. If more than 50% of the live load was required to pass the check, then more than 50% of the live load was applied to the simple span. Partially continuous systems were much less effective than fully continuous systems as a result. It is important to note that the degree of continuity did not affect the development of restraint moments. According to Section 5.14.1.4.9, a positive moment connection can resist the larger of the factored positive restraint moment or 60% of the section’s cracking moment, regardless of the effectiveness of the connection.

6.2 Parametric Study

In order to evaluate the economic benefit of continuity, a parametric study was conducted to compare simple-span and continuous system designs for eight sample bridges with varied span length configurations. These configurations covered the range of feasible PCSSS bridge lengths in order to provide a general recommendation. Table 6.1 shows the span length configurations for the eight sample bridges. Sixteen designs in all (simple and continuous for each of the eight sample bridges) were used to compare design economy. Before the full set of bridges was compared, a subset of three bridges was used to choose a creep and shrinkage model and a reasonable precast beam age. This subset is highlighted in Table 6.1. The preliminary studies for creep and shrinkage and precast age are presented in Section 6.2.1 and Section 6.2.2, respectively. The main parametric study for continuous design economy is presented in Section 6.2.3.

A specific design methodology was developed for the flexural capacity of the precast sections in order to compare different configurations. Three primary design parameters were identified for the flexural design of the precast sections: beam depth, concrete strength, and number of strands. These parameters were used to evaluate the economy of a particular precast section, as well as to optimize the sections within design constraints. Each design started with precast concrete strengths of $f'_c = 6.0$ ksi and $f'_{ci} = 4.0$ ksi and typical precast beam depths based on previous designs with similar span lengths. Beam depth and concrete strengths were held consistent for all spans in a particular bridge, while the strand pattern could change between the

middle and end spans. The middle span was designed first for the three-span configurations, because the depth of the longer center span controlled the depth of the precast sections overall.

The remaining design parameters were based on existing PCSSS bridge designs. Bridges had a design life of 20 years to develop over 99% of the total creep and shrinkage, thereby developing the largest positive restraint moment. Design live loads were defined by the HL-93 load specification in AASHTO. Assuming full composite slab action, live loads were distributed using equivalent strip widths for slab spans for multiple loaded lanes, defined in AASHTO Section 4.6.2.3. Bridges had a consistent width of 48 ft., corresponding to 8 precast beams. Designs were for interior precast beams only, so external member effects were neglected. Prestress losses were calculated using the Refined Method from AASHTO Section 5.9.5.4 because the high volume-to-surface ratio of the inverted-tee precluded the application of the Approximate Method. The CIP concrete strength was assumed to be 4.0 ksi and prestressing strand was 0.5 in., low-lax, Grade 270.

For each span, the primary design parameters were modified sequentially. First, the strand pattern design was optimized for the Service III limit state at midspan. The strand design was limited to two rows, one at 2 in. and one at 4 in. from the bottom of precast. Following common practice, each row had either an equal number of strands or two additional strands in the bottom row. This kept the center of gravity of prestressing around 3 in. from the bottom. If Service III could not be reasonably satisfied with strand design alone, concrete strength was increased up to 10 ksi. Finally, if the increased concrete strength up to 10 ksi did not satisfy the Service III limit state, the beam depth was increased by 2 in. and the sequence was repeated. Once the Service III limit state was satisfied, concrete strengths were adjusted to satisfy any strength limit states for Service I compression that had been exceeded by increasing the prestressing force. Secondary design, such as positive moment connection design, was done after flexural design optimization. None of the flexural designs needed to be changed based on secondary design considerations.

The simple-span designs were completed prior to the continuous system designs. Simple-span designs did not require considerations for restraint moment or partial continuity as described previously because these are continuous system effects. The simple-span designs were used as starting points for the corresponding continuous system designs.

6.2.1 Part 1: Creep and Shrinkage Model

The creep and shrinkage models from AASHTO LRFD 2010 and AASHTO LRFD 2004 were compared for PCSSS design. A three configuration subset of eight configurations listed in Table 6.1 was used for Part 1 and Part 2 (Section 6.2.2) of the parametric study. The optimized designs for the subset of all configurations are shown in Table 6.2. Designs are shown for each configuration, using both 2004 and 2010 models, and for both end and center spans for the three-span configurations. The controlling limit state was determined by reducing the number of strands until a limit state failed. Differential shrinkage was taken as the difference in predicted shrinkage strain of the deck and precast beam after continuity. The initial precast creep factor, due to loads applied at prestressing release, was taken as the predicted creep factor for the precast beam at the time of continuity with the CIP concrete. The restraint moment was defined by the maximum values at the pier due to time-dependent and thermal gradient components. Positive moment connections were subject to the following limit: $\max(0.6M_{cr}, RM) \leq M_n \leq 1.2M_{cr}$. Continuity degree was classified by the percentage of live load taken on as continuous

for partial continuity (i.e., “Full” if the continuity check was satisfied with no more than $0.5f_{LL}$ or “Simple” if the check could not be satisfied). For partial continuity, the percentage of live load on a continuous system is given in Table 6.2, where 100% would correspond to full continuity and 0% would correspond to the simple span case.

Both models predicted similar prestress losses; however, the AASHTO 2004 model produced restraint moments that were significantly higher than those given by the AASHTO 2010 model. The two factors contributing to this difference were the differential shrinkage and the precast beam creep prior to continuity. The AASHTO 2004 model predicted very small differential shrinkage between the CIP and precast concrete, and in many cases negative differential shrinkage, where the precast concrete underwent more shrinkage than the CIP concrete after continuity. It is unreasonable that the precast concrete would shrink more than the CIP after continuity. The large volume-to-surface ratio (V/S) of the CIP concrete reduced the ultimate shrinkage according to the 2004 model, while it had no effect according to the 2010 model. The result was a positive shrinkage moment that increased the total restraint moment. The 2004 model also predicted a smaller portion of total creep occurring between pretensioning release and continuity. This means that with the 2004 model, more positive moment due to prestressing creep developed, also increasing the total restraint moment.

In all of the designs, the restraint moment from the 2004 model limited the development of continuity according to the continuity check of AASHTO Section 5.14.1.4. For the 50-50-50 design, the positive moment connection required was greater than $1.2M_{cr}$. According to AASHTO 5.14.1.4.6, a positive moment connection is not fully effective above this limit.

Based on the prediction of unreasonably high restraint moments due to unrealistic shrinkage behavior, and the infeasibility of positive moment connection design, the AASHTO LRFD 2004 creep and shrinkage model was deemed impractical for the PCSSS. The AASHTO LRFD 2010 creep and shrinkage model was used for the remainder of the parametric study.

6.2.2 Part 2: Precast Age at Continuity

A typical design continuity time for MnDOT PCSSS is 14 days from prestressing transfer to CIP deck placement. Beam ages from the typical 14-day age to a 7-day age were compared to account for a quick fabrication turnaround. The 7-day beam age would be more conservative in design because larger positive time-dependent restraint moments would be predicted. The three sample configurations were designed using AASHTO 2010 creep and shrinkage assumptions. The optimized designs are given in Table 6.3.

For shorter spans, using a 7-day beam age resulted in higher restraint moments than for the case of the 14-day beam age, but did not change the design drastically. The only design change was an increase in the precast strength at release by at most 1.6 ksi, and in the 20-30-20 configuration, an increase in the 28-day precast strength by 0.2 ksi. Both the 20-30-20 and 22-22 configurations remained at full continuity independent of the continuity time.

For the 50-50-50 configuration, the increase in restraint moment for the 7-day continuity in comparison to the 14-day continuity was enough to exceed the $1.2M_{cr}$ limit for an effective positive moment connection. In addition, two additional strands were required and the precast strength at release had to be increased by 0.6 ksi. While it may seem conservative to design for a 7-day continuity time, exceeding the $1.2M_{cr}$ limit required that steps be taken to reduce restraint

moment. Therefore, using a 14-day continuity time was the most effective way to stay below this limit.

Based on the low impact of a 7-day continuity time on the shorter span length configurations, and the need for a 14-day continuity time for the long span configuration, a 14-day continuity time is recommended in design. The final part of the study was based on a 14-day continuity time.

6.2.3 Part 3: Continuous System vs. Simple Span Economy

Corresponding simple-span and continuous system designs were compared to evaluate economy. The results of the optimized designs in terms of the primary design parameters are shown in Table 6.4 for the continuous system designs and in Table 6.5 for the simply-supported designs. Because the precast sections for both the simple-span and continuous sections had the same depth for any given configuration, the comparison for economic benefit was made using the optimized strand number. The strand number had an associated material and labor cost and was an indication of the performance of the precast section.

Two of the configurations showed some small economic benefit with continuity: the 20-30-20 continuous design used two less strands per precast element and the 22-27-22 continuous design used 8 less strands per precast element than the respective simple designs. These configurations had short spans that did not develop large time-dependent restraint moments and maintained full continuity. In addition, the smaller section depth resulted in smaller thermal gradient restraint moments. The effect of the larger middle span was to reduce the end span restraint moment. The two-span 22-22 continuous design showed no economic benefit over the simply-supported design even though it was also fully continuous. With only two spans to provide continuity action, the time-dependent and thermal gradient restraint moments developed in this system were enough to counteract the benefit of continuity.

The continuous designs of the remaining configurations were all less economical than the corresponding simply-supported designs. These configurations were all effectively simply supported because they failed to pass the continuity check. With no continuity, the added time-dependent and thermal gradient restraint moments were large enough to control the design and require additional strand. All three three-equal-span configurations with equal end and center span lengths (i.e. 24-24-24, 34-34-34, and 50-50-50) showed similar optimized design behavior. The center spans were all equivalent to the simply-supported designs, while the end spans each required two additional strands. Restraint moments that developed in the end spans were a maximum at the pier and decreased linearly to zero at the abutment. The controlling section was still at midspan where the restraint moment stress superimposed with the live load envelope required additional capacity.

6.2.4 Recommendation

Based on the results of the parametric study, a continuous system design for PCSSS is not always more economical than a simply-supported design due to the development of time-dependent and thermal gradient restraint moments. These restraint moments significantly reduced continuity action in the continuous designs and increased loading. In many cases, providing continuity in design exhibited no net reduction in service design moment due to the addition of restraint moments to the live load envelope.

Maximum time-dependent and thermal gradient restraint moments generally increased with increasing span lengths. All of the designs had large design loads from thermal gradient. In most load combinations, the thermal gradient factor of 0.5 reduced this effect somewhat, but the moments were still large enough to cause continuity and capacity problems. Interestingly, all the designs except one had either full continuity or no continuity. This means that the continuity check either passed using $0.5 f_{LL}$ or failed using $1.0 f_{LL}$. As the span lengths increased, the time-dependent and thermal gradient restraint moments increased faster than f_{LL} . Although this was a limited set of eight configurations, this suggests that the span length range for partial continuity is small. Only shorter span bridges (about 20 ft.) can develop continuity because of low time-dependent and thermal gradient restraint moments.

It may be possible to maintain continuity if time-dependent restraint moments did not develop by letting the continuity time reach 90 days. In this case, time-dependent restraint moments are ignored since creep and shrinkage are assumed to have largely dissipated, and only thermal gradient causes tension in the bottom of the section over the pier. This would most likely result in at least partial continuity for most configurations, indicated by the restraint moment values from Table 6.4. However, the thermal gradient contribution is still significant, and overall these results show that thermal gradient should be considered for PCSSS. The importance of thermal gradients in PCSSS bridges is also shown by the instrumentation of Bridge No. 13004, discussed in Section 4.4.

The parametric study showed that designing PCSSS as a series of simple spans while also providing a continuity connection is unconservative. Many of the simple span designs required fewer strand than the corresponding continuous design. If a continuity connection were added to these simple span designs, the added restraint moments would require additional strand; the system would be under capacity if strands were not added. This contradicts the recommendation in AASHTO 5.14.1.4.1, which states that such a design would not need to consider restraint moments as a conservative approach, provided that the precast beams were aged at least 90 days. Even if positive time-dependent restraint moments did not develop, thermal gradient restraint moments would persist.

Overall, it is recommended that PCSSS be designed as a series of simple spans instead of as continuous systems. The benefits of continuous design to some span configurations do not make up for the added design complexity for restraint moments and partial continuity. For most bridges, the simple-span design is more economical. In addition, several design simplifications can be made if a simple-span approach is taken. Because the loading analysis for a simple-span design would be a function of span configuration only, design aids would be very effective. Finally, precast beams for specific span lengths could be prefabricated without having to be redesigned for each bridge.

6.3 Corollary Studies

Following the results of the parametric study and the recommendation for simply-supported PCSSS design, two related studies were done to further simplify the PCSSS design. First, a method was developed to design the PCSSS as simply-supported while also adding a continuity connection. As shown in the parametric study, designing a PCSSS bridge with this method would be unconservative without accounting for the added stress caused by restraint moments. It may be beneficial to include continuity reinforcement in a simply-supported design for purposes of rideability or to have a more integrated system across the pier. Some MnDOT

personnel have indicated that cracks may develop at the end of the continuity reinforcement, but this should not have a deleterious effect given that the prestressing strands are below the continuity reinforcement. The second study investigated negative restraint moments for designing longitudinal deck reinforcement. Longitudinal deck reinforcement is continuous over the bridge piers, even with the recommendation for a simply-supported design. As such, negative restraint moments have the potential to develop and must be considered in design. Designers at MnDOT proposed a method to approximate contributions from the negative restraint moment. The second study was used to validate the method.

6.3.1 Simplified Continuity Connection

PCSSS with a continuity connection may be designed using a simple span beam analysis and superimposing the effects of restraint moment by a simplified method. A simplified approach to restraint moment calculation is justified for several reasons. First, the effects of material creep, shrinkage and thermal gradient effects is highly variable. Second, restraint moment calculations show wide variation in negative and positive restraint moment depending on modeling assumptions. The assumptions made in restraint moment calculations are also subject to the previously noted variations in material and thermal effects. Finally, field installation timing is uncertain and an accurate design is too constraining for real-world application, especially with respect to beam age assumptions.

The simplified procedure involves first selecting positive moment connection reinforcement. The area of steel in this connection is able to develop a certain amount of restraint moment before yielding. Therefore, the positive moment connection may be designed to limit the amount of restraint moment that develops. The maximum possible restraint moment is applied as end moments at the piers, superimposing a constant moment over the center span and tapering to zero moment at the end spans. The precast beams are then redesigned with more prestressing strand for the increased demands. This simplified method does not require continuous system analysis because it is based on a simply-supported design. However, the precast beam sections would not be as efficient as with a full continuous system analysis because more prestressing strand would be needed.

Examples of using this design method were done using the eight span configurations from the parametric study. Table 6.6 contains the redesigned sections where four No. 5 bars were added to the simple-span designs. For typical PCSSS configurations, four No. 5 bars in the bottom of the each trough over the piers is reasonable. The moment capacity of the positive moment connection is shown for each span configuration. For these designs, two or four additional strands were sufficient to accommodate the restraint moment added by the yielded trough reinforcement. The method described here was shown to be viable for adding a continuity connection without needing to calculate restraint moments due to creep, shrinkage and thermal effects.

Fatigue of the trough reinforcement due to live load was a concern, especially because the trough reinforcement was assumed to yield in tension. The two types of cyclic loading cases were considered: multiple daily loadings from the fatigue truck and daily effects from thermal gradient. As an illustration of calculating the possible impact of fatigue loading, stress range calculations were performed for Bridge No. 13004 in Center City, MN. The Heavy Commercial Average Daily Traffic (HCADT) was 1,057 according to the bridge inventory report for Bridge No. 13004 (MnDOT, 2009). Because the relationship between the weight of an “average”

heavy commercial vehicle and the design fatigue truck was unknown for this location, the HCADT was conservatively taken to be representative of the number of fatigue truck crossings. Dividing the trucks over four lanes and assuming a distribution factor of 0.5 lanes per beam, the cycle count for truck loading was estimated at 48,200 per year per beam. A fully continuous system, was used to determine the stress range at the continuity reinforcement due to live load. Because the trough reinforcement assumed to be yielded in tension after the development of time-dependent restraint moments, the reinforcement would cycle in the tensile range as the live load adds compressive stress associated with negative live load moments. The negative moment generated by the fatigue truck over the pier was used to find the stress range at the reinforcement level. This method predicted a stress range in the steel on the order of 10 ksi for a bridge with 14 in. deep precast beams. A more accurate stress range could be determined if the weight of the average heavy commercial vehicle was known, however for illustrative purposes, the average weight of a heavy commercial vehicle was taken as the weight of the design fatigue truck. The section depth also affects the calculation of these stress, a deeper section would have a lower stress range, and therefore a longer fatigue life than predicted in this section. In addition, performing the fatigue load analysis assuming a cracked diaphragm and using simple-span end rotations could provide a more reasonable stress range. The stress range due to thermal gradient was taken from the strain data collected from Bridge No. 13004. From Section 4.3, it was seen that the trough reinforcement saw an average daily strain range of about 750 $\mu\epsilon$ during the summer months. This corresponded to a stress range of 22 ksi. The cycle count was conservatively estimated at 100 per year to account for 100 days of the year that were assumed to incur a large thermal gradient. Additionally, the stress range predicted for the AASHTO thermal gradient was determined to see how it compared to the measured stress range due to thermal cycles. The predicted stress range was calculated by determining the flexural deformation curvature described in 4.6.6, determining the fixed end moment, and then calculating the reinforcement stress with an elastic stress distribution. This method predicted a stress range of 88 ksi, corresponding to the design (maximum) thermal gradient. Clearly one would not expect the average thermal gradient in the summer to be as large as the design thermal gradient. For Bridge No. 13004, the measured daily stress range appears to be well predicted by using 25% of the design thermal gradient. Thus with no other experimental evidence available, it is reasonable to predict the stress range due to daily thermal cycles in the summer by using 25% of the design thermal gradient.

The fatigue life of the trough reinforcement for Bridge No. 13004 was found by applying Miner's rule. From AISC C.3.3 (2006), 60 ksi rebar is estimated to fail at 100,000 cycles of loading to full yield.

$$\text{Estimated failure: } (60 \text{ ksi})(100,000 \text{ cycles}) = 6,000,000 \text{ ksi} \cdot \text{cycles}$$

$$\text{Miner's rule: } \frac{6,000,000 \text{ ksi} \cdot \text{cycles}}{(10 \text{ ksi})(48,200 \text{ cycles/year}) + (22 \text{ ksi})(100 \text{ cycles/year})} = \mathbf{12.4 \text{ years}}$$

Using Miner's rule, the trough reinforcement would be expected to fail from fatigue after 12.4 years. If PCSSS bridges have an intended 100-year design life, the 12.4-year fatigue life of the trough reinforcement should be taken into consideration. After 12.4 years, the trough reinforcement should be assumed ineffective. Even so, the system would remain a simply-supported structure, for which the original design was done. A more refined calculation, with a

better estimate for the weight of the average heavy commercial vehicle would predict a longer fatigue life.

6.3.2 Longitudinal Deck Reinforcement

Designers at MnDOT needed a simplified approach for calculating the negative moment envelope for the longitudinal deck reinforcement. The design was controlled by the following Service I load combination:

$$DL_2 + LL + RM + 0.5TG \quad (6.2)$$

where DL_2 represents post-continuity dead loads, LL represents live loads, RM represents time-dependent restraint moments, and TG represents thermal gradient restraint moments. Restraint moments are computationally intensive, and predicted restraint moments are highly dependent on the analysis method and material properties. To avoid calculating restraint moments, MnDOT proposed investigating a simplified method of approximating the restraint moment contributions from RM and TG components. The approximate restraint moment envelope was defined by the value of LL at the pier, multiplied by a scaling factor γ . This value was then tapered from the pier to 0 at the abutment, with a constant value over the middle spans. If used, the approximation for the Service I load combination would be:

$$DL_2 + LL + \gamma LL_{RM} \quad (6.3)$$

where γ is the scaling factor and LL_{RM} is the value of LL at the pier, tapered to 0 at the abutment. Results from the design of one particular MnDOT PCSSS bridge suggested that a value of 1.0 should be used for γ .

Negative moment analyses from the parametric bridge design study were used to validate the approximate method. The parametric study investigated the design of the eight bridges covering the range of feasible span lengths and configurations. For the exact method, the moment envelope was determined by summing $DL_2 + LL + RM + 0.5TG$ for each of the eight bridge designs, where the negative live load envelope was obtained by assuming full continuity. The assumption of continuity for live load in the deck reflected the continuous deck reinforcement over the piers. Time-dependent restraint moments were calculated using the P-method for beams that were aged 90 days prior to continuity with the CIP deck. The 90-day age was used based on the assumption that it would produce the maximum negative time-dependent restraint moment. The restraint moments and live load moments were calculated at the pier of each bridge. The approximate method used the load combination of $DL_2 + LL + \gamma LL_{RM}$, where γ is a multiplier on the negative LL envelope determined from a continuous span model. The simple-span designs from the parametric study were used to emulate the recommended simple-span design method.

After comparing the results of the exact and approximate Service I negative moment envelopes, the value of γ was chosen to be 1.20. Figure 6.5 through Figure 6.8 show moment envelopes for several of the considered span configurations, along with the minimum moment capacity requirement for each case. This capacity requirement, defined in AASHTO Section 5.7.3.4 (2010) to control cracking at service levels, dictates the reinforcement cutoff point and was used to evaluate the effect of the approximate load combination. In each case, the original moment envelope from Equation 6.2 is shown with approximate envelopes from Equation 6.3,

using multipliers of 1.0 and 1.2. The approximation with a multiplier of 1.2 is close for the short span bridge but becomes an overestimate for longer span bridges. Table 6.7 shows the maximum moments of both the exact and approximate (with $\gamma = 1.2$) Service I load combinations for all eight span configurations along with the provided design moment capacity of No. 7 bars spaced at 4 in. This reinforcement detail was proposed by MnDOT as a maximum longitudinal bar size and a minimum spacing that should be allowed. All configurations provided more than enough moment capacity compared with the approximate load combination, so the No. 7 and 4 in. limit is valid. Between the pier and abutment the No. 7 bars are cutoff at two locations: 1) where the moment capacity of two bars per foot exceeds the moment envelope, and 2) where the moment capacity of one bar per foot exceeds the moment envelope.

MnDOT provided negative moment analyses from the designs of Bridge Nos. 49003 and 08006 to compare with the results of this study. Bridge No. 49003 had two 39.5-foot spans, and Bridge No. 08006 was a three-span bridge with lengths 34.5-35-34.5 ft. The second bridge was particularly comparable to the 34-34-34 configuration in Table 6.7. Compared to the parametric study results, the moment envelopes from the MnDOT designs were very similar to those found from this parametric study. It would be conservative to use the approximate negative moment envelope with a live load multiplier equal to 1.2. For any spans longer than 30 ft. this approximation would be an overestimate of the restraint moment.

Chapter 7: Conclusions and Recommendations

The MnDOT PCSSS has been under development since 2005 with the goal of providing an accelerated construction replacement for conventional slab-span bridges. Extensive research on the PCSSS has influenced several generations of design changes to improve performance, constructability, and economy. These design changes were evaluated by investigating the performance of existing PCSSS bridges and reviewing the current design practices. Field inspections were conducted for five existing PCSSS bridges, consisting of crack mapping surveys and core sample examinations, to evaluate design changes related to reflective crack control. Strain indications of reflective cracking and restraint moment cracking, as well as thermal effects were monitored using the instrumentation in Bridge No. 13004 in Center City, MN. Current design details and methods were also evaluated using the results of the field inspection. Several recommendations were made for the future of PCSSS design. Finally, a parametric design study was conducted to determine the most economical design method for the PCSSS with respect to continuity for live load.

Several behaviors were either confirmed or discovered by evaluating the combination of crack surveys and core examinations. Cracking due to poor consolidation around the composite action stirrups on Bridge No. 13004 dominated the overall surface cracking, providing more evidence that increasing the stirrup clearance was necessary. This was especially evident from crack maps of subsequent bridges that had sufficient clearance under the stirrups and did not show the same cracking pattern. The durability of Bridge No. 33008 near Mora, MN was brought into question as a result of the field inspections. The combination of long surface cracks over a number of longitudinal joints and the clear observation of two reflective cracks from the core specimens, one of which was full-depth, suggested that many of the longitudinal joints had significant reflective cracking. In addition, the abnormal camber observations from Bridge No. 33008 were investigated. The remaining three inspected bridges primarily brought to light the predominate issue of cracking from shrinkage restraint. A conventional CIP concrete slab-span bridge was also inspected to compare with the PCSSS bridges, which further highlighted the issue of restrained shrinkage particular to the PCSSS. In the case of slab-span bridges, which are constructed with shored construction, the top surface of the deck in the positive moment region is in compression at service. Because the precast inverted-tee serves as stay-in-place formwork in the case of the PCSSS, the CIP is not loaded due to self-weight. Consequently, the PCSSS is more susceptible to surface cracking than the case of slab-span systems. As a result, recent PCSSS design has focused on mitigating shrinkage restraint by using low-shrinkage concrete and improved crack control reinforcement.

The field inspections provided an extensive set of information on the performance of the existing PCSSS bridges and have laid the groundwork for future evaluations, both to compare with previously inspected bridges and to evaluate new bridges. Information gathered from the field inspections can serve as a data set with which to compare future PCSSS bridges. Procedures for crack mapping described in this report were systematic enough to provide thorough and comparable diagrams. Future crack surveys should be performed for more recent PCSSS bridges so that design changes and overall performance can continue to be evaluated. While the procedure in this report would be preferable for the sake of consistency, simpler crack surveys could be completed during routine bridge maintenance inspections. Care should be taken to map the cracks under similar environmental conditions each year as the crack widths

vary with temperature. Bridge No. 33008 should continue to be monitored due to the durability problems described above. Core extractions, while very beneficial toward finding reflective cracking, were a destructive procedure that was more involved than surface crack mapping. Even so, one or two core specimens could be taken from midspan locations of future bridges if reflective cracking was suspected.

Several important design considerations were investigated during the parametric study, which ultimately concluded that simply-supported design was most economical for the PCSSS. From a design perspective, the parametric study highlighted the impact of time-dependent and thermal gradient effects on system performance. In particular, restraint moments from these effects dominated the majority of sample PCSSS continuous system designs, effectively negating benefits from live load continuity. Furthermore, the restraint moments also contributed to the ineffectiveness of continuity per the provisions from Section 5.14.1.4 in AASHTO (2010). In most cases, the large restraint moments canceled all continuity effects, reducing the continuous system to a series of simply-supported spans. This approach is certainly conservative, but the provisions in AASHTO Section 5.14.1.4 may be excessively conservative given that the step-change in continuity at $0.5f_{LL}$ had a significant effect on the results. Even so, the recommendation to design the PCSSS as simply-supported will save hours of design time for each bridge at a marginal cost for labor and materials.

7.1 Recommendations

As a result of the research presented in this report, a number of recommendations for the design of the MnDOT PCSSS were made. These recommendations are as follows:

1. Transverse deck reinforcement should be detailed to provide a ρ_g of at least 0.0063 with spacing no greater than 9 in. to control shrinkage cracking at the level of the deck reinforcement. These recommendations are based on those of Frosch (2009). For PCSSS design, ρ_g was calculated using the 6 in. of CIP concrete above the precast webs. One way to implement these recommendations would be to increase the current detailing requirements of No. 4 bars at 6 in. spacing to No. 5 bars at 6 in. spacing ($\rho_g = 0.0086$). Alternatively, No. 5 bars at 8 in. spacing could be used ($\rho_g = 0.0065$).
2. Transverse reinforcement in the trough region consisting of the combination of trough hooks and the stirrups of the “drop-in” cage should also be detailed to satisfy Frosch (2009) recommendations. The trough hooks from adjacent precast inverted tees should be located adjacent to each other to facilitate transverse load transfer in the bridge. The drop-in cage can be staggered relative to the trough hooks to meet the Frosch 9 in. maximum spacing requirement.
3. Anchorage dowels at the piers and abutments should continue to be placed in the blockout regions to aide in construction. Typically 1 in. diameter dowels have been used, with the latest generation of beams using stainless dowels at all locations. Dowels in blockouts away from the longitudinal bridge center should be minimized as these can add restraint to shrinkage which may induce cracking in the deck. Dowels at piers should be wrapped with polystyrene sleeves to reduce restraint-induced cracking. Dowels at abutments are recommended to not be wrapped in order to reduce the likelihood of promoting separation and water intrusion between the bridge and the approach panel. No more than four dowels should be placed in each blockout. If possible, dowels should be

placed in one row per support rather than in two rows spaced longitudinally, in part to reduce moments developed in the dowel bar couple.

4. MnDOT should evaluate the performance of the bridges built for Generation 4 in 2011, which were not reviewed as part of this project, regarding the use of a bearing detail aimed at reducing lateral restraint of the superstructure. The placement of the elastomeric bearing pad was unchanged in the new bearing detail. However, polystyrene was placed to cover the entire top surface of the abutments and pier caps, excluding the area of the bearing pad. The primary function of the extended polystyrene was to prevent contact between the CIP concrete and abutment or pier cap.
5. Smooth flange surfaces should continue to be used. The shallow voids resulting from fabrication need not be patched. Subsequent to this study, MnDOT has employed the use of a bond breaker such as mastic over the longitudinal joint between adjacent inverted tees. The purpose of the mastic is to soften a potential crack initiation site. Evaluation of the effectiveness of the bond breaker was not within the scope of this report. Prewetting of the flange precast surface prior to casting the CIP should help to reduce the shrinkage of the concrete at the CIP-precast interface and has an added benefit of removing laitance from the smooth flange surface, reducing the likelihood of delamination. Water should not be allowed to pool in the voids, and if mastic is used in construction, measures should be taken to enable the water to drain prior to casting the CIP.
6. Composite action stirrups need not be used if the required shear transfer is less than 135 psi. These are typically placed to satisfy minimum horizontal shear steel requirements. Research by French et al. (2011) concluded that the bond between the CIP concrete and precast web provided enough shear capacity to achieve full composite action in this case.
7. PCSSS beams should be designed as simply-supported for live load and dead loads. Providing a positive moment connection for live load continuity produces significant time-dependent and thermal restraint moments. These restraint moments effectively negate the reduction in live load, making continuous system design equally or less economical than simply-supported design. The CIP deck should be designed as continuous for negative live load.
8. Designing the PCSSS beams as simply-supported for live load while also providing a positive moment connection should not be done without accounting for the induced restraint moments. A simple method to account for restraint moments was developed, but it required the positive moment connection to yield in order to control the maximum restraint moment that could develop. For typical PCSSS configurations, four No. 5 bars is reasonable for reinforcement in positive moment connections. However, the restraint moment developed by these bars needs to be determined so the precast beams can be properly designed. The positive moment connection reinforcement should extend a development length on either side of the pier to develop the full yield restraint moment. Fatigue issues of the positive moment connection may need to be taken into consideration, as this reinforcement could undergo significant tensile stress ranges over its life due to thermal gradient effects.
9. Deck design should be bounded by both simple span assumptions and a pseudo-continuous assumption. This bounding approach recognizes the time-dependent nature of creep and shrinkage locked into the beam and deck system. In the analysis of negative

moments for longitudinal deck reinforcement design, it was found that the controlling Service I load combination could be approximated by the following:

$$DL_2 + LL + \gamma LL_{RM}$$

where DL_2 represents the post-continuity dead load, LL represents live load, and γLL_{RM} represents a conservative approximation of the time-dependent and thermal gradient restraint moment equal to a value of 1.2 times the LL moment at the bridge pier. The approximate restraint moment envelope is tapered from a γ value of 0 at the abutment to a γ value of 1.2 times the LL moment value at the pier and constant γ value of 1.2 over the center span. This approximate analysis of negative moments was calibrated for configurations with spans around 20 ft. long and becomes increasingly conservative for spans up to 60 ft. As discussed in Section 6.3.2, for longer span lengths, even a γ value of 1.0 may yield unnecessarily large negative moments at the piers. In this case, a more refined restraint moment analysis may be called for to limit the amount of negative moment steel needed in the deck.

References

- American Association of State Highway and Transportation Officials (AASHTO). (2004). *LRFD Bridge Design Specifications*, 3rd Ed., Washington, D.C.
- AASHTO. (2010). *LRFD Bridge Design Specifications*, 5th Ed., Washington, D.C.
- American Institute of Steel Construction (AISC). (2006) *Steel Construction Manual*, 13th Ed., Chicago, IL.
- Barr, P., Halling, M., Boone, S., Toca, R., and Angomas, F. (2009). *UDOT's calibration of AASHTO's new prestress loss design equations*. Report No. UT-09.10, Utah Department of Transportation, Salt Lake City, UT.
- Bell, C., Shield, C., and French, C. (2006). *Application of precast decks and other elements to bridge structures*. Research Rep. No. 2006-37, Minnesota Department of Transportation, St. Paul, MN.
- French, C.E., Shield, C., Klaseus, D., Smith, M., Eriksson, W., Ma, Z., Zhu, P., Lewis, S, and Chapman, C. (2011). *Cast-in-place concrete connections for precast deck systems*. NCHRP Project 10-71 Web-only Report 173. Transportation Research Board, Washington, D.C. http://onlinepubs.trb.org/onlinepubs/nchrp/nchrp_w173.pdf. (Accessed October 7, 2011).
- Freyermuth, C.L. (1969). "Design of Continuous Highway Bridges with Precast, Prestressed Concrete Girders." *Journal of the Prestressed Concrete Institute*, 14(2), 14-39.
- Frosch, R. J., Bice, J. K., and Erickson, J. B. (2006). *Design methods for the control of restrained shrinkage cracking*. Publication FHWA/IN/JTRP-2006/32. Joint Transportation Research Program, Indiana Department of Transportation and Purdue University, West Lafayette, IN.
- Hagen, K, Ellis, S., Fishbein, J., Molnau, K., Wolhowe, E., and Dorgan, D. (2005). "Development and Construction of a Precast Inverted T System for Expediting Minnesota Slab Span Bridge Projects." *PCI National Bridge Conference*, Palm Springs, CA.
- Miller R., Castrodale, R., Mirmiran, A. and Hastak M. (2004). *Connection of Simple-Span Precast Concrete Girders for Continuity*. NCHRP Report 519, Transportation Research Board, Washington, D.C.
- Minnesota Department of Transportation (MnDOT). (2009). *Mn/DOT Structure Inventory Report: Bridge ID: 13004*, Minnesota Department of Transportation, St. Paul, MN.
- Naito, C. and Deschenes, D. (2006). "Horizontal Shear Capacity of Composite Concrete Beams without Ties." *Proceedings, Prestressed/Precast Concrete Institute (PCI) National Bridge Conference*, Grapevine, TX.

- Okiel, A.M., Hossain, T. and Cai, C.S. (2011). "Field Monitoring Of Positive Moment Continuity Detail In A Skewed Prestressed Concrete Bulb-T Girder Bridge." *PCI/NBC Proceedings 2011*, Salt Lake City, UT.
- O'Neill, C. and French, C. (2012). *Validation of Prestressed Concrete I-Beam Deflection and Camber Estimates. Research Rep. No. 2012-09*, Minnesota Department of Transportation, St. Paul, MN.
- Peterman, R.J. and Ramirez, J.A. (1998). "Restraint moments in bridges with full-span prestressed concrete form panels." *PCI J.*, 43(1), 54-73.
- Smith, M., Eriksson, W., Shield, C., and French, C. (2008). *Monitoring and analysis of MnDOT precast composite slab span system (PCSSS). Research Rep. No. 2008-41*, Minnesota Dept. of Transportation, St. Paul, MN.
- PCI Committee on Tolerances, (2000), *Tolerances for Precast and Prestressed Concrete Construction: MNL-135-00*.
- Youakim, S., Ghali, A., Hida, S., and Karbhari, V. (2007). "Prediction of Long-Term Prestress Losses." *PCI J.*, 52(2), 116-130.

Tables

Table 2.1: Subassemblage specimen design details (French et al. 2011)

Specimen Identification	Width	Depth	Transverse Bars (Load Trans.)			Cage (Crack Control)			Max Spacing ²	R/F Ratio ³ ρ_{cr}
	[in]	[in]	Size	Spacing	Depth ¹	Presence	Size	Spacing		
SSMBLG1-Control1	62.75	14	#4	18 in. OC	4 1/2 in.	Cage	#3	18 in. OC	9	0.0031
SSMBLG2-NoCage	67.25	14	#4	18 in. OC	4 1/2 in.	No Cage	0	0	18	0.0025
SSMBLG3-HighBars	62.75	14	#4	18 in. OC	7 in.	Cage	#3	18 in. OC	9	0.0031
SSMBLG4-Deep	62.75	18	#4	18 in. OC	4 1/2 in.	Cage	#3	18 in. OC	9	0.0022
SSMBLG5-No.6Bars	62.75	14	#6	18 in. OC	4 1/2 in.	Cage	#3	18 in. OC	9	0.0061
SSMBLG6-Frosch	64	14	#4	18 in. OC	4 1/2 in.	Cage	#3	4.5 in. OC	4.5	0.0052
SSMBLG7-Control2	62.75	14	#4	18 in. OC	4 1/2 in.	Cage	#3	18 in. OC	9	0.0031

¹The depth of the transverse reinforcement was taken from the bottom of the precast section to the center of the reinforcement

²The maximum spacing was the maximum nominal distance between reinforcement traversing the longitudinal joint, regardless of type (i.e., transverse hooked bars or cage)

³The reinforcement ratio shown is that corresponding to crack control, see above and Section 5.1

Table 2.2: Typical PCSSS details from the four design generations with changes from the previous generation in bold. Actual details may differ for particular bridges.

PCSSS Details		Generation 1	Generation 2	Generation 3	Generation 4
Development Year		2005	2007	2009	2011
Inspected Field Bridges Nos.		13004	33005, 33008	49007, 49036	None inspected
Precast Beam	Flange Thickness at End	5 ¼ in.	5 ¼ in.	3 in.	3 in.
	Roughened Flange Surfaces	Yes	Yes	No	No
	Web Corner Chamfer	¾ in.	¾ in.	2 in.	2 in.
	Flange Top Corner Chamfer	¾ in.	¾ in.	1 in.	1 in.
	Prewetted Prior to Continuity	No	No	Yes	Yes
Bearing Pad		Elastomer, polystyrene under beams only	Elastomer, polystyrene under beams only	Elastomer, polystyrene under beams only	Elastomer, polystyrene over entire pier cap
Trough	Trough Reinforcement Spacing ¹	10 in.	10 in.	6 in.	6 in.
	Joint Treatment ²	None	None	No. 3 bars	Mastic
Continuity Reinforcement		4 No. 8 at 6 in.	4 No. 8 at 5 in.	4 No. 8 at 5 in.	4 No. 8 at 5 in.
Deck Region	Longitudinal Reinforcement	1 No. 8 and 2 No. 7 at 4 in. = 1 ft. total	1 No. 8 and 2 No. 7 at 4 in. = 1 ft. total	No. 7 at 4 in.	No. 7 at 4 in.
	Transverse Reinforcement	No.5 at 1 ft.	No. 5 at 1 ft.	No. 4 at 6 in.	No. 4 at 6 in.
	Composite Action Stirrups	2 No. 5 at 1 ft.	4 No. 4 at 2 ft.	2 No. 4 at 2 ft.	2 No. 4 at 2 ft.
	Stirrup Projection above Web	Not Specified	2 in.	2 in.	2 in.
Dowels	At Piers	No. 5 at 12 in. between beam ends, center 50% of pier width	6 No. 6 at 9 in. in blockouts	4 No. 8 at 12 in. in blockouts	4 No. 8 at 12 in. in blockouts
	At Abutments	3 No. 6 at 9 in. in blockouts	3 No. 6 at 9 in. in blockouts	2 No. 8 at 12 in. in blockouts	2 No. 8 at 12 in. in blockouts
	Wrapping	None	None	Outer 2/3rds³	Outer 2/3rds ³

1. Trough Reinforcement Spacing: Maximum spacing between any transverse reinforcement in the trough, either trough hooks or cage stirrups.

2. Joint treatment: No. 3 bars tied to trough hooks to control reflective crack width; mastic bond breaker applied to longitudinal joint to prevent reflective crack initiation

3. Outer 2/3rds: Two-thirds of the blockouts in each outboard portion of the deck had wrapped dowels, leaving the center one-third of the total bridge width with unwrapped dowels

Table 2.3: Summary of design details for Bridge No. 13004 over the Center Lake Channel in Center City, MN

Bridge Number:	13004	Generation:	First	Completion Date:	11/01/2005
Contractor:	Lunda	Beam Fabricator:	County	Designers:	K. Molnau K. Hagen
Location:	MN 8 over the Center Lake Channel in Center City, metro district				
Bridge Dimensions:					
Total Length:	72 ft. - 2 in.	Span Length Ratio:	0.836		
Span 1:	22 ft. - 7 in.	Span 2:	27 ft.	Span 3:	22 ft. - 7 in.
Width:	76 ft. - 5 in.	Beams per Span:	13	Skew:	0 degrees
Precast Beam:					
Release Strength:	4500 psi	Final Strength:	6500 psi		
Depth:	12 in.	Flange Thickness:	5¼ in.	Flange Roughened:	Yes
Strand Diameter:	½ in.	Strand Number:	16	Strand Pattern:	8 at 2 in., 8 at 4 in.
Reinforcement:	2 rows of No. 5 composite action stirrups, 1 in. projection; at 12 in. over midspan No. 6 trough hooks at 12 in., staggered at 2 in. / 10 in. in trough, 1 in. from top of flanges 7 No. 8 top bars No. 4 confinement ties at 12 in.				
First Beam Cast:	08/17/05	Last Beam Cast:	09/21/05		
Deck Cast:	Not available	Open to Traffic:	Not available		
Youngest Beam:	NA	Oldest Beam:	NA	Average Beam:	NA
Cast-in-Place Deck:					
Strength:	4000 psi	Slump:	Not available	Prewetting:	No
Surface Finish:	Very shallow longitudinal tining				
Longitudinal Reinforcement:	No. 8 at 12 in.: full length with lap 2 No. 7 at 4 in. between, staggered: first cutoff at 10 ft. from pier, second cutoff 16 ft. from pier, none cutoff in center span				
Transverse Reinforcement:	No. 5 at 12 in.				
Cage Reinforcement:	No. 5 corner bars 4 No. 8 continuity bars No. 5 stirrups at 12 in., adjacent to trough hooks Total ρ_{cr} : 0.0147 (Area of trough hooks and stirrup leg crossing the longitudinal joint over the area of CIP concrete in the trough)				
Piers and Abutments:					
Bearing Pad:	Elastomeric bearing pad type 1, 6 in. strip under beam tabs Polystyrene under beam bearing, excluded from blockout and 4 in. gap				
Dowels:	Abutments: 3 No. 6 at 9 in. in blockouts Piers: No. 5 at 12 in. along CL of pier cap, over center 36 ft. Cast in place prior to beam placement				
Notes:	Staged construction (1/2 width at a time) Monitored with various instrumentation by the UMN. Included precast pier caps (both stages), precast abutments stage 1 only				

Table 2.4: Summary of design details for Bridge No. 33005 over the Ann River near Mora, MN

Bridge Number:	33005	Generation:	Second	Completion Date:	11/02/2007
Contractor:	Redstone	Beam Fabricator:	County	Designer:	K. Molnau M. Dimaculangan
Location:	TH 65 over the Anne River near Mora, D-3				
Bridge Dimensions:					
Total Length:	112 ft. - 5 in.	Span Length Ratio:	0.989		
Span 1:	36 ft. - 5 in.	Span 2:	36 ft. - 10 in.	Span 3:	36 ft. - 5 in.
Width:	47 ft. - 4 in.	Beams per Span:	8	Skew:	25 degrees
Precast Beam:					
Release Strength:	4000 psi	Final Strength:	6000 psi		
Depth:	14 in.	Flange Thickness:	5¼ in.	Flange Roughened:	Yes
Strand Diameter:	½ in.	Strand Number:	22	Strand Pattern:	12 at 2 in., 10 at 4 in.
Reinforcement:	4 rows of No. 4 composite action stirrups, 2 in. projection; at 2 ft. over midspan No. 6 trough hooks at 12 in., staggered at 3 in. / 9 in. in trough, 1 1/8 in. from top of flanges 7 No. 8 top bars No. 4 confinement stirrups at 12 in.				
First Beam Cast:	08/07/07	Last Beam Cast:	9/11/07		
Deck Cast:	10/11/07	Open to Traffic:	11/02/07		
Youngest Beam:	30 days	Oldest Beam:	65 days	Average Beam:	48.5 days
Cast-in-Place Deck:					
Strength:	4000 psi	Slump:	3 in.	Prewetting:	No
Surface Finish:	Shallow longitudinal tining				
Longitudinal Reinforcement:	No. 7 at 4 in.: full length with lap, first cutoff at 7 ft. - 5 in. from pier, second cutoff 24 ft. - 10 in. (end span), and cutoff 13 ft. - 2 in. (center span) from pier				
Transverse Reinforcement:	No. 5 at 12 in.				
Cage Reinforcement:	No. 4 corner bars 4 No. 9 continuity bars No. 4 stirrups at 12 in., adjacent to trough hooks Total ρ_{cr} : 0.0103 (Area of trough hooks and stirrup leg crossing the longitudinal joint over the area of CIP concrete in the trough)				
Piers and Abutments:					
Bearing Pad:	Elastomeric bearing pad type 1, 6 in. strip under beam tabs Polystyrene under beam bearing, excluded from blockout and 4 in. gap				
Dowels:	Abutments: 4 No. 8 at 11 in. parallel to skew, next to beam ends Piers: 4 No. 8 at 12 in., 1 ft. - 9 in. symmetric over CL pier in blockouts 1 ft. - 6 in. projection, holes drilled and grouted				
Notes:	Transverse cracking perpendicular to beam direction, not parallel to skew				

Table 2.5: Summary of design details for Bridge No. 33008 over the Groundhouse River near Mora, MN

Bridge Number:	33008	Generation:	Second	Completion Date:	11/02/2007
Contractor:	Redstone	Beam Fabricator:	County	Designers:	A. Ottman A. Staples
Location:	TH 65 over the Groundhouse River near Mora, D-3				
Bridge Dimensions:					
Total Length:	90 ft. - 8 in.	Span Length Ratio:	0.975		
Span 1:	29 ft. - 7 in.	Span 2:	30 ft. - 4 in.	Span 3:	29 ft. - 7 in.
Width:	66 ft.	Beams per Span:	11	Skew:	0 degrees
Precast Beam:					
Release Strength:	4500 psi	Final Strength:	6500 psi		
Depth:	12 in.	Flange Thickness:	5¼ in.	Flange Roughened:	Yes
Strand Diameter:	½ in.	Strand Number:	20	Strand Pattern:	10 at 2 in., 10 at 4 in.
Reinforcement:	4 rows of No. 4 composite action stirrups, 2 in. projection, at 12 in. over midspan No. 6 trough hooks at 12 in., staggered at 4 in. / 8 in. in trough, 1 in. from top of flanges 7 No. 8 top bars No. 4 confinement stirrups at 12 in.				
First Beam Cast:	07/02/07	Last Beam Cast:	07/31/07		
Deck Cast:	9/11/07	Open to Traffic:	11/02/07		
Youngest Beam:	42 days	Oldest Beam:	71 days	Average Beam:	57 days
Cast-in-Place Deck:					
Strength:	4000 psi	Slump:	3 in.	Prewetting:	No
Surface Finish:	Shallow longitudinal tining				
Longitudinal Reinforcement:	No. 8 at 4 in., staggered: full length with lap, first cutoff at 10 ft. from pier (end spans), second cutoff 16 ft. from pier (end spans), none cutoff in center span				
Transverse Reinforcement:	No. 5 at 12 in.				
Cage Reinforcement:	No. 5 corner bars 4 No. 8 continuity bars No. 5 stirrups at 12 in., adjacent to trough hooks Total ρ_{cr} : 0.0147 (Area of trough hooks and stirrup leg crossing the longitudinal joint over the area of CIP concrete in the trough)				
Piers and Abutments:					
Bearing Pad:	Elastomeric bearing pad type 1, 6 in. strip under beam tabs Polystyrene under beam bearing, excluded from blackout and 4 in. gap				
Dowels:	Abutments: 3 No. 6 at 9 in. in blockouts Piers: 6 No. 6 at 9 in., 1 ft. - 6 in. symmetric over CL pier in blockouts 12 in. projection, cast in place prior to beam placement				
Notes:	This bridge exhibited fairly extensive longitudinal deck cracking at the joints between the beams There are significant differences in camber between many adjacent beams, evidenced by inspection of the underside and from core specimens				

Table 2.6: Summary of design details for Bridge No. 49007 over the Swan River near Little Falls, MN

Bridge Number:	49007	Generation:	Third	Completion Date:	08/11/09
Contractor:	Lunda	Beam Fabricator:	Cretex	Designer:	A. Ottman / T. Lesch
Location:	TH 238 over the Swan River near Little Falls, D-3				
Bridge Dimensions:					
Total Length:	104 ft. - 2 in.	Span Length Ratio:	0.995		
Span 1:	34 ft. - 8 in.	Span 2:	34 ft. - 10 in.	Span 3:	34 ft. - 8 in.
Width:	39 ft. - 4 in.	Beams per Span:	7	Skew:	0 degrees
Precast Beam:					
Release Strength:	4500 psi	Final Strength:	6500 psi		
Depth:	16 in.	Flange Thickness:	3 in.	Flange Roughened:	No
Strand Diameter:	½ in.	Strand Number:	22	Strand Pattern:	12 at 2 in., 10 at 4 in.
Reinforcement:	4 rows of No. 4 composite action stirrups, 2 in. projection; at 6 in. for 11 ft. (from end), at 1 ft. for next 2 ft., at 2 ft. for 8 ft. to midspan, symmetric No. 6 transverse trough hooks at 12 in., not staggered, 1 1/8 in. from top of flanges 7 No. 8 top bars No. 4 confinement stirrups at 12 in.				
First Beam Cast:	06/04/09	Last Beam Cast:	07/07/09		
Deck Cast:	07/22/09	Open to Traffic:	08/11/09		
Youngest Beam:	15 days	Oldest Beam:	48 days	Average Beam:	31 days
Cast-in-Place Deck:					
Strength:	4000 psi	Slump:	Not available	Prewetting:	Yes
Surface Finish:	Deep longitudinal tining				
Longitudinal Reinforcement:	No. 7 at 1 ft. full length with lap 2 No. 7 at 4 in. between, staggered; first cutoff at 7 ft. - 5 in. (end spans), second cutoff at 24 ft. - 10 in. from pier (end spans), none cutoff in center span				
Transverse Reinforcement:	No. 4 at 6 in.				
Cage Reinforcement:	No. 5 corner bars 4 No. 8 continuity bars No. 5 stirrups at 12 in., staggered 6" from trough hooks (6 in. total spacing) Total ρ_{cr} : 0.00763 (Area of trough hooks and stirrup leg crossing the longitudinal joint over the area of CIP concrete in the trough)				
Piers and Abutments:					
Bearing Pad:	Elastomeric bearing pad type 1, 6 in. strip under beam tabs Polystyrene under beam bearing, excluded from blockout and 4 in. gap				
Dowels:	Abutments: 2 No. 8 at 1 ft. in blockouts Piers: 4 No. 8 at 1 ft. square in blockouts 1 ft. - 6 in. projection, holes drilled and grouted Polystyrene wrapped outer 4 sets				
Notes:	Designed as simply supported but used continuous reinforcement over the piers. 30 minute wet curing spec was used for the deck. No wire mesh used, and dowel wrapping only on the south pier				

Table 2.7: Summary of design details for Bridge No. 49036 over Pike Creek near Little Falls, MN

Bridge Number:	49036	Generation:	Third	Completion Date:	08/11/09
Contractor:	Lunda	Beam Fabricator:	Cretex	Designer:	J. Lin / G. Feyissa
Location:	TH 238 over Pike Creek near Little Falls, D-3				
Bridge Dimensions:					
Total Length:	72 ft. - 2 in.	Span Length Ratio:	0.969		
Span 1:	23 ft. - 5 in.	Span 2:	24 ft. - 2 in.	Span 3:	23 ft. - 5 in.
Width:	43 ft. - 4 in.	Beams per Span:	8	Skew:	0 degrees
Precast Beam:					
Release Strength:	4000 psi	Final Strength:	6000 psi		
Depth:	12 in.	Flange Thickness:	3 in.	Flange Roughened:	No
Strand Diameter:	½ in.	Strand Number:	16	Strand Pattern:	8 at 2 in., 8 at 4 in.
Reinforcement:	2 rows of No. 4 composite action stirrups, 2 in. projection; at 6 in. to 10 in. for 19 ft. (from end), at 12 in. for 5 ft. to midspan, symmetric No. 6 transverse hooks at 12 in., not staggered, 1 1/8 in. from top of flanges 7 No. 8 top bars No. 4 confinement stirrups at 12 in.				
First Beam Cast:	06/17/09	Last Beam Cast:	07/16/09		
Deck Cast:	07/31/09	Open to Traffic:	08/11/09		
Youngest Beam:	15 days	Oldest Beam:	44 days	Average Beam:	28.1 days
Cast-in-Place Deck:					
Strength:	4000 psi	Slump:	Not available	Prewetting:	Yes
Surface Finish:	Deep transverse tining				
Longitudinal Reinforcement:	No. 7 at 4 in. staggered: full length with lap, first cutoff at 10 ft. from pier (end spans), second cutoff at 16 ft. from pier (end spans), none cutoff in center span				
Transverse Reinforcement:	No. 4 at 6 in.				
Cage Reinforcement:	No. 4 corner bars 4 No. 9 continuity bars No. 4 stirrups at 12 in., adjacent to hooks Total ρ_{cr} : 0.0100 (Area of trough hooks and stirrup leg crossing the longitudinal joint over the area of CIP concrete in the trough)				
Piers and Abutments:					
Bearing Pad:	Elastomeric bearing pad type 1, 6 in. strip under beam tabs Polystyrene under beam bearing, excluded from blockout and 4 in. gap				
Dowels:	Abutments: 2 No. 8 at 12 in. in blockouts Piers: 4 No. 8 at 1 ft. - 6 in. square in blockouts 12 in. projection, holes drilled and grouted Polystyrene wrapped outer 4 sets				
Notes:	Consider adding more room at the substructures to allow for beams that are slightly longer than plan, which was issue on this bridge. Used No. 3 bars @ 6 in. in lieu of welded wire fabric 30 minute wet curing spec was used for the deck.				

Table 3.1: Original crack width classification categories

Crack Classification	Crack Width
A	< 0.007 in.
B	0.008 in. – 0.022 in.
C	0.023 in. – 0.200 in.
D	> 0.200 in.

Table 3.2: Refined crack width classification categories

Crack Classification	Crack Width
A1	< 0.003 in.
A2	0.003 in. – 0.007 in.
B1	0.008 in. – 0.015 in.
B2	0.016 in. – 0.022 in.
C1	0.023 in. – 0.100 in.
C2	0.100 in. – 0.200 in.
D	> 0.200 in.

Table 3.3: List of cores taken from in-field PCSSS bridges with coordinate locations and rationale

Core Name	Longitudinal-Coordinate ¹	Transverse-Coordinate ²	Rationale
13004-1	38'-1" W	10'-8.5" S	Reflective cracking indicated by instrumentation
13004-2	38'-1" W	22'-8.5" S	Reflective cracking indicated by instrumentation
13004-3	8'-10" W	11'-8.5" S	Surface crack over web corner
13004-4	38'-1" W	9'-8.5" S	Web corner adjacent to 13004-1
33005-1	19'-7" S	11'-0.5" E	Joint adjacent to 33005-2
33005-2	19'-7" S	12'-1.75" E	Surface crack over web corner
33008-1	45'-4"	16'-6" W	Surface crack over longitudinal joint
33008-2	45'-4" N	22'-6" W	Longitudinal joint between likely reflective cracks
33008-3	45'-4" N	28'-6" W	Joint adjacent to 33008-4
33008-4	45'-4" N	29'-6" W	Surface crack over web corner
49007-1	52'-1" S	9'-0" E	Midspan of center span, possible cracking
49007-2	52'-1" S	15'-0" E	Midspan of center span, possible cracking
49007-3	19'-10" S	16'-0" E	Surface crack over web corner
49007-4	20'-2" S	15'-0" E	Joint adjacent to 49007-3
49036-1	12'-0" N	14'-0" W	Joint adjacent to 49036-3
49036-2	12'-0" N	8'-0" W	Longitudinal joint adjacent to possible cracking
49036-3	10'-3" N	15'-0" W	Surface crack over web corner

1. The coordinate location of a core is with respect to the working point (WP) indicated on the corresponding bridge diagram (Figure 3.1 through Figure 3.7). Longitudinal coordinate is in the direction parallel to the span direction, roughly in the indicated cardinal direction

2. Transverse coordinate is in the direction perpendicular to the span direction, roughly in the indicated cardinal direction

Table 3.4: Dates and bridge ages for each field bridge inspection

Bridge No.	Inspection No.	Date	Bridge Age (years)
13004	1	November 18 and 23, 2009	4.05
	2	June 22 and 24, 2010	4.63
33005	1	November 2, 2009	2.00
	2	June 29, 2010	2.66
	3	August 9, 2011	3.77
33008	1	November 4, 2009	2.00
	2	May 24, 2010	2.56
	3	June 16 and August 10, 2011	3.62
49007	1	October 12, 14, and 19, 2009	0.17
	2	June 14, 2010	0.84
	3	June 29, 2011	1.88
49036	1	November 6, 2009	0.24
	2	May 26, 2010	0.79
	3	June 24, 2011	1.87

Table 3.5: Summary of the observed cracks from the core examinations

Core Characteristics			Crack Characteristics			
Number ¹	Location ²	Diameter	Type ³	Location ⁴	Length ⁵	Width: Depth ⁶
13004-1	Joint	3¾"	Shrinkage Shrinkage	North - 1" W South - 0"	½" ¼"	(N) A1: 0"-½" (S) A1: 0"-¼"
13004-2	Joint	3¾"	Reflective Reflective Horizontal Shrinkage	North - 1¼" E South - 1½" E North - N/A ⁷ East - N/A ⁷	1" 1¼" 1 ¾" ½"	(N) A1: 12½"-13½" (S) A1: 12¼"-13½" (Horiz.) A2: 12" (E) A1: 0"-½"
<i>13004-3⁸</i>	<i>Web-CIP</i>	<i>3¾"</i>	<i>Shrinkage</i>	<i>West - N/A⁷</i>	<i>¼"</i>	<i>A1: 0"-¼"</i>
<i>13004-4⁸</i>	<i>Web-CIP</i>	<i>3¾"</i>	<i>Shrinkage</i>	<i>West - N/A⁷</i>	<i>½"</i>	<i>A1: 0"-½"</i>
33005-1	Joint	5½"	NONE ⁹			
33005-2	Web-CIP	3¾"	Shrinkage	South - ¾" E	¼"	A1: 0"-¼"
33008-1	Joint	5¾"	Reflective Reflective	North - ¼" E South - 0"	13¼" 13¼"	(N) B1: 0"-¾", A2: ¾"-3", A1: 3"- 3¼", A2: 3¼"-3¾", A1: 3¾"-4½", A2: 4½"-6", A1 6"- 13 ½" (S) B1: 0"-1", A2: 1"-3¼", A1: 3¼"-5½", A2: 5½"- 7", A1: 7"-13½"
33008-2	Joint	3¾"	Shrinkage Shrinkage	North - 1" E South - 1¼" E	½" ¼"	(N) A2: 0"-½" (S) A2: 0"-¼"
33008-3	Joint	5¾"	Reflective Reflective	North - 1" W South - 1" W	5¾" 2½"	(N) A1: 10"-12½" (S) A1: 6¾"-12½"
<i>33008-4⁸</i>	<i>Web-CIP</i>	<i>3¾"</i>	<i>Shrinkage</i> <i>Shrinkage</i>	<i>North - ¼" E</i> <i>South - ¼" E</i>	<i>3½"</i> <i>3½"</i>	(N) B1: 0"-1", A2: 1"-1½", B1: 1½"-2", A1: 2"-3½" (S) B1: 0"-1", A1: 1"-1½", A2: 1½"-3", A1: 3"-3½"
<i>49007-1⁸</i>	<i>Joint</i>	<i>3¾"</i>	<i>NONE⁹</i>			
<i>49007-2⁸</i>	<i>Joint</i>	<i>3¾"</i>	<i>NONE⁹</i>			
<i>49007-3⁸</i>	<i>Web-CIP</i>	<i>3¾"</i>	<i>Shrinkage</i>	<i>North - 0"</i>	<i>1"</i>	<i>A2: 0"-1"</i>
<i>49007-4⁸</i>	<i>Joint</i>	<i>3¾"</i>	<i>NONE⁹</i>			
<i>49036-1⁸</i>	<i>Joint</i>	<i>3¾"</i>	<i>NONE⁹</i>			
<i>49036-2⁸</i>	<i>Joint</i>	<i>3¾"</i>	<i>NONE⁹</i>			
<i>49036-3⁸</i>	<i>Web-CIP</i>	<i>3¾"</i>	<i>Shrinkage</i>	<i>East - 1¼" N</i>	<i>½"</i>	<i>A1: 0"-½"</i>

1 Bridge No. number followed by core number from the crack maps
 2 Intended core location in the cross section
 3 Identified as either reflective or shrinkage cracks
 4 Location defined by the core face followed by the transverse distance away from the joint or web-CIP interface
 5 Total length of the crack
 6 Width classifications given in Table 1 over the given depth. Depth given relative to the top of the core

7 N/A indicates the crack location could not be given in terms of the joint or web-CIP interface
 8 Entries in italics indicate the actual location of the core could not be verified with physical identification of a joint or web corner. In this case the core was unreliable with respect to whether or not the joint or web-CIP interface initiated reflective cracking in the general region of the core
 9 "NONE" indicates there were no cracks observed on the core

Table 3.6: Precasting data related to the in-field relative camber measurements of beams from Bridge No. 33008

	Beam Number ¹	Cast Date	Release Date	Curing Age (hr)	Beam Age at Erection ² (days)	Beam Age at Deck Placement ³ (days)	Release Camber (in.)	Relative Camber ⁴ (in.)
North End Span	B1-1	07-05-07	07-06-07	15.50	46	68	1/2	3/4
	B2-2	07-24-07	07-25-07	11.50	27	49	1/2	0
	B2-3	07-24-07	07-25-07	11.50	27	49	7/16	3/4
	B2-4	07-24-07	07-25-07	11.50	27	49	7/16	1
	B2-5	07-27-07	07-30-07	70.50	24	46	1/2	1/4
	B2-6	07-27-07	07-30-07	70.50	24	46	7/16	1/2
	B2-7	07-27-07	07-30-07	70.50	24	46	1/2	1/2
	B2-8	07-31-07	08-01-07	15.25	20	42	1/2	3/4
	B2-9	07-31-07	08-01-07	15.25	20	42	1/2	1 1/4
	B2-10	07-31-07	08-01-07	15.25	20	42	1/2	1
	B3-11	07-05-07	07-06-07	15.50	46	68	9/16	1 3/4
South End Span	B1-23	07-02-07	07-03-07	17.50	36	71	1/2	3/4
	B2-24	07-16-07	07-17-07	12.75	29	64	1/2	1/4
	B2-25	07-16-07	07-17-07	12.75	29	64	5/8	3/4
	B2-26	07-16-07	07-17-07	12.75	29	64	9/16	1/2
	B2-27	07-18-07	07-19-07	14.75	27	62	1/2	5/8
	B2-28	07-18-07	07-19-07	14.75	27	62	1/2	7/8
	B2-29	07-18-07	07-19-07	14.75	27	62	1/2	0
	B2-30	07-20-07	07-21-07	15.75	25	60	1/2	0
	B2-31	07-20-07	07-21-07	15.75	25	60	7/16	1/2
	B2-32	07-20-07	07-21-07	15.75	25	60	1/2	1/4
	B3-33	07-05-07	07-06-07	15.50	36	71	1/2	3/4

1 Beams were fabricated in groups of three, indicated by shading. Beams B1-1 and B3-11 were fabricated together.

2 North end span beams were placed on 08-20-07, south end span beams were placed on 08/28/07

3 CIP concrete deck was cast on 09-11-07

4 Observed camber relative to the minimum observed camber in each span. These values are shown in Figure 3.20 and Figure 3.21

Table 3.7: Beam age statistics for Bridge No. 33008 compared to the remaining field bridges

Bridge No.	Number of Beams per Span	Age at Beam Placement (days)			Age at Deck Casting (days)		
		Minimum	Maximum	Average	Minimum	Maximum	Average
33008	11	20	57	33.3	42	71	57.0
13004 ¹	13	4	15	9.4	21	32	26.2
33005	8	22	63	38.2	30	65	48.5
49007	7	6	40	22.7	15	48	31.0
49036	8	2	30	15.1	15	44	28.1

1. Beam age information for Bridge No. 13004 was only available for Stage I construction (north half)

Table 4.1: Aspect ratios of the five inspected bridges

Bridge Number	Aspect Ratio (L/W)
13004	0.945
33005	2.375 (25° skew)
33008	1.374
49007	2.648
49036	1.665

Table 5.1: Transverse deck reinforcement details compared to the recommendation by Frosh (2006)

	Original Design	Revised Design	Frosch Recommendation
Area, A_s (in ² /ft)	0.31	0.40	--
Spacing, s (in.)	12	6	9 (max)
Reinforcement ratio ¹ , ρ	0.0043	0.0056	0.0063 (min)

1. Reinforcement ratios were calculated using only the top 6 in. for the deck thickness: $\rho = (A_s)/(6 \text{ in})(12 \text{ in}) = A_s/(72 \text{ in}^2)$

Table 5.2: Dowel details for the five inspected PCSSS bridges

Bridge No.	At Piers	At Abutments	Wrapping [†]
13004	On CL of pier, No. 5 at 12 in. along center 36 ft. (outer 25% on each side had no dowels)	In blockouts, 3 No. 6 at 9 in.	No
33005	In blockouts, 4 No. 8 at 12 in. x 18 in. [‡]	In blockouts, 4 No. 6 at 11 in. [‡]	No
33008	In blockouts, 6 No. 6 at 9 in. x 18 in.	In blockouts, 3 No. 6 at 9 in.	No
49007	In blockouts, 4 No. 8 at 12 in. square	In blockouts, 2 No. 8 at 12 in.	Yes [¥]
49036	In blockouts, 4 No. 8 at 18 in. square	In blockouts, 2 No. 8 at 12 in.	Yes

[†] Polystyrene sleeves wrapped on dowels in outer two-thirds of blockouts

[‡] Rows were aligned with substructure skew

[¥] Only dowels on the south pier cap were wrapped

Table 6.1: Span length configurations covering the range of feasible designs for the parametric study to investigate simple vs. continuous system designs. The highlighted configurations were used to compare creep and shrinkage models and precast beam ages for design

Two Spans	Three Equal Spans	Three Unequal Spans
22 ft. – 22 ft.	24 ft. – 24 ft. – 24 ft.	22 ft. – 27 ft. – 22 ft.
62 ft. – 62 ft.	34 ft. – 34 ft. – 34 ft.	20 ft. – 30 ft. – 20 ft.
	50 ft. – 50 ft. – 50 ft.	45 ft. – 62 ft. – 45 ft.

Table 6.2: Results of the parametric study comparing the AASHTO 2004 and AASHTO 2010 creep and shrinkage model for use in PCSSS design

Configuration ¹ Creep and shrinkage model Span	50-50-50				20-30-20				22-22	
	AASHTO 2004		AASHTO 2010		AASHTO 2004		AASHTO 2010		AASHTO 2004	AASHTO 2010
	End	Center	End	Center	End	Center	End	Center		
Optimized Design										
Beam depth (in.)	20		18		12		12		10	10
Strand number	34	36	36	34	12	22	8	16	14	12
Precast concrete strength ² (ksi)	10.4		7.0		7.0		6.0		7.2	6.0
Precast concrete release strength ² (ksi)	5.0		6.0		4.0		4.0		4.0	4.0
Controlling limit state ³	SER III Pier	SER III Midspan	SER III Midspan	SER III Midspan	STR I	SER III Midspan	STR I	SER III Midspan	SER III Midspan	SER III Midspan
Restraint Moment										
Total loss percentage	17%	18%	18%	17%	14%	17%	13%	17%	14%	15%
Differential shrinkage (μϵ)	4		311		-117		196		-65	192
Initial precast creep (% of total creep)	9.1%		26.3%		16.0%		22.7%		18.8%	22.8%
Time-dependent restraint moment at pier (k-ft)	313	234	118	71	97	110	-4	20	88	14
Thermal gradient restraint moment at pier (k-ft)	414	277	348	233	202	140	196	136	161	156
Positive moment connection limit ⁴	1.2M _{cr}		RM		RM		RM		RM	RM
Continuity degree ⁵	Simple		Simple		5%		Full		Simple	Full

1 Configurations are named according to the span lengths in ft., e.g. 20-30-20 is a bridge with 20 ft. end spans and a 30 ft. center span

2 Nominal concrete strengths were $f'_c = 6.0$ ksi and $f'_{ci} = 4.0$ ksi

3 SERIII is the Service III limit state for bottom tension of prestressed elements; STRI is the Strength I limit state; locations Pier and Midspan are locations where SERIII was limited

4 Positive moment connection is limited by the lesser of $1.2M_{cr}$ and the total restraint moment, time-dependent and thermal (RM)

5 Continuity degree is "Full" if the continuity check passes and "Simple" if the continuity check fails with $1.0f_{LL}$. For partial continuity, the percentage of live load on a continuous system is given. In terms of percentages, "Full" corresponds to 100% and "Simple" corresponds to 0%.

Table 6.3: Results of the parametric study comparing 7-day and 14-day precast ages for use in PCSSS design

Configuration ¹	50-50-50				20-30-20				22-22	
Continuity time	7 Days		14 Days		7 Days		14 Days		7 Days	14 Days
Span	End	Center	End	Center	End	Center	End	Center		
Optimized Design										
Precast depth (in.)	18		18		12		12		10	10
Strand number	36	36	36	34	8	16	8	16	12	12
Precast concrete strength ² (ksi)	7.0		7.0		6.2		6.0		6.0	6.0
Precast concrete release strength ² (ksi)	6.6		6.0		5.6		4.0		5.2	4.0
Controlling limit state ³	SER III Midspan	SER III Midspan	SER III Midspan	SER III Midspan	STR I Midspan	SER III Midspan	STR I Midspan	SER III Midspan	SER III Midspan	SER III Midspan
Restraint Moment										
Time-dependent restraint moment at pier (k-ft)	194	134	118	71	-4	28	0	20	22	14
Thermal gradient restraint moment at pier (k-ft)	348	233	348	233	198	137	196	136	156	156
Positive moment connection limit ⁴	1.2M _{cr}		RM		RM		RM		RM	RM
Continuity degree ⁵	Simple		Simple		Full		Full		Full	Full

1 Configurations are named according to the span lengths in ft., e.g. 20-30-20 is a bridge with 20 ft. end spans and a 30 ft. center span

2 Nominal concrete strengths were $f'_c = 6.0$ ksi and $f'_{ci} = 4.0$ ksi

3 SERIII is the Service III limit state for bottom tension of prestressed elements; STRI is the Strength I limit state; locations Pier and Midspan are locations where SERIII was limited

4 Positive moment connection is limited by the lesser of $1.2M_{cr}$ and the total restraint moment, time-dependent and thermal (RM)

5 Continuity degree is "Full" if the continuity check passes and "Simple" if the continuity check fails with $1.0f_{LL}$. For partial continuity, the percentage of live load on a continuous system is given. In terms of percentages, "Full" corresponds to 100% and "Simple" corresponds to 0%.

Table 6.4: Continuous system designs for comparison in the parametric study. More economical designs are highlighted.

Configuration ¹	22-22		62-62		24-24-24		34-34-34		50-50-50		20-30-20		22-27-22		45-62-45	
	Span				End	Center	End	Center								
Precast depth (in.)	10	24	10		14		18		12		10		22			
Strand number	12	46	16	14	22	20	36	34	8	16	10	16	24	50		
Precast concrete strength (ksi)	6.0	7.0	6.0		6.0		7.0		6.0		6.0		7.4			
Precast concrete release strength (ksi)	4.0	6.0	4.0		4.0		6.0		4.0		4.0		6.0			
Controlling limit state ²	SER III	SER III	SER III		SER III		SER III		STR I	SER III	SER III		SER III			
Continuity degree ³	Full	Simple	17%		Simple		Simple		Full		Full		Simple			

1 Configurations are named according to the span lengths in ft., e.g. 20-30-20 is a bridge with 20 ft. end spans and a 30 ft. center span

2 SERIII is the Service III limit state for bottom tension of prestressed elements; STRI is the Strength I limit state

3 Continuity degree is "Full" if the continuity check passes and "Simple" if the continuity check fails with $1.0f_{LL}$. For partial continuity, the percentage of live load on a continuous system is given. In terms of percentages, "Full" corresponds to 100% and "Simple" corresponds to 0%.

Table 6.5: Simply-supported designs for comparison in the parametric study. More economical designs are highlighted

Configuration ¹	22-22		62-62		24-24-24		34-34-34		50-50-50		20-30-20		22-27-22		45-62-45	
	Span										End	Center	End	Center	End	Center
Precast depth (in.)	10	24	10		14		18		12		10		22			
Strand number	12	44	14		20		34		10	18	12	20	22	48		
Precast concrete strength (ksi)	6.0	7.0	6.0		6.0		7.0		6.0		6.0		7.0			
Precast concrete release strength (ksi)	4.0	6.0	4.0		4.0		6.0		4.0		4.0		6.0			
Controlling limit state ²	SER III	SER III	SER III		SER III		SER III		STR I	SER III	SER III		STR I	SER III		

1 Configurations are named according to the span lengths in ft., e.g. 20-30-20 is a bridge with 20 ft end spans and a 30 ft. center span

2 SERIII is the Service III limit state for bottom tension of prestressed elements; STRI is the Strength I limit state

Table 6.6: Redesigned prestressed beams for superimposed restraint moment with 4 No. 5 bars for positive moment connection (PMC) reinforcement

Configuration	Beam Depth (in.)	PMC Capacity, M_n (k-ft)	Original Strand Number*	Redesigned Strand Number*
22-22	10	70	12	14
62-62	24	223	44	46
24-24-24	10	70	14	16
34-34-34	14	94	20	24
50-50-50	18	120	34	36
20-30-20	12	83	10, 18	10, 20
22-27-22	10	70	12, 20	14, 24
45-62-45	22	200	22, 48	22, 52

* For two numbers shown, the first is for the end spans and the second is for the center span

Table 6.7: Comparison of the governing Service I load combination, the approximate Service I load combination with $\gamma = 1.2$, and the design moment capacity of No. 7 bars at 4 in., all at the pier

Span Configuration	SER I (k-ft)	Approx. SER I (k-ft)	ΦM_n of No. 7 at 4 in.
22 – 22	-233	-258	-546
62 – 62	-708	-961	-1227
24 – 24 – 24	-249	-250	-546
34 – 34 – 34	-348	-390	-741
50 – 50 – 50	-496	-611	-935
20 – 30 – 20	-275	-281	-643
22 – 27 – 22	-255	-261	-546
45 – 62 – 45	-599	-761	-1129

Figures

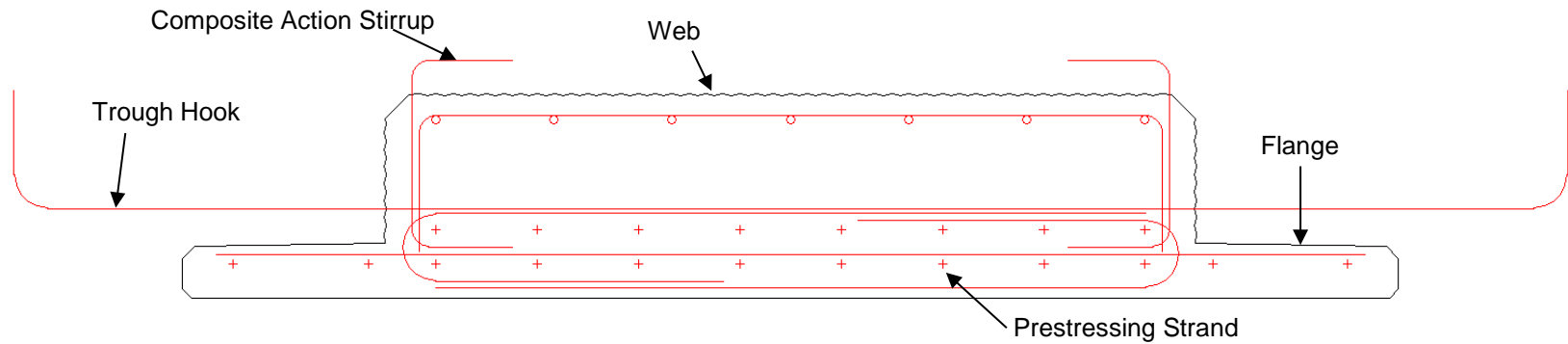


Figure 1.1: Typical cross section of a PCSSS inverted-tee beam at midspan

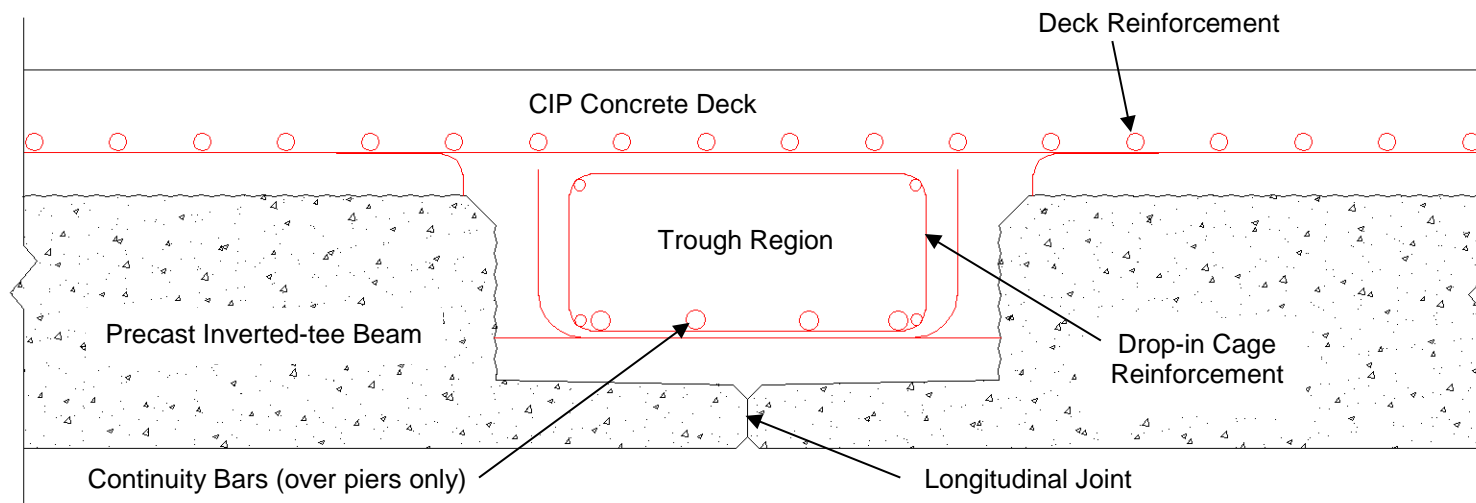
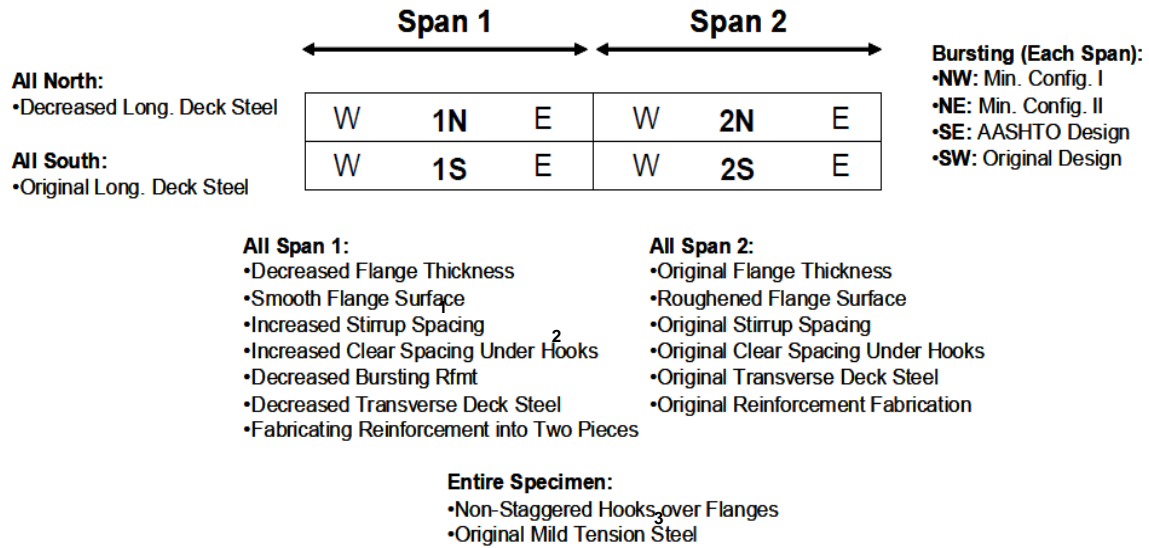
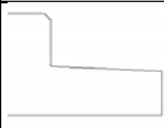
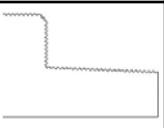
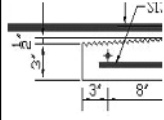
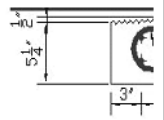
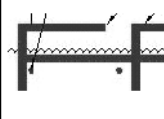
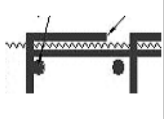
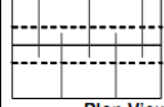
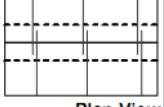


Figure 1.2: Typical cross section of the PCSSS precast beam joint with transverse and drop-in cage reinforcement and continuity bars (only over pier)



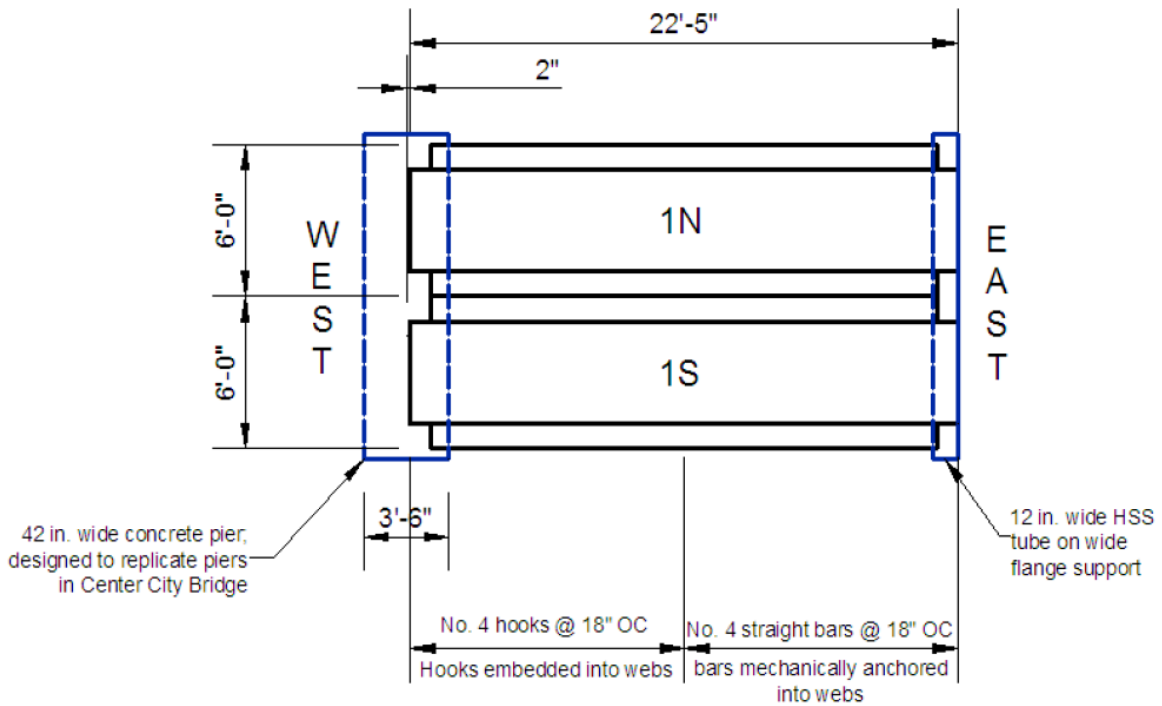
Figure 1.3: Photograph of Bridge No. 49036 during construction showing the drop-in cage reinforcement prior to placement of deck reinforcement and CIP concrete (MnDOT 2009)



		Proposed	Original			Proposed	Original
A	Smooth Flange Surface			F	Separating Web Reinforcement into Two Pieces		
B	Increased Stirrup Spacing	24 in.	12 in.	G	Decreased Bursting Reinforcement	#4 Stirrups @ 2 in. or #3 Stirrups @ 2 and 4 in.	2 #5 Stirrups @ 2, 4, and 6 in.
C	Decreased Flange Thickness			H	Decreased Longitudinal Deck Steel	#6 @ 6 in.	#7, #7, #8 @ 12 in.
D	Increased Clear Spacing Under Hooks			I	Decreased Transverse Deck Steel	#4 @ 12 in.	#5 @ 12 in.
E	Staggering Transverse Hooks over Flanges			J	Increased Chamfer @ Web Corner	1-1/2 in.	3/4 in.

1. "Stirrup Spacing" refers to the composite action stirrups
2. "Clear Spacing Under Hooks" refers to the composite action stirrups
3. "Mild Tension Steel" refers to the top longitudinal bars in the precast beam web.

Figure 2.1: Conceptual layout of the Concept 1 laboratory bridge specimen and accompanying table with descriptions of each design change (Smith et al. 2008).



Overall Details:

- 3 in. thick, smooth flanges
- 9 in. maximum trough reinforcement spacing
- No composite action stirrups

Figure 2.2: Plan layout of Concept bridge 2 with details of each half-span indicated (French et al. 2011)

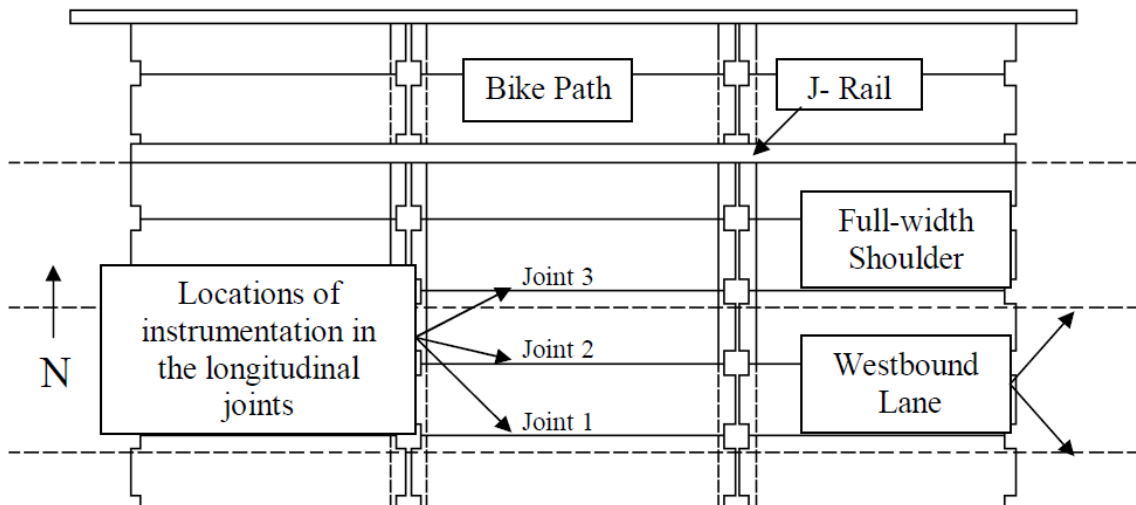


Figure 2.3: Plan view of Stage 1 of bridge construction for Bridge No. 13004 showing the instrumented joints (Bell et al. 2006)

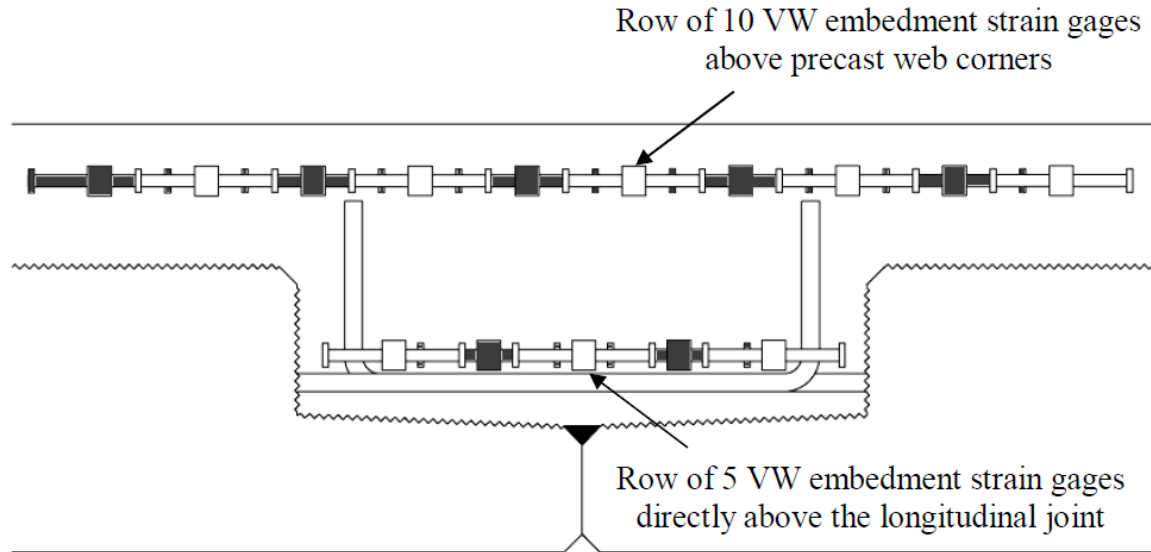


Figure 2.4: Cross-sectional view of the instrumentation detail for the embedment VW strain gauges over each longitudinal joint (Bell et al. 2006)

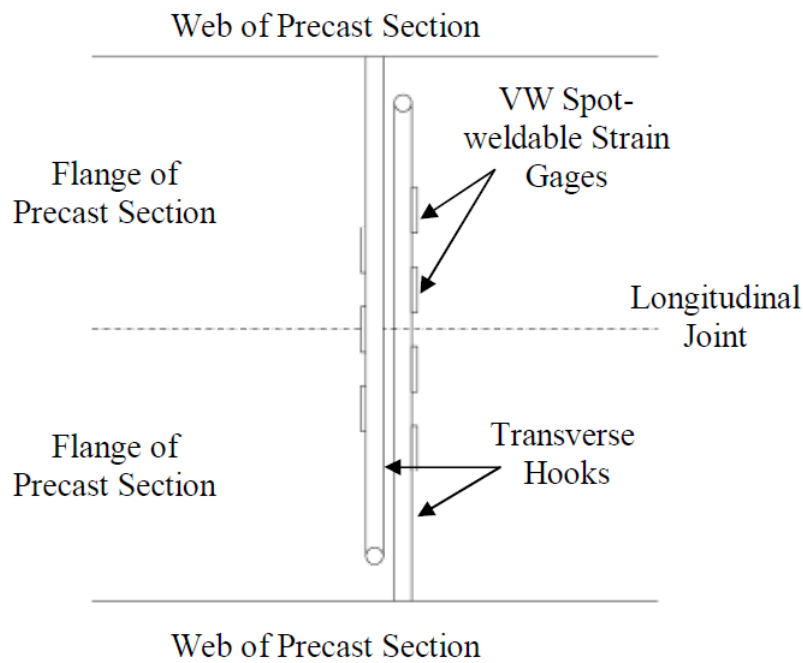


Figure 2.5: Plan view of instrumentation detail for VW spot-weldable strain gauges on transverse (trough) hooks (Bell et al. 2006)

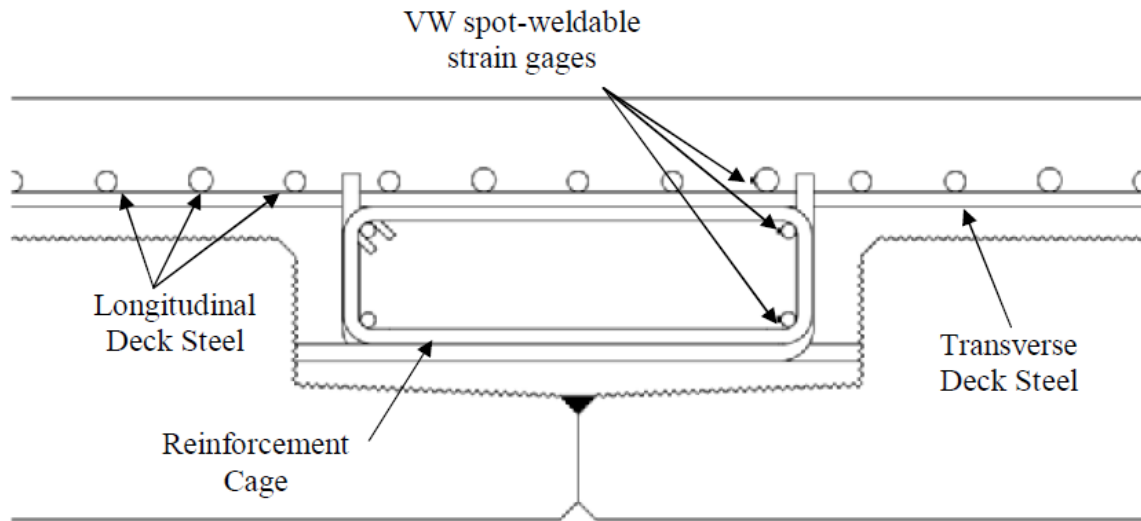


Figure 2.6: Cross-sectional view of the instrumentation detail for locations with 3 VW spot-weldable strain gauges, typical at midspan (Bell et al. 2006)

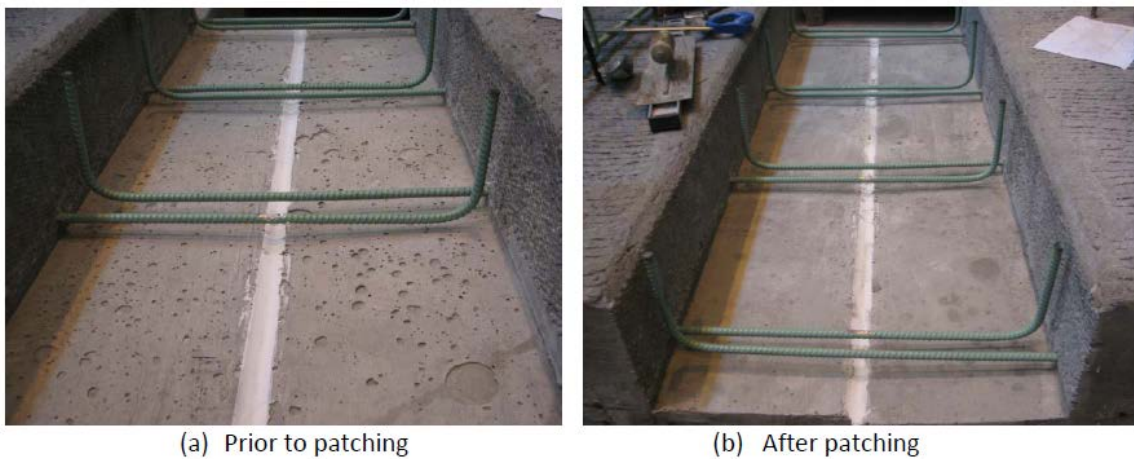


Figure 2.7: Precast flange surface (a) with voids from fabrication and (b) after patching preparation (French et al. 2011)

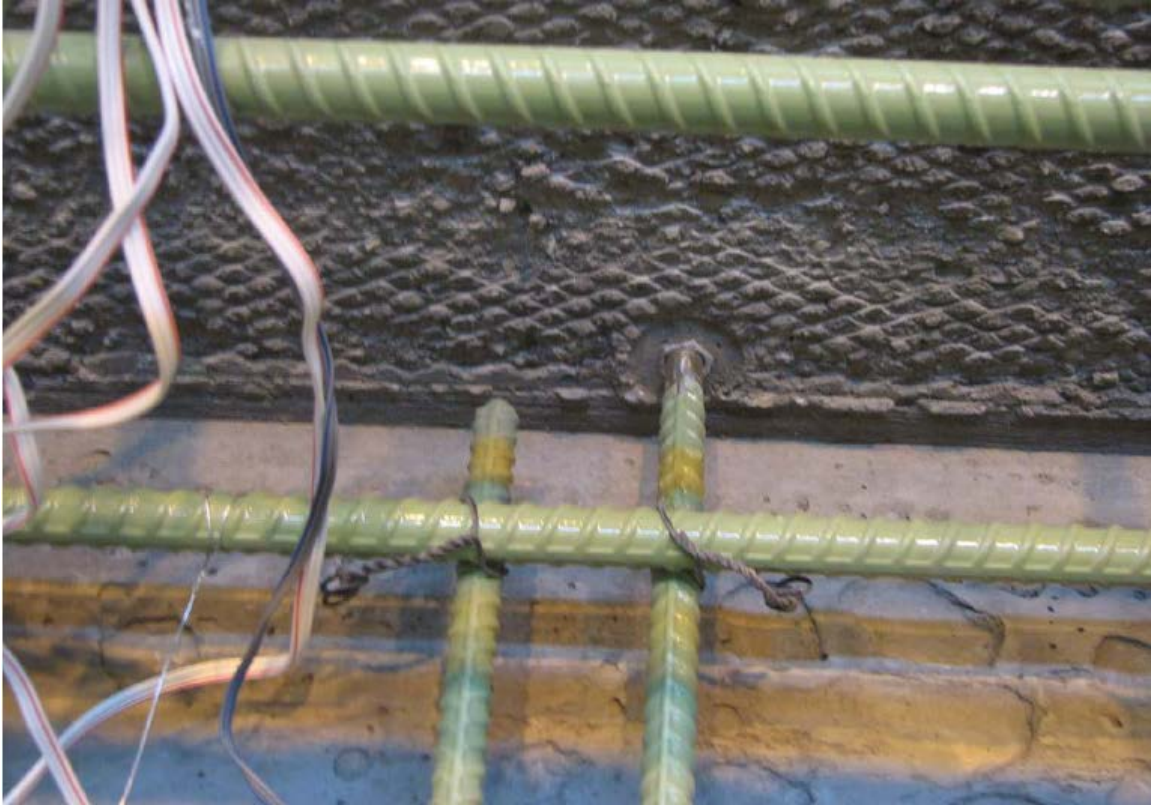


Figure 2.8: Photograph of threaded transverse reinforcement mechanically anchored into the precast web and the non-hooked terminal end (French et al. 2011)

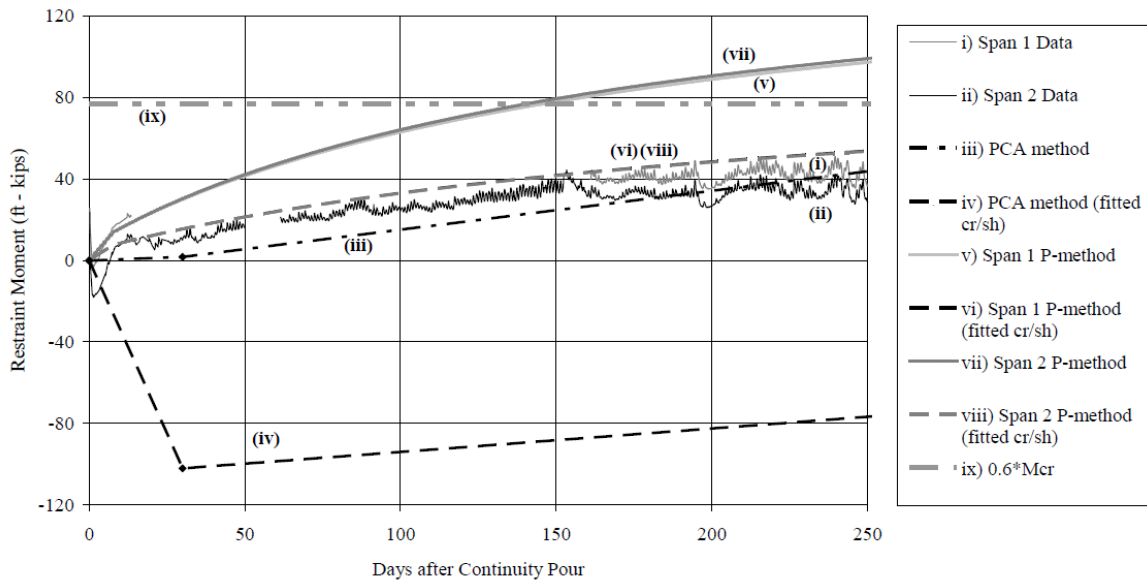


Figure 2.9: Restraint moments from the laboratory bridge specimen compared to PCA and P-method with creep and shrinkage models fitted to data (Smith et al. 2008)

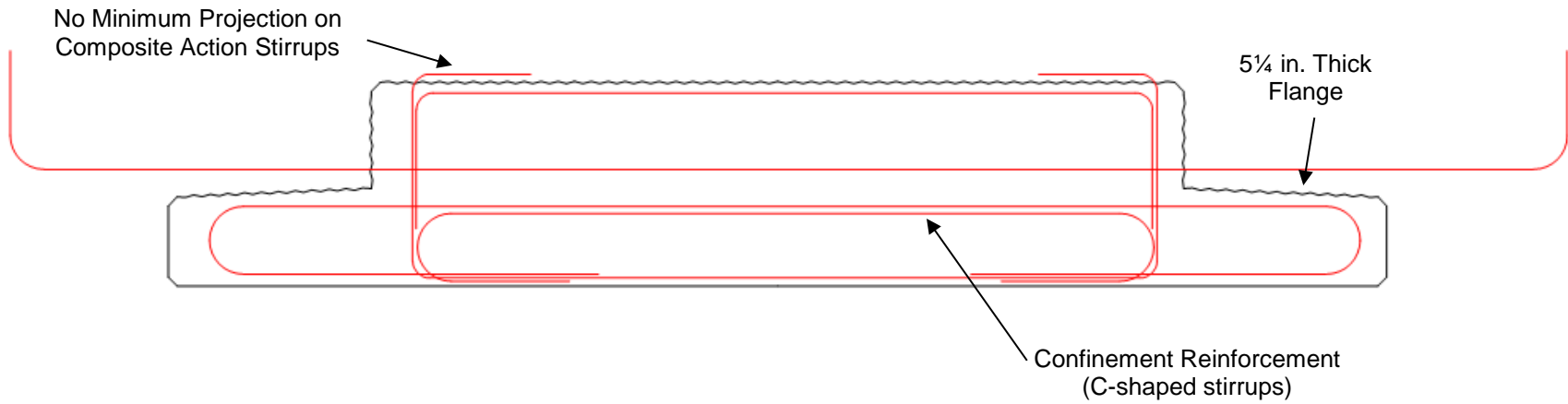


Figure 2.10: Typical PCSSS inverted-tee beam reinforcement at midspan from Generation 1

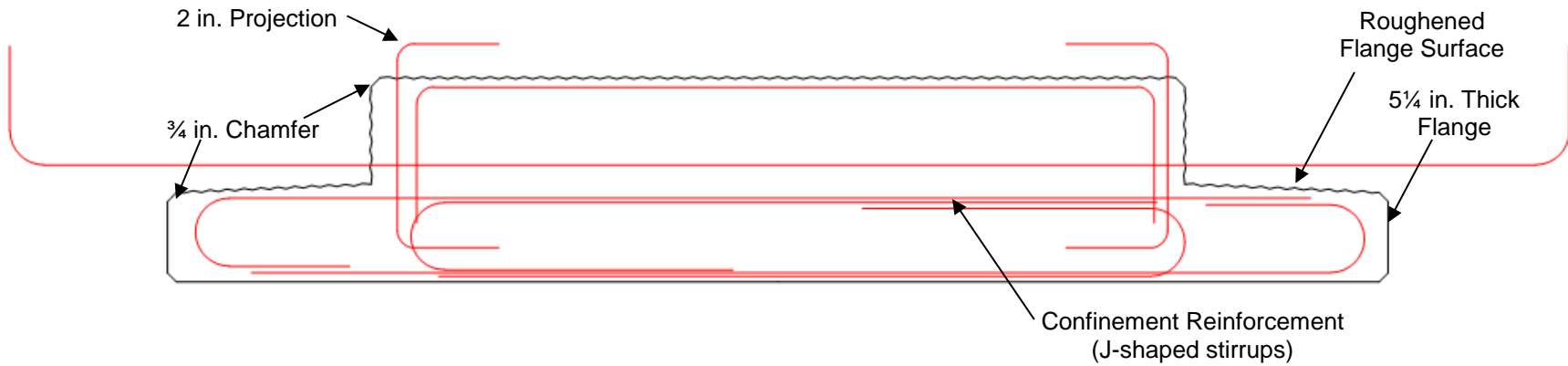


Figure 2.11: Typical PCSSS inverted-tee beam reinforcement at midspan from Generation 2

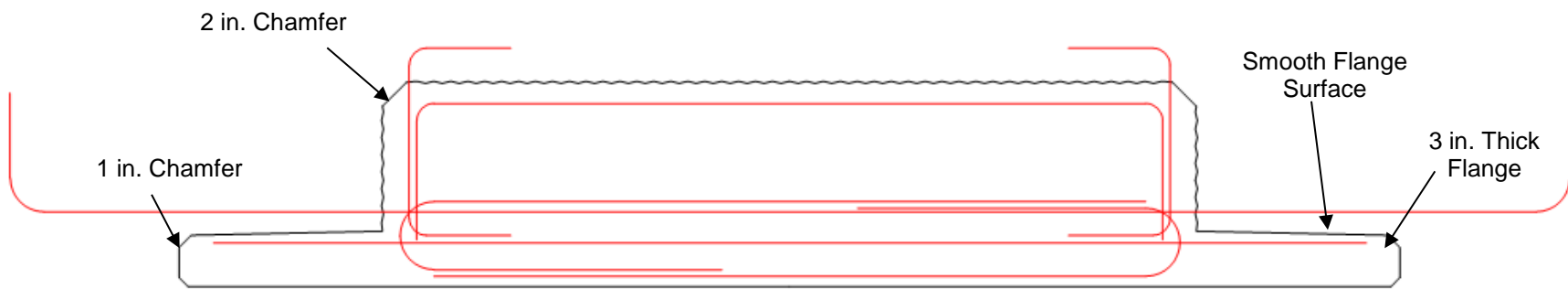


Figure 2.12: Typical PCSSS inverted-tee beam reinforcement at midspan from Generation 3

Bridge No. 13004

Scale: 1" = 11'-0"
 Built: 11/02/2005 (Generation 1)
 Inspection No. 2: 6/22 and 6/24, 2010

Age: 4.63 years
 Temperature: 53°F - 87°F (70°F average)
 Average Humidity: 72%
 Clouds/Precipitation: Clear

Precast Concrete
 Release Strength: 4500 psi
 Final Strength: 6500 psi
 Depth: 12 in.
 Flange Thickness: 5.25 in.
 Strand: 16 - 0.5 in. Ø

Cast-in-Place Concrete
 Strength: 4000 psi
 Slump: Not available
 Prewetted: No
 Surface Finish: Very shallow longitudinal tining

Reinforcement

- Precast:**
- No. 5 composite hooks at 1 ft over midspan, 1 in. projection
 - No. 6 transverse hooks at 1 ft, stag. at 2 in. and 10 in.
 - 7 No. 8 top bars
 - No. 4 ties at spacing of top hooks
- Deck Longitudinal:**
- No. 8 at 12 in., full length with lap splice
 - 2 No. 7 at 4 in. between, first cutoff at 10 ft from pier (end span and center span), second cutoff 16 ft from pier (end span only)
- Deck Transverse:**
- No. 5 at 12 in. with lap at staged construction joint
- Trough:**
- No. 5 corner bars
 - 4 No. 8 continuity bars at 6 in.
 - No. 5 stirrups at 12 in., adjacent to hooks
 - Overall spacing at 2 in., 10 in.

Piers and Abutments

- Dowels:**
- Cast in place prior to beam placement
 - In block-outs at abutments, 3 No. 6 @ 9 in.
 - Along CL of pier cap, between beam ends, No. 5 at 1 ft over center 36 ft
- Bearing:**
- Polystyrene under beam bearing, not at block-out or 4 in. gap
 - Elastomeric bearing pad type 1, 6 in. strip under beam tabs

Core Summary

- 1) Shrinkage crack: AI, 1/2 in. deep from surface
- 2) Reflective crack: AI, 1 1/4 in. deep from joint
- 3) Shrinkage crack: AI, 1/2 in. deep from surface
- 4) Shrinkage crack: AI, 1/2 in. deep from surface

Crack Classification

Class AI	< 0.003"
Class AII	0.003" - 0.007"
Class BI	0.008" - 0.015"
Class BII	0.016" - 0.022"
Class CI	0.023" - 0.100"
Class CII	0.100" - 0.200"
Class D	> 0.200"

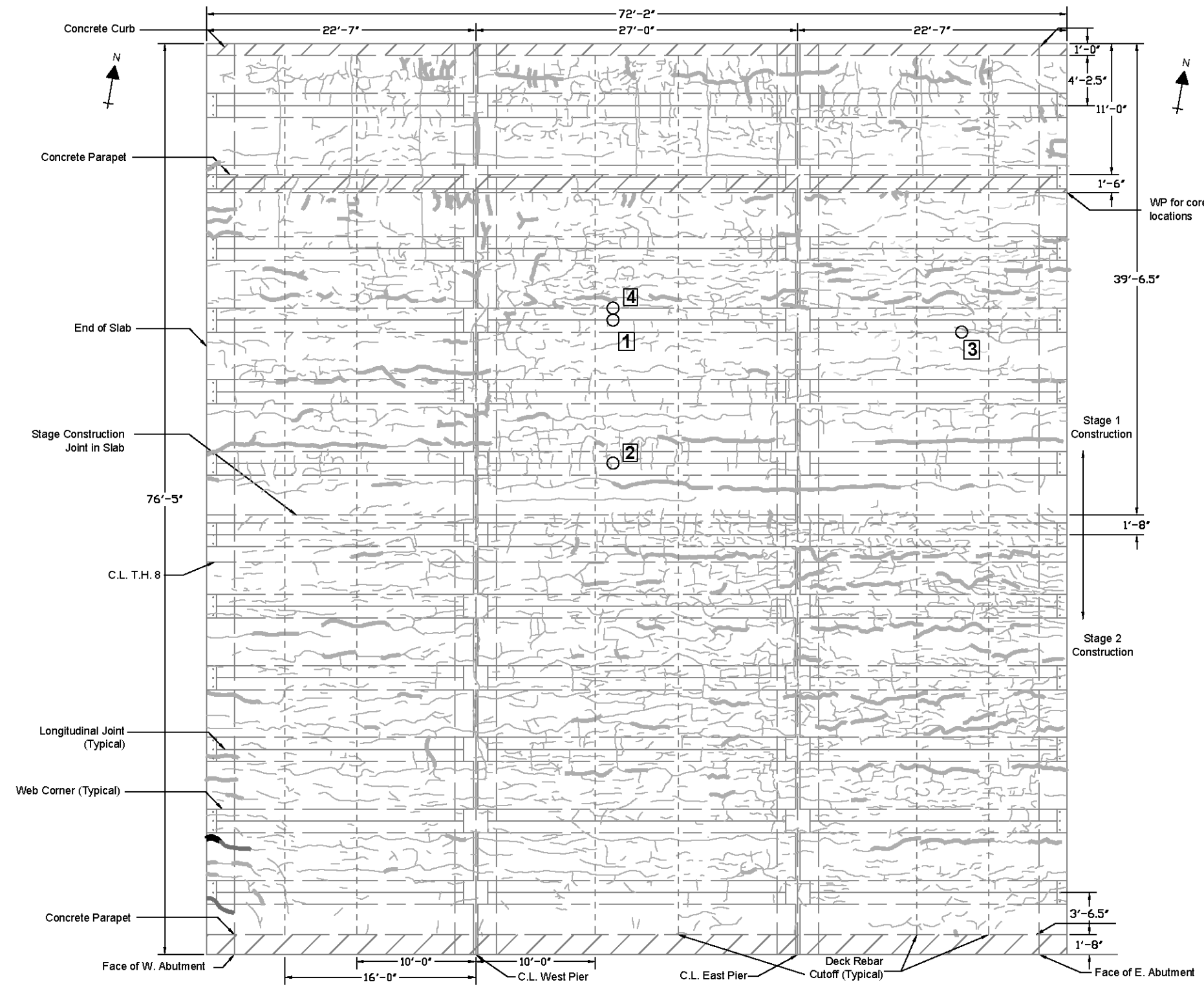


Figure 3.1: Crack map for Bridge No. 13004, Inspection No. 2, June 22 and 24, 2010 with core specimen locations indicated

Bridge No. 33005 (North)

Scale: 1" = 7'-0"
 Built: 11/02/2007 (Generation 2)
 Inspection No. 3: 08/09/2011

Age: 3.77 years
 Temperature: 55°F - 69°F (62°F average)
 Average Humidity: 57%
 Clouds/Precipitation: Overcast

Precast Concrete
 Release Strength: 4000 psi
 Final Strength: 6000 psi
 Depth: 14 in.
 Flange Thickness: 5.25 in.
 Strand: 22 - 0.5 in. Ø

Cast-in-Place Concrete
 Strength: 4000 psi
 Slump: 3 in.
 Prewetted: No
 Surface Finish: Shallow longitudinal tining

Reinforcement

- Precast:**
- No. 4 composite hooks at 2 ft over midspan, 2 in. projection
 - No. 6 transverse hooks at 1 ft, stag. at 3 in. and 9 in.
 - 7 No. 8 top bars
 - No. 4 ties at spacing of top hooks
- Deck Longitudinal:**
- No. 7 at 4 in.
 - Full length with lap, first cutoff at 7 ft -5 in. from pier (end span), second cutoff at 24 ft -10 in. (end span), 13 ft -2 in. from pier (center span)
- Deck Transverse:**
- No. 5 at 12 in.
- Trough:**
- No. 4 corner bars
 - 4 No. 9 continuity bars at 5 in.
 - No. 4 stirrups at 12 in., adjacent to hooks
 - Overall spacing at 3 in. and 9 in.

Piers and Abutments

- Dowels:**
- 1 ft. - 6 in. projection
 - Holes drilled after beams placed, grouted
 - Next to ends at abutments, 4 No. 8 at 11 in.
 - In block-outs at piers, 4 No. 8 at 12 in., 1 ft - 9 in. symmetric over CL pier
- Bearing:**
- Polystyrene under beam bearing, not at block-out or 4 in. gap
 - Elastomeric bearing pad type 1, 6 in. strip under beam tabs

Core Summary

- 1) No cracking
- 2) Shrinkage crack: AI, 1/4 in. deep from surface

Crack Classification

Class AI	< 0.003"
Class AII	0.003" - 0.007"
Class BI	0.008" - 0.015"
Class BII	0.016" - 0.022"
Class CI	0.023" - 0.100"
Class CII	0.100" - 0.200"
Class D	> 0.200"
---	Sealed, unknown width

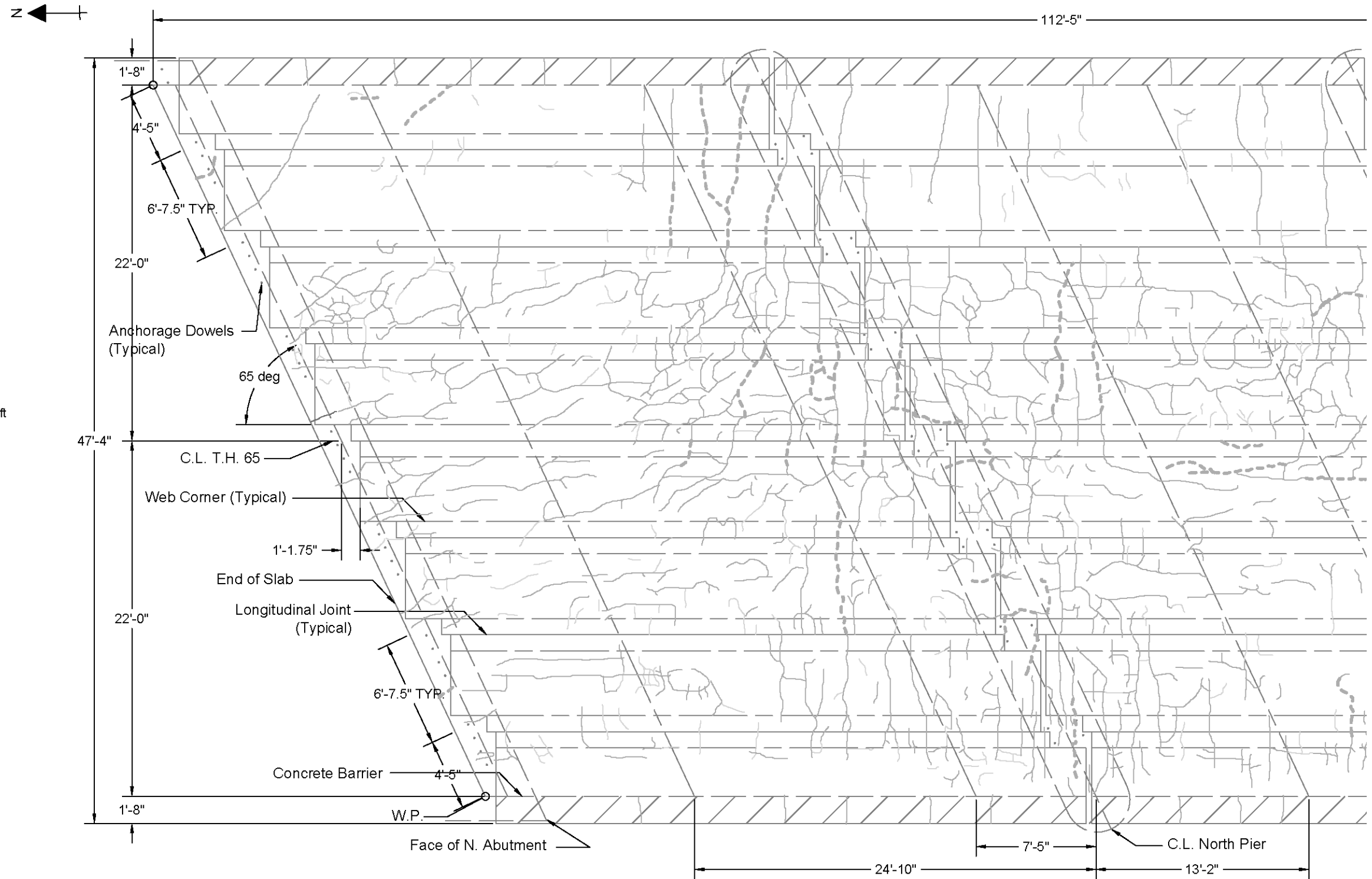


Figure 3.2: Crack map for the north side of Bridge No. 33005, Inspection No. 3, August 9, 2011

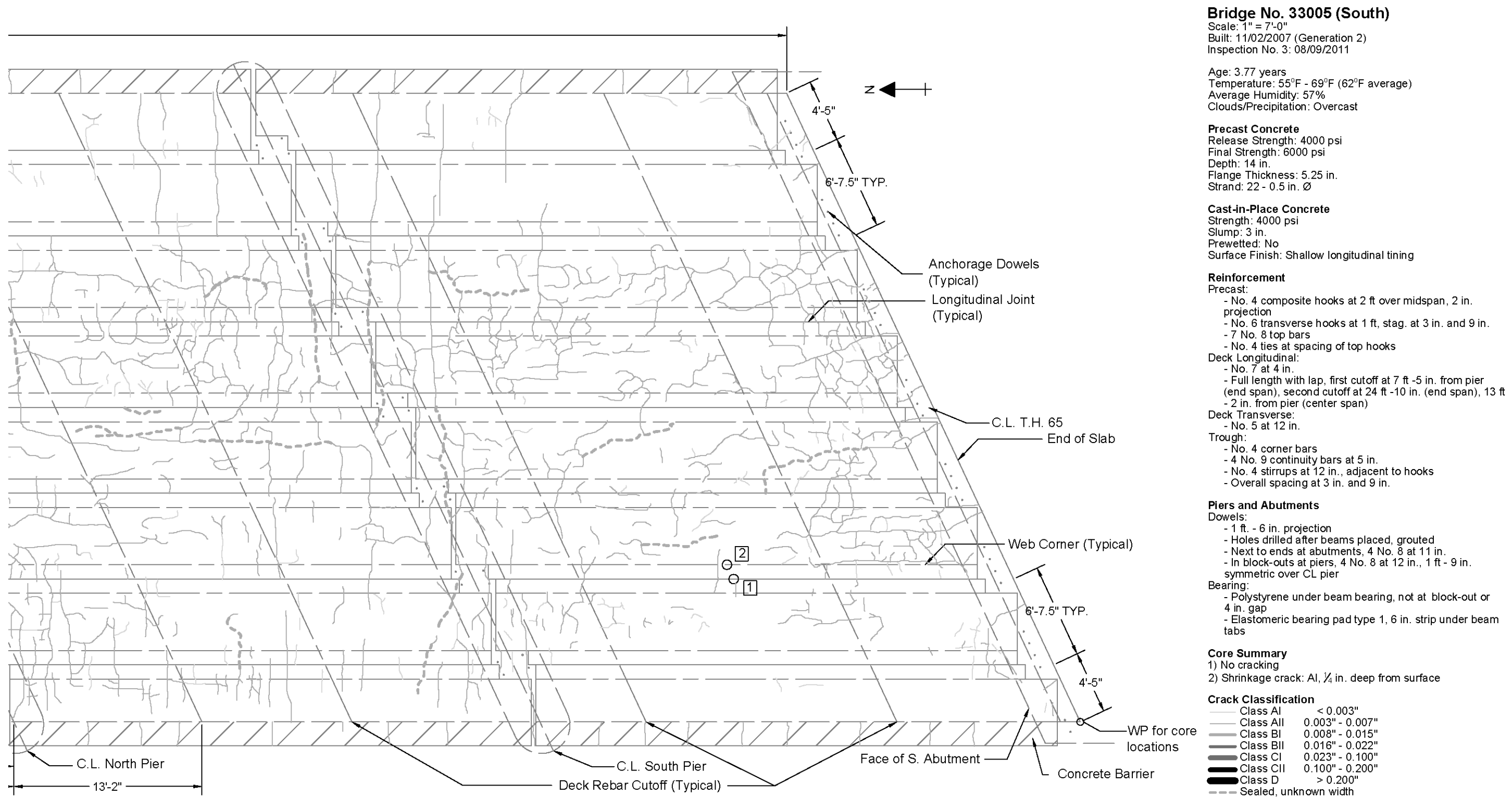


Figure 3.3: Crack map for the south side of Bridge No. 33005, Inspection No. 3, August 9, 2011 with core specimen locations indicated

Bridge No. 33008

Scale: 1" = 10'-0"
 Built: 11/02/2007 (Generation 2)
 Inspection No. 3: 06/16 and 08/10, 2011

Age: 1.62 years
 Temp.: 53°F-68°F (60°F average); 62°F-75°F (65°F average)
 Average Humidity: 76%
 Clouds/Precipitation: Overcast; clear

Precast Concrete
 Release Strength: 4500 psi
 Final Strength: 6500 psi
 Depth: 12 in.
 Flange Thickness: 5.25 in.
 Strand: 20 - 0.5 in. Ø

Cast-in-Place Concrete
 Strength: 4000 psi
 Slump: 3 in.
 Prewetted: No
 Surface Finish: Shallow longitudinal tining

Reinforcement

- Precast:**
- No. 5 composite hooks at 12 in. over midspan, 2 in. projection
 - No. 6 transverse hooks at 12 in., stag. at 4 in. and 8 in.
 - 7 No. 8 top bars
 - No. 4 ties at spacing of top hooks
- Deck Longitudinal:**
- No. 8 at 4 in.
 - Full length with lap; first cutoff at 10 ft from pier (end and center spans); second cutoff at 16 ft from pier (end span only)
- Deck Transverse:**
- No. 5 at 12 in.
- Trough:**
- No. 5 corner bars
 - 4 No. 8 continuity bars at 5 in.
 - No. 5 stirrups at 12 in., adjacent to hooks
 - Overall spacing at 4 in. and 8 in.

Piers and Abutments

- Dowels:**
- 12 in. projection
 - Cast in place with cap
 - In block-outs at abutments, 3 No. 6 at 9 in.
 - In block-outs at piers, 6 No. 6 at 9 in., 1 ft. - 6 in. symmetric over CL pier
- Bearing:**
- Polystyrene under bearing, not at blockout or 4 in. gap
 - Elastomeric bearing pad type 1, 6 in. strip under beam tabs

Core Summary

- 1) Reflective crack: AI - BI, full depth
- 2) Shrinkage crack: All, 1/2 in. deep from surface
- 3) Reflective crack: AI, 5 3/4 in. deep from joint
- 4) Shrinkage crack: AI - BI, 3 1/2 in. deep from surface

Crack Classification

Class AI	< 0.003"
Class AII	0.003" - 0.007"
Class BI	0.008" - 0.015"
Class BII	0.016" - 0.022"
Class CI	0.023" - 0.100"
Class CII	0.100" - 0.200"
Class D	> 0.200"
--- (dashed)	Sealed (unknown width)

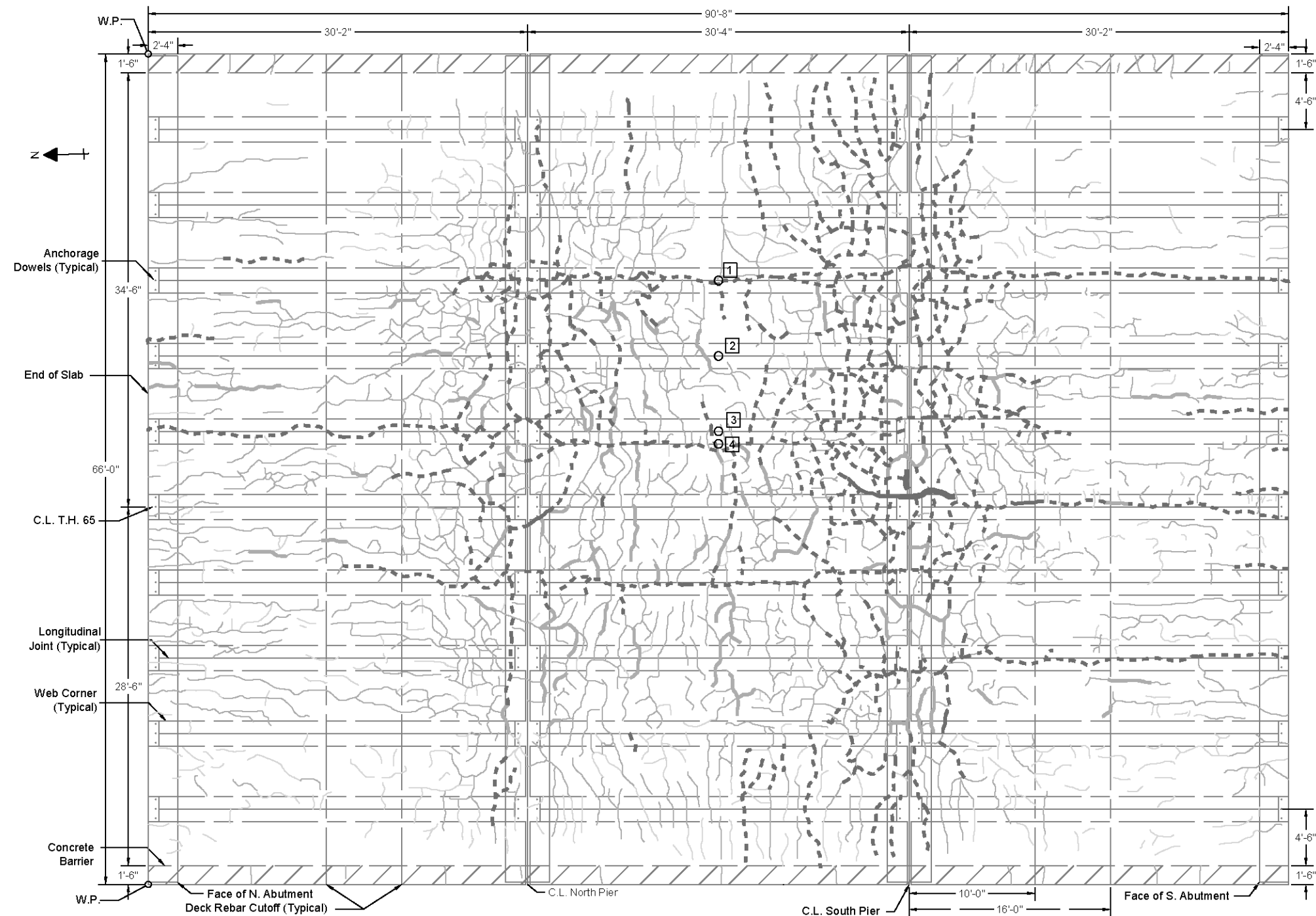


Figure 3.4: Crack map for Bridge No. 33008, Inspection No. 3, June 16 and August 10, 2011 with core specimen locations indicated

Bridge No. 49007 (South)

Scale: 1" = 6'-0"
 Built: 08/11/2009 (Generation 3)
 Inspection No. 3: 06/29/2011

Age: 1.88 years
 Temperature: 50°F - 80°F (65°F average)
 Average Humidity: 68%
 Clouds/Precipitation: Clear, some scattered clouds

Precast Concrete
 Release Strength: 4500 psi
 Final Strength: 6500 psi
 Depth: 16 in.
 Flange Thickness: 3 in.
 Strand: 22 - 0.5 in. Ø

Cast-in-Place Concrete
 Strength: 4000 psi
 Slump: Not available
 Prewetted: Yes
 Surface Finish: Deep longitudinal tining

Reinforcement

Precast:
 - No. 4 composite hooks at 6 in. for 11 ft, at 12 in. for 2 ft, at 2 ft for 8 ft (sym.), 2 in. projection
 - No. 6 transverse hooks at 12 in., stag. at 6 in.
 - 7 No. 8 top bars
 - No. 4 ties at spacing of top hooks

Deck Longitudinal:
 - No. 7 at 4 in.
 - Full length with lap, first cutoff at 7 ft. - 5 in. from pier (end span), second cutoff at 24 ft - 10 in. (end span), 13 ft - 2 in. from pier (center span)

Deck Transverse:
 - No. 4 at 6 in.

Trough:
 - No. 5 corner bars
 - 4 No. 8 continuity bars at 4.5 in.
 - No. 5 stirrups at 12 in., adjacent to hooks
 - Overall spacing at 6 in.

Piers and Abutments

Dowels:
 - 1 ft - 6 in. projection
 - Holes drilled after beams placed, grouted
 - Polystyrene wrapped 4 outer sets
 - In blockouts at abutments, 2 No. 8 at 12 in.
 - In blockouts at piers, 4 No. 8 at 12 in., 12 in. symmetric over CL pier

Bearing:
 - Polystyrene under bearing, not at blockout or 4 in. gap
 - Elastomeric bearing pad type 1, 6 in. strip under beam tabs

Core Summary

- 1) No cracking
- 2) No cracking
- 3) Shrinkage crack: All, 1 in. deep from surface
- 4) No cracking

Crack Classification

Class AI	< 0.003"
Class AII	0.003" - 0.007"
Class BI	0.008" - 0.015"
Class BII	0.016" - 0.022"
Class CI	0.023" - 0.100"
Class CII	0.100" - 0.200"
Class D	> 0.200"

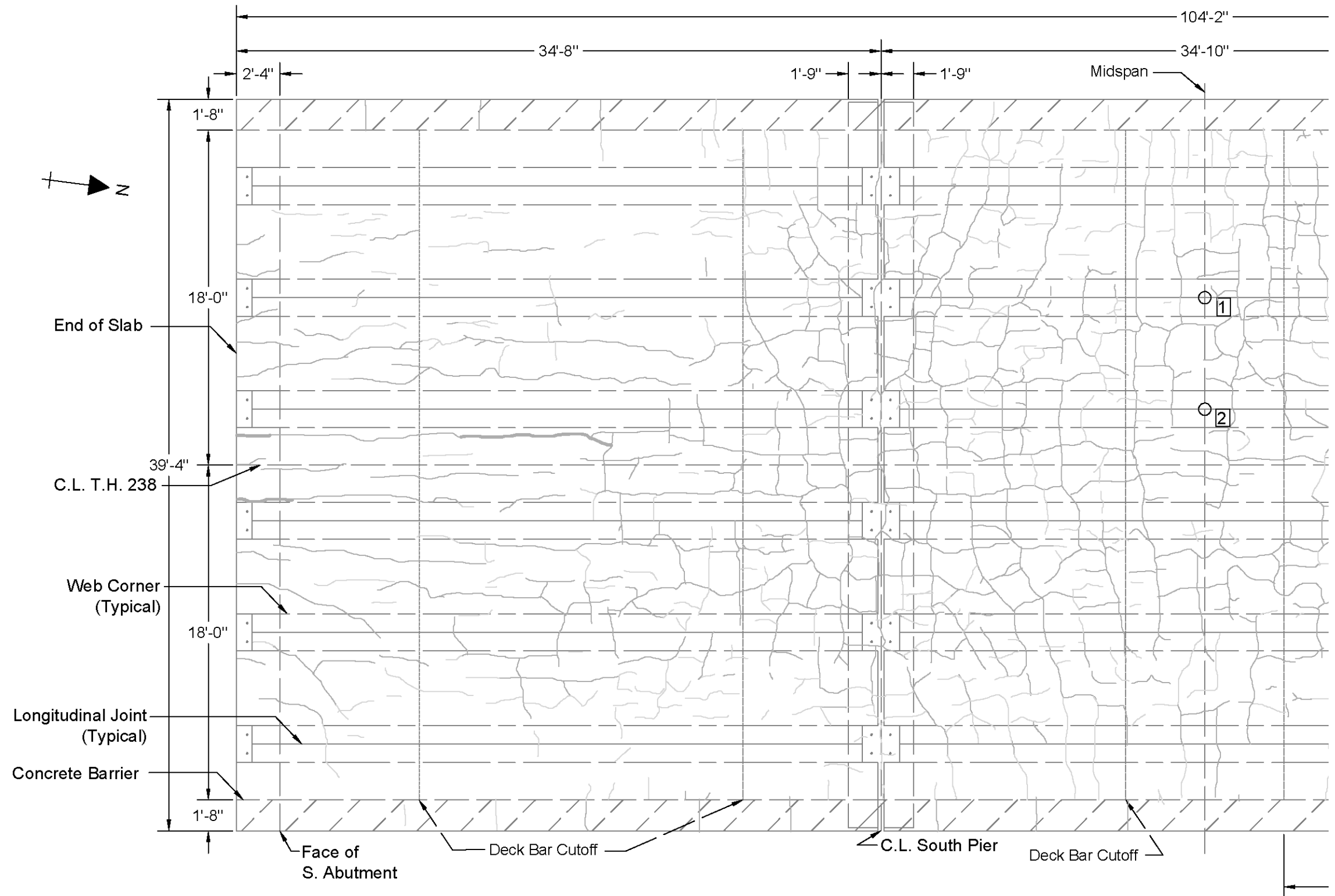
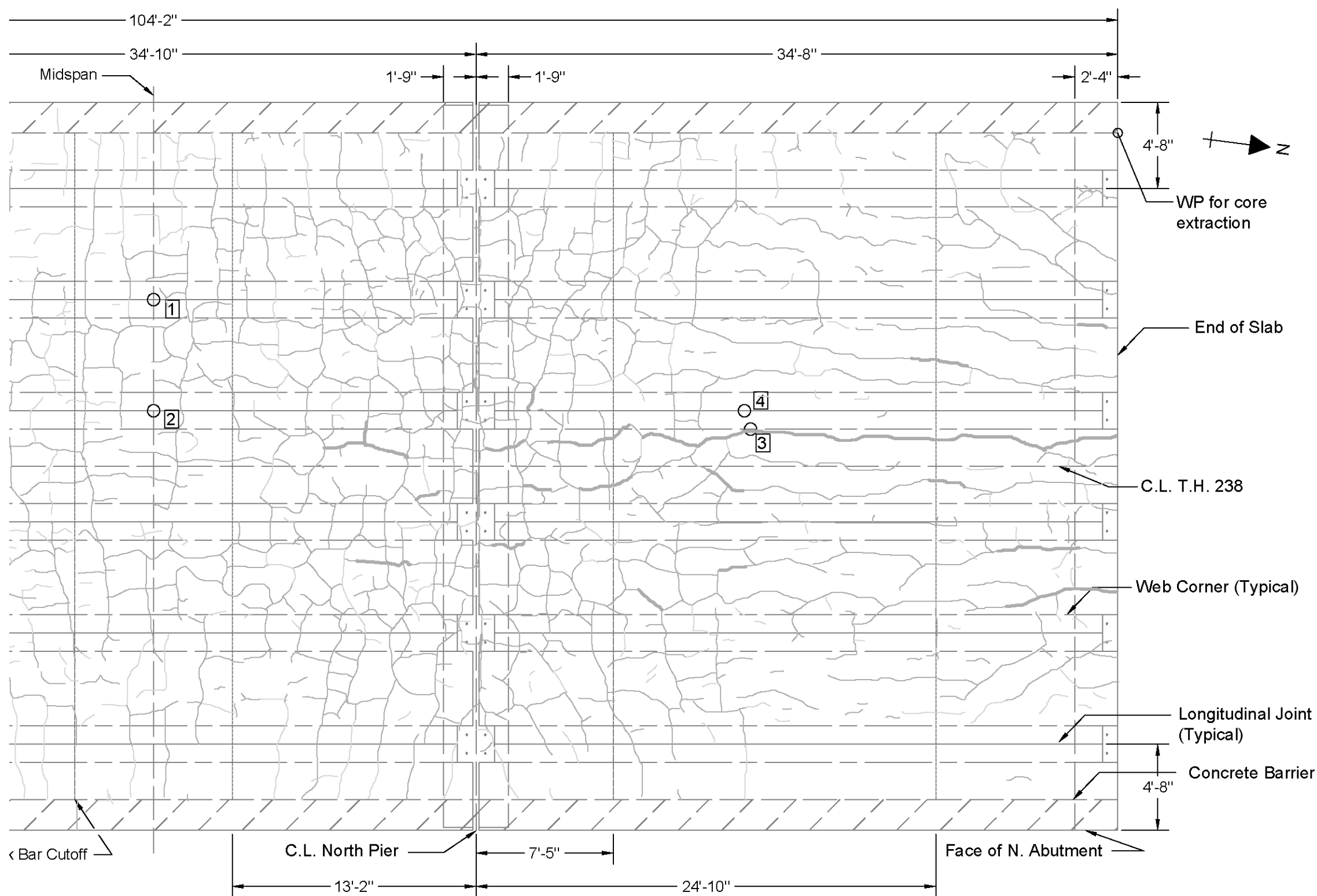


Figure 3.5: Crack map for the south side of Bridge No. 49007, Inspection No. 3, June 29, 2011 with core specimen locations indicated



Bridge No. 49007 (North)

Scale: 1" = 6'-0"
 Built: 08/11/2009 (Generation 3)
 Inspection No. 3: 06/29/2011

Age: 1.88 years
 Temperature: 50°F - 80°F (65°F average)
 Average Humidity: 68%
 Clouds/Precipitation: Clear, some scattered clouds

Precast Concrete

Release Strength: 4500 psi
 Final Strength: 6500 psi
 Depth: 16 in.
 Flange Thickness: 3 in.
 Strand: 22 - 0.5 in. Ø

Cast-in-Place Concrete

Strength: 4000 psi
 Slump: Not available
 Prewetted: Yes
 Surface Finish: Deep longitudinal tining

Reinforcement

Precast:

- No. 4 composite hooks at 6 in. for 11 ft, at 12 in. for 2 ft, at 2 ft for 8 ft (sym.), 2 in. projection
- No. 6 transverse hooks at 12 in., stag. at 6 in.
- 7 No. 8 top bars
- No. 4 ties at spacing of top hooks

Deck Longitudinal:

- No. 7 at 4 in.
- Full length with lap, first cutoff at 7 ft. - 5 in. from pier (end span), second cutoff at 24 ft - 10 in. (end span), 13 ft - 2 in. from pier (center span)

Deck Transverse:

- No. 4 at 6 in.

Trough:

- No. 5 corner bars
- 4 No. 8 continuity bars at 4.5 in.
- No. 5 stirrups at 12 in., adjacent to hooks
- Overall spacing at 6 in.

Piers and Abutments

Dowels:

- 1 ft - 6 in. projection
- Holes drilled after beams placed, grouted
- Polystyrene wrapped 4 outer sets
- In blockouts at abutments, 2 No. 8 at 12 in.
- In blockouts at piers, 4 No. 8 at 12 in., 12 in. symmetric over CL pier

Bearing:

- Polystyrene under bearing, not at blockout or 4 in. gap
- Elastomeric bearing pad type 1, 6 in. strip under beam tabs

Core Summary

- 1) No cracking
- 2) No cracking
- 3) Shrinkage crack: All, 1 in. deep from surface
- 4) No cracking

Crack Classification

Class AI	< 0.003"
Class AII	0.003" - 0.007"
Class BI	0.008" - 0.015"
Class BII	0.016" - 0.022"
Class CI	0.023" - 0.100"
Class CII	0.100" - 0.200"
Class D	> 0.200"

Figure 3.6: Crack map for the north side of Bridge No. 49007, Inspection No. 3, June 29, 2011 with core specimen locations indicated

Bridge No. 49036

Scale: 1" = 7'-0"
 Built: 08/11/2009 (Generation 3)
 Inspection No. 3: 06/24/2011

Age: 1.87 years
 Temperature: 42°F - 73°F (58°F average)
 Average Humidity: 67%
 Clouds/Precipitation: Clear

Precast Concrete
 Release Strength: 4000 psi
 Final Strength: 6000 psi
 Depth: 12 in.
 Flange Thickness: 3 in.
 Strand: 16, 0.5 in.

Cast-in-Place Concrete
 Strength: 4000 psi
 Slump: Not available
 Prewetted: Yes
 Surface Finish: Deep transverse tining

Reinforcement
Precast:
 - No. 4 composite hooks at 6 in. to 10 in. for 19 ft, at 12 in. for 5 ft (sym.), 2 in. projection
 - No. 6 transverse hooks at 1 ft, not staggered
 - 7 No. 8 top bars
 - No. 4 ties at spacing of top hooks
Deck Longitudinal:
 - No. 7 at 4 in.
 - Full length with lap, first cutoff at 10 ft from pier (end and center span), second cutoff at 16 ft from pier (end span only)
Deck Transverse:
 - No. 4 at 6 in.
Trough:
 - No. 5 corner bars
 - 4 No. 9 continuity bars at 4.5 in.
 - No. 5 stirrups at 12 in., adjacent to hooks
 - Overall spacing at 12 in.

Piers and Abutments
Dowels:
 - 12 in. projection
 - Holes drilled after beams placed, grouted
 - Polystyrene wrapped 4 outer sets
 - In block-outs at abutments, 2 No. 8 at 12 in.
 - In block-outs at piers, 4 No. 8 at 1 ft - 6 in., 1 ft - 6 in. symmetric over CL pier
Bearing:
 - Polystyrene under beam bearing, not at block-out or 4 in. gap
 - Elastomeric bearing pad type 1, 6 in. strip under beam tabs

Core Summary
 1) No cracking
 2) No cracking
 3) Shrinkage crack: AI, 1/2 in. deep from surface

Crack Classification

Class AI	< 0.003"
Class AII	0.003" - 0.007"
Class BI	0.008" - 0.015"
Class BII	0.016" - 0.022"
Class CI	0.023" - 0.100"
Class CII	0.100" - 0.200"
Class D	> 0.200"

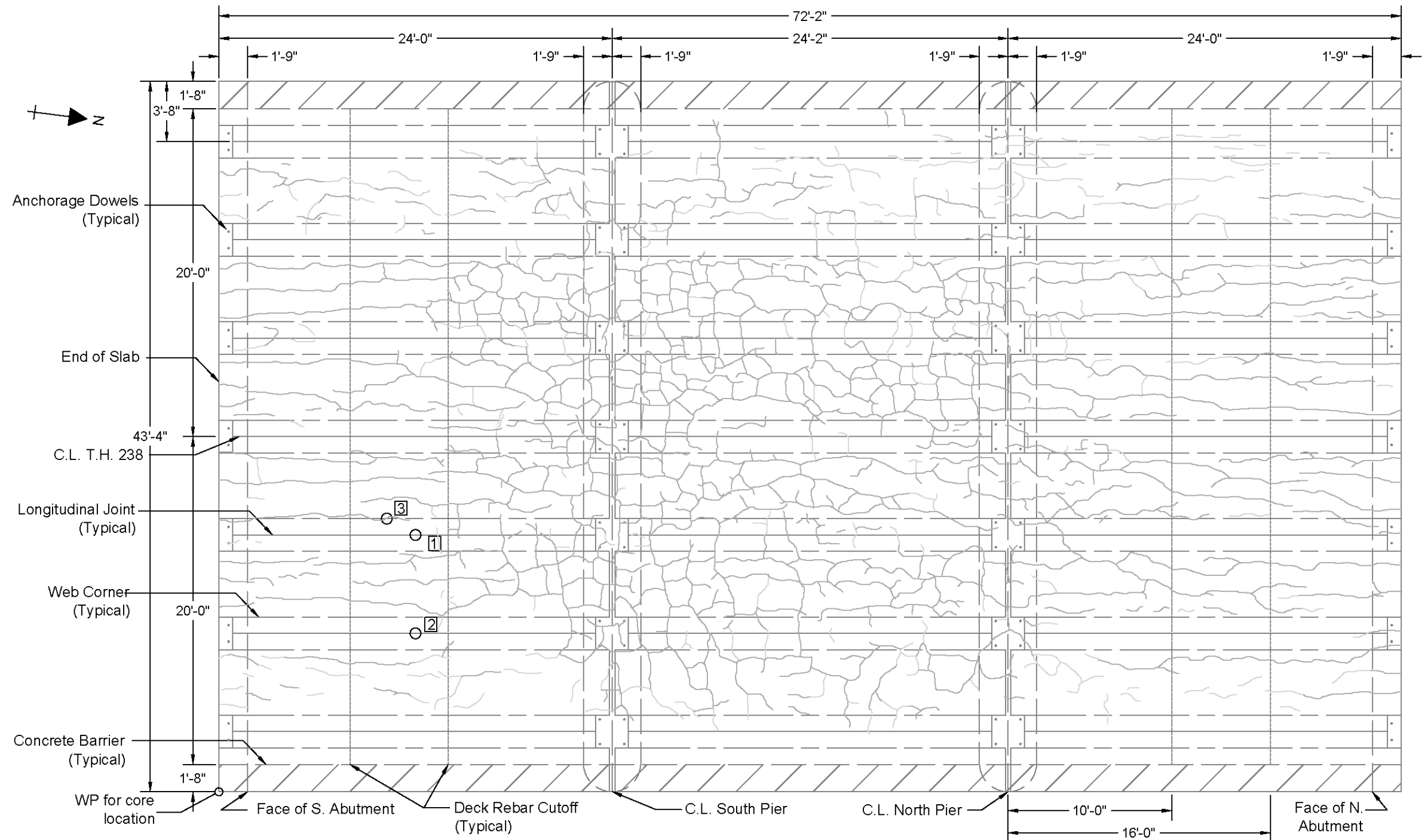


Figure 3.7: Crack map for Bridge No. 49036, Inspection No. 3, June 24, 2011 with core specimen locations indicated

Bridge No. 33532
 Scale: 1" = 8'-0"
 Built: 1995 (Slab Span)
 Inspection No. 1: 09/16/2010

Age: 15 years
 Temperature: 32°F - 55°F (42°F average)
 Average Humidity: 70%
 Clouds/Precipitation: Overcast

Slab Concrete
 Strength: 4000 psi
 Slump: Not available
 Prewetted: No
 Surface Finish: Transverse tining

Reinforcement
 Top Longitudinal:
 - No. 8 at 12 in., cutoff at 16 ft - 10 in.
 - Alt. No. 8 at 12 in., cutoff at 11 ft - 5 in. and 6 ft - 3 in.
 Bottom Longitudinal:
 - No. 7 at 12 in. full length
 - Alt. No. 7 at 12 in. cutoff over piers
 Transverse:
 - Top No. 4 at 1 ft - 6 in.
 - Bottom No. 5 at 12 in.

Pier Anchorage
 - No. 6 paired hooks at 12 in.

Crack Classification

Class AI	< 0.003"
Class AII	0.003" - 0.007"
Class BI	0.008" - 0.015"
Class BII	0.016" - 0.022"
Class CI	0.023" - 0.100"
Class CII	0.100" - 0.200"
Class D	> 0.200"

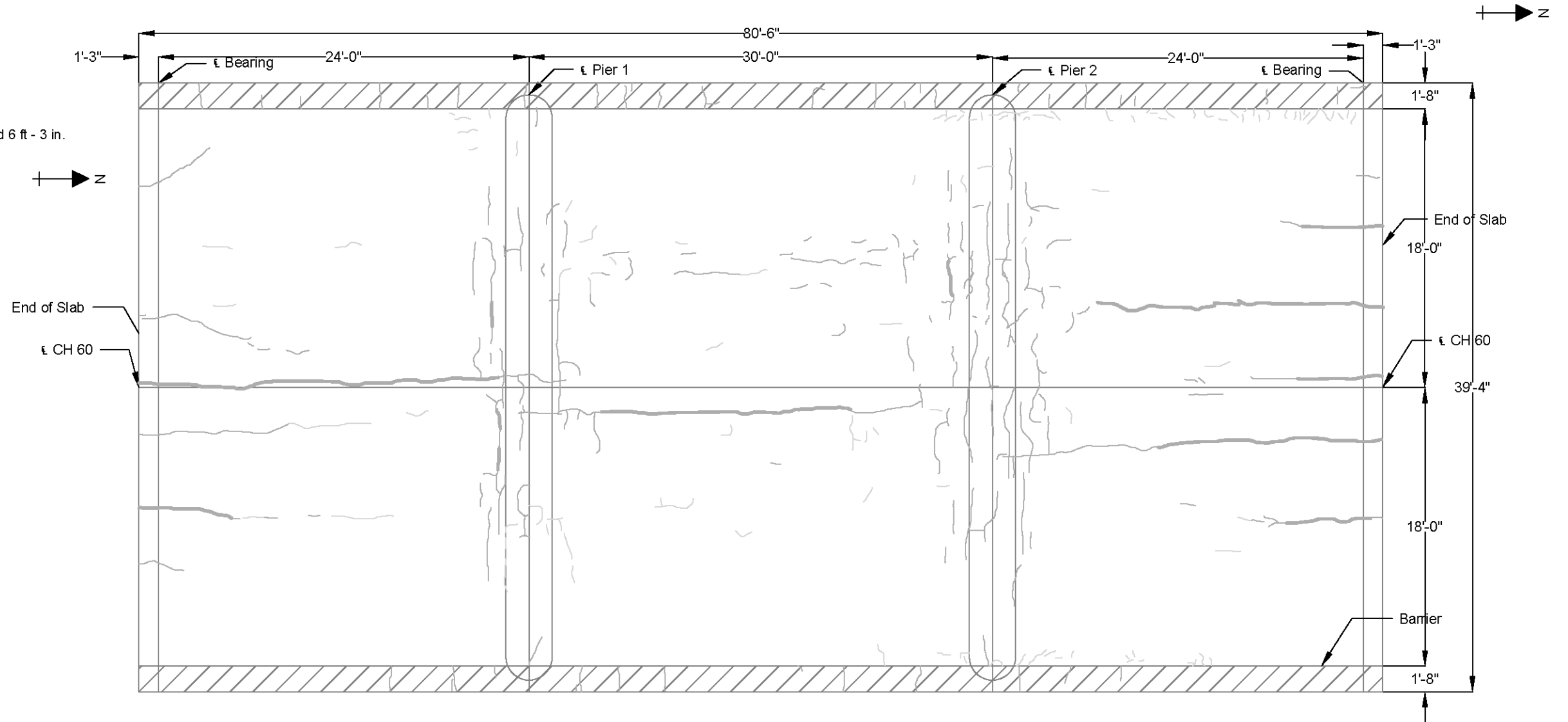


Figure 3.8: Crack map for Bridge No. 33532 (conventional slab-span) from September 16, 2010



Figure 3.9: Efflorescence at a longitudinal joint underneath Bridge No. 49007

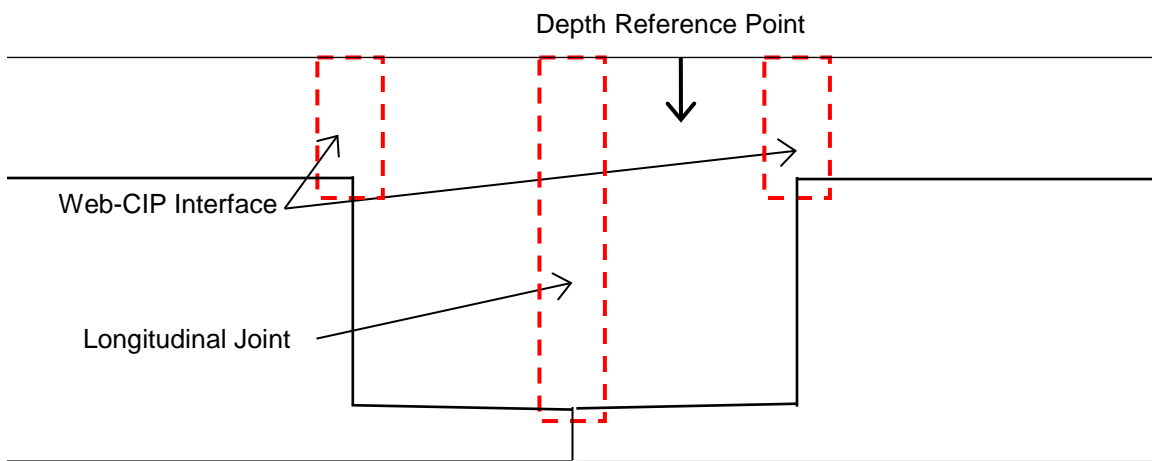


Figure 3.10: Terminology for the location and depth of cores

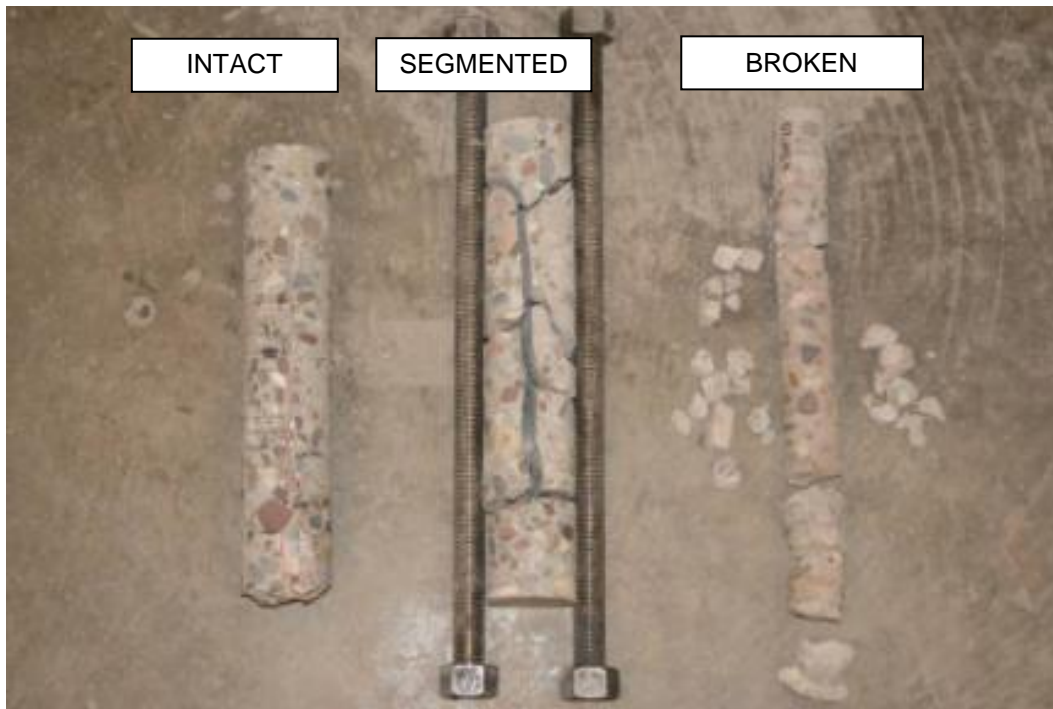


Figure 3.11: Definitions for core condition due to extraction; Intact: very few sections, easy to reassemble; Segmented: many sections, easy to reassemble; Broken: very many sections, difficult to reassemble



Figure 3.12: Examples of a physically identifiable longitudinal joint (left) and web corner (right)



Figure 3.13: Crack on the surface of Core 33008-1 labeled by a dotted red line

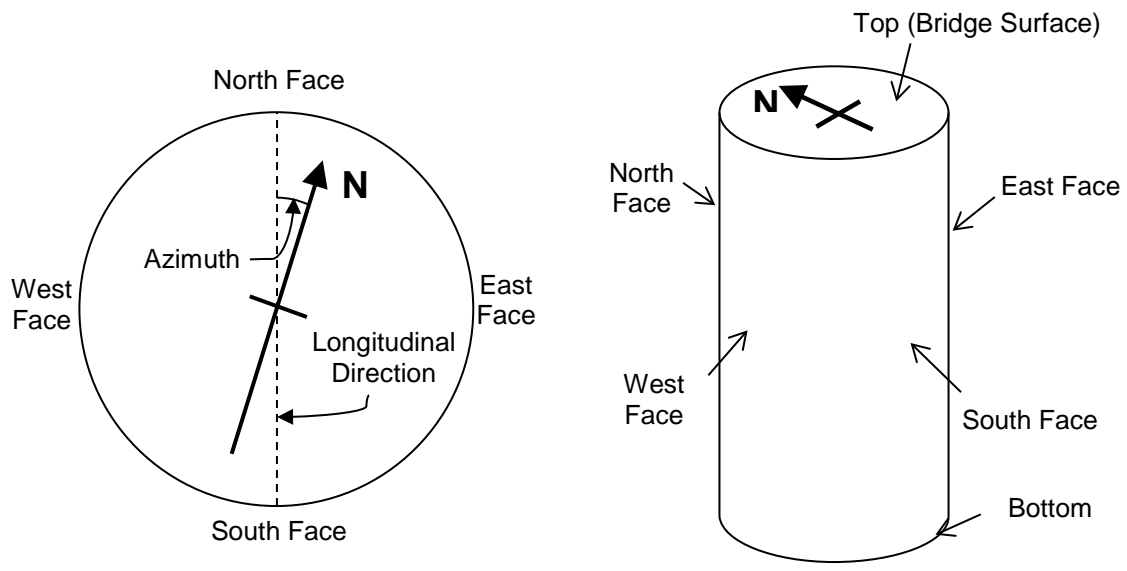


Figure 3.14: Orientation of core faces for locating cracks and reinforcement. The local faces (north, south, east and west) are associated with the longitudinal and transverse directions of the bridge, as shown. The azimuth for each core is the angle between true North and the local north face direction.

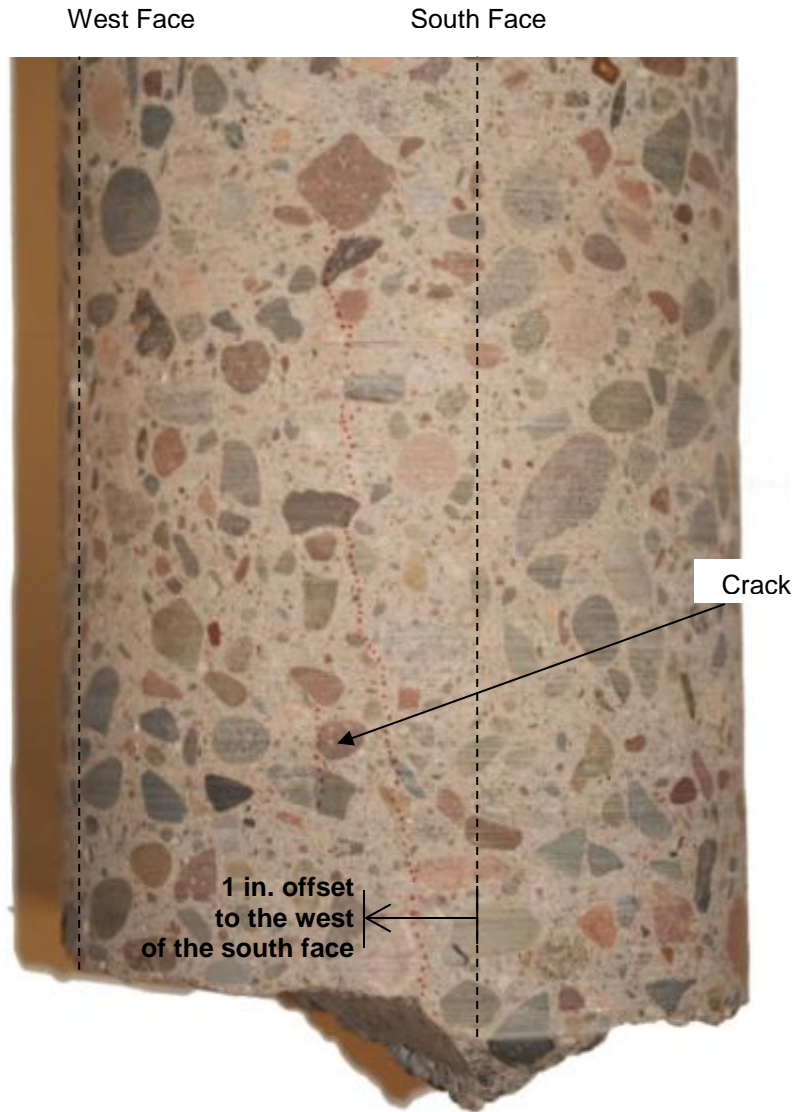


Figure 3.15: Crack on the pseudo-local south face of Core 33008-3 with a 1 in. offset to the west

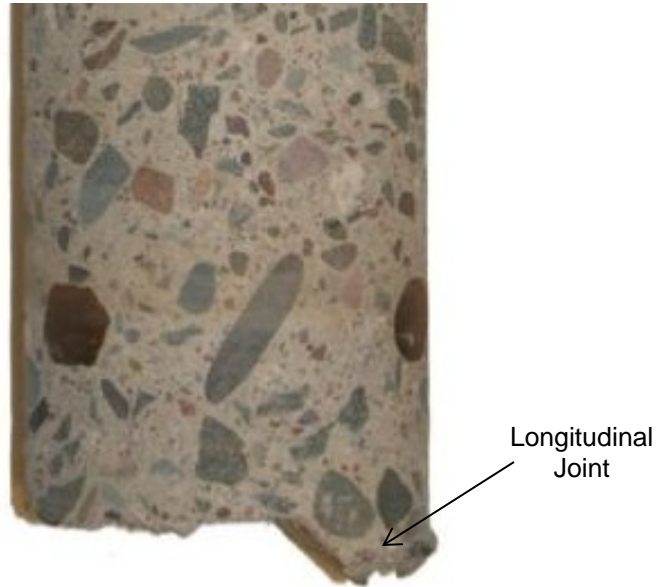


Figure 3.16: The west face of Core 13004-1 showing that the core only captured one side of the joint

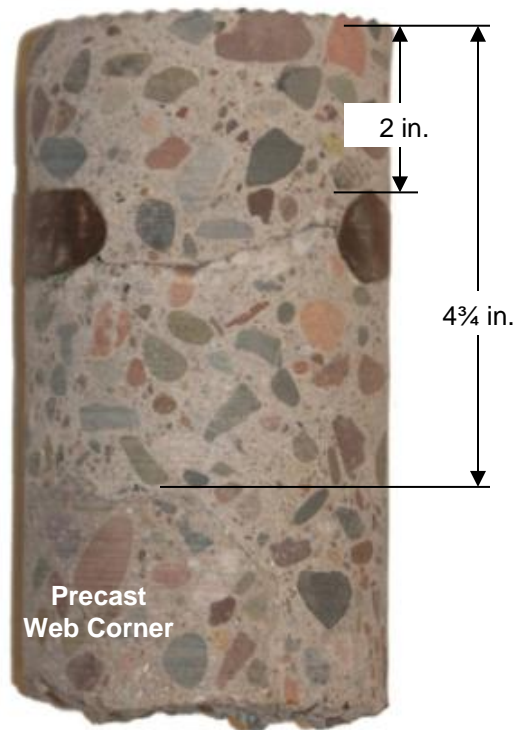


Figure 3.17: Core 33005-2 showing the precast web corner and 4 3/4 in. of CIP concrete above the precast web and less than 3 in. of cover



Figure 3.18: Uneven bearings of end-span precast beams at the north pier of Bridge No. 33005



Figure 3.19: Observed differential camber of the inverted-tee beams from Bridge No. 33008

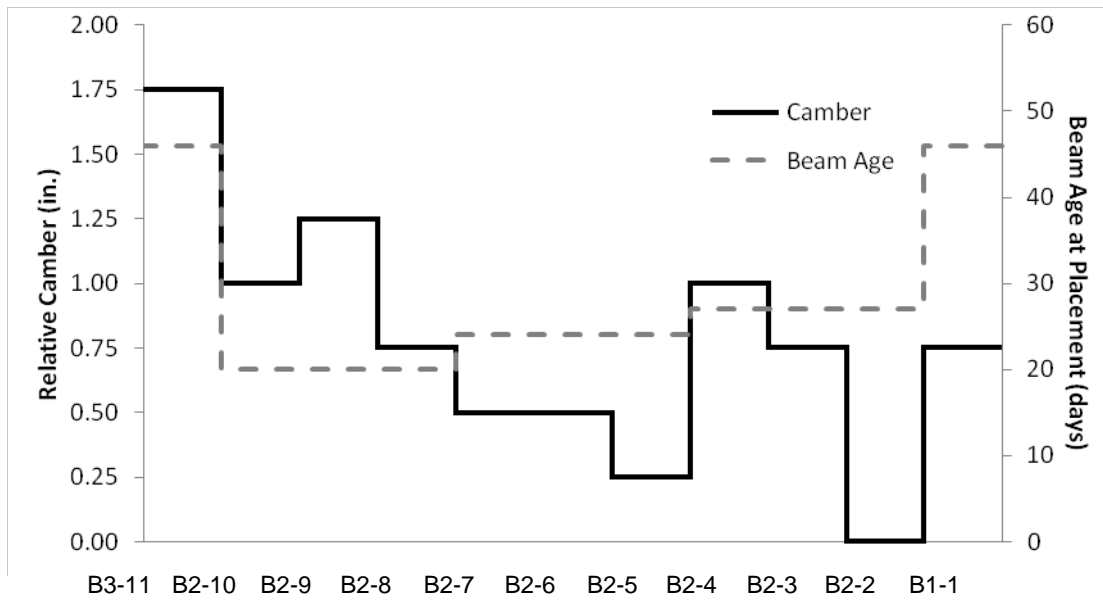


Figure 3.20: Observed differential camber from the north span of Bridge No. 33008. Camber is measured relative to minimum observed camber in the span. Beam age at placement is shown for comparison

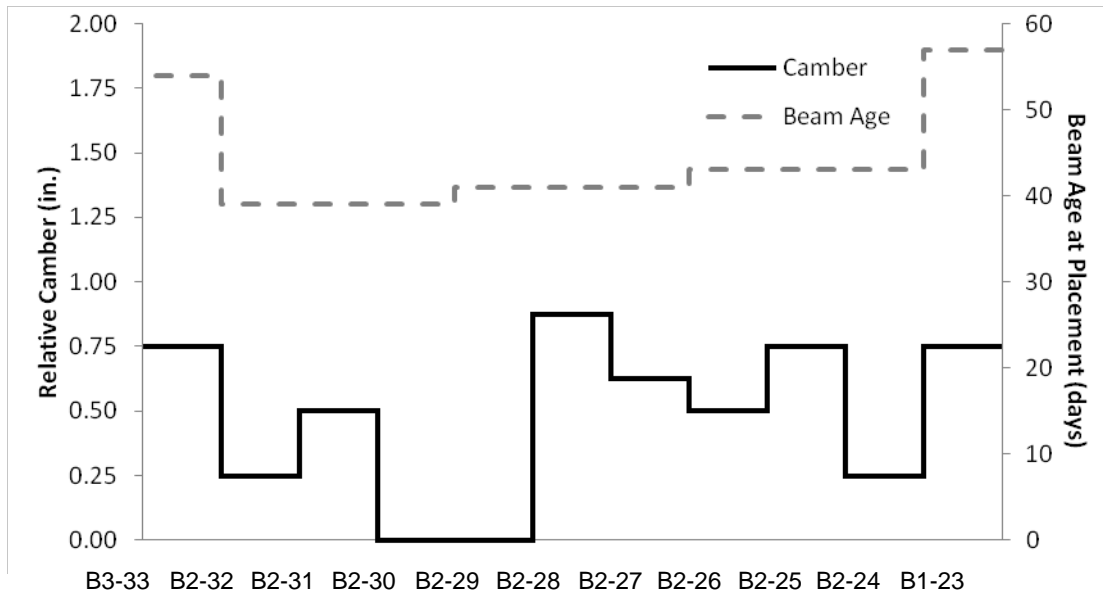


Figure 3.21: Observed differential camber from the south span of Bridge No. 33008. Camber is measured relative to the minimum camber in the span. Beam age at placement is shown for comparison

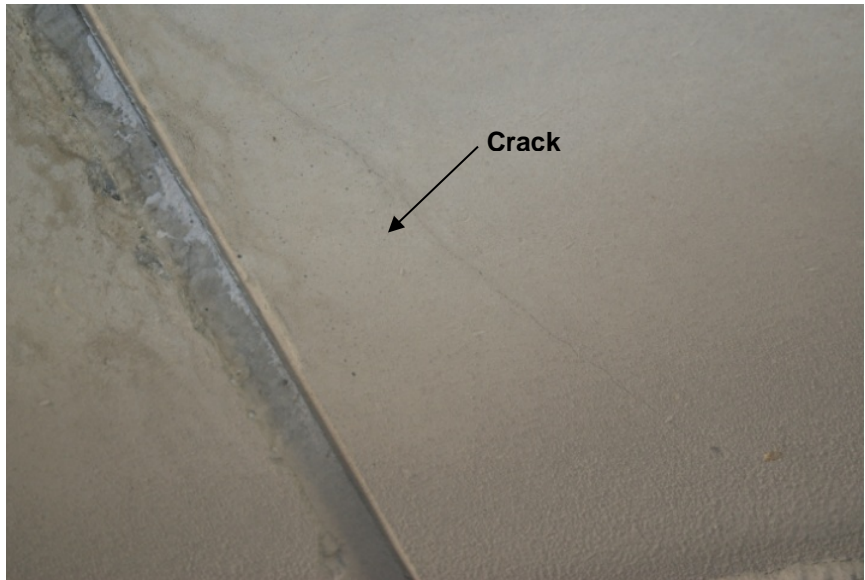
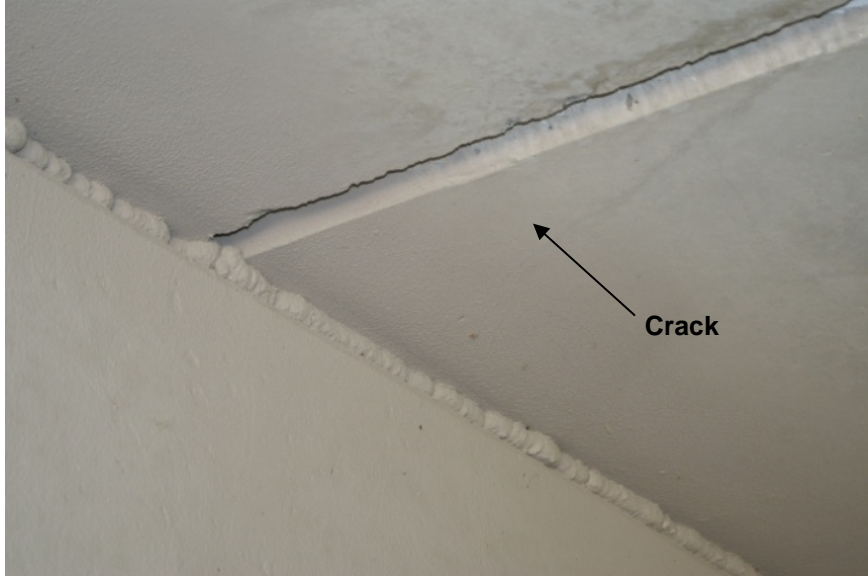


Figure 3.22: Cracked end-span beam at the north pier of Bridge No. 49007

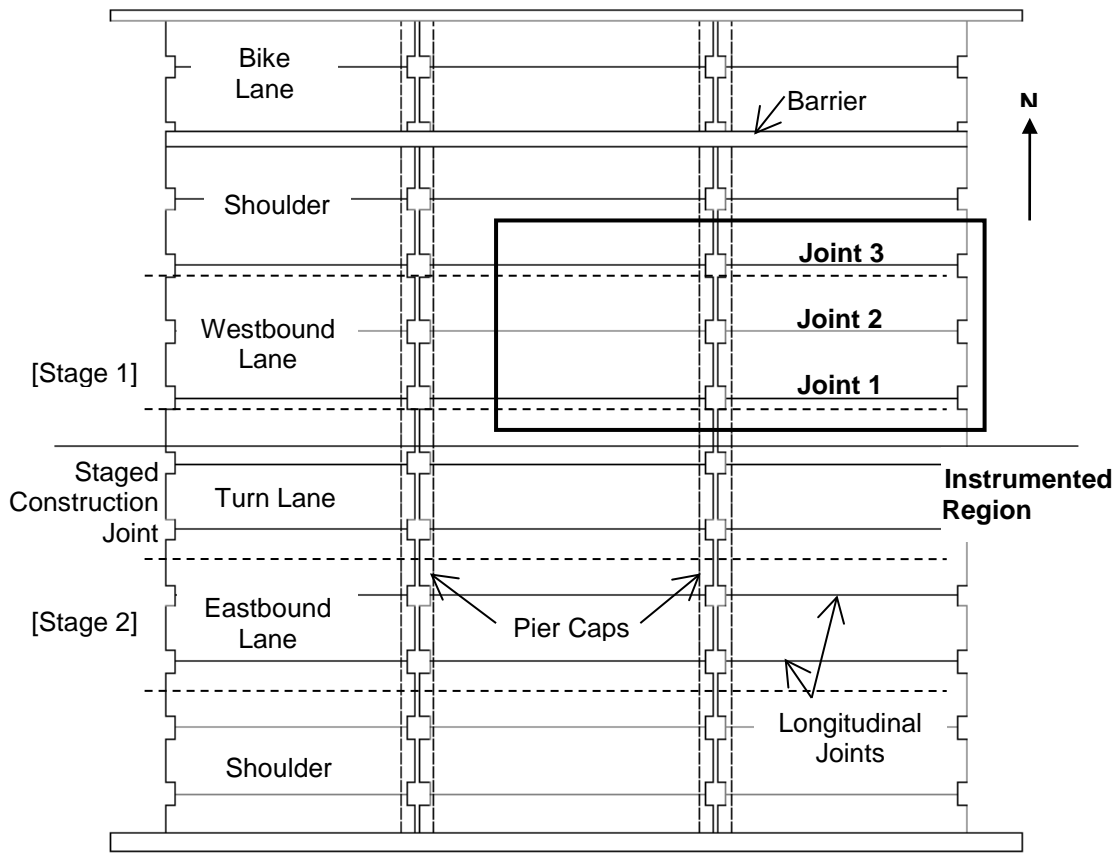


Figure 4.1: Plan view of MnDOT Bridge No. 13004 in Center City, MN

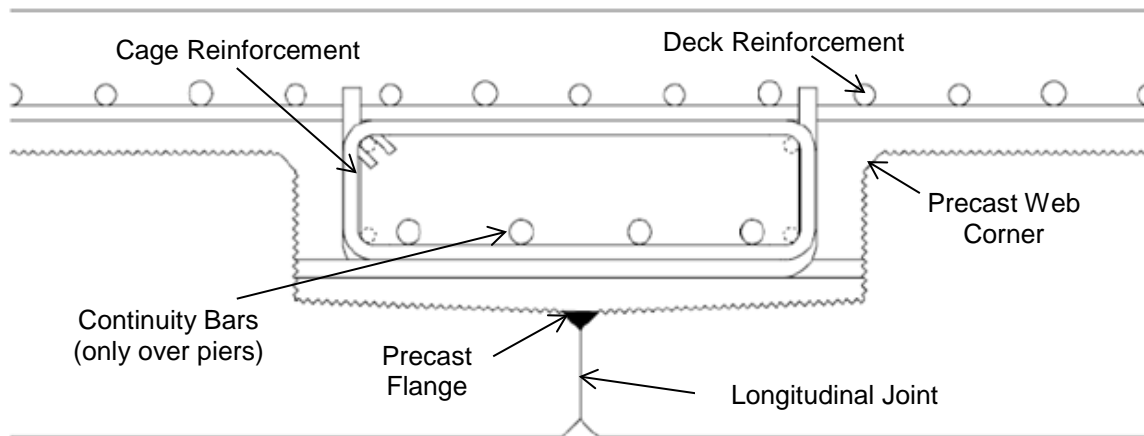


Figure 4.2: Cross-sectional view of a typical precast longitudinal joint from Bridge No. 13004, taken at the pier

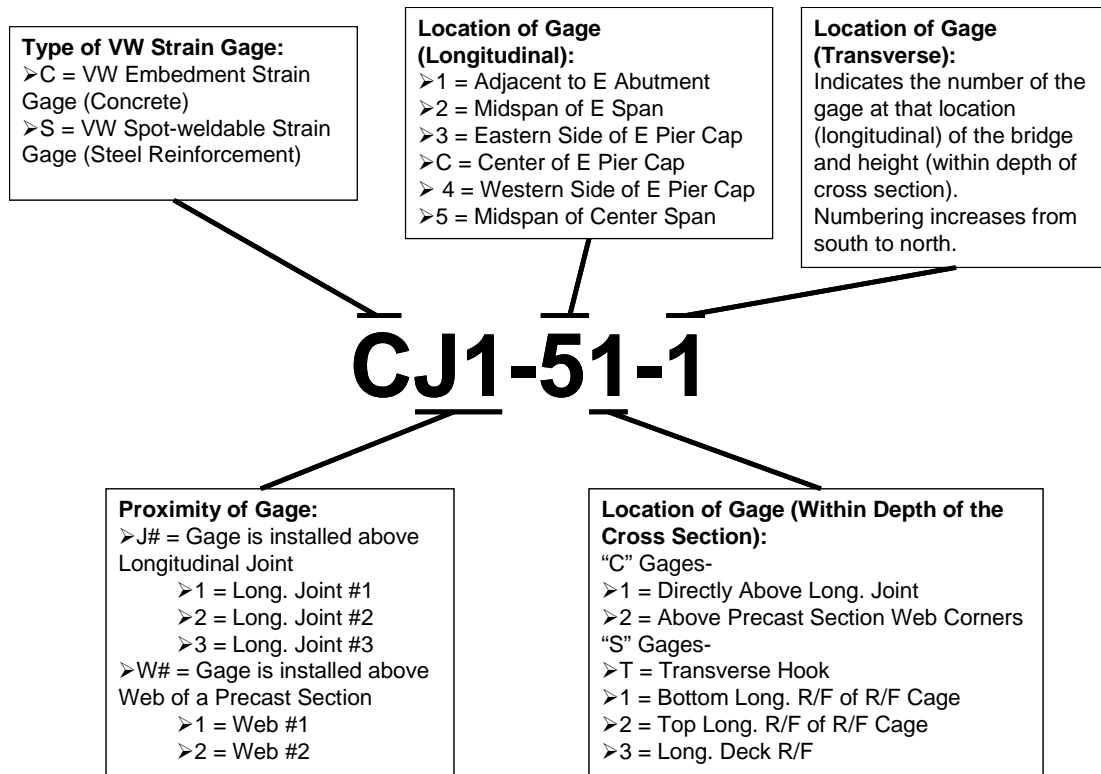


Figure 4.3: Naming convention for the instrumentation of Bridge No. 13004 (Smith et al. 2008)

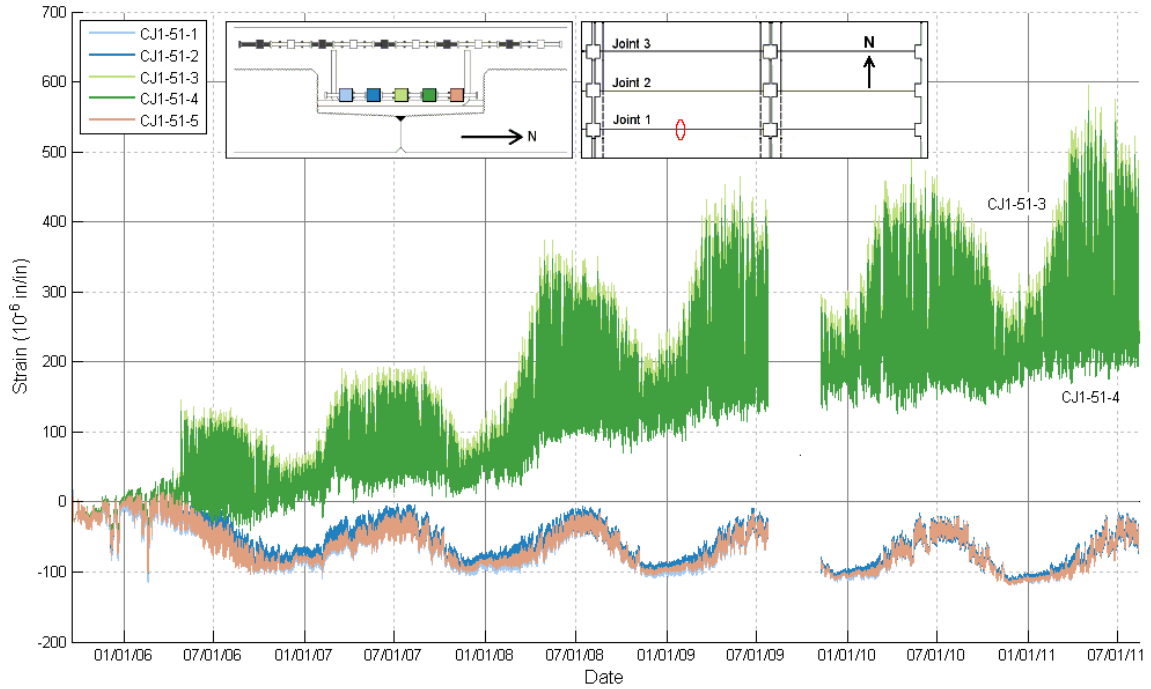


Figure 4.4: Transverse strain data from concrete embedment gauges directly above longitudinal Joint 1 at midspan of the center span. Gauges CJ1-51-3 and CJ1-51-4 show increasing strain

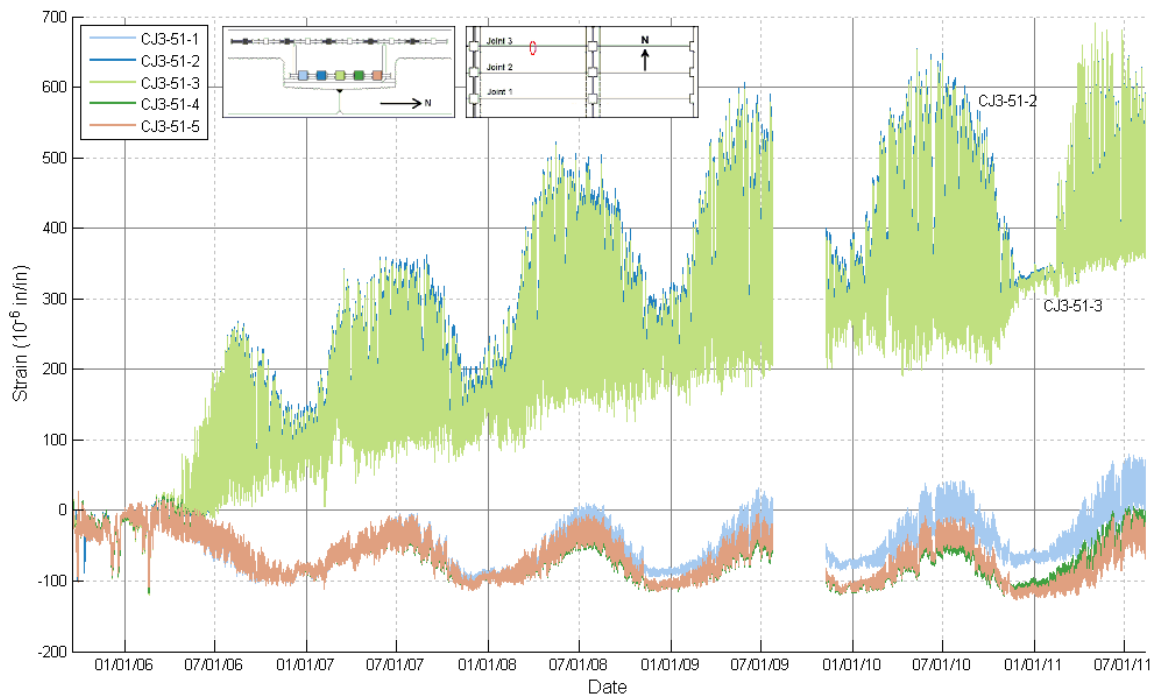


Figure 4.5: Transverse strain data from concrete embedment gauges directly above longitudinal Joint 3 at midspan of the center span. Gauges CJ3-51-2 and CJ3-51-3 show increasing strain

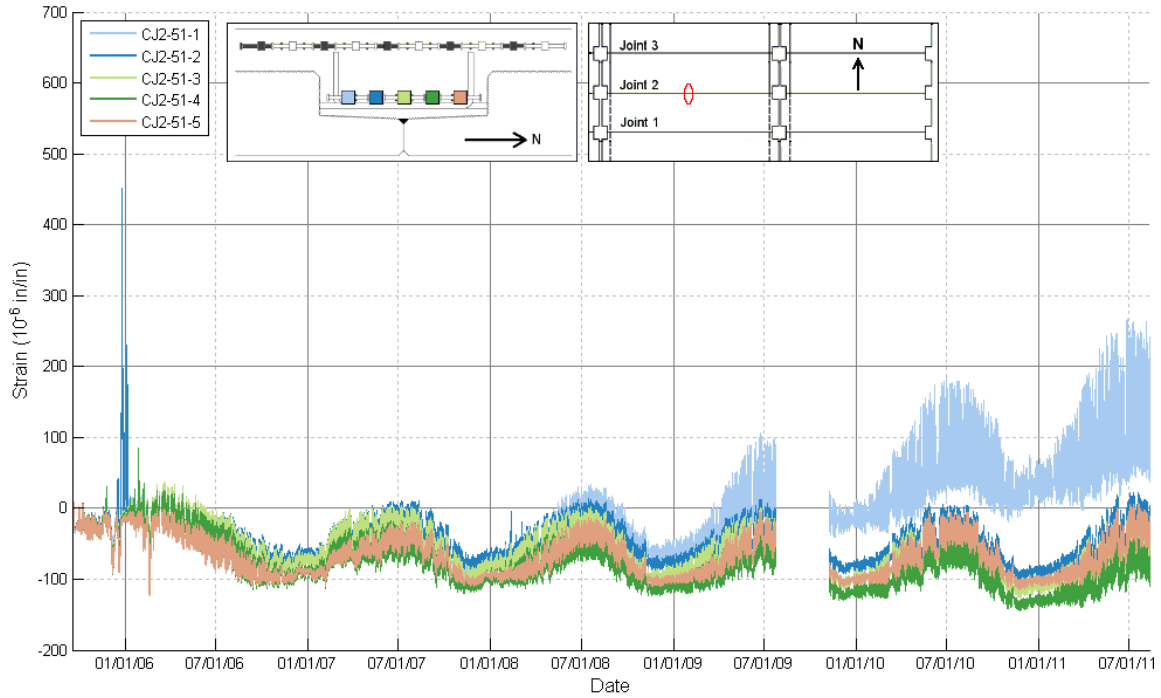


Figure 4.6: Transverse strain data from concrete embedment gauges directly above longitudinal Joint 2 at midspan of the center span. Gauge CJ2-51-1 shows increasing strain

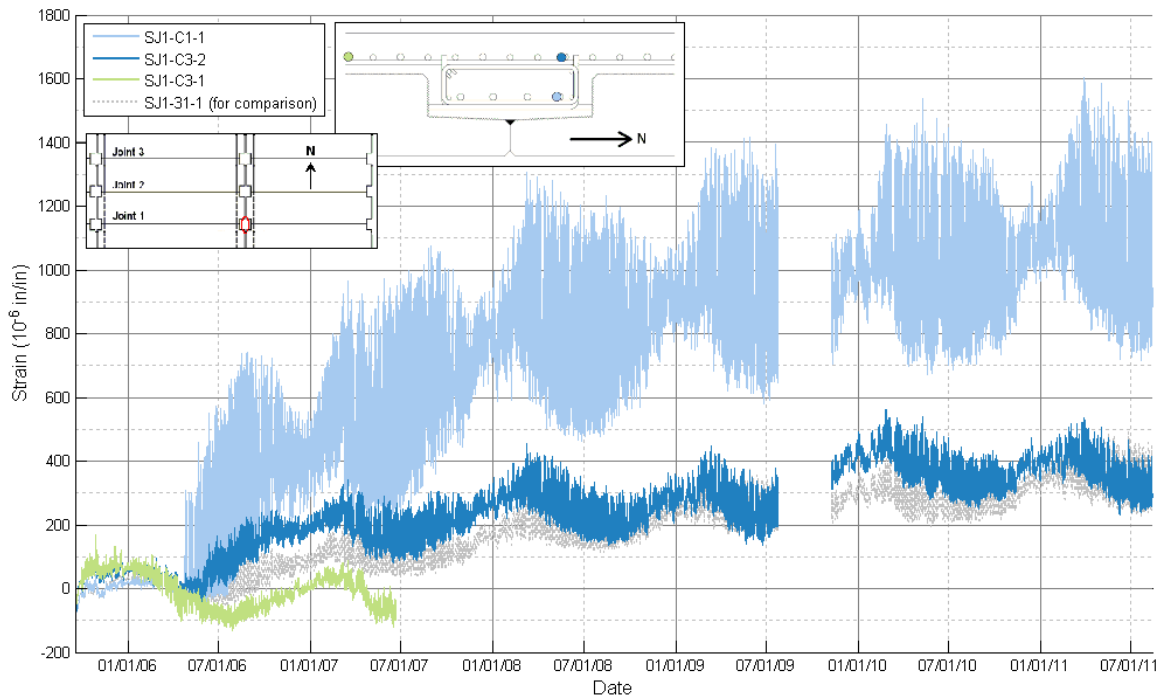


Figure 4.7: Longitudinal strain data from spot-weldable gauges on continuity and deck reinforcement along Joint 1 over the center of the pier cap. Data from gauge SJ1-31-1 (grey line) is shown for comparison

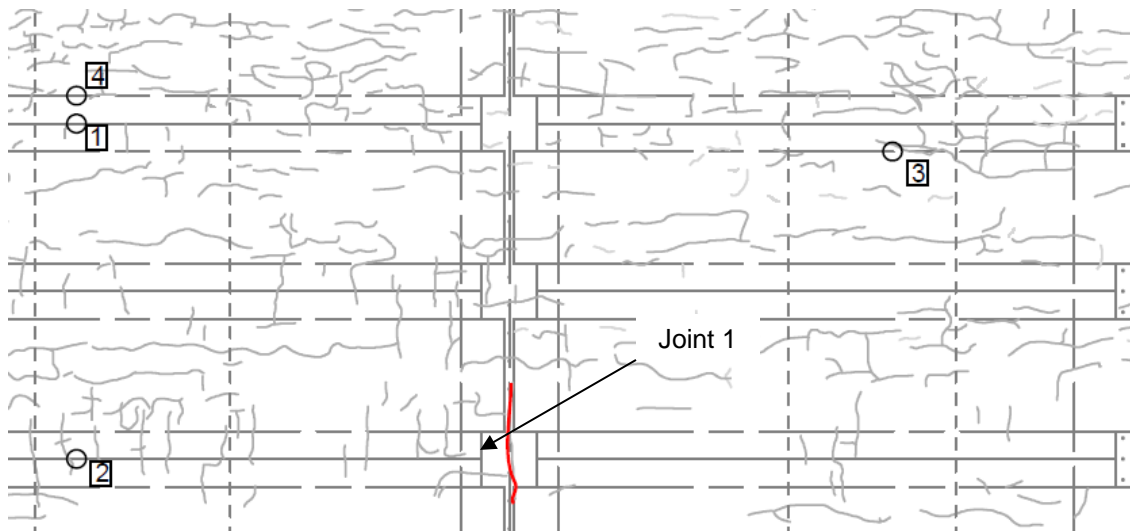


Figure 4.8: Crack map of Bridge 13004 showing a transverse crack at the pier over Joint 1 corresponding to the location of gauge SJ1-C3-2 from Figure 4.7

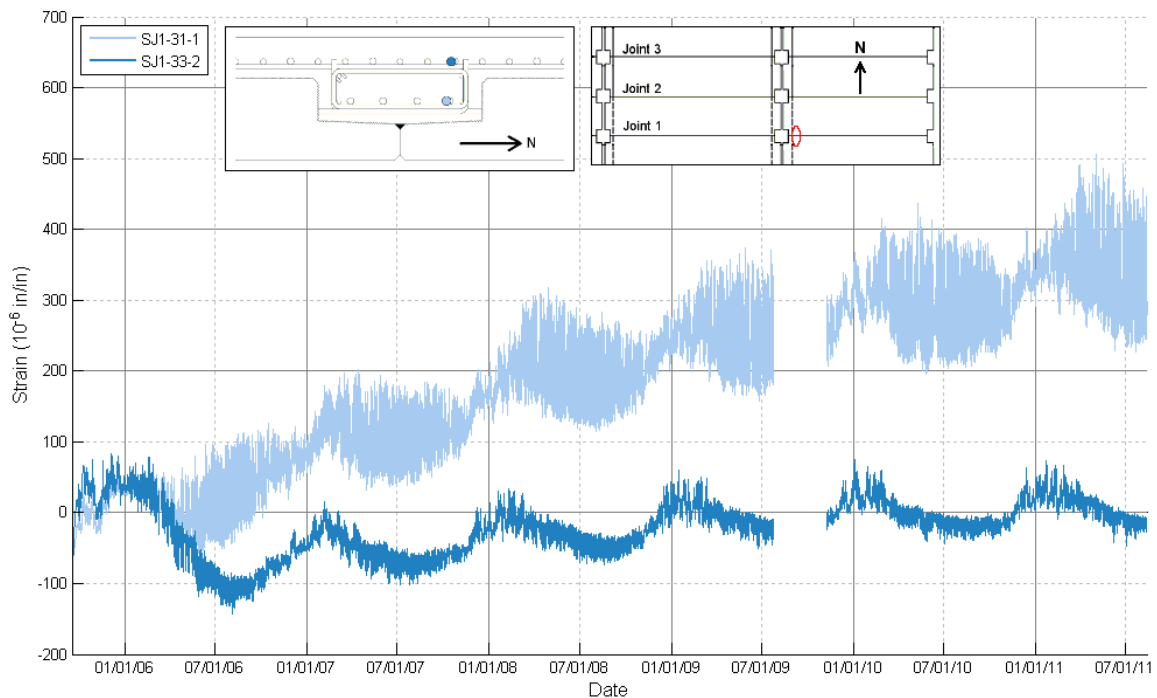


Figure 4.9: Longitudinal strain data from spot-weldable gauges on continuity and deck rebar over Joint 1 at the east side of the pier cap

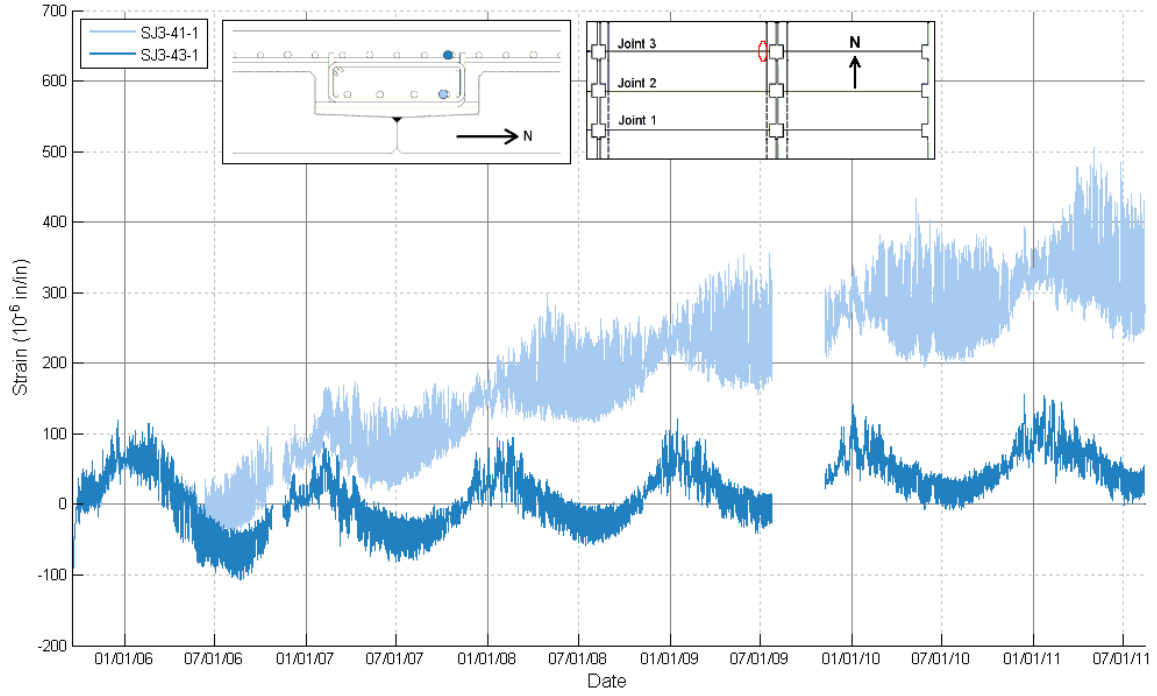


Figure 4.10: Longitudinal strain data from spot-weldable gauges on continuity and deck rebar over Joint 3 at the west side of the pier cap

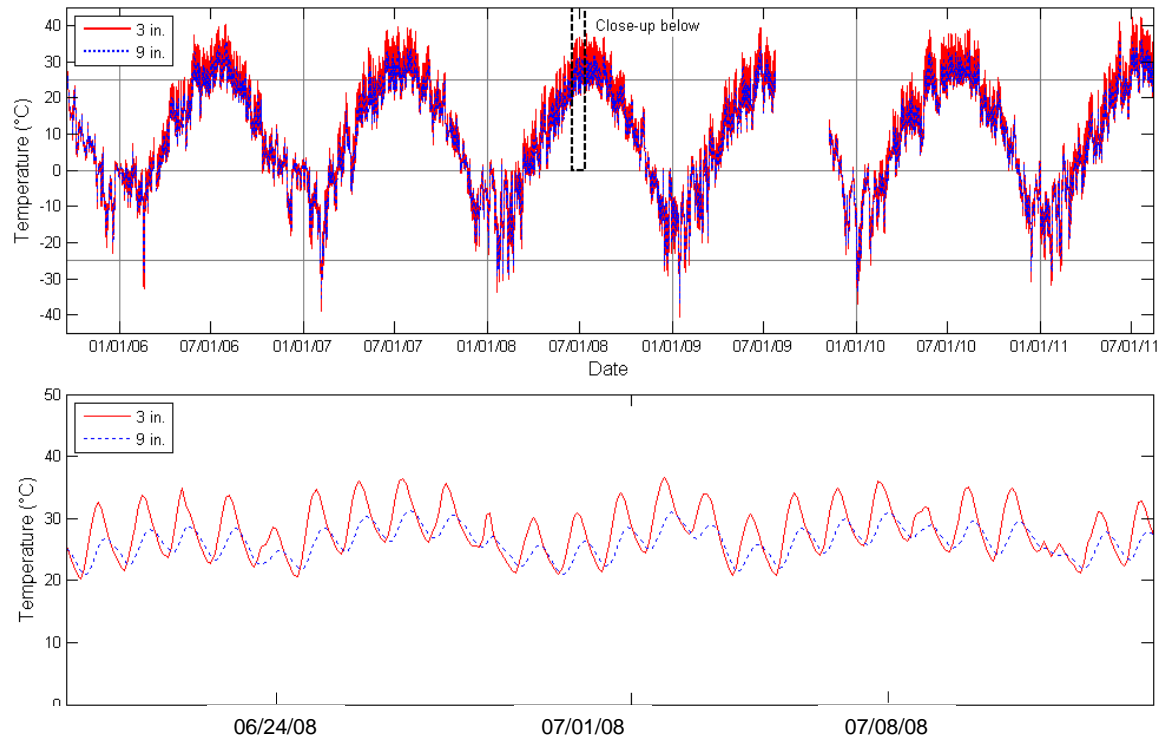
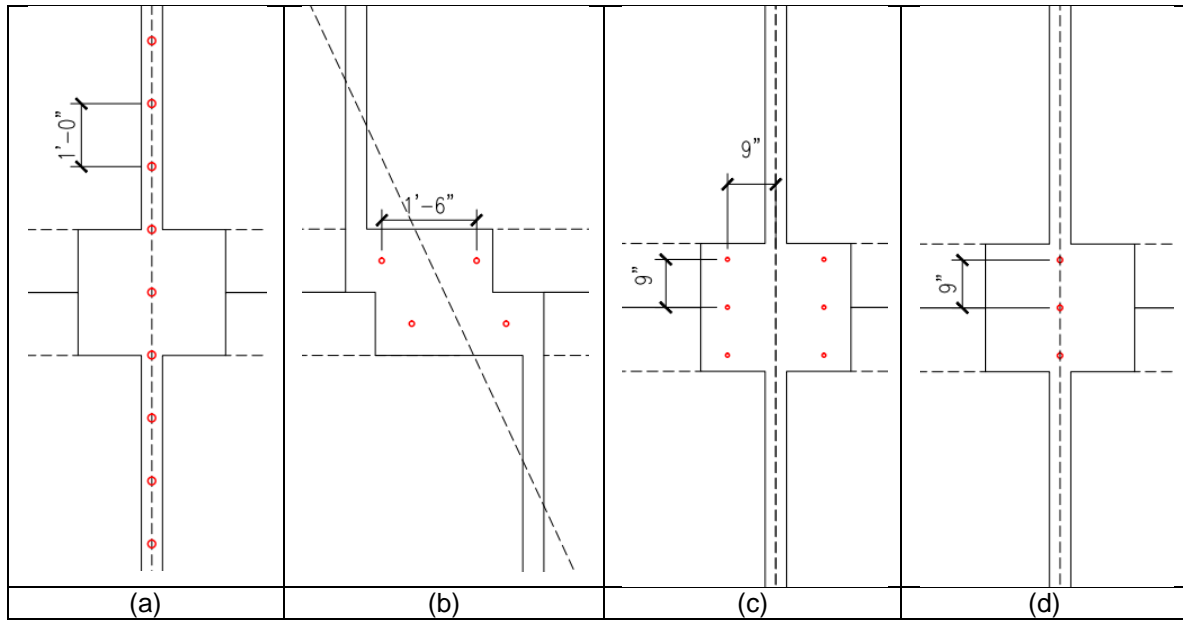


Figure 4.11: Temperature data at points 3 in and 9 in from the bridge surface at Joint 1 at midspan of the center span. A close-up of peak temperatures in 2008 shows daily temperature variations



- (a): One row of dowels at 12" along the pier centerline between beam ends (Bridge No. 13004).
- (b): Two rows of two dowels each in the blockout. Rows are aligned with pier skew, each 9" from the pier centerline (Bridge No. 33005).
- (c): Two rows of three dowels each in the blockout. Dowels are spaced at 9" and each row is 9" from the pier centerline (Bridge No. 33008).
- (d): One row of dowels along the pier centerline in the blockout (recommended).

Figure 5.1: Example dowel layouts for the five inspected PCSSS bridges and a recommended dowel layout

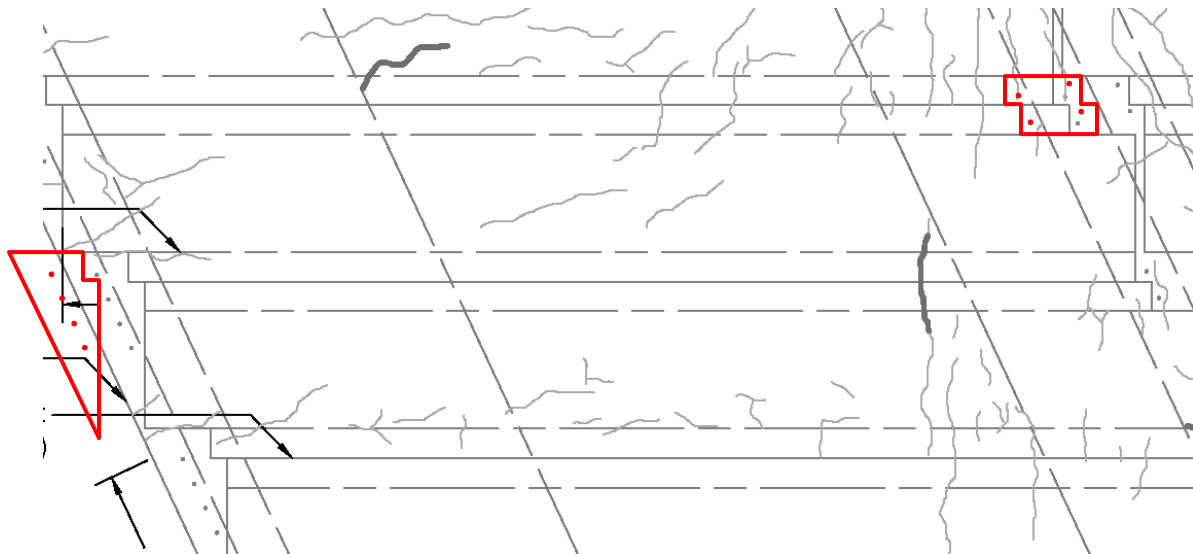


Figure 5.2: Skewed blockout regions from Bridge No. 33005 with dowels, all highlighted in red.

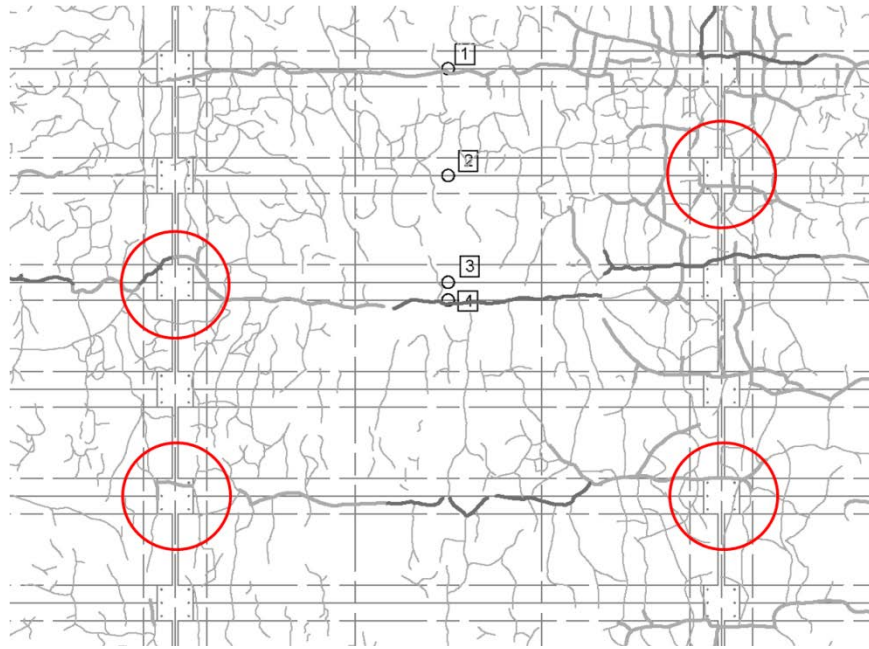


Figure 5.3: Crack map from inspection No. 2 of Bridge No. 33008 showing cracking in the region of precast beam blockouts



Figure 5.4: Construction photograph showing the placement of a mastic bond breaker on Bridge No. 08006

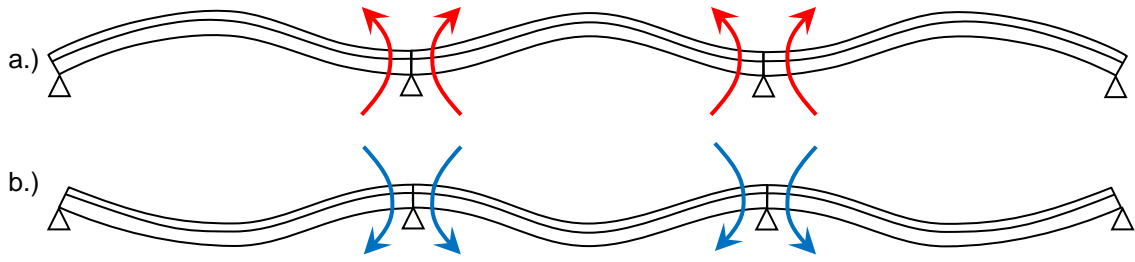


Figure 6.1: Deflections and restraint moments for simple beams made continuous: a.) positive and b.) negative restraint moments

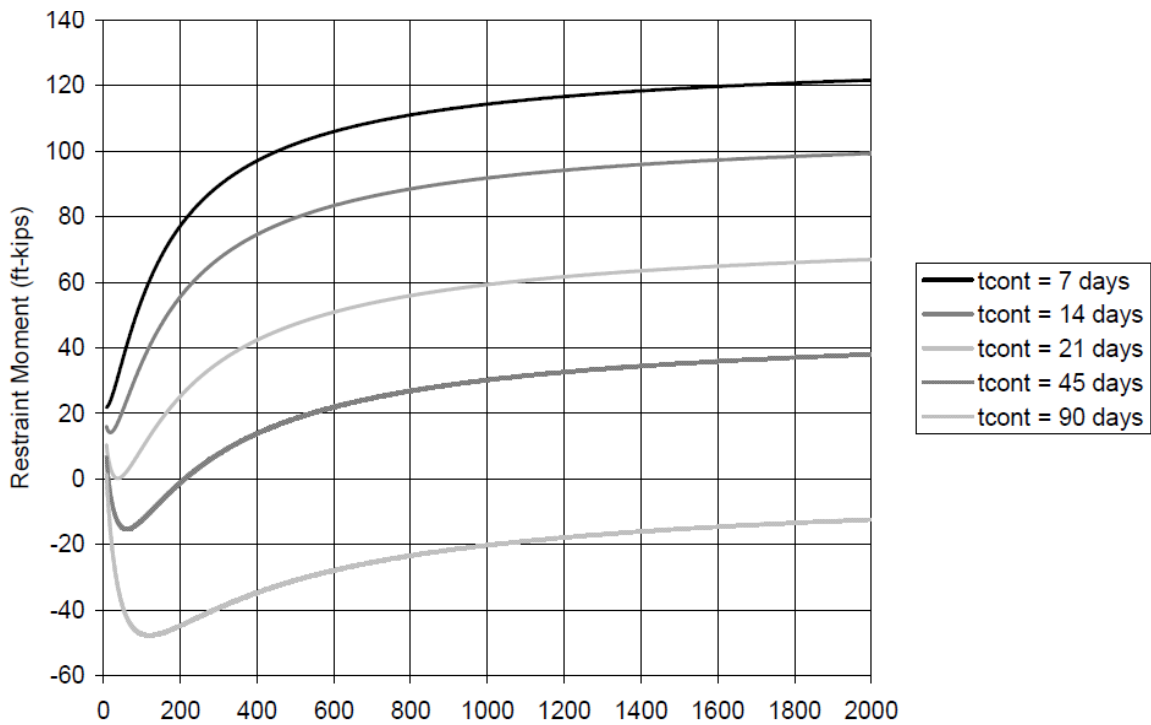


Figure 6.2: Predicted time-dependent restraint moment for Bridge No. 13004 for various ages of the precast beams at the time of continuity, represented by tcont (Smith et al. 2008)

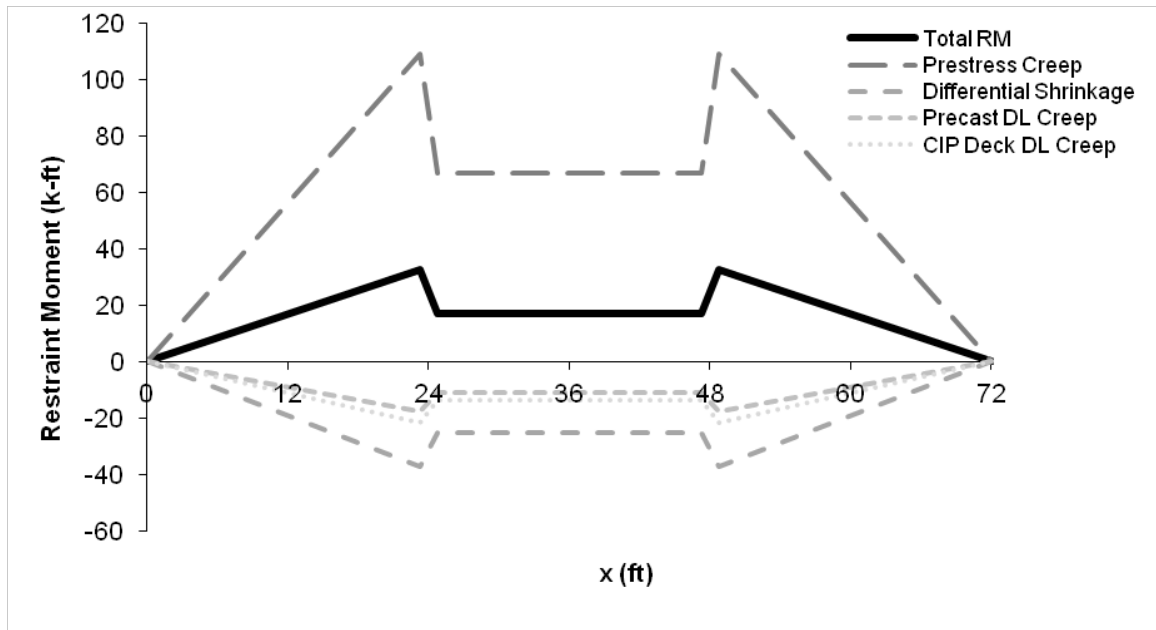


Figure 6.3: Typical time-dependent restraint moment (RM) for PCSSS design using the P-method with separate components shown. Precast beam age is 14 days at the time of continuity. The differences in moment at the piers (24 ft. and 48 ft.) are due to the effective diaphragm stiffness

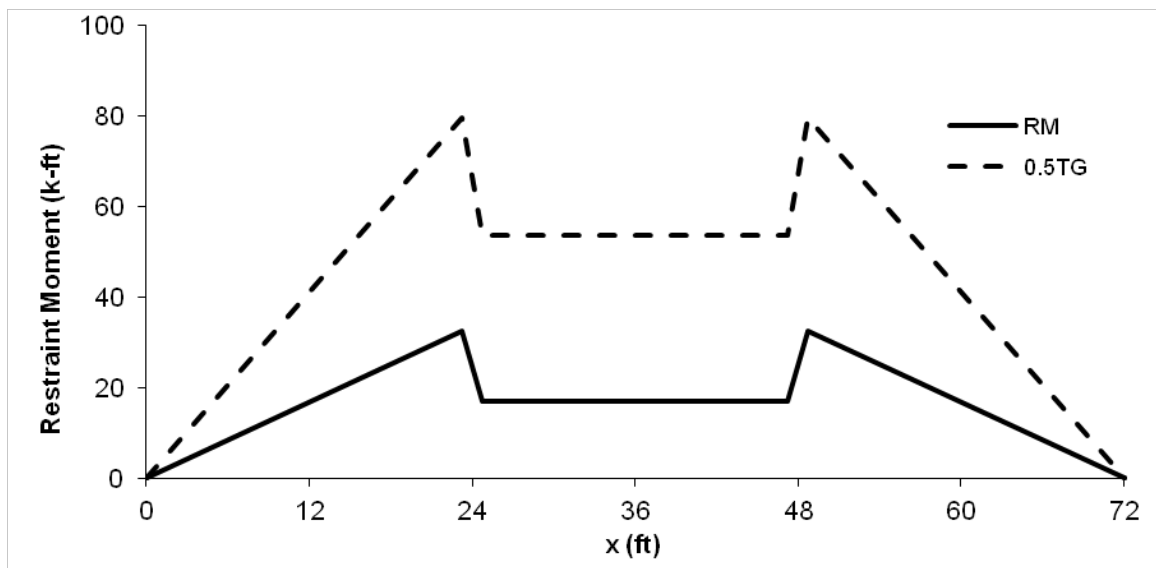


Figure 6.4: Typical time-dependent and thermal gradient restraint moment envelopes (24-24 configuration). The 0.5TG is the factored thermal gradient restraint moment used in the Service III load combination

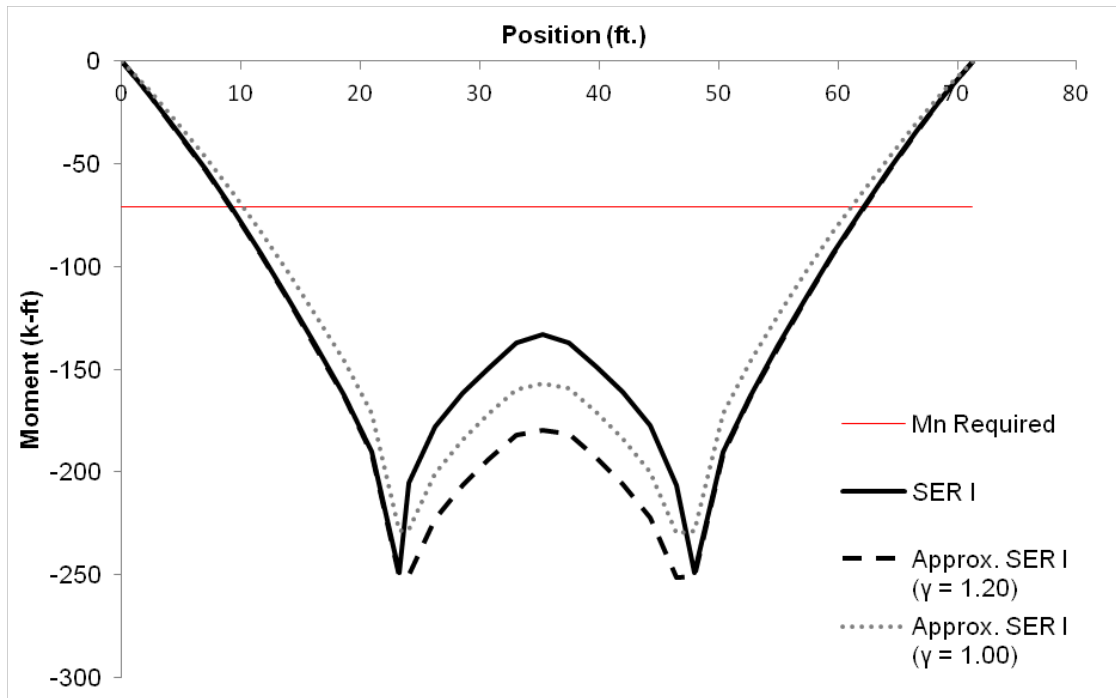


Figure 6.5: Service I and approximate Service I negative moment envelopes for a 24-24-24 bridge. The intersection between M_n Required and the service moment envelopes indicate the reinforcement cutoff locations

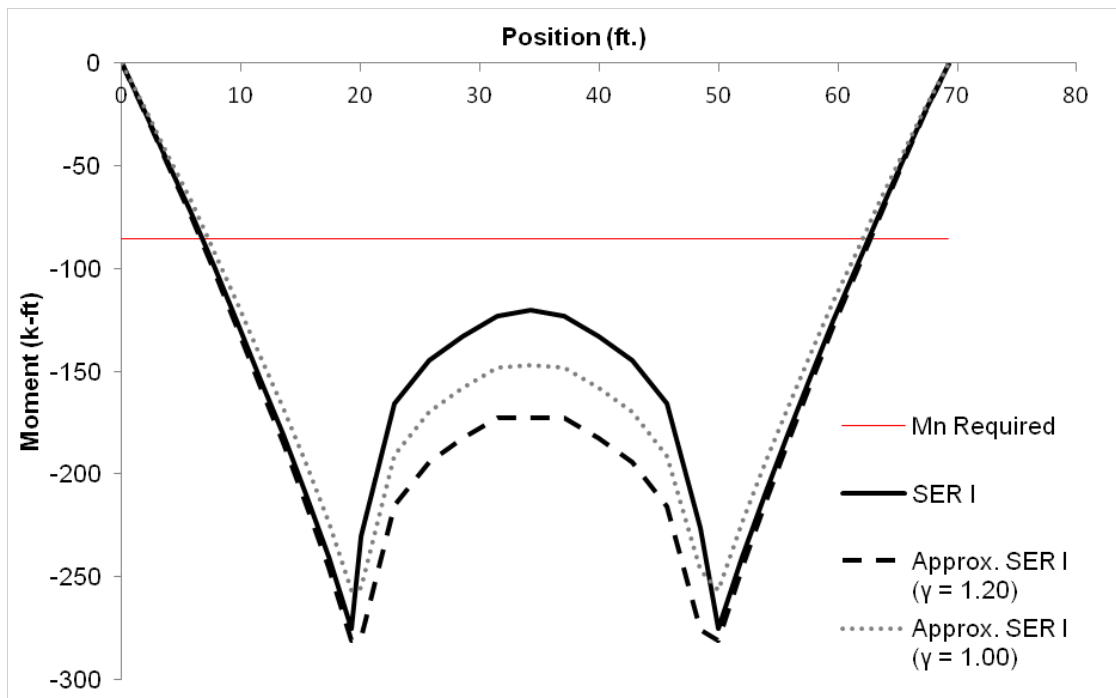


Figure 6.6: Service I and approximate Service I negative moment envelopes for a 20-30-20 bridge. The intersection between M_n Required and the service moment envelopes indicate the reinforcement cutoff locations

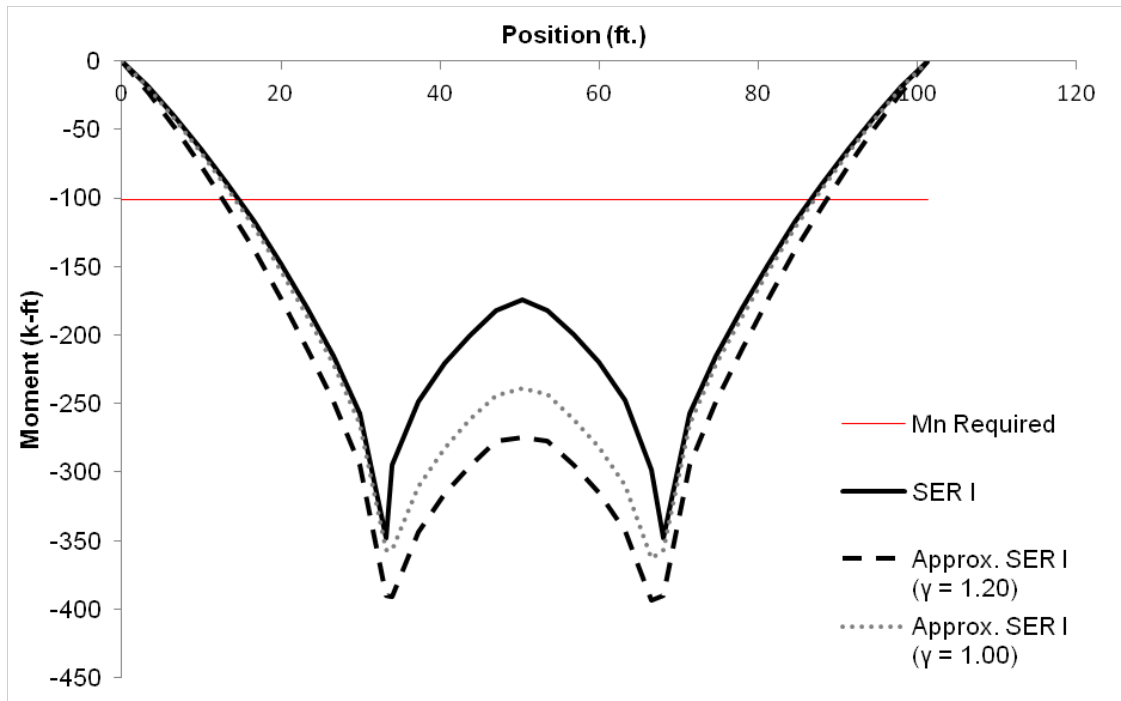


Figure 6.7: Service I and approximate Service I negative moment envelopes for a 34-34-34 bridge. The intersection between M_n Required and the service moment envelopes indicate the reinforcement cutoff locations

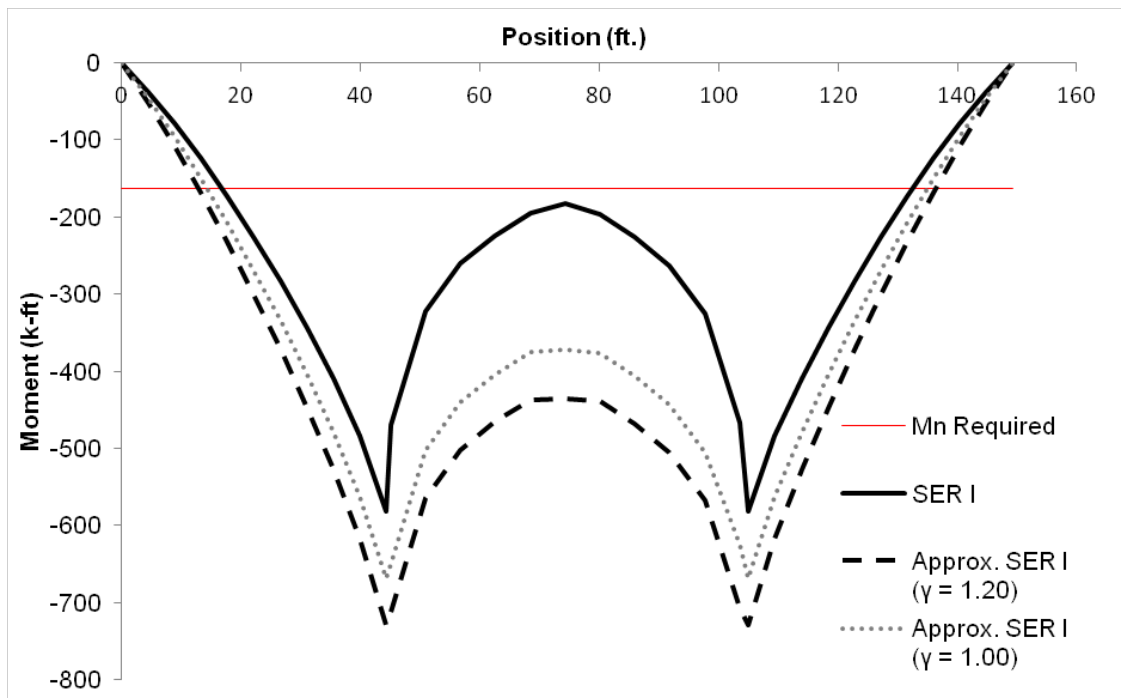


Figure 6.8: Service I and approximate Service I negative moment envelopes for a 45-62-45 bridge. The intersection between M_n Required and the service moment envelopes indicate the reinforcement cutoff locations

Appendix A: Crack Mapping Procedure and Results

The procedure for locating and documenting the cracks for the field inspections entailed identifying a crack on the surface of the bridge and recording its characteristics on paper, such as crack length, crack width, and location with respect to the structural precast member. Plan-view drawings of each bridge were prepared using AutoCAD 2010, and were plotted to scale on 11 in. × 17 in. paper. These drawings were used in the field to record the observed cracks.

Each plan-view drawing showed the structural features of the bridge (i.e., end of slab, barriers, pier locations, etc.). The locations of cracks identified and marked on the surface of the bridge were recorded to their respective locations on the plan-view drawings. The plan-view drawings showing both the structural features of the bridge and observed cracks are referred to as crack maps. The area of investigation for surface cracks was between the barriers at each side of the bridge and the expansion joints at both ends of the bridge span. Any visible cracks identified in this area were documented on the crack maps using the following procedure.

Loose debris was removed from the bridge deck surface prior to inspections by pressure washing the entire deck. Pre-wetting the deck was an effective method for locating cracks because the water from the bridge deck evaporated faster than the water in the surface cracks, making the cracks more visible for a short period of time. Crack mapping generally took place on days when the environmental conditions were favorable for pre-wetting the deck to enhance the appearance of the cracks. These were days when the temperature was above 32°F and the relative humidity was low. Once a crack was spotted, it was marked along its length using colored chalk. The chalk could be used on a wet or dry deck. It was preferable to mark the cracks while the water evaporated. Unfortunately, the chalk would wash away if the deck was wetted a second time, so cracks had to be identified with one wetting.

After the surface cracks were located, the characteristics of length, width, and location with respect to the precast members were recorded to paper. To expedite the process of recording the cracks onto the crack maps while maintaining acceptable accuracy, a 1 ft. × 1 ft. square grid was superimposed on the crack map to be used as a reference for locating cracks with respect to their physical locations on the bridge deck surface. Instead of marking a 1 ft. × 1 ft. square grid on the surface of each bridge, a prefabricated 6 ft. × 6 ft. wooden frame with an interior 1 ft. × 1 ft. grid of string was used. This frame, shown in Figure A.1, was advantageous for several reasons. First, it was more efficient than measuring out a 1 ft. × 1 ft. grid over the entire bridge deck. Second, it was light and small enough to be handled easily in the field. Finally, the precast members of the PCSSS bridges were 6 ft. wide, so the 6 ft. × 6 ft. frame could be aligned with the underlying beams. In order to correlate the 6 ft. × 6 ft. frame with the location of the structural features, a 6 ft. × 6 ft. grid was superimposed on the crack maps.

An example of a crack map used to record cracks in the field is shown in Figure A.2, complete with both a 1 ft. × 1 ft. and 6 ft. × 6 ft. grid. The grid on this crack map is aligned with the locations of the precast members, which was typical. The 6 ft. × 6 ft. grid was marked on the bridge deck using paint dots, as shown in Figure A.3, at the intersection of grid lines. Using four adjacent paint dots (i.e., grid line intersections), the 6 ft. × 6 ft. square frame was placed such that each of the four corners of the square frame was resting over a paint dot. In practice, two square frames were used by two teams of crack mappers to speed up the process, systematically moving around the bridge surface recording all observed cracks.

With the crack locations documented on the crack map, the remaining characteristic to document was the crack width. Knowing that the crack widths would vary along the length of

the crack, the following method of documenting the crack widths was developed. The crack widths were initially grouped into four different categories ranging from very small cracks to progressively larger cracks, originally given in Table 3.1. To mark which group the crack belonged to on the crack map, the crack categories were color coded. While the crack locations were being recorded, the width of each crack was measured with a crack gauge, shown in Figure A.4, and marked with the corresponding color on the crack map. Changes in crack widths were generally not recorded over crack lengths of less than 1 ft. so that the variations could be seen more clearly on the crack maps. The crack maps contain a description of the environmental conditions encountered during crack mapping because the crack widths correlated with the temperature (i.e., in cooler temperatures, the cracks were wider than observed in warmer temperatures). It is desirable to conduct annual crack maps during similar environmental conditions each year.

As a final step, the hand-drawn crack maps were transcribed into AutoCAD and superimposed on the bridge plans electronically. This final copy of the crack map was produced to cleanly present a map of the surface cracks in relation to the significant structural features. Final copies of the crack maps from all of the field inspections are provided in this appendix. The original crack width classification is shown for inspection No. 1 crack maps while the refined crack width classification is shown for inspection Nos. 2 and 3. The line widths and shades for the original classification were the same as the larger of the refined classification (e.g., Class B in the original classification had the same line width and shade as Class B2 in the refined classification). In addition, a summary of these and other relevant design details are listed on each crack map. Much of this information is also given in Table 2.3 through Table 2.7.

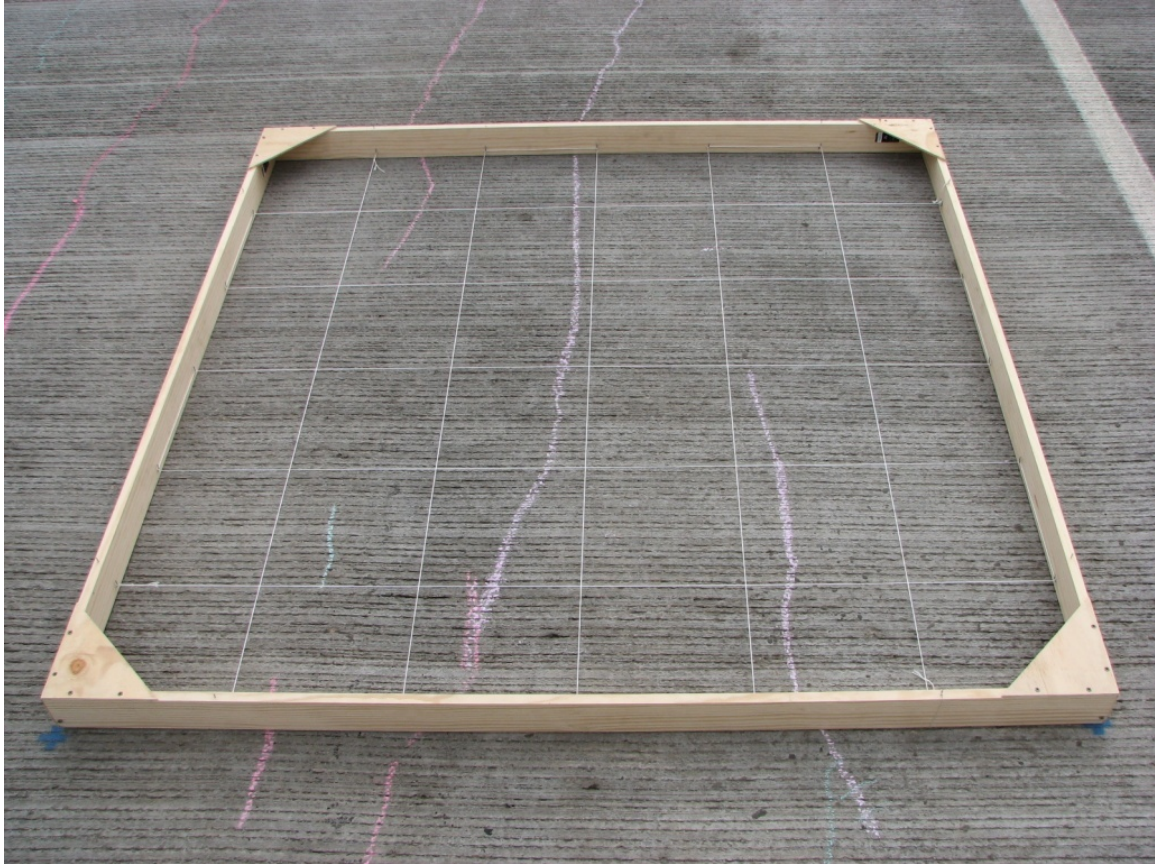


Figure A.1: Photograph of wood fabricated square frame used to create movable 1 ft. × 1 ft. grid

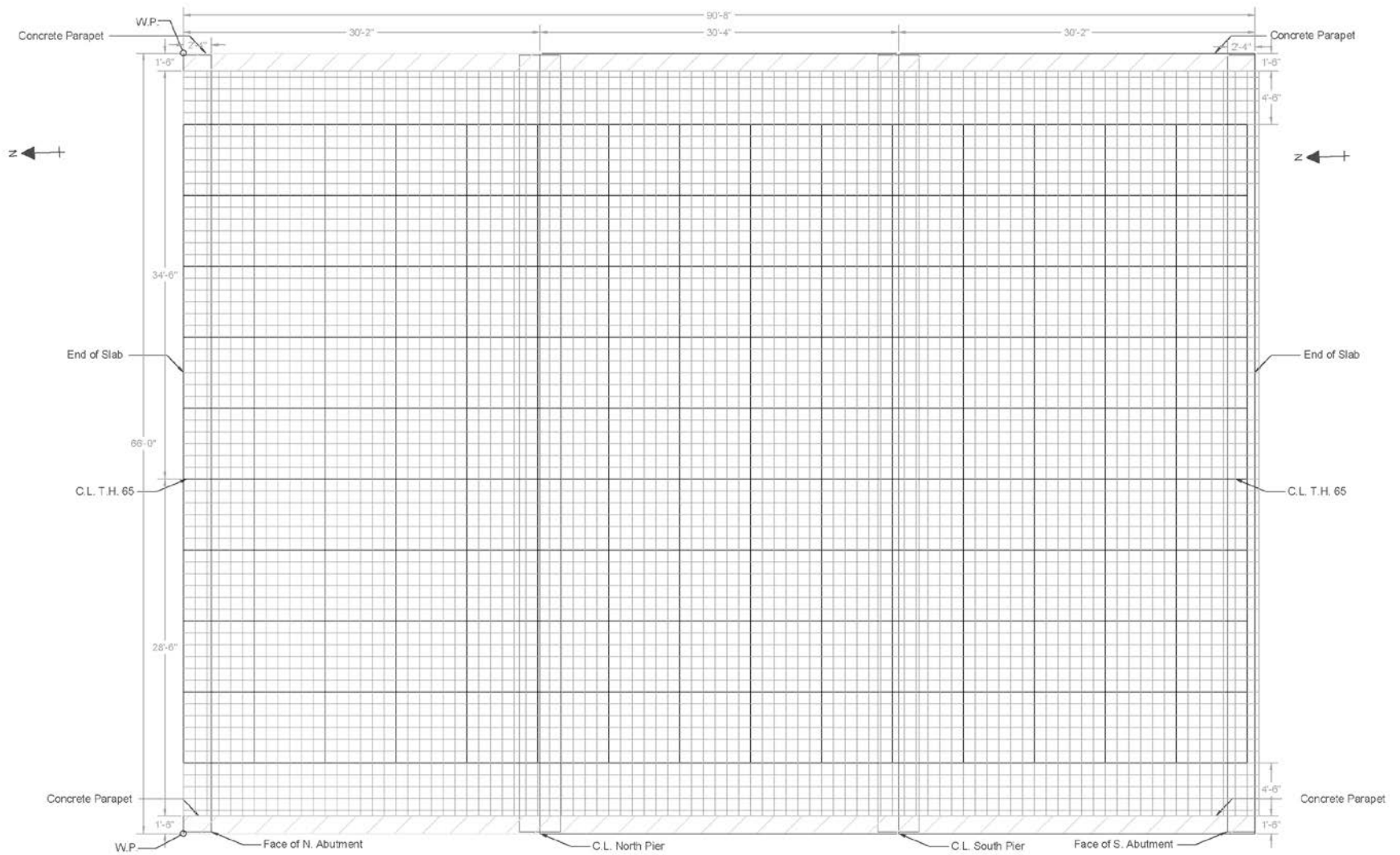


Figure A.2: Example of a gridded crack map used in the field to document observed surface cracks



Figure A.3: Photograph of 6 ft. x 6 ft. square area on bridge surface indicated by four blue painted dots with crack locations marked in chalk

INCHES	Crack Comparator		MILLIMETERS
.002			0.0508
.004			0.1016
.006			0.1524
.008			0.2032
.010			0.2540
.012			0.3048
.014			0.3556
.016			0.4064
.018			0.4572
.020			0.5080
.022			0.5588
.024	<0.007	Class A	<0.178
.026	0.008-0.022	Class B	0.179-0.559
.028	0.023-0.200	Class C	0.560-5.08
.030		Class D	>5.08
.032	>0.200		0.8128

CRACK CLASSIFICATIONS

Figure A.4: Crack width measurement gauge used for the crack mapping surveys

Bridge No. 33532
 Scale: 1" = 8'-0"
 Built: 1995 (Slab Span)
 Inspection No. 1: 09/16/2010

Age: 15 years
 Temperature: 32°F - 55°F (42°F average)
 Average Humidity: 70%
 Clouds/Precipitation: Overcast

Slab Concrete
 Strength: 4000 psi
 Slump: Not available
 Prewetted: No
 Surface Finish: Transverse tining

Reinforcement
 Top Longitudinal:
 - No. 8 at 12 in., cutoff at 16 ft - 10 in.
 - Alt. No. 8 at 12 in., cutoff at 11 ft - 5 in. and 6 ft - 3 in.
 Bottom Longitudinal:
 - No. 7 at 12 in. full length
 - Alt. No. 7 at 12 in. cutoff over piers
 Transverse:
 - Top No. 4 at 1 ft - 6 in.
 - Bottom No. 5 at 12 in.

Pier Anchorage
 - No. 6 paired hooks at 12 in.

Crack Classification

Class AI	< 0.003"
Class AII	0.003" - 0.007"
Class BI	0.008" - 0.015"
Class BII	0.016" - 0.022"
Class CI	0.023" - 0.100"
Class CII	0.100" - 0.200"
Class D	> 0.200"

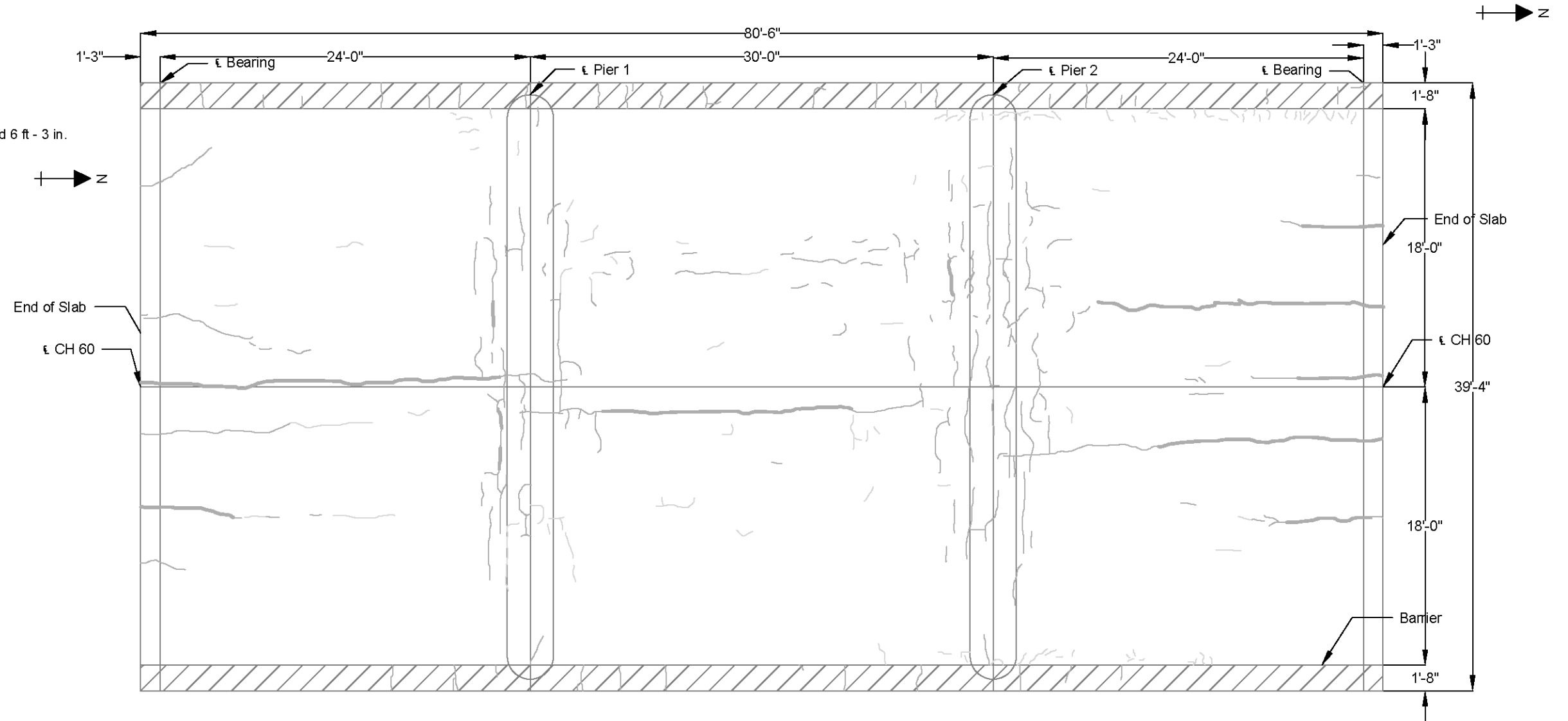


Figure A.5: Crack map for Bridge No. 33532 (conventional slab-span) from September 16, 2010

Bridge No. 13004

Scale: 1" = 11'-0"
 Built: 11/01/2005 (Generation 1)
 Inspection No. 1: 11/18 and 11/23, 2009

Age: 4.05 years
 Temperature: 21°F - 51°F (36°F average)
 Average Humidity: 72%
 Clouds/Precipitation: Clear

Precast Concrete
 Release Strength: 4500 psi
 Final Strength: 6500 psi
 Depth: 12 in.
 Flange Thickness: 5.25 in.
 Strand: 16 - 0.5 in. Ø

Cast-in-Place Concrete
 Strength: 4000 psi
 Slump: Not available
 Prewetted: No
 Surface Finish: Very shallow longitudinal tining

Reinforcement

- Precast:**
- No. 5 composite hooks at 1 ft over midspan, 1 in. projection
 - No. 6 transverse hooks at 1 ft, stag. at 2 in. and 10 in.
 - 7 No. 8 top bars
 - No. 4 ties at spacing of top hooks
- Deck Longitudinal:**
- No. 8 at 12 in., full length with lap splice
 - 2 No. 7 at 4 in. between, first cutoff at 10 ft from pier (end span and center span), second cutoff 16 ft from pier (end span only)
- Deck Transverse:**
- No. 5 at 12 in. with lap at staged construction joint
- Trough:**
- No. 5 corner bars
 - 4 No. 8 continuity bars at 6 in.
 - No. 5 stirrups at 12 in., adjacent to hooks
 - Overall spacing at 2 in., 10 in.

Piers and Abutments

- Dowels:**
- Cast in place prior to beam placement
 - In block-outs at abutments, 3 No. 6 @ 9 in.
 - Along CL of pier cap, between beam ends, No. 5 at 1 ft over center 36 ft
- Bearing:**
- Polystyrene under beam bearing, not at block-out or 4 in. gap
 - Elastomeric bearing pad type 1, 6 in. strip under beam tabs

Core Summary

- 1) Shrinkage crack: Al, 1/2 in. deep from surface
- 2) Reflective crack: Al, 1 1/4 in. deep from joint
- 3) Shrinkage crack: Al, 1/2 in. deep from surface
- 4) Shrinkage crack: Al, 1/2 in. deep from surface

Crack Classification

Class A	< 0.007"
Class B	0.008" - 0.022"
Class C	0.023" - 0.200"
Class D	> 0.200"

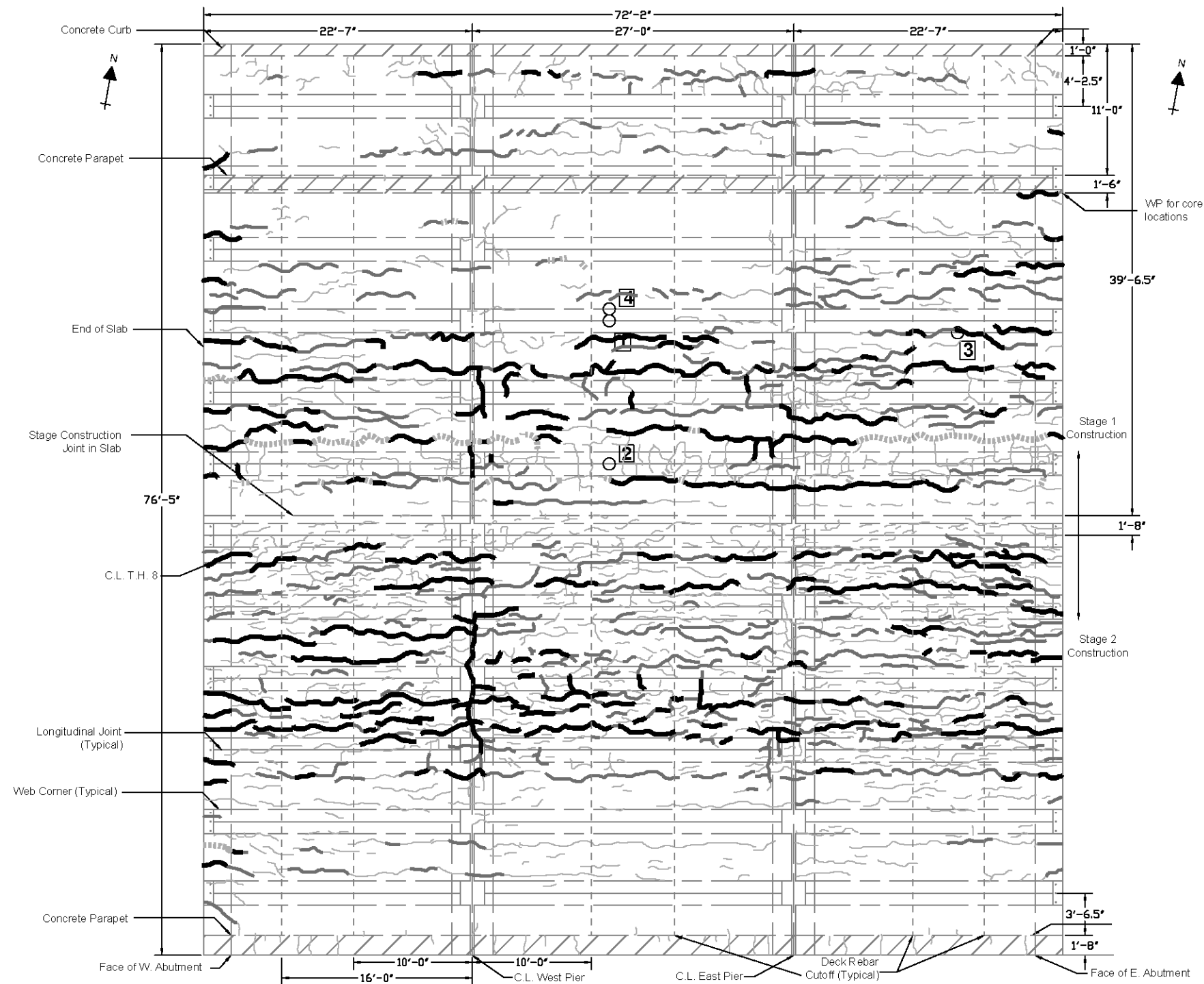


Figure A.6: Crack map for Bridge No. 13004 from Inspection No. 1, November 18 and 23, 2009

Bridge No. 13004

Scale: 1" = 11'-0"
 Built: 11/02/2005 (Generation 1)
 Inspection No. 2: 6/22 and 6/24, 2010

Age: 4.63 years
 Temperature: 53°F - 87°F (70°F average)
 Average Humidity: 72%
 Clouds/Precipitation: Clear

Precast Concrete
 Release Strength: 4500 psi
 Final Strength: 6500 psi
 Depth: 12 in.
 Flange Thickness: 5.25 in.
 Strand: 16 - 0.5 in. Ø

Cast-in-Place Concrete
 Strength: 4000 psi
 Slump: Not available
 Prewetted: No
 Surface Finish: Very shallow longitudinal tining

Reinforcement

- Precast:**
- No. 5 composite hooks at 1 ft over midspan, 1 in. projection
 - No. 6 transverse hooks at 1 ft, stag. at 2 in. and 10 in.
 - 7 No. 8 top bars
 - No. 4 ties at spacing of top hooks
- Deck Longitudinal:**
- No. 8 at 12 in., full length with lap splice
 - 2 No. 7 at 4 in. between, first cutoff at 10 ft from pier (end span and center span), second cutoff 16 ft from pier (end span only)
- Deck Transverse:**
- No. 5 at 12 in. with lap at staged construction joint
- Trough:**
- No. 5 corner bars
 - 4 No. 8 continuity bars at 6 in.
 - No. 5 stirrups at 12 in., adjacent to hooks
 - Overall spacing at 2 in., 10 in.

Piers and Abutments

- Dowels:**
- Cast in place prior to beam placement
 - In block-outs at abutments, 3 No. 6 @ 9 in.
 - Along CL of pier cap, between beam ends, No. 5 at 1 ft over center 36 ft
- Bearing:**
- Polystyrene under beam bearing, not at block-out or 4 in. gap
 - Elastomeric bearing pad type 1, 6 in. strip under beam tabs

Core Summary

- 1) Shrinkage crack: AI, 1/2 in. deep from surface
- 2) Reflective crack: AI, 1 1/4 in. deep from joint
Shrinkage crack: AI, 1/2 in. deep from surface
- 3) Shrinkage crack: AI, 1/4 in. deep from surface
- 4) Shrinkage crack: AI, 1/2 in. deep from surface

Crack Classification

Class AI	< 0.003"
Class AII	0.003" - 0.007"
Class BI	0.008" - 0.015"
Class BII	0.016" - 0.022"
Class CI	0.023" - 0.100"
Class CII	0.100" - 0.200"
Class D	> 0.200"

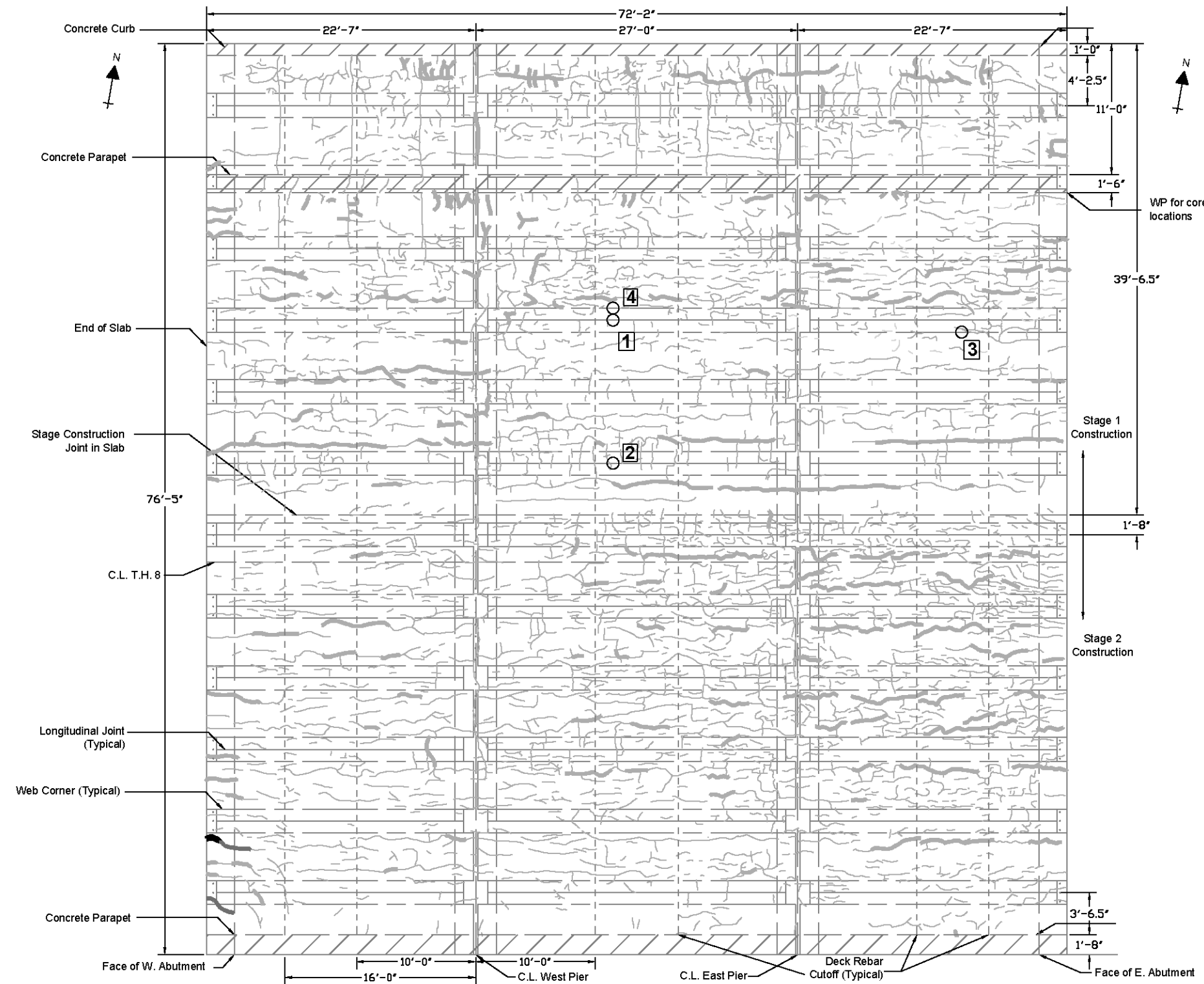


Figure A.7: Crack map for Bridge No. 13004 from Inspection No. 2, June 22 and 24, 2010

Bridge No. 33005 (North)

Scale: 1" = 7'-0"
 Built: 11/02/2007 (Generation 2)
 Inspection No. 1: 11/02/2009

Age: 2 years
 Temperature: 32°F - 44°F (38°F average)
 Average Humidity: 68%
 Clouds/Precipitation: Clear, clouds in afternoon

Precast Concrete
 Release Strength: 4000 psi
 Final Strength: 6000 psi
 Depth: 14 in.
 Flange Thickness: 5.25 in.
 Strand: 22 - 0.5 in. Ø

Cast-in-Place Concrete
 Strength: 4000 psi
 Slump: 3 in.
 Prewetted: No
 Surface Finish: Shallow longitudinal tining

Reinforcement

- Precast:**
- No. 4 composite hooks at 2 ft over midspan, 2 in. projection
 - No. 6 transverse hooks at 1 ft, stag. at 3 in. and 9 in.
 - 7 No. 8 top bars
 - No. 4 ties at spacing of top hooks
- Deck Longitudinal:**
- No. 7 at 4 in.
 - Full length with lap, first cutoff at 7 ft -5 in. from pier (end span), second cutoff at 24 ft -10 in. (end span), 13 ft -2 in. from pier (center span)
- Deck Transverse:**
- No. 5 at 12 in.
- Trough:**
- No. 4 corner bars
 - 4 No. 9 continuity bars at 5 in.
 - No. 4 stirrups at 12 in., adjacent to hooks
 - Overall spacing at 3 in. and 9 in.

Piers and Abutments

- Dowels:**
- 1 ft. - 6 in. projection
 - Holes drilled after beams placed, grouted
 - Next to ends at abutments, 4 No. 8 at 11 in.
 - In block-outs at piers, 4 No. 8 at 12 in., 1 ft - 9 in. symmetric over CL pier
- Bearing:**
- Polystyrene under beam bearing, not at block-out or 4 in. gap
 - Elastomeric bearing pad type 1, 6 in. strip under beam tabs

Core Summary

- 1) No cracking
- 2) Shrinkage crack: AI, 1/4 in. deep from surface

Crack Classification

Class A	< 0.007"
Class B	0.008" - 0.022"
Class C	0.023" - 0.200"
Class D	> 0.200"

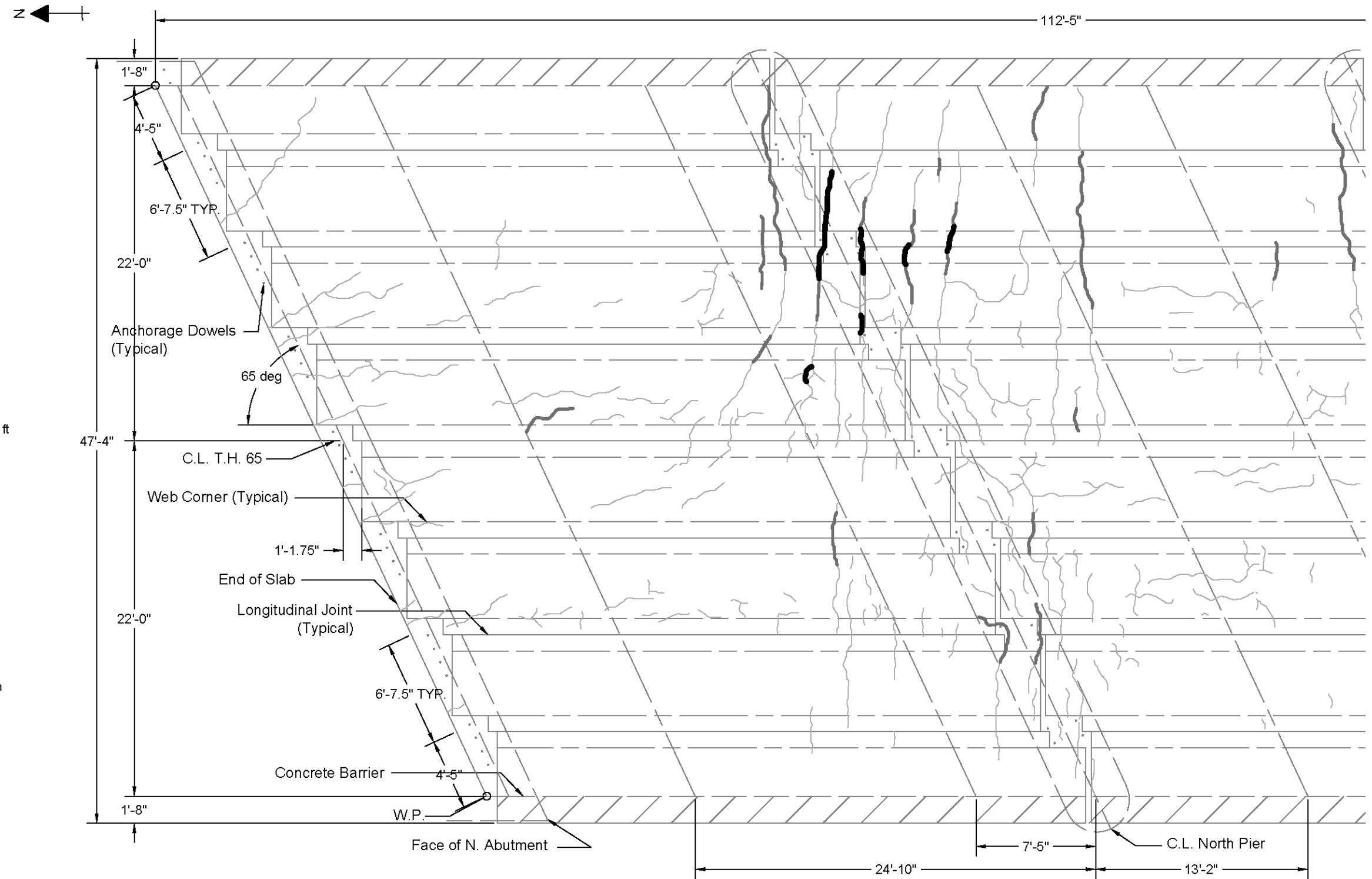
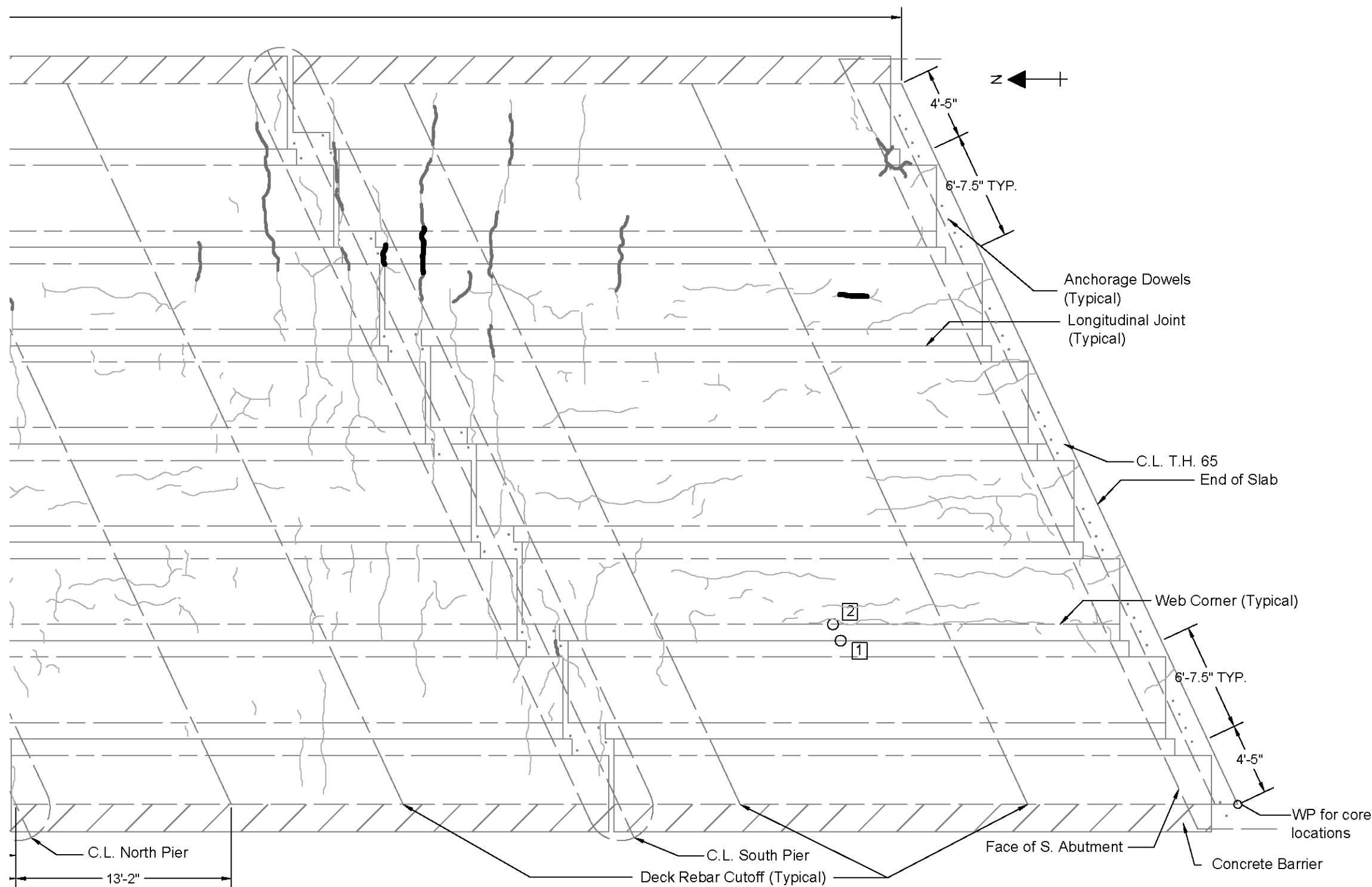


Figure A.8: Crack map for the north side of Bridge No. 33005 Inspection No. 1, November 2, 2009



Bridge No. 33005 (South)

Scale: 1" = 7'-0"
 Built: 11/02/2007 (Generation 2)
 Inspection No. 1: 11/02/2009

Age: 2 years
 Temperature: 32°F - 44°F (38°F average)
 Average Humidity: 68%
 Clouds/Precipitation: Clear, clouds in afternoon

Precast Concrete

Release Strength: 4000 psi
 Final Strength: 6000 psi
 Depth: 14 in.
 Flange Thickness: 5.25 in.
 Strand: 22 - 0.5 in. Ø

Cast-in-Place Concrete

Strength: 4000 psi
 Slump: 3 in.
 Prewetted: No
 Surface Finish: Shallow longitudinal tining

Reinforcement

Precast:

- No. 4 composite hooks at 2 ft over midspan, 2 in. projection
- No. 6 transverse hooks at 1 ft, stag. at 3 in. and 9 in.
- 7 No. 8 top bars
- No. 4 ties at spacing of top hooks

Deck Longitudinal:

- No. 7 at 4 in.
- Full length with lap, first cutoff at 7 ft -5 in. from pier (end span), second cutoff at 24 ft -10 in. (end span), 13 ft - 2 in. from pier (center span)

Deck Transverse:

- No. 5 at 12 in.

Trough:

- No. 4 corner bars
- 4 No. 9 continuity bars at 5 in.
- No. 4 stirrups at 12 in., adjacent to hooks
- Overall spacing at 3 in. and 9 in.

Piers and Abutments

Dowels:

- 1 ft. - 6 in. projection
- Holes drilled after beams placed, grouted
- Next to ends at abutments, 4 No. 8 at 11 in.
- In block-outs at piers, 4 No. 8 at 12 in., 1 ft - 9 in. symmetric over CL pier

Bearing:

- Polystyrene under beam bearing, not at block-out or 4 in. gap
- Elastomeric bearing pad type 1, 6 in. strip under beam tabs

Core Summary

- 1) No cracking
- 2) Shrinkage crack: AI, 1/4 in. deep from surface

Crack Classification

Class A	< 0.007"
Class B	0.008" - 0.022"
Class C	0.023" - 0.200"
Class D	> 0.200"

Figure A.9: Crack map for the south side of Bridge No. 33005 Inspection No. 1, November 2, 2009

Bridge No. 33005 (North)

Scale: 1" = 7'-0"
 Built: 11/02/2007 (Generation 2)
 Inspection No. 2: 06/29/2010

Age: 2.66 years
 Temperature: 46°F - 69°F (58°F average)
 Average Humidity: 57%
 Clouds/Precipitation: Clear

Precast Concrete
 Release Strength: 4000 psi
 Final Strength: 6000 psi
 Depth: 14 in.
 Flange Thickness: 5.25 in.
 Strand: 22 - 0.5 in. Ø

Cast-in-Place Concrete
 Strength: 4000 psi
 Slump: 3 in.
 Prewetted: No
 Surface Finish: Shallow longitudinal tining

Reinforcement

- Precast:**
- No. 4 composite hooks at 2 ft over midspan, 2 in. projection
 - No. 6 transverse hooks at 1 ft, stag. at 3 in. and 9 in.
 - 7 No. 8 top bars
 - No. 4 ties at spacing of top hooks
- Deck Longitudinal:**
- No. 7 at 4 in.
 - Full length with lap, first cutoff at 7 ft -5 in. from pier (end span), second cutoff at 24 ft -10 in. (end span), 13 ft -2 in. from pier (center span)
- Deck Transverse:**
- No. 5 at 12 in.
- Trough:**
- No. 4 corner bars
 - 4 No. 9 continuity bars at 5 in.
 - No. 4 stirrups at 12 in., adjacent to hooks
 - Overall spacing at 3 in. and 9 in.

Piers and Abutments

- Dowels:**
- 1 ft. - 6 in. projection
 - Holes drilled after beams placed, grouted
 - Next to ends at abutments, 4 No. 8 at 11 in.
 - In block-outs at piers, 4 No. 8 at 12 in., 1 ft - 9 in. symmetric over CL pier
- Bearing:**
- Polystyrene under beam bearing, not at block-out or 4 in. gap
 - Elastomeric bearing pad type 1, 6 in. strip under beam tabs

Core Summary

- 1) No cracking
- 2) Shrinkage crack: AI, 1/4 in. deep from surface

Crack Classification

Class AI	< 0.003"
Class AII	0.003" - 0.007"
Class BI	0.008" - 0.015"
Class BII	0.016" - 0.022"
Class CI	0.023" - 0.100"
Class CII	0.100" - 0.200"
Class D	> 0.200"

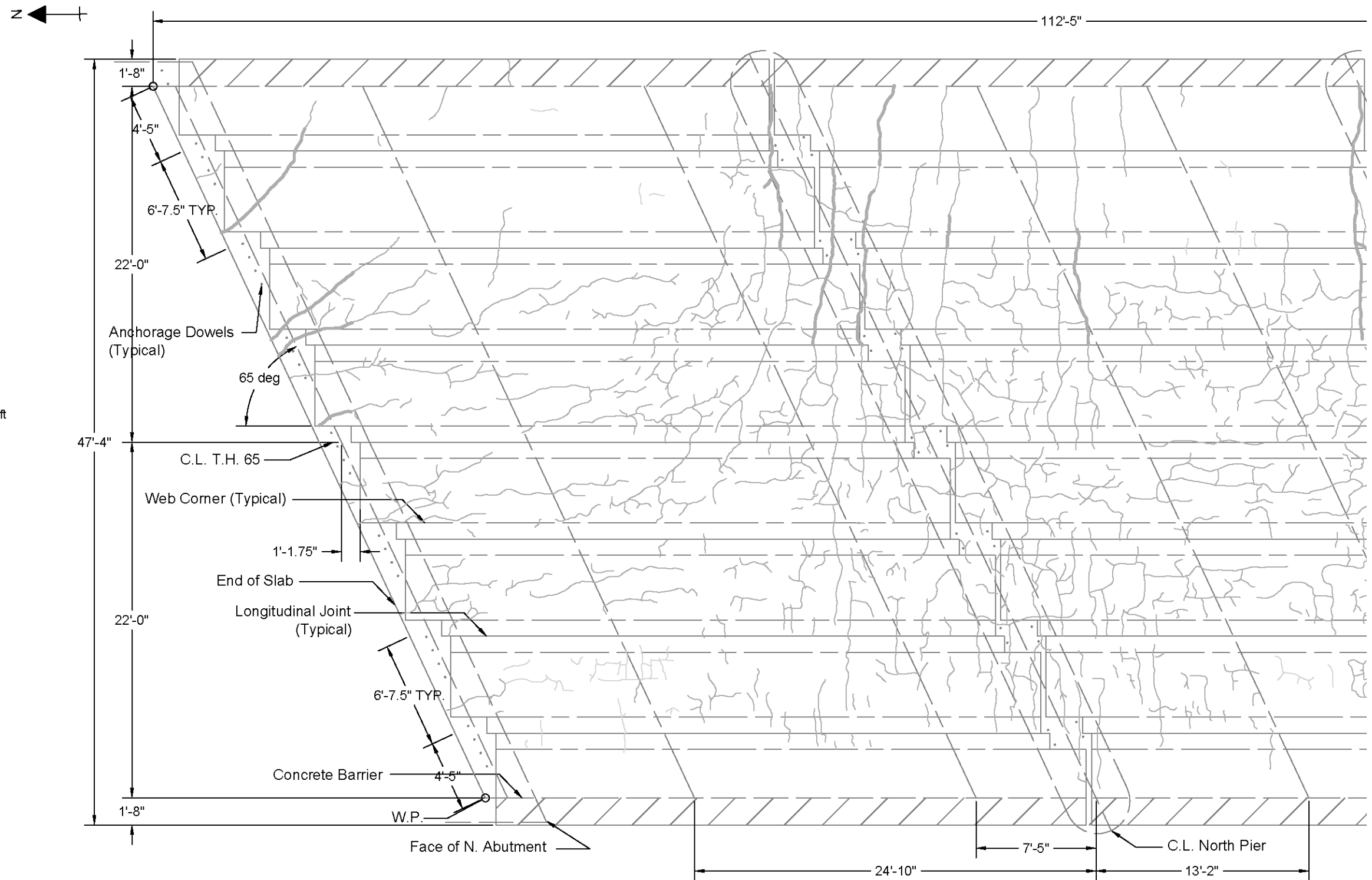
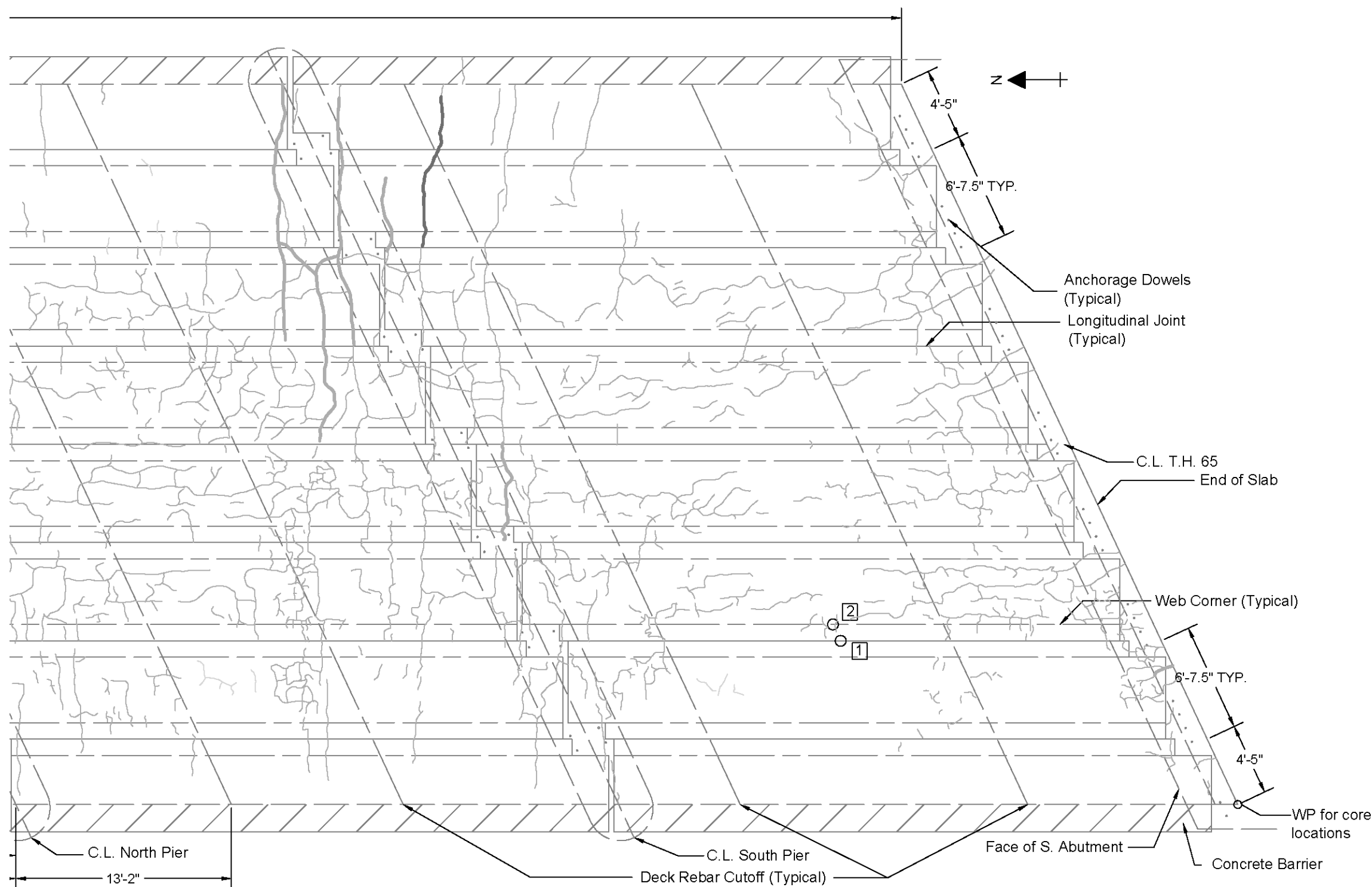


Figure A.10: Crack map for the north side of Bridge No. 33005 Inspection No. 2, June 29, 2010



Bridge No. 33005 (South)

Scale: 1" = 7'-0"
 Built: 11/02/2007 (Generation 2)
 Inspection No. 2: 06/29/2010

Age: 2.66 years
 Temperature: 46°F - 69°F (58°F average)
 Average Humidity: 57%
 Clouds/Precipitation: Clear

Precast Concrete

Release Strength: 4000 psi
 Final Strength: 6000 psi
 Depth: 14 in.
 Flange Thickness: 5.25 in.
 Strand: 22 - 0.5 in. Ø

Cast-in-Place Concrete

Strength: 4000 psi
 Slump: 3 in.
 Prewetted: No
 Surface Finish: Shallow longitudinal tining

Reinforcement

- Precast:**
- No. 4 composite hooks at 2 ft over midspan, 2 in. projection
 - No. 6 transverse hooks at 1 ft, stag. at 3 in. and 9 in.
 - 7 No. 8 top bars
 - No. 4 ties at spacing of top hooks
- Deck Longitudinal:**
- No. 7 at 4 in.
 - Full length with lap, first cutoff at 7 ft -5 in. from pier (end span), second cutoff at 24 ft -10 in. (end span), 13 ft -2 in. from pier (center span)
- Deck Transverse:**
- No. 5 at 12 in.
- Trough:**
- No. 4 corner bars
 - 4 No. 9 continuity bars at 5 in.
 - No. 4 stirrups at 12 in., adjacent to hooks
 - Overall spacing at 3 in. and 9 in.

Piers and Abutments

- Dowels:**
- 1 ft. - 6 in. projection
 - Holes drilled after beams placed, grouted
 - Next to ends at abutments, 4 No. 8 at 11 in.
 - In block-outs at piers, 4 No. 8 at 12 in., 1 ft - 9 in. symmetric over CL pier
- Bearing:**
- Polystyrene under beam bearing, not at block-out or 4 in. gap
 - Elastomeric bearing pad type 1, 6 in. strip under beam tabs

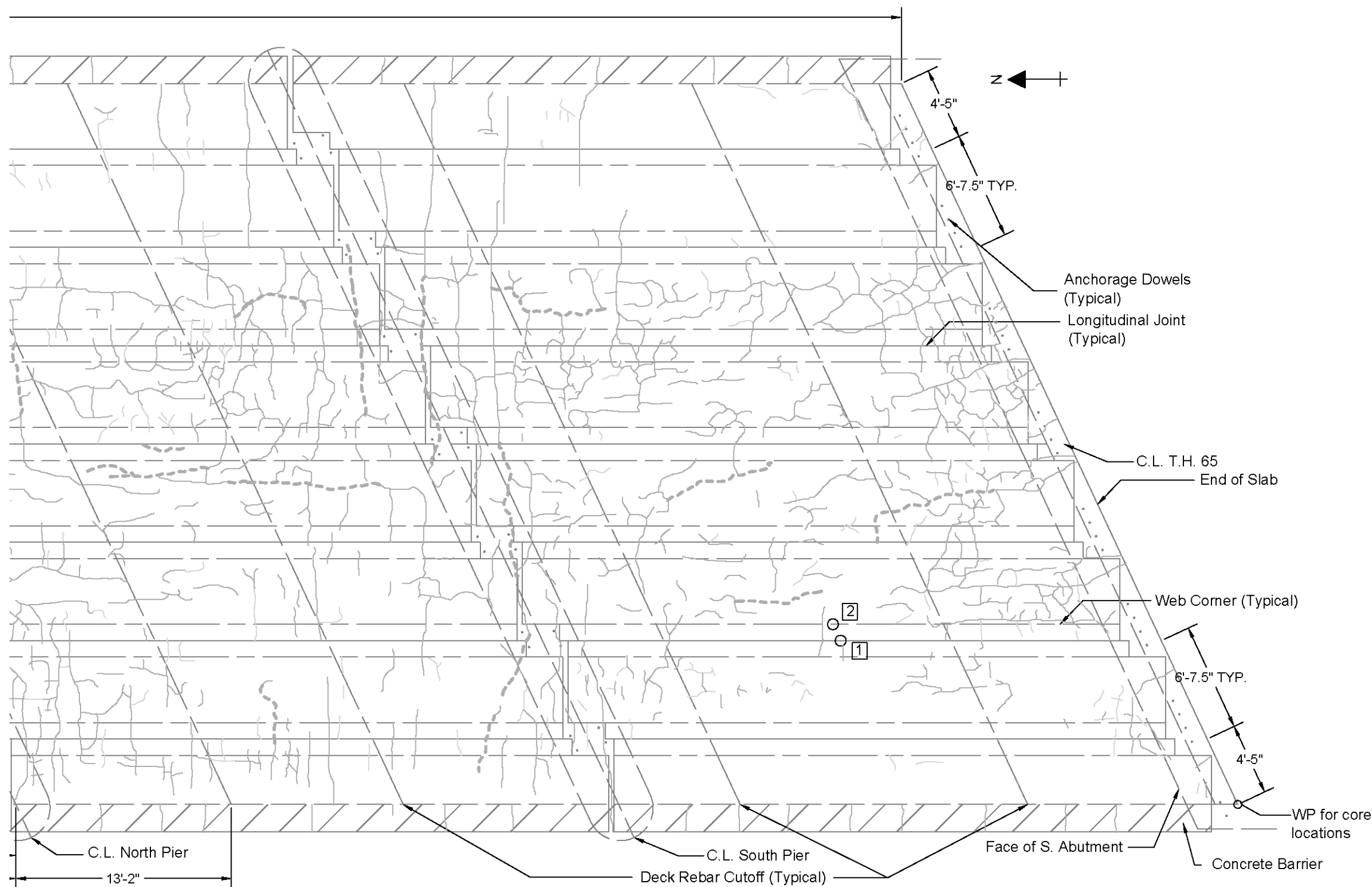
Core Summary

- 1) No cracking
- 2) Shrinkage crack: AI, 1/4 in. deep from surface

Crack Classification

Class	Crack Width Range (inches)
Class AI	< 0.003"
Class AII	0.003" - 0.007"
Class BI	0.008" - 0.015"
Class BII	0.016" - 0.022"
Class CI	0.023" - 0.100"
Class CII	0.100" - 0.200"
Class D	> 0.200"

Figure A.11: Crack map for the south side of Bridge No. 33005 Inspection No. 2, June 29, 2010



Bridge No. 33005 (South)

Scale: 1" = 7'-0"
 Built: 11/02/2007 (Generation 2)
 Inspection No. 3: 08/09/2011

Age: 3.77 years
 Temperature: 55°F - 69°F (62°F average)
 Average Humidity: 57%
 Clouds/Precipitation: Overcast

Precast Concrete

Release Strength: 4000 psi
 Final Strength: 6000 psi
 Depth: 14 in.
 Flange Thickness: 5.25 in.
 Strand: 22 - 0.5 in. Ø

Cast-in-Place Concrete

Strength: 4000 psi
 Slump: 3 in.
 Prewetted: No
 Surface Finish: Shallow longitudinal tining

Reinforcement

- Precast:**
- No. 4 composite hooks at 2 ft over midspan, 2 in. projection
 - No. 6 transverse hooks at 1 ft, stag. at 3 in. and 9 in.
 - 7 No. 8 top bars
 - No. 4 ties at spacing of top hooks
- Deck Longitudinal:**
- No. 7 at 4 in.
 - Full length with lap, first cutoff at 7 ft -5 in. from pier (end span), second cutoff at 24 ft -10 in. (end span), 13 ft - 2 in. from pier (center span)
- Deck Transverse:**
- No. 5 at 12 in.
- Trough:**
- No. 4 corner bars
 - 4 No. 9 continuity bars at 5 in.
 - No. 4 stirrups at 12 in., adjacent to hooks
 - Overall spacing at 3 in. and 9 in.

Piers and Abutments

- Dowels:**
- 1 ft. - 6 in. projection
 - Holes drilled after beams placed, grouted
 - Next to ends at abutments, 4 No. 8 at 11 in.
 - In block-outs at piers, 4 No. 8 at 12 in., 1 ft - 9 in. symmetric over CL pier
- Bearing:**
- Polystyrene under beam bearing, not at block-out or 4 in. gap
 - Elastomeric bearing pad type 1, 6 in. strip under beam tabs

Core Summary

- 1) No cracking
- 2) Shrinkage crack: AI, 1/4 in. deep from surface

Crack Classification

Class AI	< 0.003"
Class AII	0.003" - 0.007"
Class BI	0.008" - 0.015"
Class BII	0.016" - 0.022"
Class CI	0.023" - 0.100"
Class CII	0.100" - 0.200"
Class D	> 0.200"
---	Sealed, unknown width

Figure A.13: Crack map for the south side of Bridge No. 33005 Inspection No. 3, August 9, 2011

Bridge No. 33008

Scale: 1" = 10'-0"
 Built: 11/02/2007 (Generation 2)
 Inspection No. 1: 11/04/2009

Age: 2.00 years
 Temperature: 32°F - 41°F (36°F average)
 Average Humidity: 86%
 Clouds/Precipitation: Overcast

Precast Concrete
 Release Strength: 4500 psi
 Final Strength: 6500 psi
 Depth: 12 in.
 Flange Thickness: 5.25 in.
 Strand: 20 - 0.5 in. Ø

Cast-in-Place Concrete
 Strength: 4000 psi
 Slump: 3 in.
 Prewetted: No
 Surface Finish: Shallow longitudinal tining

Reinforcement

- Precast:**
- No. 5 composite hooks at 12 in. over midspan, 2 in. projection
 - No. 6 transverse hooks at 12 in., stag. at 4 in. and 8 in.
 - 7 No. 8 top bars
 - No. 4 ties at spacing of top hooks
- Deck Longitudinal:**
- No. 8 at 4 in.
 - Full length with lap; first cutoff at 10 ft from pier (end and center spans); second cutoff at 16 ft from pier (end span only)
- Deck Transverse:**
- No. 5 at 12 in.
- Trough:**
- No. 5 corner bars
 - 4 No. 8 continuity bars at 5 in.
 - No. 5 stirrups at 12 in., adjacent to hooks
 - Overall spacing at 4 in. and 8 in.

Piers and Abutments

- Dowels:**
- 12 in. projection
 - Cast in place with cap
 - In block-outs at abutments, 3 No. 6 at 9 in.
 - In block-outs at piers, 6 No. 6 at 9 in., 1 ft. - 6 in. symmetric over CL pier
- Bearing:**
- Polystyrene under beam bearing, not at block-out or 4 in. gap
 - Elastomeric bearing pad type 1, 6 in. strip under beam tabs

Core Summary

- 1) Reflective crack: AI - BI, full depth
- 2) Shrinkage crack: AI, 1/2 in. deep from surface
- 3) Reflective crack: AI, 5 3/4 in. deep from joint
- 4) Shrinkage crack: AI - BI, 3 1/2 in. deep from surface

Crack Classification

Class A	< 0.007"
Class B	0.008" - 0.022"
Class C	0.023" - 0.200"
Class D	> 0.200"

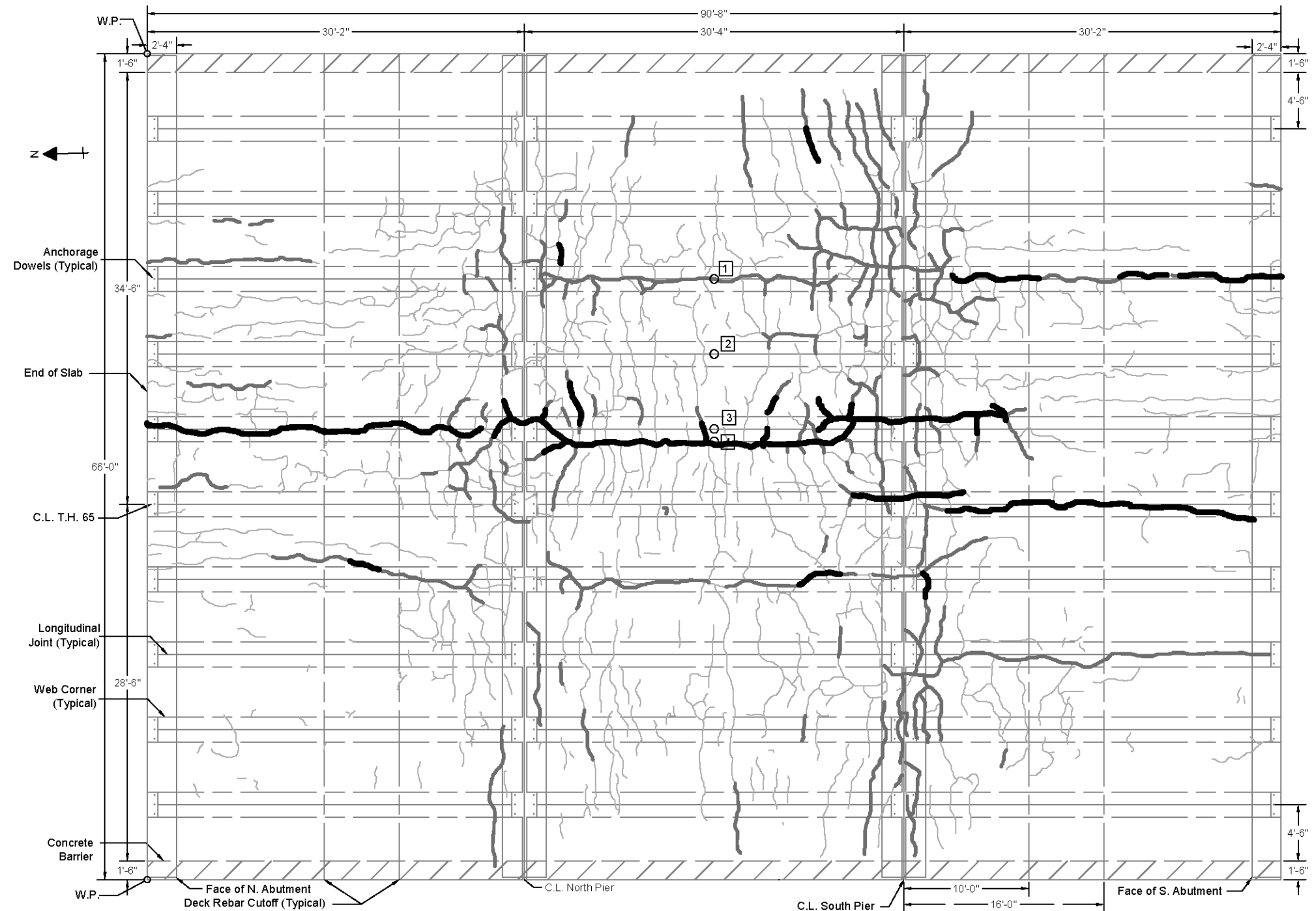


Figure A.14: Crack map for Bridge No. 33008 Inspection No. 1, November 4, 2009

Bridge No. 33008

Scale: 1" = 10'-0"
 Built: 11/02/2007 (Generation 2)
 Inspection No. 2: 05/24/2010

Age: 2.56 years
 Temperature: 64°F - 89°F (76°F average)
 Average Humidity: 66%
 Clouds/Precipitation: Partly Cloudy

Precast Concrete
 Release Strength: 4500 psi
 Final Strength: 6500 psi
 Depth: 12 in.
 Flange Thickness: 5.25 in.
 Strand: 20 - 0.5 in. Ø

Cast-in-Place Concrete
 Strength: 4000 psi
 Slump: 3 in.
 Prewetted: No
 Surface Finish: Shallow longitudinal tining

Reinforcement

Precast:
 - No. 5 composite hooks at 12 in. over midspan, 2 in. projection
 - No. 6 transverse hooks at 12 in., stag. at 4 in. and 8 in.
 - 7 No. 8 top bars
 - No. 4 ties at spacing of top hooks

Deck Longitudinal:
 - No. 8 at 4 in.
 - Full length with lap; first cutoff at 10 ft from pier (end and center spans); second cutoff at 16 ft from pier (end span only)

Deck Transverse:
 - No. 5 at 12 in.

Trough:
 - No. 5 corner bars
 - 4 No. 8 continuity bars at 5 in.
 - No. 5 stirrups at 12 in., adjacent to hooks
 - Overall spacing at 4 in. and 8 in.

Piers and Abutments

Dowels:
 - 12 in. projection
 - Cast in place with cap
 - In block-outs at abutments, 3 No. 6 at 9 in.
 - In block-outs at piers, 6 No. 6 at 9 in., 1 ft. - 6 in. symmetric over CL pier

Bearing:
 - Polystyrene under beam bearing, not at block-out or 4 in. gap
 - Elastomeric bearing pad type 1, 6 in. strip under beam tabs

Core Summary

- 1) Reflective crack: AI - BI, full depth
- 2) Shrinkage crack: All, 1/2 in. deep from surface
- 3) Reflective crack: AI, 5 3/4 in. deep from joint
- 4) Shrinkage crack: AI - BI, 3 1/2 in. deep from surface

Crack Classification

Class AI	< 0.003"
Class All	0.003" - 0.007"
Class BI	0.008" - 0.015"
Class BII	0.016" - 0.022"
Class CI	0.023" - 0.100"
Class CII	0.100" - 0.200"
Class D	> 0.200"

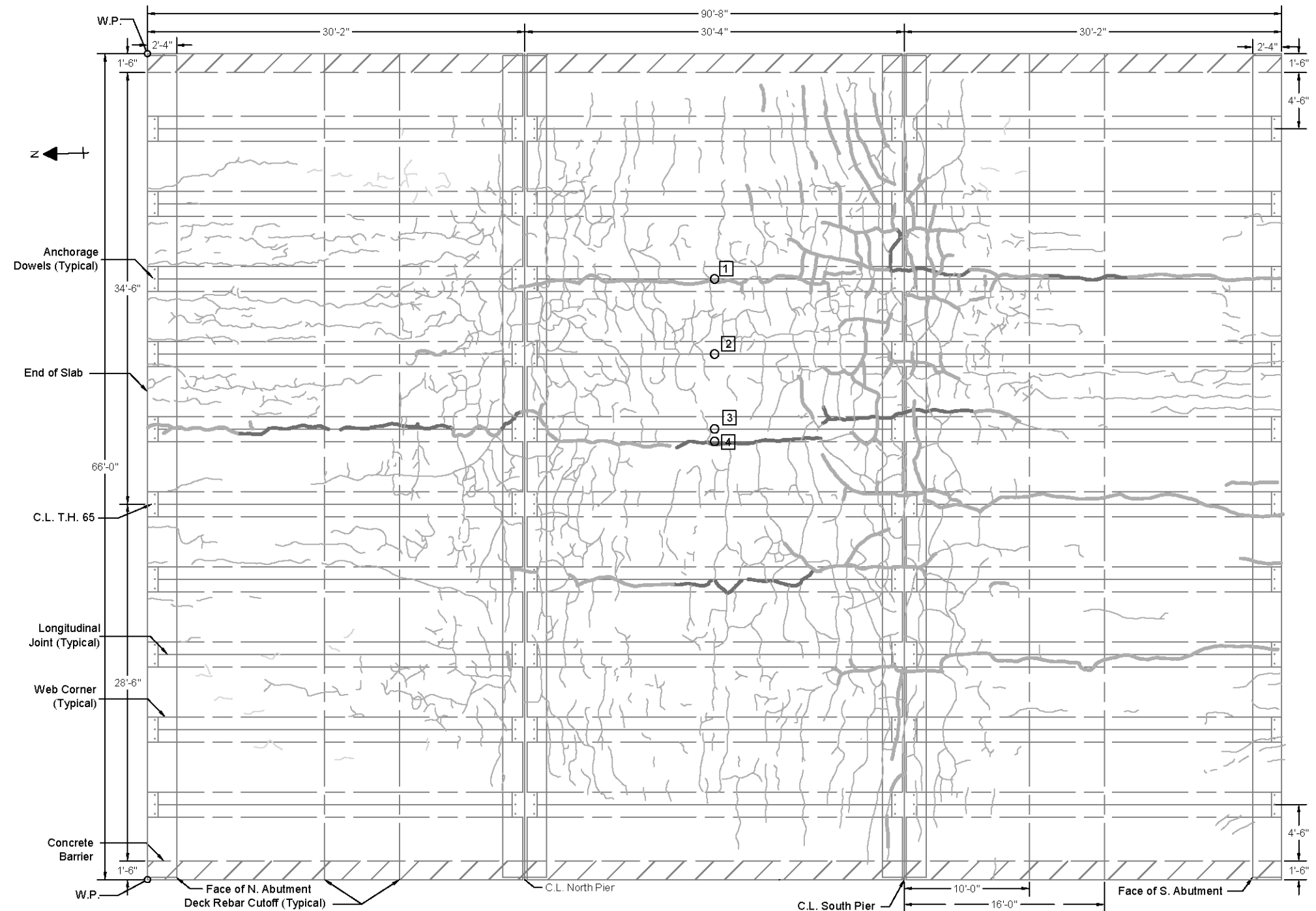


Figure A.15: Crack map for Bridge No. 33008 Inspection No. 2, May 24, 2010

Bridge No. 33008

Scale: 1" = 10'-0"
 Built: 11/02/2007 (Generation 2)
 Inspection No. 3: 06/16 and 08/10, 2011

Age: 1.62 years
 Temp.: 53°F-68°F (60°F average); 62°F-75°F (65°F average)
 Average Humidity: 76%
 Clouds/Precipitation: Overcast; clear

Precast Concrete
 Release Strength: 4500 psi
 Final Strength: 6500 psi
 Depth: 12 in.
 Flange Thickness: 5.25 in.
 Strand: 20 - 0.5 in. Ø

Cast-in-Place Concrete
 Strength: 4000 psi
 Slump: 3 in.
 Prewetted: No
 Surface Finish: Shallow longitudinal tining

Reinforcement

Precast:
 - No. 5 composite hooks at 12 in. over midspan, 2 in. projection
 - No. 6 transverse hooks at 12 in., stag. at 4 in. and 8 in.
 - 7 No. 8 top bars
 - No. 4 ties at spacing of top hooks

Deck Longitudinal:
 - No. 8 at 4 in.
 - Full length with lap; first cutoff at 10 ft from pier (end and center spans); second cutoff at 16 ft from pier (end span only)

Deck Transverse:
 - No. 5 at 12 in.

Trough:
 - No. 5 corner bars
 - 4 No. 8 continuity bars at 5 in.
 - No. 5 stirrups at 12 in., adjacent to hooks
 - Overall spacing at 4 in. and 8 in.

Piers and Abutments

Dowels:
 - 12 in. projection
 - Cast in place with cap
 - In block-outs at abutments, 3 No. 6 at 9 in.
 - In block-outs at piers, 6 No. 6 at 9 in., 1 ft. - 6 in. symmetric over CL pier

Bearing:
 - Polystyrene under bearing, not at blockout or 4 in. gap
 - Elastomeric bearing pad type 1, 6 in. strip under beam tabs

Core Summary

- 1) Reflective crack: AI - BI, full depth
- 2) Shrinkage crack: All, 1/2 in. deep from surface
- 3) Reflective crack: AI, 5 3/4 in. deep from joint
- 4) Shrinkage crack: AI - BI, 3 1/2 in. deep from surface

Crack Classification

Class AI	< 0.003"
Class All	0.003" - 0.007"
Class BI	0.008" - 0.015"
Class BII	0.016" - 0.022"
Class CI	0.023" - 0.100"
Class CII	0.100" - 0.200"
Class D	> 0.200"
--- Sealed	(unknown width)

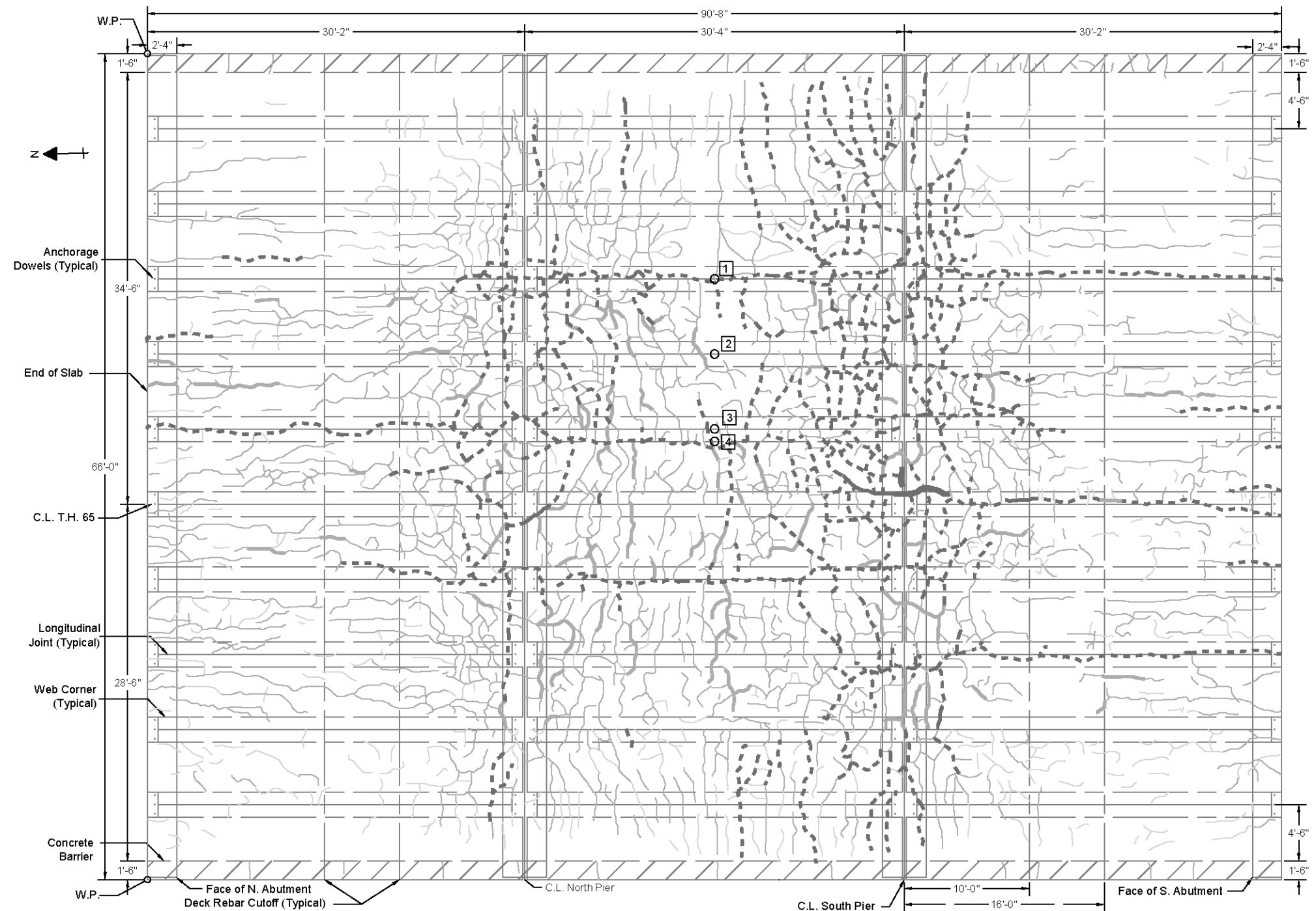


Figure A.16: Crack map for Bridge No. 33008 Inspection No. 3, June 16 and August 10, 2011

Bridge No. 49007 (South)

Scale: 1" = 6'-0"
 Built: 08/11/2009 (Generation 3)
 Inspection No. 1: 10/12, 10/14 and 10/19, 2009

Age: 0.17 years
 Temperature: 28°F - 54°F (40°F average)
 Average Humidity: 80%
 Clouds/Precipitation: Cloudy, snow on first day

Precast Concrete
 Release Strength: 4500 psi
 Final Strength: 6500 psi
 Depth: 16 in.
 Flange Thickness: 3 in.
 Strand: 22 - 0.5 in. Ø

Cast-in-Place Concrete
 Strength: 4000 psi
 Slump: Not available
 Prewetted: Yes
 Surface Finish: Deep longitudinal tining

Reinforcement
 Precast:
 - No. 4 composite hooks at 6 in. for 11 ft, at 12 in. for 2 ft, at 2 ft for 8 ft (sym.), 2 in. projection
 - No. 6 transverse hooks at 12 in., stag. at 6 in.
 - 7 No. 8 top bars
 - No. 4 ties at spacing of top hooks
 Deck Longitudinal:
 - No. 7 at 4 in.
 - Full length with lap, first cutoff at 7 ft. - 5 in. from pier (end span), second cutoff at 24 ft - 10 in. (end span), 13 ft - 2 in. from pier (center span)
 Deck Transverse:
 - No. 4 at 6 in.
 Trough:
 - No. 5 corner bars
 - 4 No. 8 continuity bars at 4.5 in.
 - No. 5 stirrups at 12 in., adjacent to hooks
 - Overall spacing at 6 in.

Piers and Abutments
 Dowels:
 - 1 ft - 6 in. projection
 - Holes drilled after beams placed, grouted
 - Polystyrene wrapped 4 outer sets
 - In blockouts at abutments, 2 No. 8 at 12 in.
 - In blockouts at piers, 4 No. 8 at 12 in., 12 in. symmetric over CL pier
 Bearing:
 - Polystyrene under bearing, not at blockout or 4 in. gap
 - Elastomeric bearing pad type 1, 6 in. strip under beam tabs

Core Summary
 1) No cracking
 2) No cracking
 3) Shrinkage crack: All, 1 in. deep from surface
 4) No cracking

Crack Classification

Class A	< 0.007"
Class B	0.008" - 0.022"
Class C	0.023" - 0.200"
Class D	> 0.200"

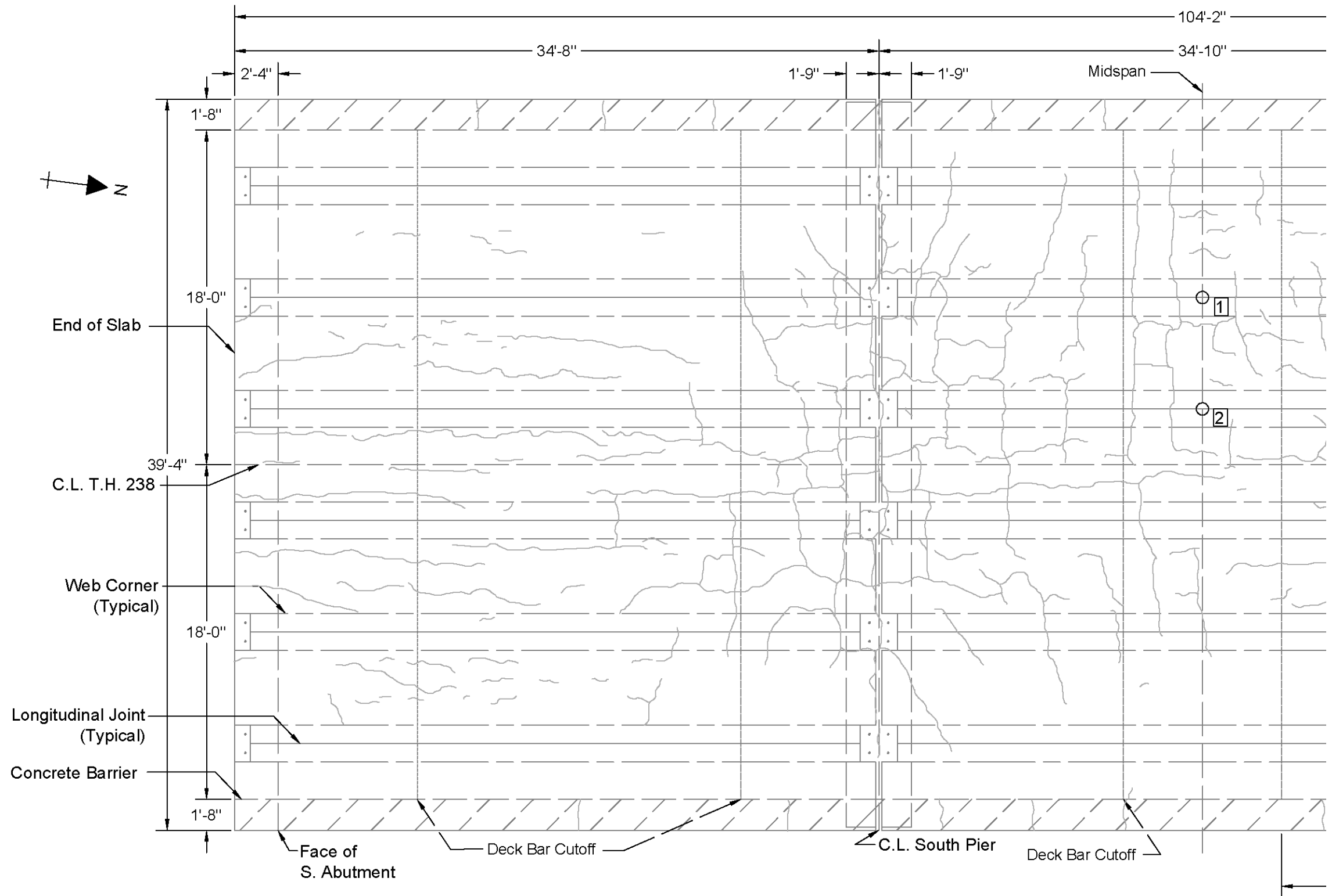
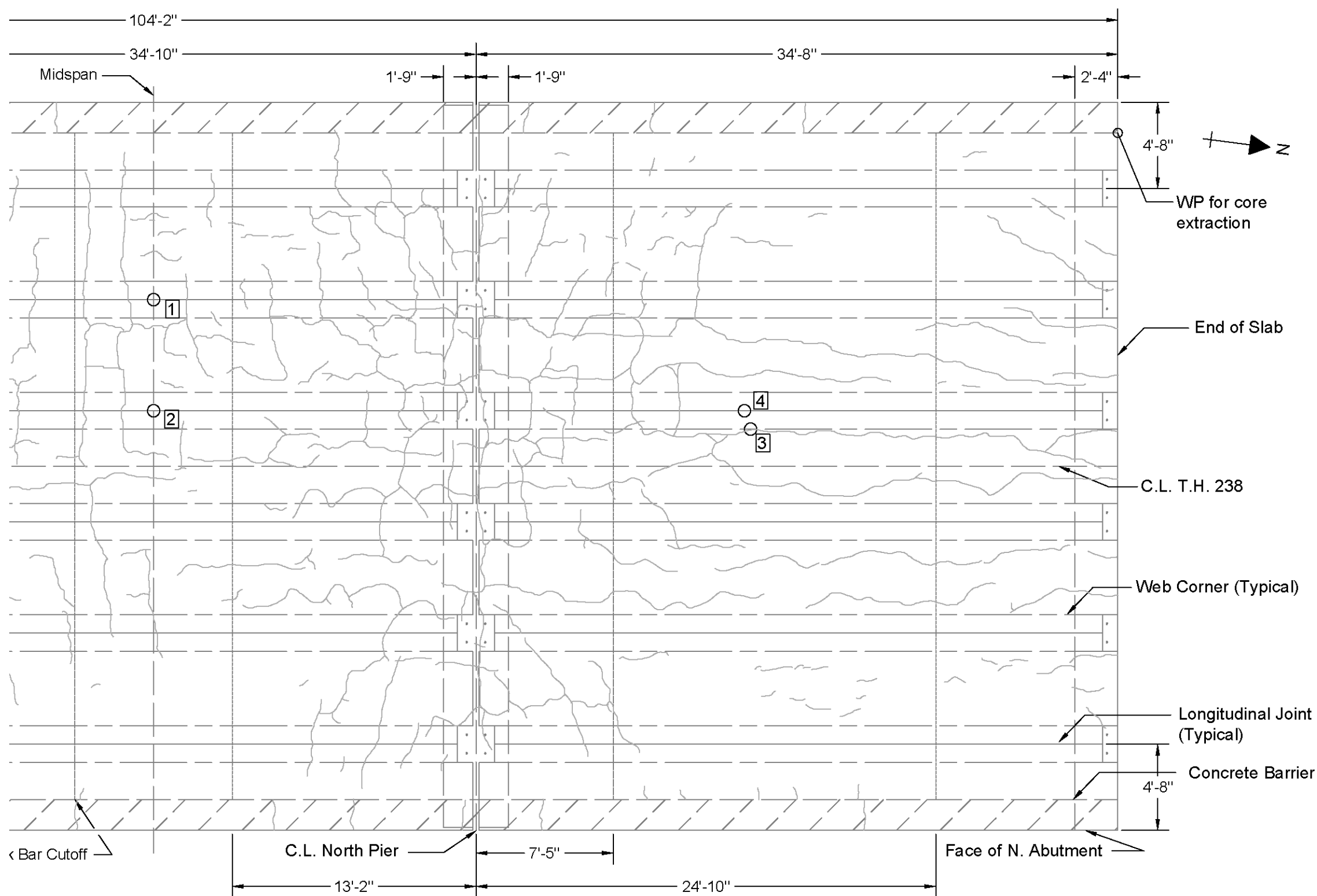


Figure A.17: Crack map for the south side of Bridge No. 49007 Inspection No. 1, October 14 and 19, 2009



Bridge No. 49007 (North)

Scale: 1" = 6'-0"
 Built: 08/11/2009 (Generation 3)
 Inspection No. 1: 10/12, 10/14 and 10/19, 2009

Age: 0.17 years
 Temperature: 28°F - 54°F (40°F average)
 Average Humidity: 80%
 Clouds/Precipitation: Cloudy, snow on first day

Precast Concrete
 Release Strength: 4500 psi
 Final Strength: 6500 psi
 Depth: 16 in.
 Flange Thickness: 3 in.
 Strand: 22 - 0.5 in. Ø

Cast-in-Place Concrete
 Strength: 4000 psi
 Slump: Not available
 Prewetted: Yes
 Surface Finish: Deep longitudinal tining

Reinforcement
Precast:
 - No. 4 composite hooks at 6 in. for 11 ft, at 12 in. for 2 ft, at 2 ft for 8 ft (sym.), 2 in. projection
 - No. 6 transverse hooks at 12 in., stag. at 6 in.
 - 7 No. 8 top bars
 - No. 4 ties at spacing of top hooks
Deck Longitudinal:
 - No. 7 at 4 in.
 - Full length with lap, first cutoff at 7 ft. - 5 in. from pier (end span), second cutoff at 24 ft - 10 in. (end span), 13 ft - 2 in. from pier (center span)
Deck Transverse:
 - No. 4 at 6 in.
Trough:
 - No. 5 corner bars
 - 4 No. 8 continuity bars at 4.5 in.
 - No. 5 stirrups at 12 in., adjacent to hooks
 - Overall spacing at 6 in.

Piers and Abutments
Dowels:
 - 1 ft - 6 in. projection
 - Holes drilled after beams placed, grouted
 - Polystyrene wrapped 4 outer sets
 - In blockouts at abutments, 2 No. 8 at 12 in.
 - In blockouts at piers, 4 No. 8 at 12 in., 12 in. symmetric over CL pier
Bearing:
 - Polystyrene under bearing, not at blockout or 4 in. gap
 - Elastomeric bearing pad type 1, 6 in. strip under beam tabs

Core Summary
 1) No cracking
 2) No cracking
 3) Shrinkage crack: All, 1 in. deep from surface
 4) No cracking

Crack Classification
 — Class A < 0.007"
 — Class B 0.008" - 0.022"
 — Class C 0.023" - 0.200"
 — Class D > 0.200"

Figure A.18: Crack map for the north side of Bridge No. 49007 Inspection No. 1, October 14 and 19, 2009

Bridge No. 49007 (South)

Scale: 1" = 6'-0"
 Built: 08/11/2009 (Generation 3)
 Inspection No. 2: 06/14/2010

Age: 0.84 years
 Temperature: 55°F - 64°F (60°F average)
 Average Humidity: 85%
 Clouds/Precipitation: Clear

Precast Concrete
 Release Strength: 4500 psi
 Final Strength: 6500 psi
 Depth: 16 in.
 Flange Thickness: 3 in.
 Strand: 22 - 0.5 in. Ø

Cast-in-Place Concrete
 Strength: 4000 psi
 Slump: Not available
 Prewetted: Yes
 Surface Finish: Deep longitudinal tining

Reinforcement

Precast:
 - No. 4 composite hooks at 6 in. for 11 ft, at 12 in. for 2 ft, at 2 ft for 8 ft (sym.), 2 in. projection
 - No. 6 transverse hooks at 12 in., stag. at 6 in.
 - 7 No. 8 top bars
 - No. 4 ties at spacing of top hooks

Deck Longitudinal:
 - No. 7 at 4 in.
 - Full length with lap, first cutoff at 7 ft. - 5 in. from pier (end span), second cutoff at 24 ft - 10 in. (end span), 13 ft - 2 in. from pier (center span)

Deck Transverse:
 - No. 4 at 6 in.

Trough:
 - No. 5 corner bars
 - 4 No. 8 continuity bars at 4.5 in.
 - No. 5 stirrups at 12 in., adjacent to hooks
 - Overall spacing at 6 in.

Piers and Abutments

Dowels:
 - 1 ft - 6 in. projection
 - Holes drilled after beams placed, grouted
 - Polystyrene wrapped 4 outer sets
 - In blockouts at abutments, 2 No. 8 at 12 in.
 - In blockouts at piers, 4 No. 8 at 12 in., 12 in. symmetric over CL pier

Bearing:
 - Polystyrene under bearing, not at blockout or 4 in. gap
 - Elastomeric bearing pad type 1, 6 in. strip under beam tabs

Core Summary

- 1) No cracking
- 2) No cracking
- 3) Shrinkage crack: All, 1 in. deep from surface
- 4) No cracking

Crack Classification

Class AI	< 0.003"
Class AII	0.003" - 0.007"
Class BI	0.008" - 0.015"
Class BII	0.016" - 0.022"
Class CI	0.023" - 0.100"
Class CII	0.100" - 0.200"
Class D	> 0.200"

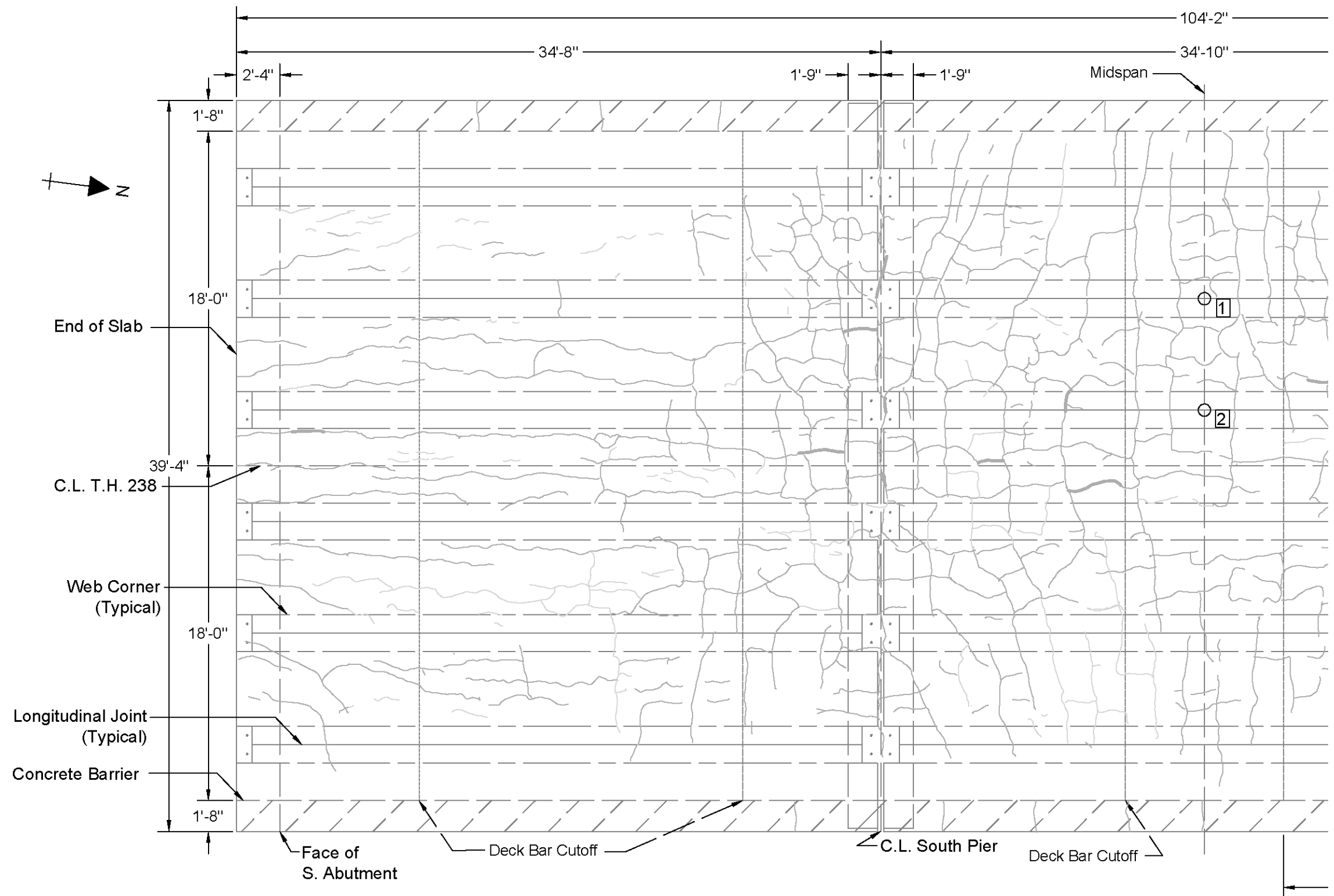
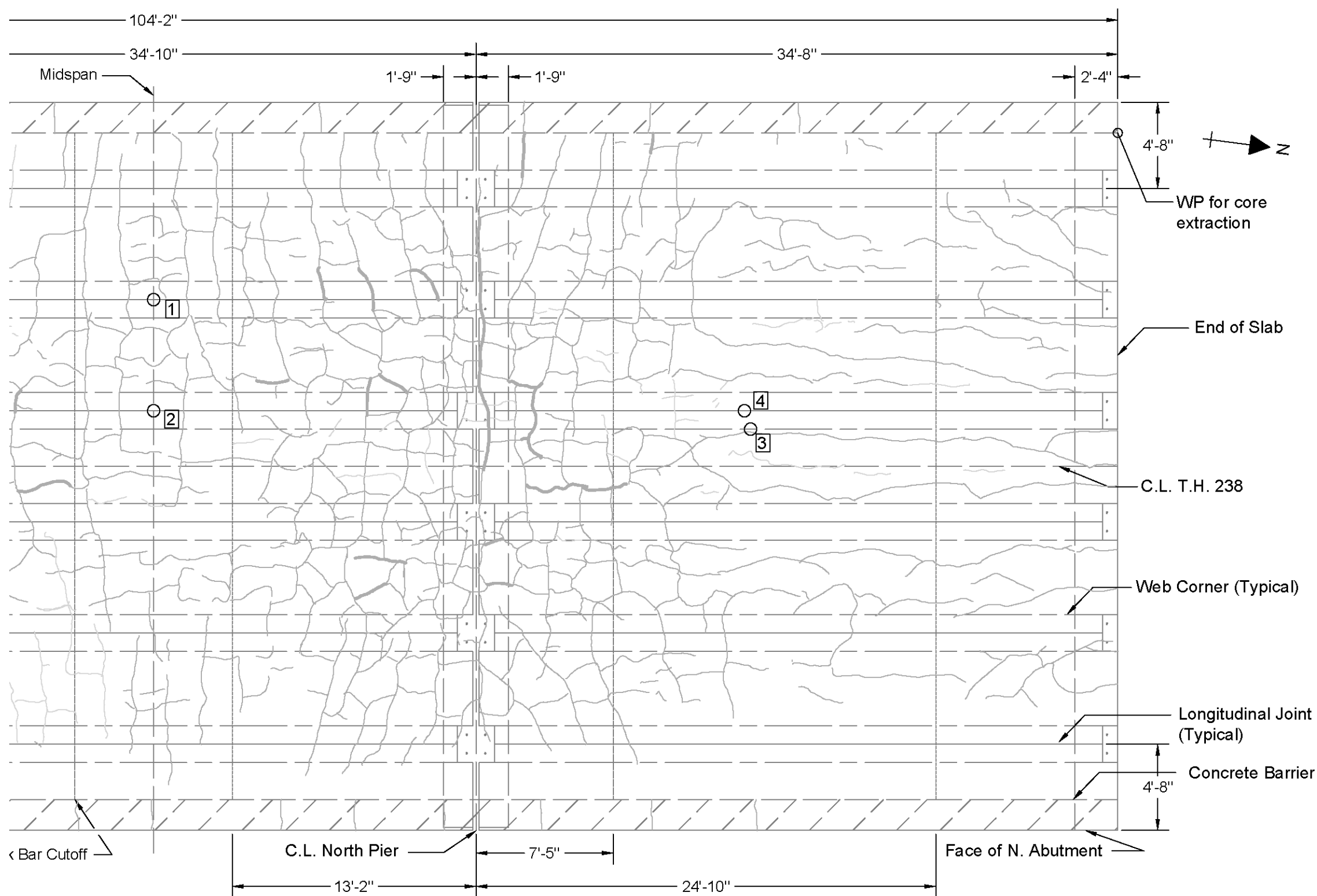


Figure A.19: Crack map for the south side of Bridge No. 49007 Inspection No. 2, June 14, 2010



Bridge No. 49007 (North)

Scale: 1" = 6'-0"
 Built: 08/11/2009 (Generation 3)
 Inspection No. 2: 06/14/2010

Age: 0.84 years
 Temperature: 55°F - 64°F (60°F average)
 Average Humidity: 85%
 Clouds/Precipitation: Clear

Precast Concrete
 Release Strength: 4500 psi
 Final Strength: 6500 psi
 Depth: 16 in.
 Flange Thickness: 3 in.
 Strand: 22 - 0.5 in. Ø

Cast-in-Place Concrete
 Strength: 4000 psi
 Slump: Not available
 Prewetted: Yes
 Surface Finish: Deep longitudinal tining

Reinforcement
 Precast:
 - No. 4 composite hooks at 6 in. for 11 ft, at 12 in. for 2 ft, at 2 ft for 8 ft (sym.), 2 in. projection
 - No. 6 transverse hooks at 12 in., stag. at 6 in.
 - 7 No. 8 top bars
 - No. 4 ties at spacing of top hooks

Deck Longitudinal:
 - No. 7 at 4 in.
 - Full length with lap, first cutoff at 7 ft. - 5 in. from pier (end span), second cutoff at 24 ft - 10 in. (end span), 13 ft - 2 in. from pier (center span)

Deck Transverse:
 - No. 4 at 6 in.

Trough:
 - No. 5 corner bars
 - 4 No. 8 continuity bars at 4.5 in.
 - No. 5 stirrups at 12 in., adjacent to hooks
 - Overall spacing at 6 in.

Piers and Abutments
 Dowels:
 - 1 ft - 6 in. projection
 - Holes drilled after beams placed, grouted
 - Polystyrene wrapped 4 outer sets
 - In blockouts at abutments, 2 No. 8 at 12 in.
 - In blockouts at piers, 4 No. 8 at 12 in., 12 in. symmetric over CL pier

Bearing:
 - Polystyrene under bearing, not at blockout or 4 in. gap
 - Elastomeric bearing pad type 1, 6 in. strip under beam tabs

Core Summary
 1) No cracking
 2) No cracking
 3) Shrinkage crack: All, 1 in. deep from surface
 4) No cracking

Crack Classification

Class AI	< 0.003"
Class AII	0.003" - 0.007"
Class BI	0.008" - 0.015"
Class BII	0.016" - 0.022"
Class CI	0.023" - 0.100"
Class CII	0.100" - 0.200"
Class D	> 0.200"

Figure A.20: Crack map for the north side of Bridge No. 49007 Inspection No. 2, June 14, 2010

Bridge No. 49007 (South)

Scale: 1" = 6'-0"
 Built: 08/11/2009 (Generation 3)
 Inspection No. 3: 06/29/2011

Age: 1.88 years
 Temperature: 50°F - 80°F (65°F average)
 Average Humidity: 68%
 Clouds/Precipitation: Clear, some scattered clouds

Precast Concrete
 Release Strength: 4500 psi
 Final Strength: 6500 psi
 Depth: 16 in.
 Flange Thickness: 3 in.
 Strand: 22 - 0.5 in. Ø

Cast-in-Place Concrete
 Strength: 4000 psi
 Slump: Not available
 Prewetted: Yes
 Surface Finish: Deep longitudinal tining

Reinforcement

Precast:
 - No. 4 composite hooks at 6 in. for 11 ft, at 12 in. for 2 ft, at 2 ft for 8 ft (sym.), 2 in. projection
 - No. 6 transverse hooks at 12 in., stag. at 6 in.
 - 7 No. 8 top bars
 - No. 4 ties at spacing of top hooks

Deck Longitudinal:
 - No. 7 at 4 in.
 - Full length with lap, first cutoff at 7 ft. - 5 in. from pier (end span), second cutoff at 24 ft - 10 in. (end span), 13 ft - 2 in. from pier (center span)

Deck Transverse:
 - No. 4 at 6 in.

Trough:
 - No. 5 corner bars
 - 4 No. 8 continuity bars at 4.5 in.
 - No. 5 stirrups at 12 in., adjacent to hooks
 - Overall spacing at 6 in.

Piers and Abutments

Dowels:
 - 1 ft - 6 in. projection
 - Holes drilled after beams placed, grouted
 - Polystyrene wrapped 4 outer sets
 - In blockouts at abutments, 2 No. 8 at 12 in.
 - In blockouts at piers, 4 No. 8 at 12 in., 12 in. symmetric over CL pier

Bearing:
 - Polystyrene under bearing, not at blockout or 4 in. gap
 - Elastomeric bearing pad type 1, 6 in. strip under beam tabs

Core Summary

- 1) No cracking
- 2) No cracking
- 3) Shrinkage crack: All, 1 in. deep from surface
- 4) No cracking

Crack Classification

Class AI	< 0.003"
Class AII	0.003" - 0.007"
Class BI	0.008" - 0.015"
Class BII	0.016" - 0.022"
Class CI	0.023" - 0.100"
Class CII	0.100" - 0.200"
Class D	> 0.200"

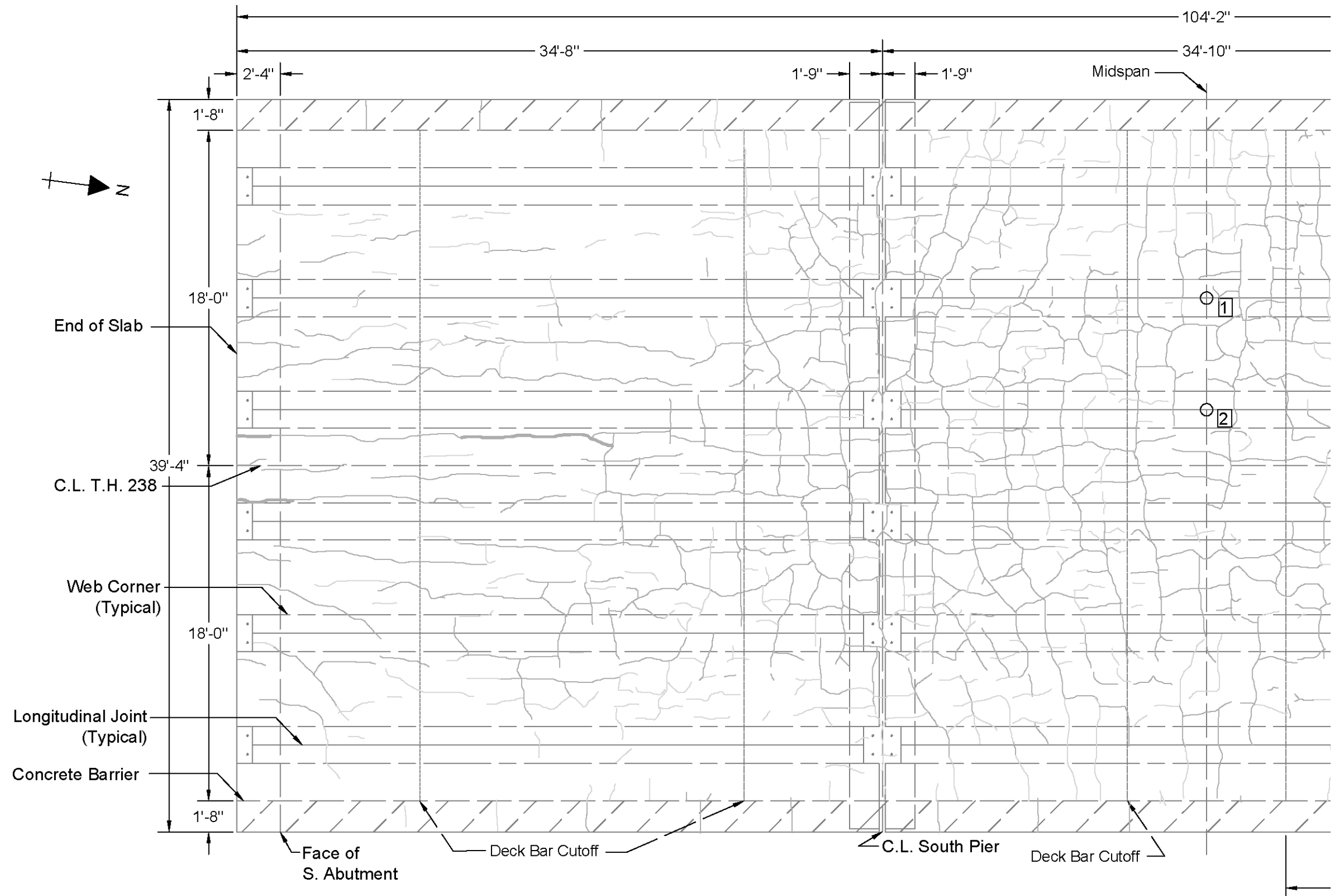
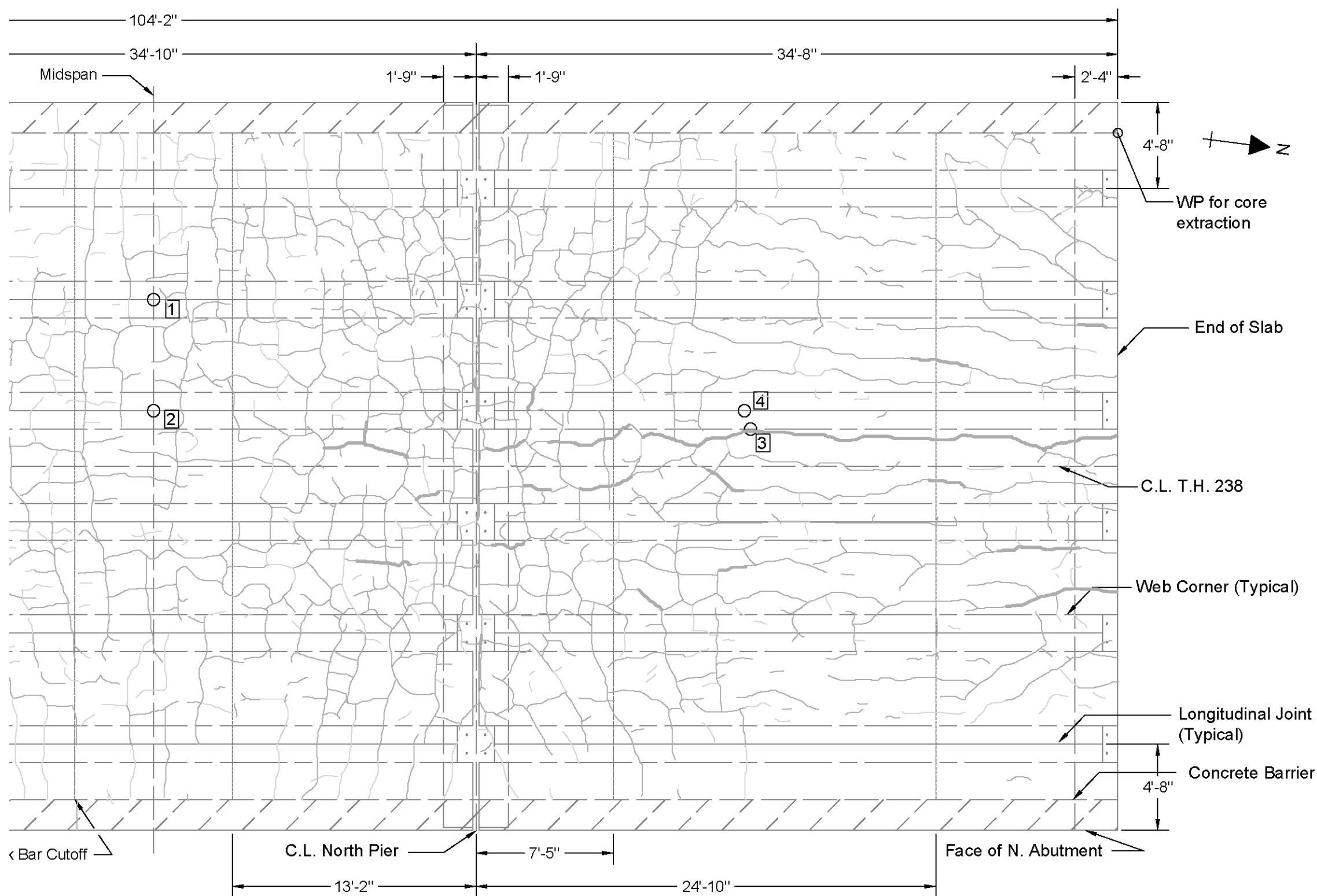


Figure A.21: Crack map for the south side of Bridge No. 49007 Inspection No. 3, June 29, 2011



Bridge No. 49007 (North)

Scale: 1" = 6'-0"
 Built: 08/11/2009 (Generation 3)
 Inspection No. 3: 06/29/2011

Age: 1.88 years
 Temperature: 50°F - 80°F (65°F average)
 Average Humidity: 68%
 Clouds/Precipitation: Clear, some scattered clouds

Precast Concrete

Release Strength: 4500 psi
 Final Strength: 6500 psi
 Depth: 16 in.
 Flange Thickness: 3 in.
 Strand: 22 - 0.5 in. Ø

Cast-in-Place Concrete

Strength: 4000 psi
 Slump: Not available
 Prewetted: Yes
 Surface Finish: Deep longitudinal tining

Reinforcement

Precast:

- No. 4 composite hooks at 6 in. for 11 ft, at 12 in. for 2 ft, at 2 ft for 8 ft (sym.), 2 in. projection
- No. 6 transverse hooks at 12 in., stag. at 6 in.
- 7 No. 8 top bars
- No. 4 ties at spacing of top hooks

Deck Longitudinal:

- No. 7 at 4 in.
- Full length with lap, first cutoff at 7 ft. - 5 in. from pier (end span), second cutoff at 24 ft - 10 in. (end span), 13 ft - 2 in. from pier (center span)

Deck Transverse:

- No. 4 at 6 in.

Trough:

- No. 5 corner bars
- 4 No. 8 continuity bars at 4.5 in.
- No. 5 stirrups at 12 in., adjacent to hooks
- Overall spacing at 6 in.

Piers and Abutments

Dowels:

- 1 ft - 6 in. projection
- Holes drilled after beams placed, grouted
- Polystyrene wrapped 4 outer sets
- In blockouts at abutments, 2 No. 8 at 12 in.
- In blockouts at piers, 4 No. 8 at 12 in., 12 in. symmetric over CL pier

Bearing:

- Polystyrene under bearing, not at blockout or 4 in. gap
- Elastomeric bearing pad type 1, 6 in. strip under beam tabs

Core Summary

- 1) No cracking
- 2) No cracking
- 3) Shrinkage crack: All, 1 in. deep from surface
- 4) No cracking

Crack Classification

Class AI	< 0.003"
Class AII	0.003" - 0.007"
Class BI	0.008" - 0.015"
Class BII	0.016" - 0.022"
Class CI	0.023" - 0.100"
Class CII	0.100" - 0.200"
Class D	> 0.200"

Figure A.22: Crack map for the north side of Bridge No. 49007 Inspection No. 3, June 29, 2011

Bridge No. 49036

Scale: 1" = 7'-0"
 Built: 08/11/2009 (Generation 3)
 Inspection No. 1: 11/06/2009

Age: 0.24 years
 Temperature: 37°F - 57°F (47°F average)
 Average Humidity: 74%
 Clouds/Precipitation: Clear

Precast Concrete
 Release Strength: 4000 psi
 Final Strength: 6000 psi
 Depth: 12 in.
 Flange Thickness: 3 in.
 Strand: 16, 0.5 in.

Cast-in-Place Concrete
 Strength: 4000 psi
 Slump: Not available
 Prewetted: Yes
 Surface Finish: Deep transverse tining

Reinforcement
 Precast:
 - No. 4 composite hooks at 6 in. to 10 in. for 19 ft, at 12 in. for 5 ft (sym.), 2 in. projection
 - No. 6 transverse hooks at 1 ft, not staggered
 - 7 No. 8 top bars
 - No. 4 ties at spacing of top hooks
 Deck Longitudinal:
 - No. 7 at 4 in.
 - Full length with lap, first cutoff at 10 ft from pier (end and center span), second cutoff at 16 ft from pier (end span only)
 Deck Transverse:
 - No. 4 at 6 in.
 Trough:
 - No. 5 corner bars
 - 4 No. 9 continuity bars at 4.5 in.
 - No. 5 stirrups at 12 in., adjacent to hooks
 - Overall spacing at 12 in.

Piers and Abutments
 Dowels:
 - 12 in. projection
 - Holes drilled after beams placed, grouted
 - Polystyrene wrapped 4 outer sets
 - In block-outs at abutments, 2 No. 8 at 12 in.
 - In block-outs at piers, 4 No. 8 at 1 ft - 6 in., 1 ft - 6 in. symmetric over CL pier
 Bearing:
 - Polystyrene under beam bearing, not at block-out or 4 in. gap
 - Elastomeric bearing pad type 1, 6 in. strip under beam tabs

Core Summary
 1) No cracking
 2) No cracking
 3) Shrinkage crack: AI, 1/2 in. deep from surface

Crack Classification

Class A	< 0.007"
Class B	0.008" - 0.022"
Class C	0.023" - 0.200"
Class D	> 0.200"

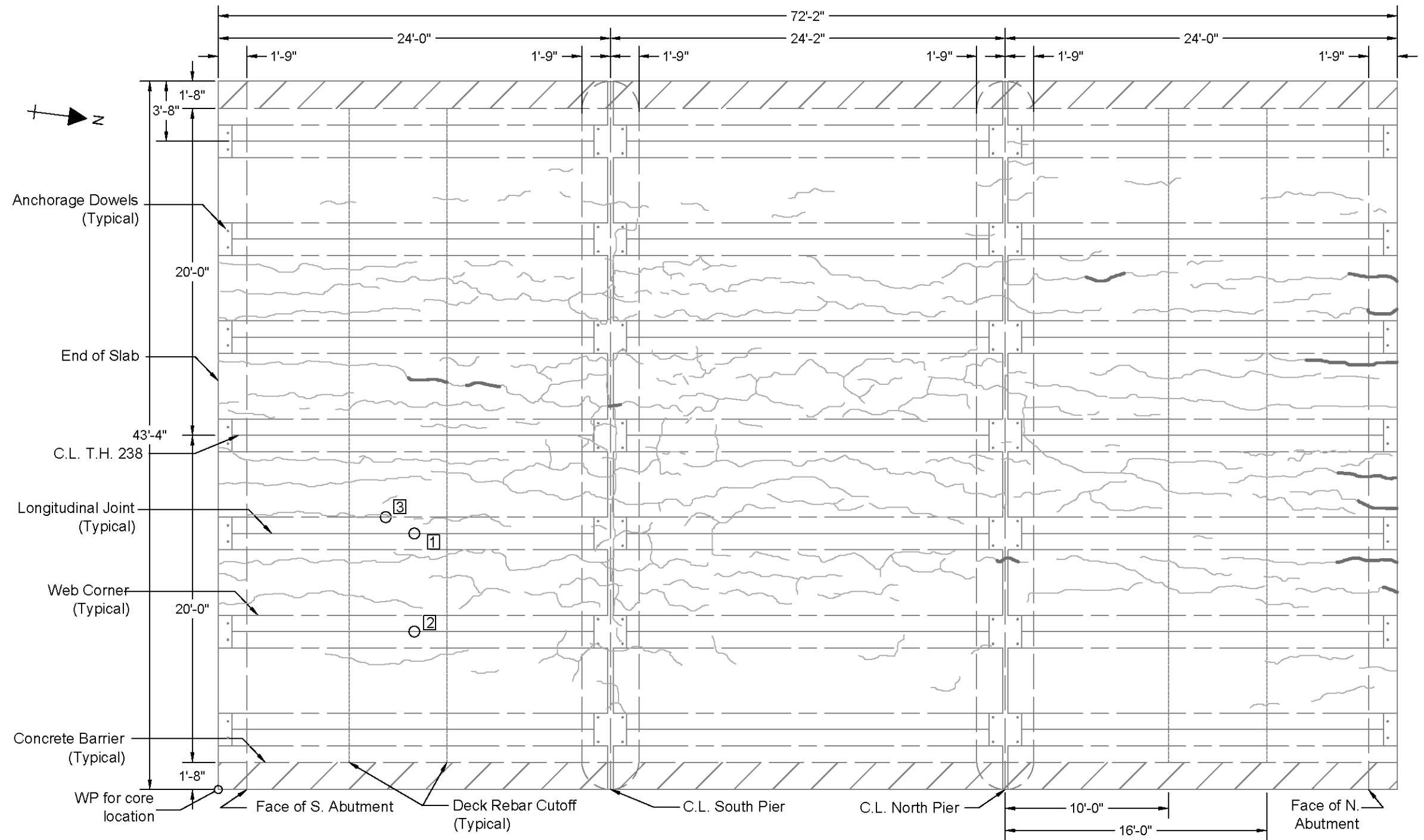


Figure A.23: Crack map for Bridge No. 49036 Inspection No. 1, November 6, 2009

Bridge No. 49036

Scale: 1" = 7'-0"
 Built: 08/11/2009 (Generation 3)
 Inspection No. 2: 05/26/2010

Age: 0.79 years
 Temperature: 46°F - 77°F (62°F average)
 Average Humidity: 56%
 Clouds/Precipitation: Clear

Precast Concrete
 Release Strength: 4000 psi
 Final Strength: 6000 psi
 Depth: 12 in.
 Flange Thickness: 3 in.
 Strand: 16, 0.5 in.

Cast-in-Place Concrete
 Strength: 4000 psi
 Slump: Not available
 Prewetted: Yes
 Surface Finish: Deep transverse tining

Reinforcement
Precast:
 - No. 4 composite hooks at 6 in. to 10 in. for 19 ft, at 12 in. for 5 ft (sym.), 2 in. projection
 - No. 6 transverse hooks at 1 ft, not staggered
 - 7 No. 8 top bars
 - No. 4 ties at spacing of top hooks
Deck Longitudinal:
 - No. 7 at 4 in.
 - Full length with lap, first cutoff at 10 ft from pier (end and center span), second cutoff at 16 ft from pier (end span only)
Deck Transverse:
 - No. 4 at 6 in.
Trough:
 - No. 5 corner bars
 - 4 No. 9 continuity bars at 4.5 in.
 - No. 5 stirrups at 12 in., adjacent to hooks
 - Overall spacing at 12 in.

Piers and Abutments
Dowels:
 - 12 in. projection
 - Holes drilled after beams placed, grouted
 - Polystyrene wrapped 4 outer sets
 - In block-outs at abutments, 2 No. 8 at 12 in.
 - In block-outs at piers, 4 No. 8 at 1 ft - 6 in., 1 ft - 6 in. symmetric over CL pier
Bearing:
 - Polystyrene under beam bearing, not at block-out or 4 in. gap
 - Elastomeric bearing pad type 1, 6 in. strip under beam tabs

Core Summary
 1) No cracking
 2) No cracking
 3) Shrinkage crack: AI, 1/2 in. deep from surface

Crack Classification

Class AI	< 0.003"
Class AII	0.003" - 0.007"
Class BI	0.008" - 0.015"
Class BII	0.016" - 0.022"
Class CI	0.023" - 0.100"
Class CII	0.100" - 0.200"
Class D	> 0.200"

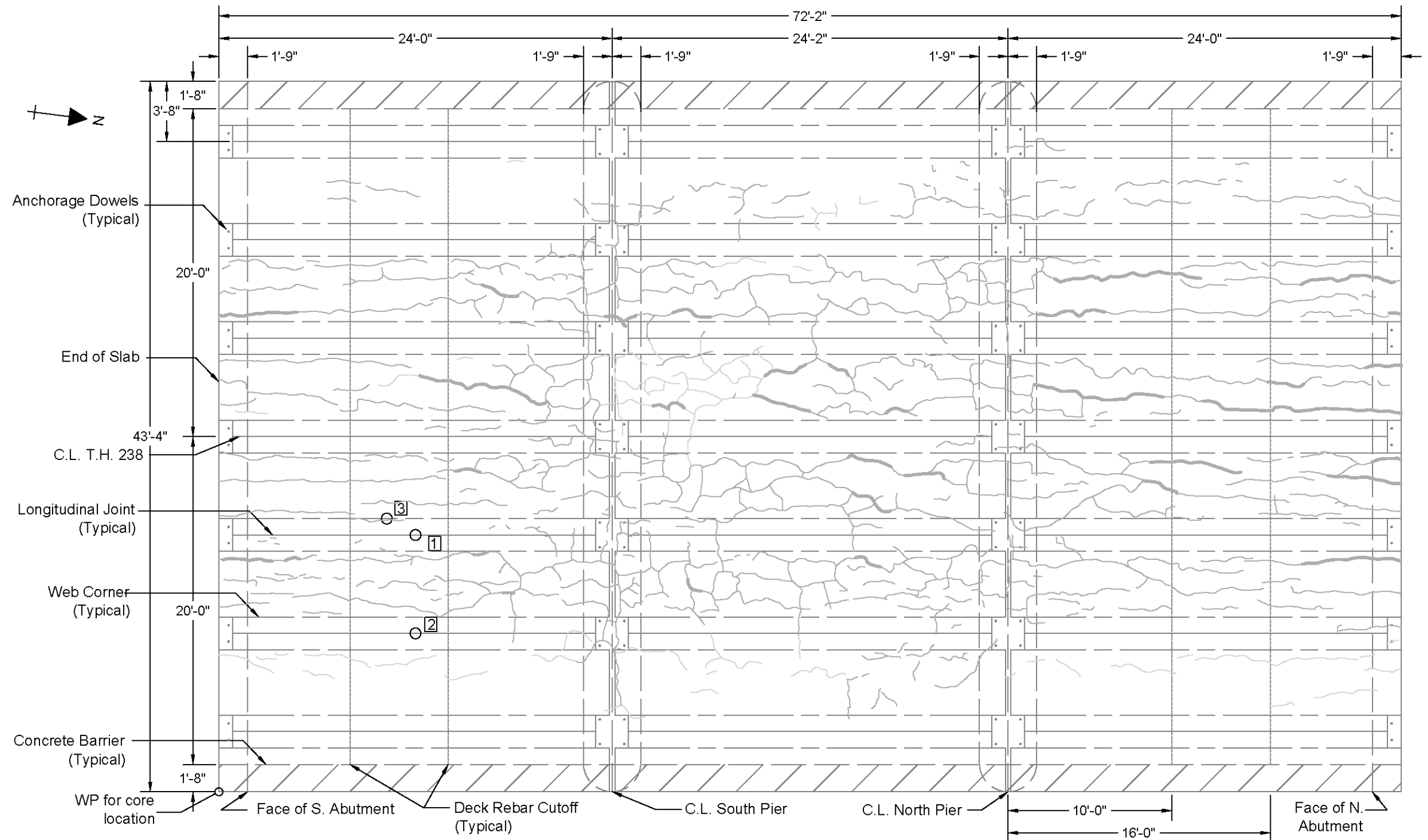


Figure A.24: Crack map for Bridge No. 49036 Inspection No. 2, May 26, 2010

Bridge No. 49036

Scale: 1" = 7'-0"
 Built: 08/11/2009 (Generation 3)
 Inspection No. 3: 06/24/2011

Age: 1.87 years
 Temperature: 42°F - 73°F (58°F average)
 Average Humidity: 67%
 Clouds/Precipitation: Clear

Precast Concrete
 Release Strength: 4000 psi
 Final Strength: 6000 psi
 Depth: 12 in.
 Flange Thickness: 3 in.
 Strand: 16, 0.5 in.

Cast-in-Place Concrete
 Strength: 4000 psi
 Slump: Not available
 Prewetted: Yes
 Surface Finish: Deep transverse tining

Reinforcement
Precast:
 - No. 4 composite hooks at 6 in. to 10 in. for 19 ft, at 12 in. for 5 ft (sym.), 2 in. projection
 - No. 6 transverse hooks at 1 ft, not staggered
 - 7 No. 8 top bars
 - No. 4 ties at spacing of top hooks
Deck Longitudinal:
 - No. 7 at 4 in.
 - Full length with lap, first cutoff at 10 ft from pier (end and center span), second cutoff at 16 ft from pier (end span only)
Deck Transverse:
 - No. 4 at 6 in.
Trough:
 - No. 5 corner bars
 - 4 No. 9 continuity bars at 4.5 in.
 - No. 5 stirrups at 12 in., adjacent to hooks
 - Overall spacing at 12 in.

Piers and Abutments
Dowels:
 - 12 in. projection
 - Holes drilled after beams placed, grouted
 - Polystyrene wrapped 4 outer sets
 - In block-outs at abutments, 2 No. 8 at 12 in.
 - In block-outs at piers, 4 No. 8 at 1 ft - 6 in., 1 ft - 6 in. symmetric over CL pier
Bearing:
 - Polystyrene under beam bearing, not at block-out or 4 in. gap
 - Elastomeric bearing pad type 1, 6 in. strip under beam tabs

Core Summary
 1) No cracking
 2) No cracking
 3) Shrinkage crack: AI, 1/2 in. deep from surface

Crack Classification

Class AI	< 0.003"
Class AII	0.003" - 0.007"
Class BI	0.008" - 0.015"
Class BII	0.016" - 0.022"
Class CI	0.023" - 0.100"
Class CII	0.100" - 0.200"
Class D	> 0.200"

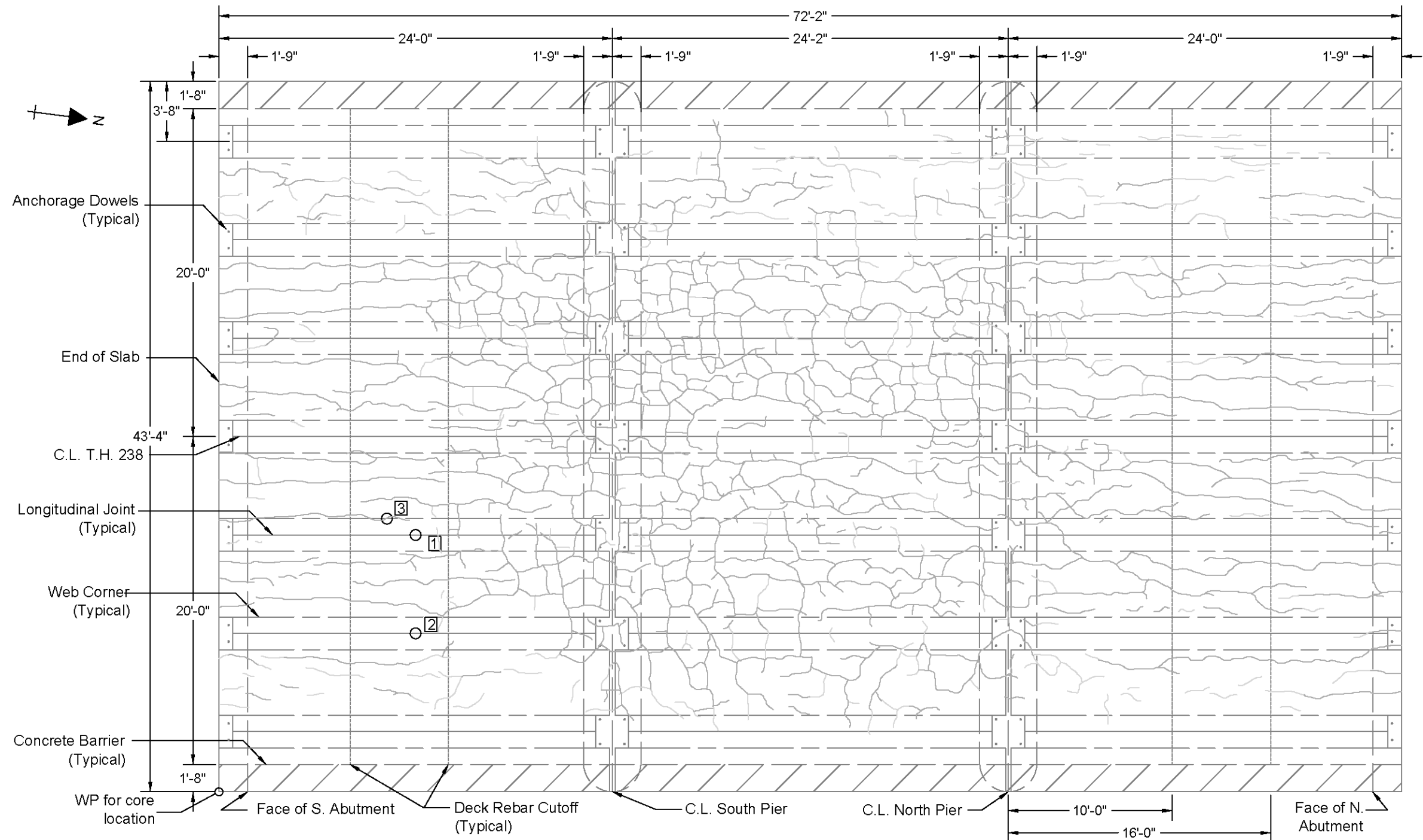


Figure A.25: Crack map for Bridge No. 49036 Inspection No. 3, June 24, 2011

Appendix B: Core Examination Records

Pictures of core specimens are all oriented with the top of the core towards the top of the page, unless otherwise indicated. The following explanations correlate with superscripts in Table B.1 but apply for all examination records:

1. **Number:** Bridge No. number followed by the core number, as indicated on crack maps (e.g. Core 3 from Bridge 49007 is named 49007-3).
2. **Condition:** Condition due to extraction was intact, segmented, or broken, as shown in Figure 3.11. This damage may be due to the extraction procedure, rather than in situ conditions.
3. **Coordinates:** Coordinate location with respect to southwest corner of the bridge plan and crack maps, in the pseudo-north coordinates of the bridge (see Azimuth).
4. **Azimuth:** Azimuth of the longitudinal direction (pseudo-north) of the bridge with respect to true North.
5. **Offset:** Transverse offset of core from intended location. “Unknown” indicates the actual location of the core could not be verified with physical identification of a joint or web corner. In this case the core was unreliable with respect to whether or not the joint or web-CIP interface initiated reflective cracking in the general region of the core.
6. **Reinforcement Location:** Faces on which reinforcement was observed followed by an offset distance measured circumferentially from the centerline of the face (relative to the pseudo-local coordinate system).
7. **Crack Location:** Location on the core, as shown in Figure 3.14, and the circumferential offset.
8. **Crack Width:** Width along the crack with the classifications in Table 3.2. Widths defined over depth ranges, with 0” at the top of the core.

B.1 Bridge No. 13004 – T.H. 8 over the Center Lake channel, Center City, MN

Table B.1: Core examination record of Core 13004-1

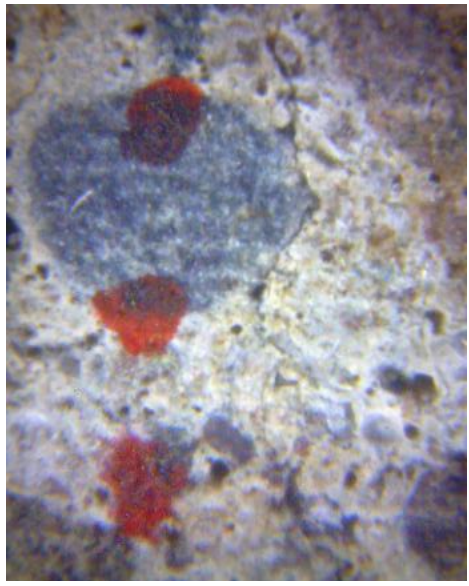
Number ¹ :	13004-1	Condition ² :	Intact	
Coordinates ³ :	38'-1" W, 10'-8.5" S	Azimuth ⁴ :	79°50'53.85"	
Location:	Long. Joint, Midspan	Offset ⁵ :	1¼" W	
Diameter:	3¾"	Depth:	14"	
REINFORCEMENT:				
Type/Size		Location ⁶	Depth	
Longitudinal, No. 8		N-S, 0"	4"	
Transverse, No. 5		E-W, 1" S	4¾"	
Transverse Hook, No. 6		E-W, 1" S	11¾"	
Transverse Hook, No. 6		N-S, 1" S	11¾"	
CRACKS:				
Description	Origination	Location ⁷	Length	Width: Depth ⁸
Shrinkage	Top of Core	N Face, ¼" E	½"	A1: 0"-½"
Shrinkage	Top of Core	S Face, 1¼" E	¼"	A1: 0"-¼"
NOTES:				
The core was broken into three pieces during extraction, at the intersection of the longitudinal and transverse deck reinforcement. No reflective cracks were observed. However, the core was offset from the joint by 1¼", only capturing one side of the joint. A reflective crack could be present on the other side of the joint. The instrumentation data indicated a reflective crack.				
PICTURES:				
				
<p>Figure B.1 North face (left) and west face (right) of core 13004-1. The shrinkage crack is highlighted by the red box, with adjacent close-up</p>		<p>Figure B.2: Close up of the shrinkage crack on the west face of core 13004-1</p>		

Table B.2: Core examination record of Core 13004-2

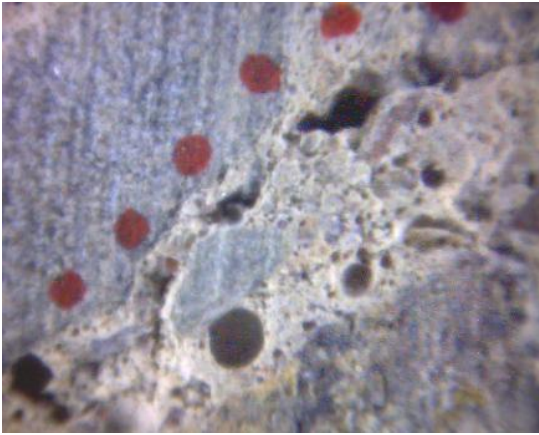
Name:	13004-2	Condition:	Intact	
Coordinates:	38'-1" W, 22'-8.5" S	Azimuth:	79°50'53.85"	
Location:	Longitudinal Joint, Midspan	Offset:	0"	
Diameter:	3¾"	Depth:	14"	
REINFORCEMENT:				
	Type/Size	Location	Depth	
	Longitudinal, No. 8	N-S, 1/2" W	3¾"	
	Transverse, No. 5	E-W, ¾" N	4¾"	
	Transverse, No. 5	E-W, 1¾" N	5½"	
	Transverse Hook, No. 6	E-W, ¼" S	11¼"	
	Transverse Hook, No. 6	E-W, ¾" N	11¼"	
CRACKS:				
Description	Origination	Location	Length	Width: Depth
Reflective	Bottom of Core	N Face, 1¼" E	1"	A1: 13½"-12½"
Reflective	Bottom of Core	S Face, 1 ½" E	1¼"	A1: 13½"-12¼"
Horizontal	N/A	N Face, 1" E – ¾" W 3" from Bottom	1 ¾"	A2: 0"-1¾"
Shrinkage	Top of Core	E Face, ½" S	½"	A1: 0"-½"
NOTES:				
The core was broken into two pieces during extraction, at the longitudinal deck rebar. A reflective crack was observed on both the east and west faces originating from the flange joint. The crack was also visible along the bottom of the core at the joint. The camber of the precast beams appeared to be different, looking at the bottom of the core. This camber difference was not noticeable in the field. The reflective crack confirmed the instrumentation data from Joint 1.				
PICTURES:				
				
<p>Figure B.3: Reflective crack on core 13004-2</p>		<p>Figure B.4: Close up of the reflective crack on the west face of core 13004-2</p>		



Figure B.5: North face (left) and east face (right) of core 13004-2



Figure B.6: Visible camber difference in the joint of core 13004-2.

Table B.3: Core examination record of Core 13004-3

Name:	13004-3		Condition:	Segmented	
Coordinates:	8'-10" W, 11'-8.5" S		Azimuth:	79°50'53.85"	
Location:	Web-CIP Interface, Midspan		Offset:	Unknown	
Diameter:	3¾"		Depth:	7 ¾"	
REINFORCEMENT:					
Type/Size		Location		Depth	
Longitudinal, No. 8		N-S, 1" W		4"	
Transverse, No. 5		E-W, 1 ¼" S		4¾"	
Transverse Hook (Vertical)		E Face, 0"		Bar end at 5¼"	
CRACKS:					
Description	Origination	Location	Length	Width: Depth	
Shrinkage	Top of Core	W Face, ¾" S	¼"	A1: 0"-¼"	
NOTES:					
The core intercepted the vertical section of a transverse hook. It broke apart around the transverse bar into four pieces during extraction.					
PICTURES:					

Figure B.7: North face (left) and east face (right) of core 13004-3

Table B.4: Core examination record of Core 13004-4

Name:	13004-4		Condition:	Intact	
Coordinates:	38'-1" W, 11'-8.5" S		Azimuth:	79°50'53.85"	
Location:	Web-CIP Joint, Midspan		Offset:	0"	
Diameter:	3¾"		Depth:	7 ¾"	
REINFORCEMENT:					
Type/Size		Location		Depth	
Longitudinal, No. 8		N-S, 1" W		4"	
CRACKS:					
Description	Origination	Location	Length	Width: Depth	
Shrinkage	Top of Core	W Face, 0"	½"	A1: 0"-½"	
NOTES:					
The core broke off just at the top of the precast web, leaving traces of the precast concrete. The precast was visible by the different coloration in the concrete.					
One shrinkage crack was observed on the west face, extending ½" from the top of the core					
PICTURES:					
					
<p>Figure B.8: Bottom of core 13004-4 showing differing coloration between the precast web and cast-in-place concrete. Pseudo-local north is inset.</p>					



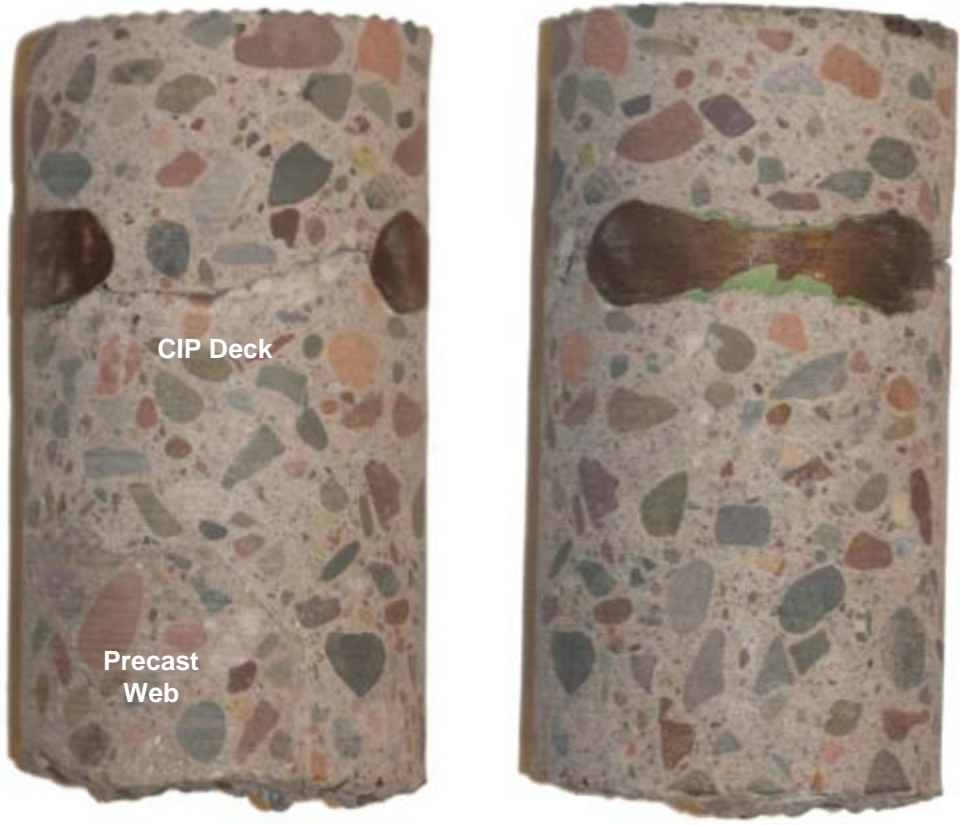
Figure B.9: North face (left) and east face (right) of core 13004-4

B.2 Bridge No. 33005 – T.H. 65 over the Ann River, Mora, MN

Table B.5: Core examination record of Core 33005-1

Name:	33005-1	Condition:	Intact
Coordinates:	19'-7" N, 11'-0.5" E	Azimuth:	0°37'58.0"
Location:	Longitudinal Joint	Offset:	½" W
Diameter:	5¾"	Depth:	15"
REINFORCEMENT:			
Type/Size	Location	Depth	
Longitudinal, No. 7	N-S, 2" W	2½"	
Longitudinal, No. 7	N-S, 2½" E	2½"	
Transverse, No. 5	E-W, 2¼" N	3 ¼"	
Transverse, No. 4	E-W, 0"	5¼"	
Transverse, No. 6	E-W, 1" S	12"	
Transverse, No. 6	E-W, 2 ½" N	12"	
Transverse No. 4	E-W, ¾" N	12"	
CRACKS:			
None Observed			
NOTES:			
<p>The core intercepted a substantial amount of rebar: two longitudinal deck bars spaced at about 4", a transverse deck bar, the top and bottom legs of a trough hoop, and two transverse hooks from the precast webs spaced at about 3". These spacings were all consistent with the bridge plans. However, the cover on the deck bars was only about 2", with only 5¼" of CIP concrete above the precast webs (instead of 6").</p> <p>No observed cracks. Core was extracted in two parts, with a horizontal break at a depth of 12" (at the transverse hooks).</p>			
PICTURES:			
			
<p>Figure B.10: North face (left) and east face (right) of core 33005-1</p>			

Table B.6: Core examination record of Core 33005-2

Name:	33005-2	Condition:	Intact	
Coordinates:	19'-7" N, 12'-1.75" E	Azimuth:	0°37'58.0"	
Location:	Web-CIP Joint, Midspan	Offset:	¼" E	
Diameter:	3 ¾"	Depth:	7"	
REINFORCEMENT:				
Type/Size	Location	Depth		
Longitudinal, No. 8	N-S, 1½" W	2"		
Longitudinal, No. 8	N-S, 1 ½" E	2"		
CRACKS:				
Description	Origination	Location	Length	Width: Depth
Shrinkage	Top of Core	S Face, ½" E	¼"	A1: 0"-¼"
NOTES:				
The web-CIP interface was clearly visible through the core. No cracks were observed originating from the web corner. The CIP deck thickness was smaller than indicated on the bridge plans: there was 4¾" of CIP concrete above the web, where there should be at least 6". Also, the longitudinal bars were close to the surface (1½" cover).				
PICTURES:				
				
<p>Figure B.11: North face (left) and east face (right) of core 33005-2. The web-CIP interface was visible at the bottom of the north face.</p>				

B.3 Bridge No. 33008 – T.H. 65 over the Groundhouse River near Mora, MN

Table B.7: Core examination record of Core 33008-1

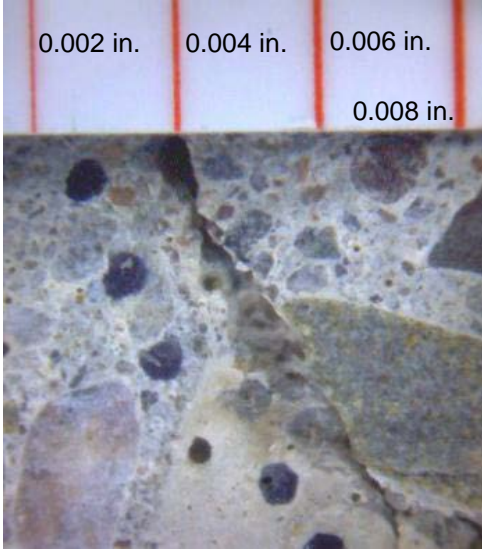
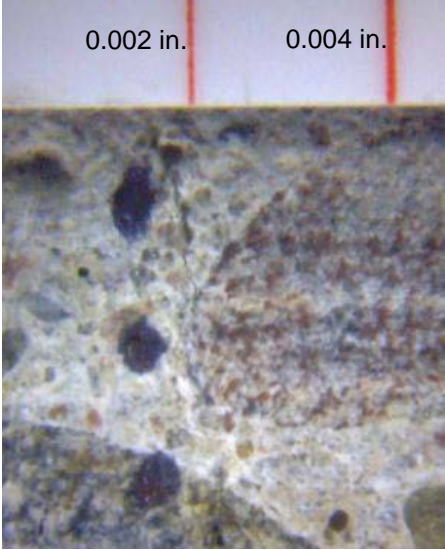
Name:	33008-1		Condition:	Intact	
Coordinates:	45'-4" N, 16'-6" E (Midspan)		Orientation:	3.67° E	
Location:	Longitudinal Joint		Offset ⁵ :	0"	
Diameter:	5¾"		Depth:	13¼"	
REINFORCEMENT:					
	Type/Size	Location		Depth (on center)	
	Longitudinal, No. 8	N-S, ½" W		3 ¼"	
	Transverse, No. 5	E-W, ½" S		4 ¼"	
CRACKS:					
	Description	Origination	Location	Length	Width: Depth
	Shrinkage, Reflective	Undefined	N Face, 1" E - ¼" E	13¼"	B1: 0"-¾", A2: ¾"-3", A1: 3"-3¼", A2: 3¼"-3¾", A1: 3¾"-4½", A2: 4½"-6", A1 6"-13½"
	Shrinkage, Reflective	Undefined	S Face, 2½" E - 0"	13¼"	B1: 0"-1", A2: 1"-3¼", A1: 3¼"-5½", A2: 5½"-7", A1: 7"-13½"
NOTES:					
No rebar from the trough cage or transverse hooks was intercepted. Two full-depth cracks were observable without the microscope. These cracks connected on the top of the core and most likely continued over the bottom, though the connecting crack could not be seen. The cracks were widest (B1) within the top three inches of the core, diminishing to class A1 at the bottom. The crack widths decreased at the region of transverse reinforcement that intercepted the crack. Two lateral cracks extended no more than 1½" from the south crack, width A1, at a depth of 6". The top of the reflective cracks was the widest section, indicating shrinkage cracking dominated.					
PICTURES:					
					
<p>Figure B.12: A2 crack on the south face. Crack width was determined from the interior of the cracks, neglecting spalling at the surface of the core from the coring process.</p>			<p>Figure B.13: A1 crack on the south face. The smallest width on the crack gauge was 0.002", which was larger than the crack shown.</p>		



Table B.8: Core examination record of Core 33008-2

Name:	33008-2	Condition:	Intact	
Coordinates:	45'-4" N, 22'-6" E	Orientation:	3.67° E	
Location:	Longitudinal Joint, Midspan	Offset:	¼" E	
Diameter:	3¾"	Depth:	13¼"	
REINFORCEMENT:				
Type/Size	Location		Depth	
Longitudinal, No. 8	N-S, ¼" E		3¼"	
Transverse, No. 5	E-W, 0"		4¼"	
CRACKS:				
Description	Origination	Location	Length	Width: Depth
Shrinkage	Top of core	N Face, ¾" E	½"	A2: 0"-½"
Shrinkage	Top of core	S Face, 1" E	¼"	A2: 0"-¼"
NOTES:				
The core was in good condition, in one piece. The core intercepted two deck bars, one longitudinal and one transverse. No trough reinforcement was intercepted. The two shrinkage cracks were continuous over the top of the core. No reflective cracks were observed, which supports the prediction that reflective cracks would occur on alternating longitudinal joints, not adjacent ones.				
PICTURES:				
				
<p>Figure B.15: Close-up of the shrinkage crack on the north face of core 33008-2</p>				



Figure B.16: North face (left) and south face (right) of core 33008-2

Table B.9: Core examination record of Core 33008-3

Name:	33008-3	Condition:	Intact	
Coordinates:	45'-4" N, 28'-6" E	Orientation:	3.67° E	
Location:	Longitudinal Joint, Midspan	Offset:	0"	
Diameter:	5¾"	Depth:	13½"	
REINFORCEMENT:				
Type/Size	Location	Depth (on center)		
Longitudinal, No.8	N-S, 0"	3¼"		
Transverse, No. 5	E-W, ¼" S	4¼"		
Tie Wire	N Face, 2" E	12½"		
CRACKS:				
Description	Origination	Location	Length	Width: Depth
Reflective	Bottom, chamfer corner	S Face, 1" W	5¾"	A1: 6¾"-12½"
Reflective	Bottom of core	N Face, 1" W	2½"	A1: 10"-12½"
NOTES:				
<p>The precast panels appeared to have different cambers. This confirmed that in-field observations of differential camber on the end spans were also present in the middle span. This differential camber was present at the time of the CIP deck placement, and did not occur after CIP concrete curing. The cracks from each side did not appear to meet at the bottom of the core, but the cracks may have been obscured by the chamfer corner.</p>				
PICTURES:				
				
<p>Figure B.17: Reflective crack originating at the flange joint on the north face</p>				



Figure B.18: North face (left) and east face (right) of core 33008-3



Figure B.19: Reflective crack on the south face. There was a small crack adjacent to the reflective crack. Also note the uneven bottom surface due to differential camber.

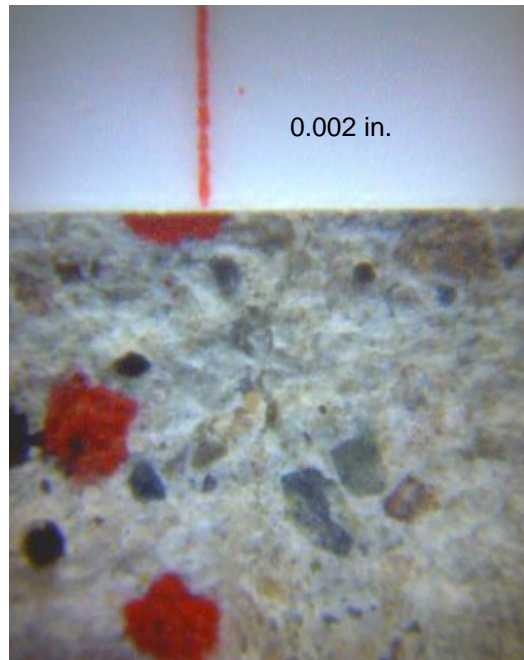


Figure B.20: Close-up of the reflective crack on the south face, highlighted by the red box, A1: less than 0.002".

Table B.10: Core examination record of Core 33008-4

Name:	33008-4	Condition:	Segmented	
Coordinates:	45'-4" N, 29'-6" E	Orientation:	3.67° E	
Location:	Web-CIP Interface, Midspan	Offset:	Unknown	
Diameter:	3¾"	Depth:	6½"	
REINFORCEMENT:				
Type/Size		Location	Depth (on center)	
Longitudinal, No. 8		N-S, 1" E	3 ¼"	
Transverse, No. 5		E-W, 0"	4"	
CRACKS:				
Description	Origination	Location	Length	Width: Depth
Shrinkage	Top of core	S Face, ¼" E	3½"	B1: 0"-1", A1: 1"-1½", A2: 1½"-3", A1: 3"-3½"
Shrinkage	Top of core	N Face, ¼" E	3 ½"	B1: 0"-1", A2: 1"-1½", B1: 1½"-2", A1: 2"-3 ½"
NOTES:				
<p>The core broke into at least 10 pieces while being extracted. The 7 pieces that could be put back together were numbered sections 1 through 7. Some of the precast web corner could be seen on section 6 at a depth of 5¾". The precast did not appear on sections 5 or 7, which have portions just as deep as section 6. This indicated that the core was somewhere over the web-CIP interface, although the exact offset was unknown.</p> <p>The vertical cracks connected on the bottom of section 1, along the longitudinal deck reinforcement. The transverse reinforcement intercepted the crack where it crossed the longitudinal reinforcement, though whether the crack stopped there could not be determined. It is possible that this could be a reflective crack from the web corner that was parallel with the longitudinal deck reinforcement. The crack was widest at the surface, likely due to shrinkage.</p>				
PICTURES:				
				
<p>Figure B.21: North face (left) and east face (right) of core 33008-4</p>				



Figure B.22: Precast concrete at the web-CIP interface

B.4 Bridge No. 49007 – T.H. 238 over the Swan River near Little Falls, MN

Table B.11: Core examination record of Core 49007-1

Name:	49007-1	Condition:	Intact
Coordinates:	52'-1" S, 9'-0" E	Azimuth:	352°49'01.0"
Location:	Longitudinal Joint	Offset:	Unknown
Diameter:	3¾"	Depth:	19¾"
REINFORCEMENT:			
Type/Size	Location	Depth (on center)	
Longitudinal, No. 7	N-S, ¼" E	5 ¾"	
Transverse, No. 4	E-W, 0"	6½"	
Transverse, No. 5	E-W, 1" S	15"	
CRACKS:			
None observed			
NOTES:			
No observed cracks. Core was extracted in two pieces, with horizontal break at depth of 14½"			
PICTURES:			
			
<p>Figure B.23: North face (left) and east face (right) of Core 49007-1. The horizontal break occurred during extraction.</p>			

Table B.12: Core examination record of Core 49007-2

Name:	49007-2	Condition:	Intact
Coordinates:	52'-1" S, 15'-0" E	Azimuth:	352°49'01.0"
Location:	Longitudinal Joint	Offset:	Unknown
Diameter:	3¾"	Depth:	20 ¼"
REINFORCEMENT:			
Type/Size	Location	Depth (on center)	
Longitudinal, No. 7	N-S, ¾" E	5 ½"	
CRACKS:			
None observed			
NOTES:			
No observed cracks. Core was extracted in two pieces, with a horizontal break at depth of 14"			
PICTURES:			
			

Figure B.24: North face (left) and east face (right) of Core 49007-2

Table B.13: Core examination record of Core 49007-3

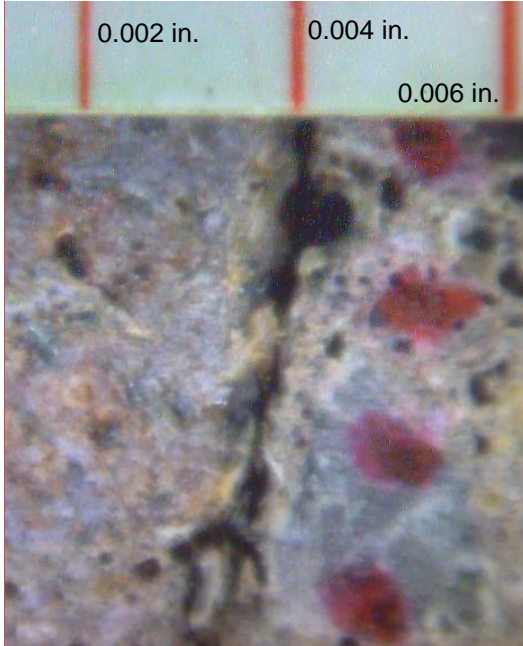
Name:	49007-3			Condition:	Intact
Coordinates:	19'-10" S, 16'-0" E			Azimuth:	352°49'01.0"
Location:	Web-CIP Interface			Offset:	Unknown
Diameter:	3¾"			Depth:	6½"
REINFORCEMENT:					
	Type/Size	Location		Depth	
	Transverse, No. 4	E-W, 1" N		6¼"	
CRACKS:					
	Description	Origination	Location	Length	Width: Depth
	Shrinkage	Top of Core	N Face, 0"	1"	A2: 0"-1"
NOTES:					
The one observed shrinkage crack had a ½" horizontal offshoot about 1/8" from the surface.					
PICTURES:					
					
<p>Figure B.25: North face (left) and east face (right) of Core 49007-3.</p>			<p>Figure B.26: Shrinkage crack on the north face of Core 49007-3. The crack gauge is shown for width reference.</p>		

Table B.14: Core examination record of Core 49007-4

Name:	49007-4	Condition:	Intact
Coordinates:	20'-2" S, 15'-0" E	Azimuth:	352°49'01.0"
Location:	Longitudinal Joint	Offset:	Unknown
Diameter:	3¾"	Depth:	20¼"
REINFORCEMENT:			
Type/Size		Location	Depth
Transverse, No. 4		E-W, ¾" S	6¼"
Transverse, No. 5		E-W, 1¼" S	6¾"
CRACKS:			
None observed			
NOTES:			
No cracks observed.			
PICTURES:			
			
<p>Figure B.27: North face (left) and east face (right) of Core 49007-4.</p>			

B.5 Bridge No. 49036 – T.H. 238 over Pike Creek near Little Falls, MN

Table B.15: Core examination record of Core 49036-1

Name:	49036-1	Condition:	Intact
Coordinates:	12'-0" N, 14'-0" W	Azimuth:	3°33'51.0"
Location:	Longitudinal Joint	Offset:	Unknown
Diameter:	3¾"	Depth:	14½"
REINFORCEMENT:			
Type/Size	Location	Depth	
Longitudinal, No. 7	N-S, 1½" W	4½"	
Transverse, No. 5	E-W, 1 ¾" S	5¼"	
CRACKS:			
None observed			
NOTES:			
No cracks observed. The core was extracted in two pieces, with a horizontal break at a depth of 6".			
PICTURES:			
			
<p>Figure B.28: North Face (left) and east face (right) of Core 49036-1</p>			

Table B.16: Core examination record of Core 49036-2

Name:	49036-2	Condition:	Intact
Coordinates:	12'-0" N, 8'-0" W	Azimuth:	3°33'51.0"
Location:	Longitudinal Joint	Offset:	Unknown
Diameter:	3¾"	Depth:	15½"
REINFORCEMENT:			
Type/Size		Location	Depth
Longitudinal, No. 3		N-S, ½" E	15"
CRACKS:			
None observed.			
NOTES:			
No cracks observed. The core was extracted in two pieces, with a horizontal break at a depth of 8½"			
PICTURES:			
			
<p>Figure B.29: North face (left) and east face (right) of Core 49036-2</p>			

Table B.17: Core examination record of Core 49036-3

Name:	49036-3		Condition:	Intact	
Coordinates:	10'-3" N, 15'-0" W		Azimuth:	3°33'51.0"	
Location:	Web-CIP Interface		Offset:	Unknown	
Diameter:	3¾"		Depth:	5"	
REINFORCEMENT:					
Type/Size		Location		Depth	
Longitudinal, No. 7		N-S, ½" E		4½"	
CRACKS:					
Description	Origination	Location	Length	Width: Depth	
Shrinkage	Top of Core	E Face, 1¼" N	½"	A1: 0"-½"	
NOTES:					
One shrinkage crack was observed on the east face at the top of the core. The core did not intercept the the precast web corner, so the exact location could not be verified.					
PICTURES:					
					
Figure B.30: North face (left) and east face (right) of Core 49036-3					

Appendix C: Center City Bridge Data

The figures in this appendix show the data collected from the strain gauge instrumentation installed in Bridge No. 13004, located over the Center Lake channel in Center City, MN. An overview of the instrumentation plan is given in Section 4.1. Each of the following figures shows strain data for the six-year monitoring period (September 2005 to August 2011). The location of each strain gauge is shown inset on the appropriate plot, on both a plan view of the instrumented region and in the cross section. During the fall of 2009 there was a failure in the collection system that resulted in three months of missing data, indicated on all plots by a gap in the data.

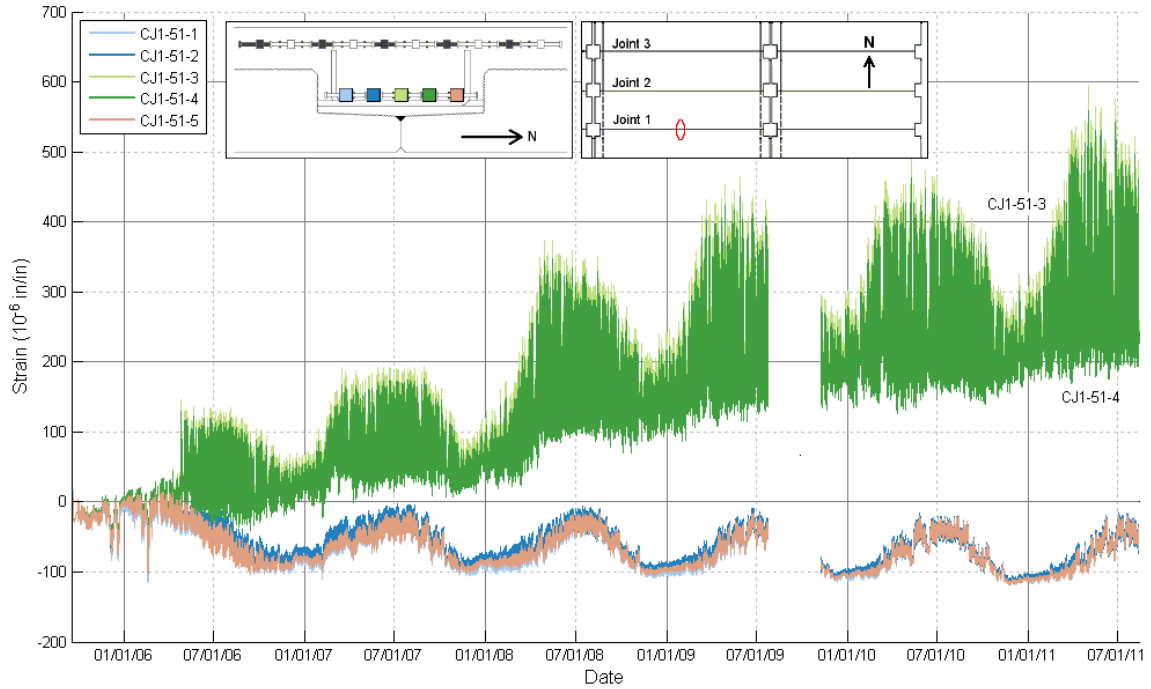


Figure C.1: Transverse strain data from concrete embedment gauges directly above longitudinal Joint 1 at midspan of the center span. Gauges CJ1-51-3 and CJ1-51-4 show increasing strain

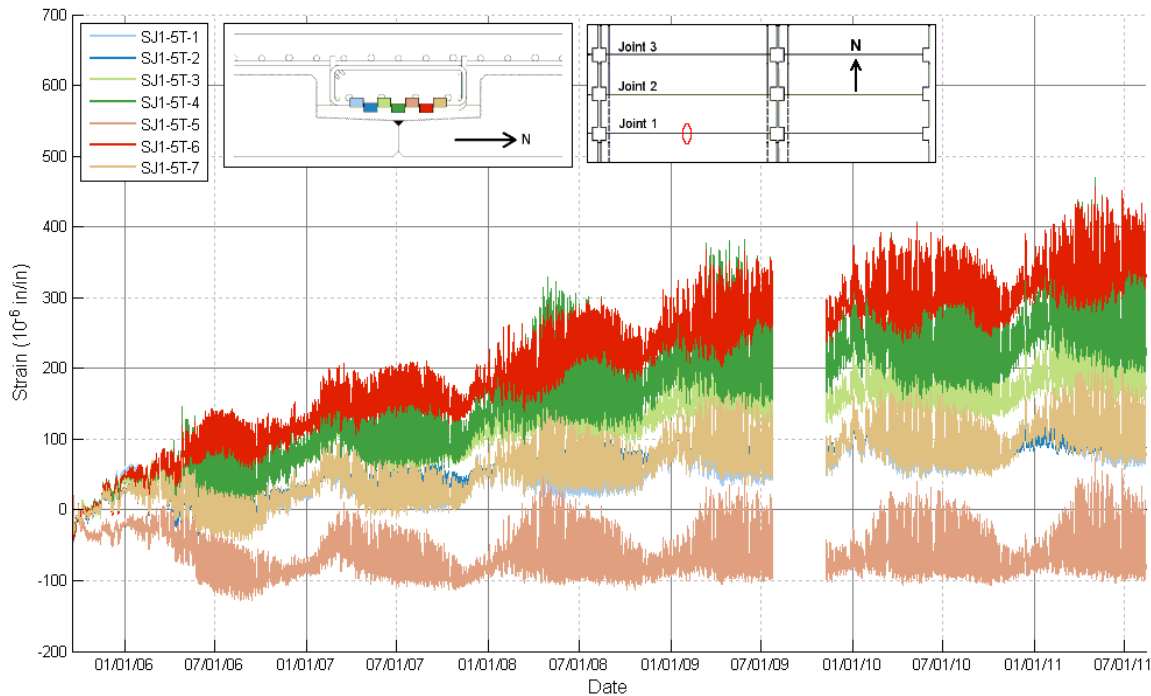


Figure C.2: Transverse strain data from spot-weldable strain gauges on the transverse hooks over Joint 1 at midspan of the center span

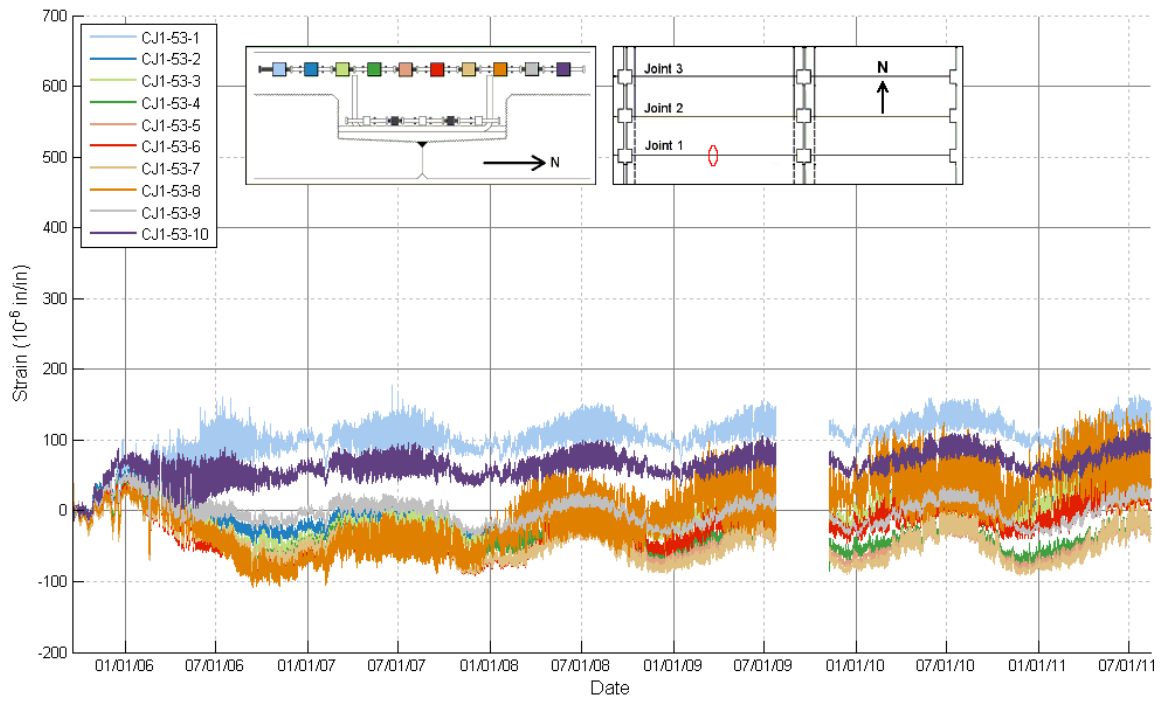


Figure C.3: Transverse strain data from concrete embedment gauges over the precast webs at Joint 1 at midspan of the center span

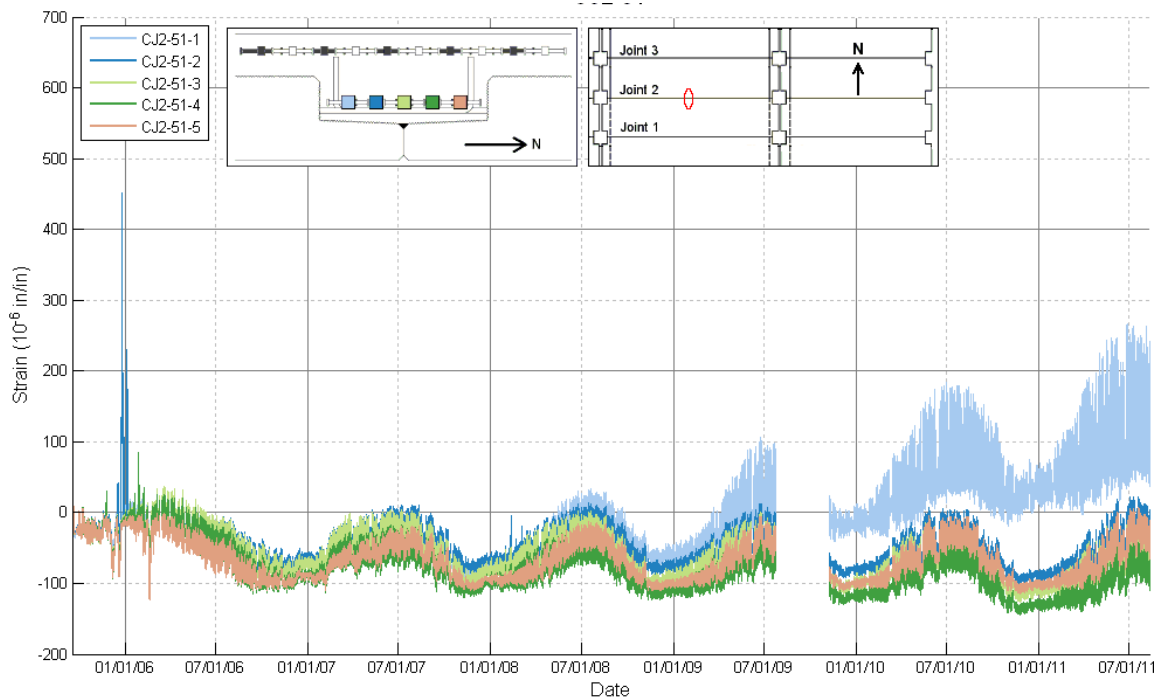


Figure C.4: Transverse strain data from concrete embedment gauges directly above longitudinal Joint 2 at midspan of the center span

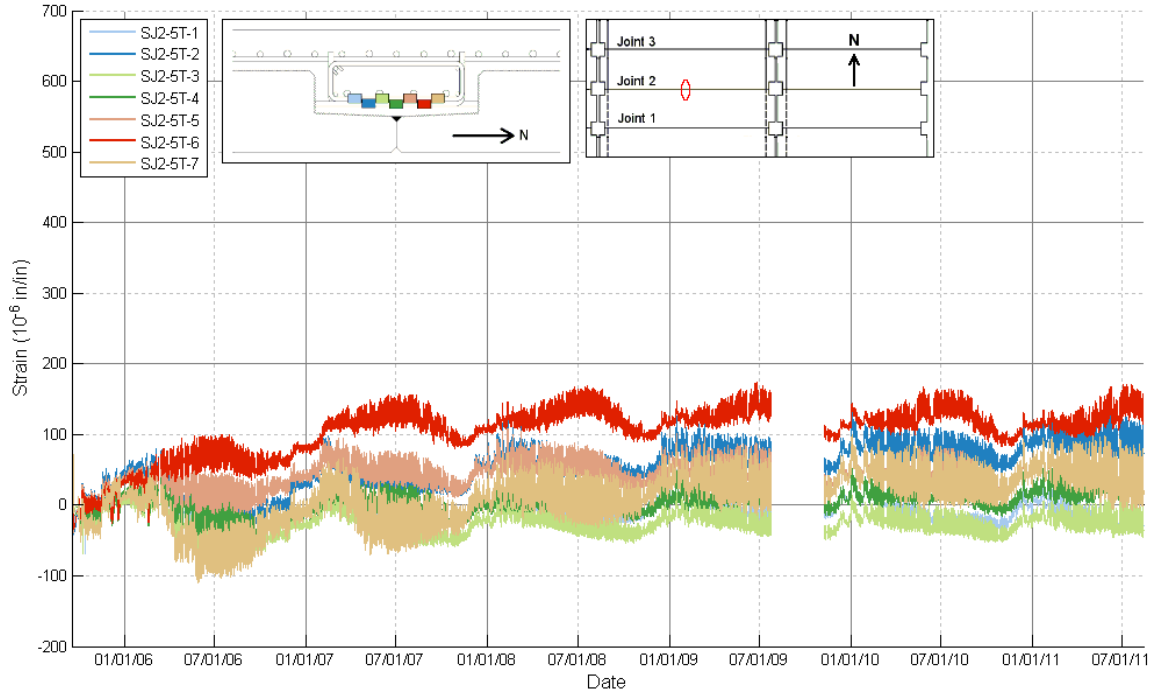


Figure C.5: Transverse strain data from spot-weldable gauges on the transverse hooks above Joint 2 at midspan of the center span

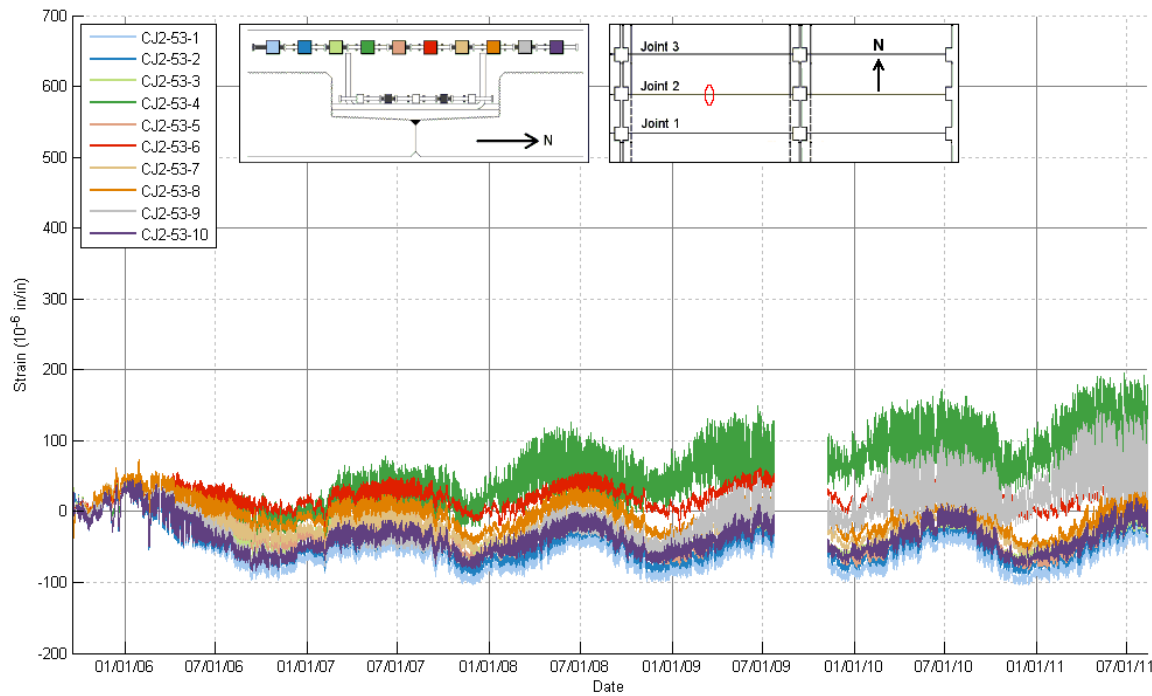


Figure C.6: Transverse strain data from concrete embedment gauges over the precast webs at Joint 2 at midspan of the center span

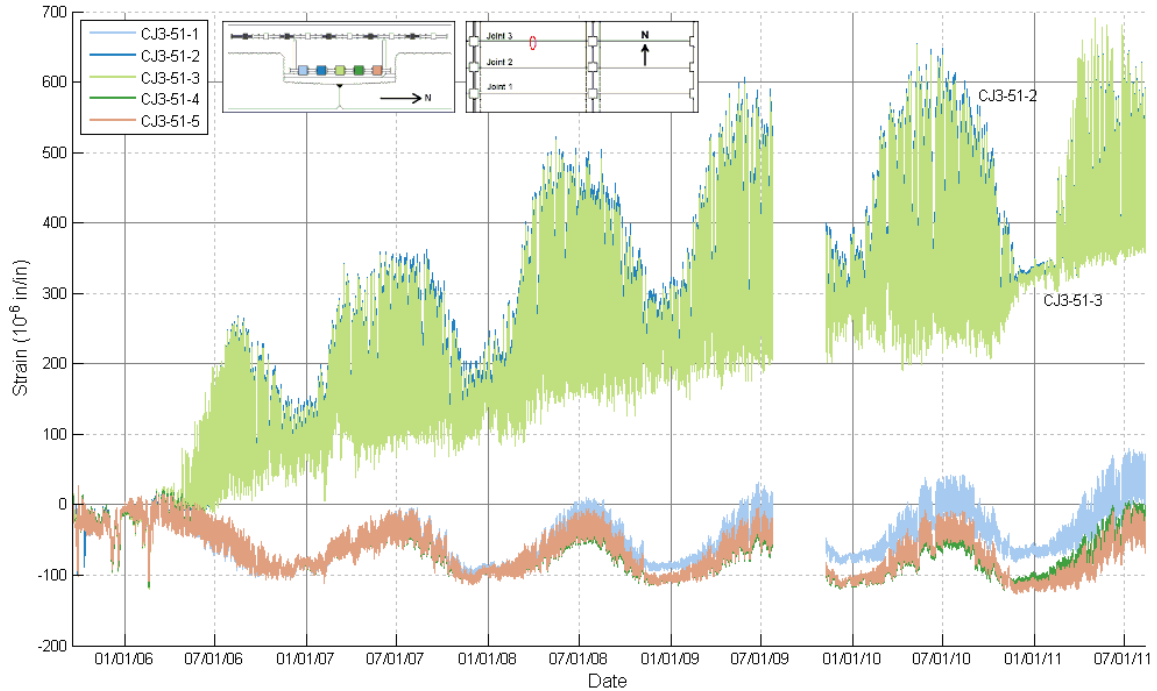


Figure C.7: Transverse strain data from concrete embedment gauges directly above longitudinal Joint 3 at midspan of the center span. Gauges CJ3- 51-2 and CJ3-51-3 show increasing strains

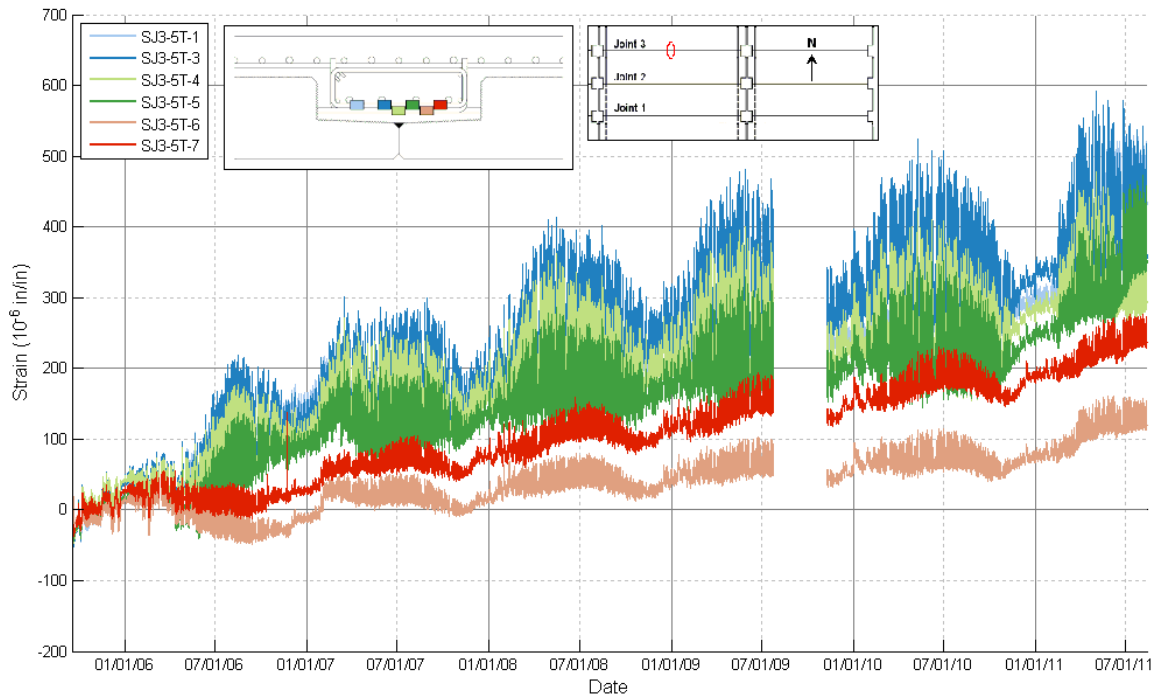


Figure C.8: Transverse strain data from spot-weldable gauges on the transverse hooks above Joint 3 at midspan of the center span. Gauge SJ3-5T-2 is not shown because it malfunctioned and did not collect data

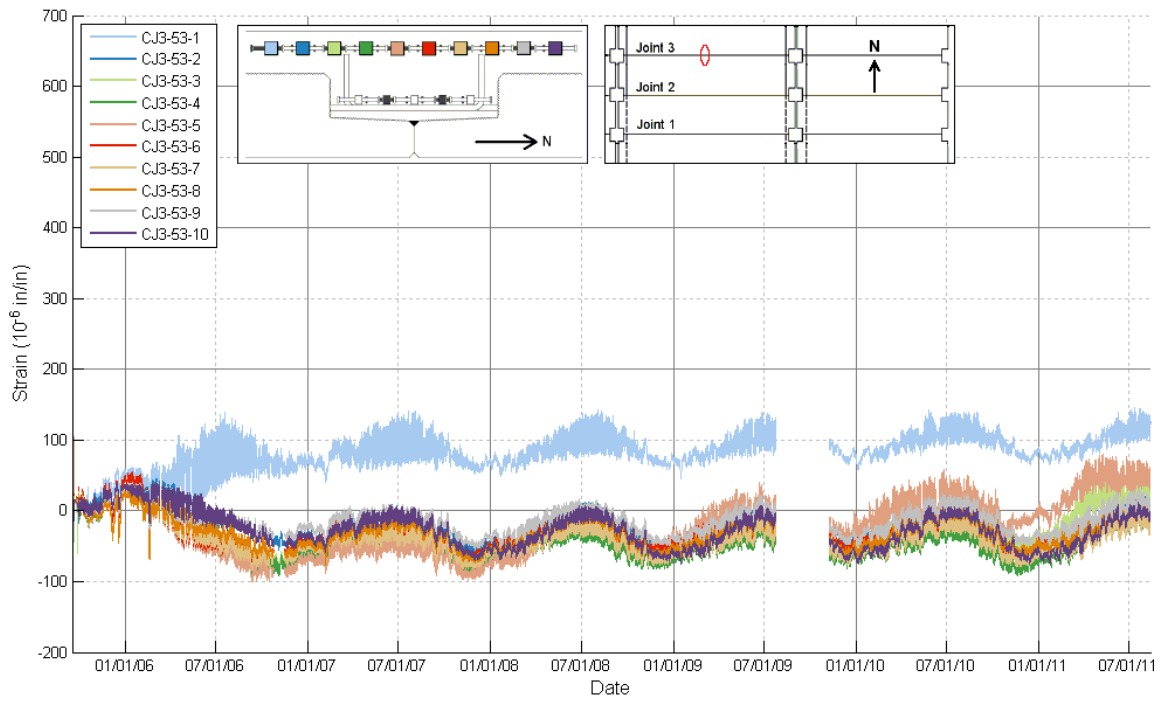


Figure C.9: Transverse strain data from concrete embedment gauges over the precast webs at Joint 3 at midspan of the center span

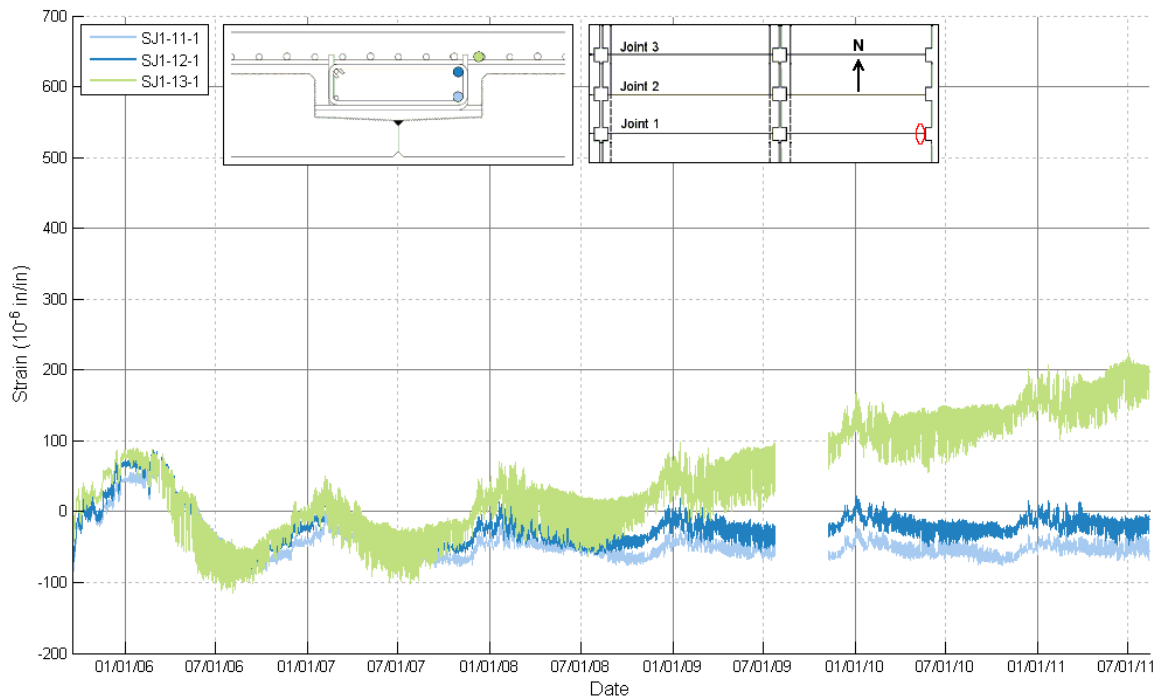


Figure C.10: Longitudinal strain data from spot-weldable gauges on cage and deck rebar over Joint 1 at the east abutment

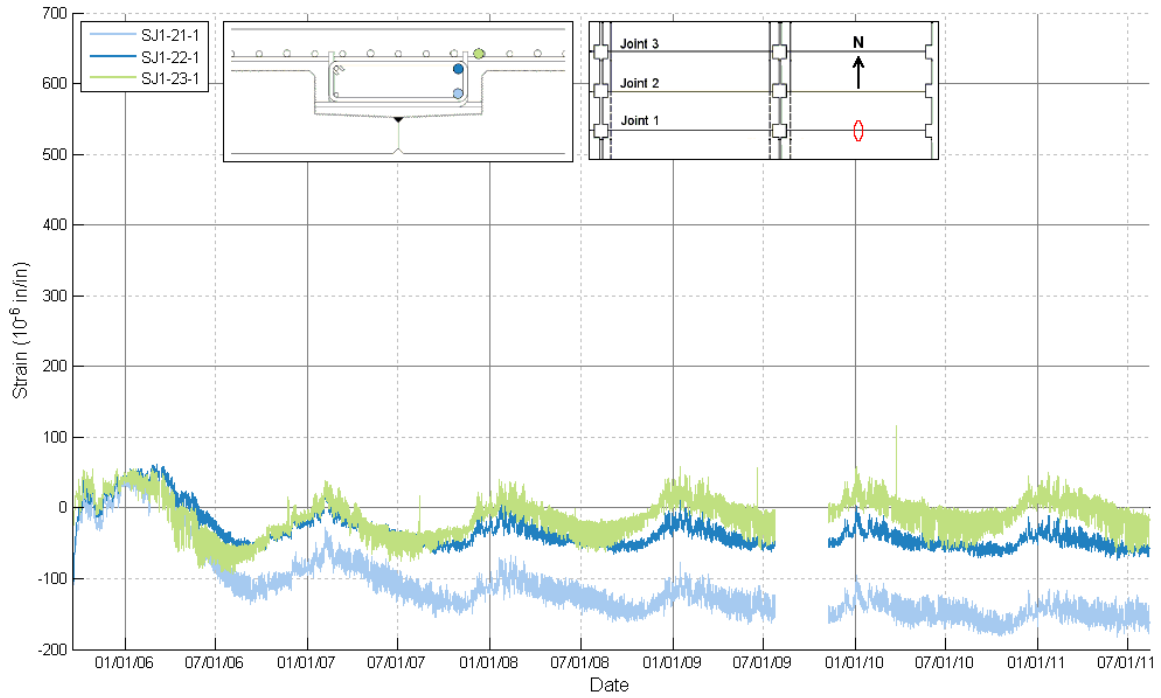


Figure C.11: Longitudinal strain data from spot-weldable gauges on cage and deck rebar over Joint 1 at midspan of the east span

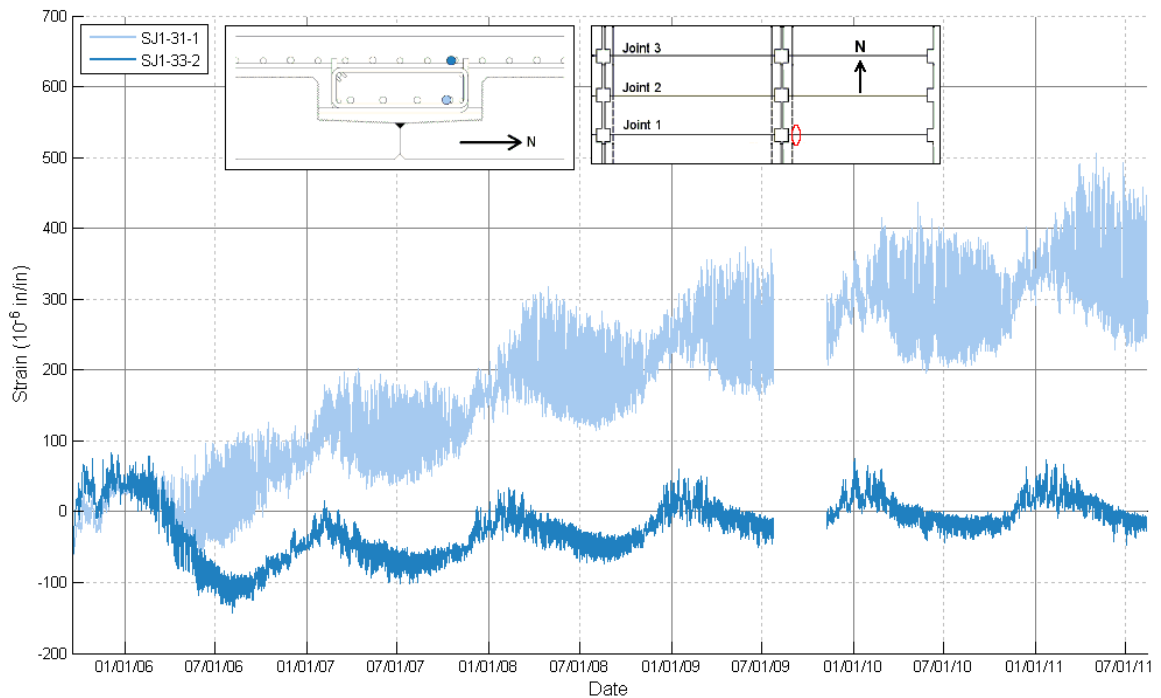


Figure C.12: Longitudinal strain data from spot-weldable gauges on continuity and deck rebar over Joint 1 at the east side of the pier cap

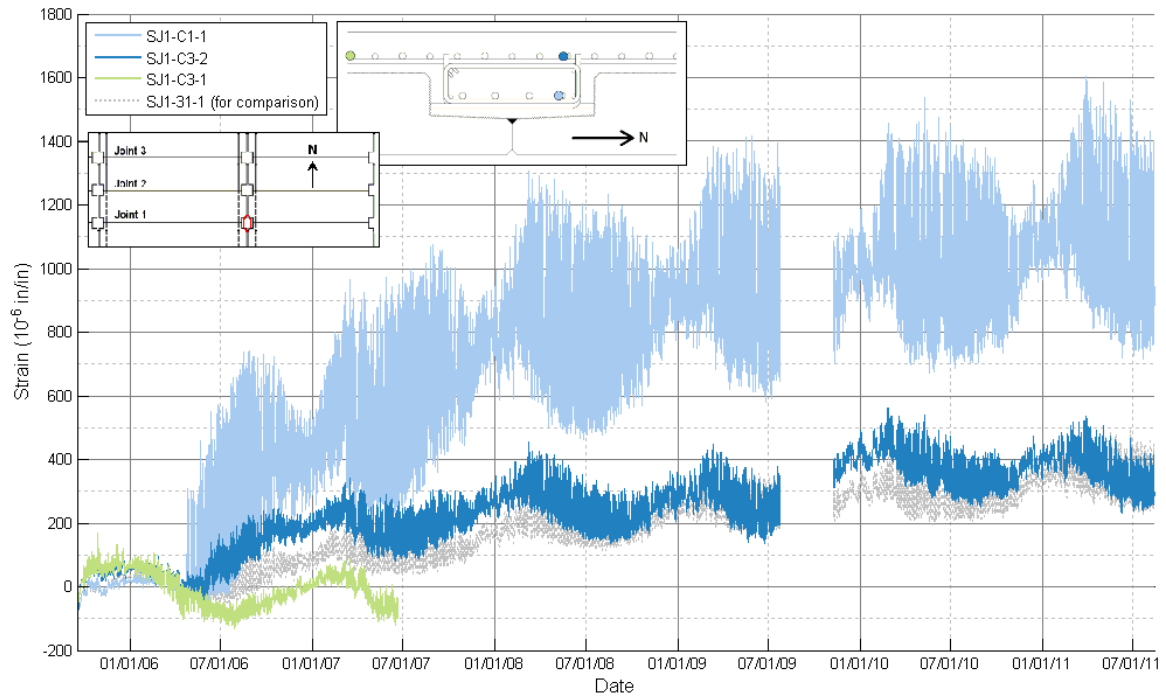


Figure C.13: Longitudinal strain data from spot-weldable gauges on continuity and deck rebar over Joint 1 at the center of the pier cap. Note that strains from gauge SJ1-31-1 are shown for comparison, highlighting the larger strains from gauge SJ1-C1-1

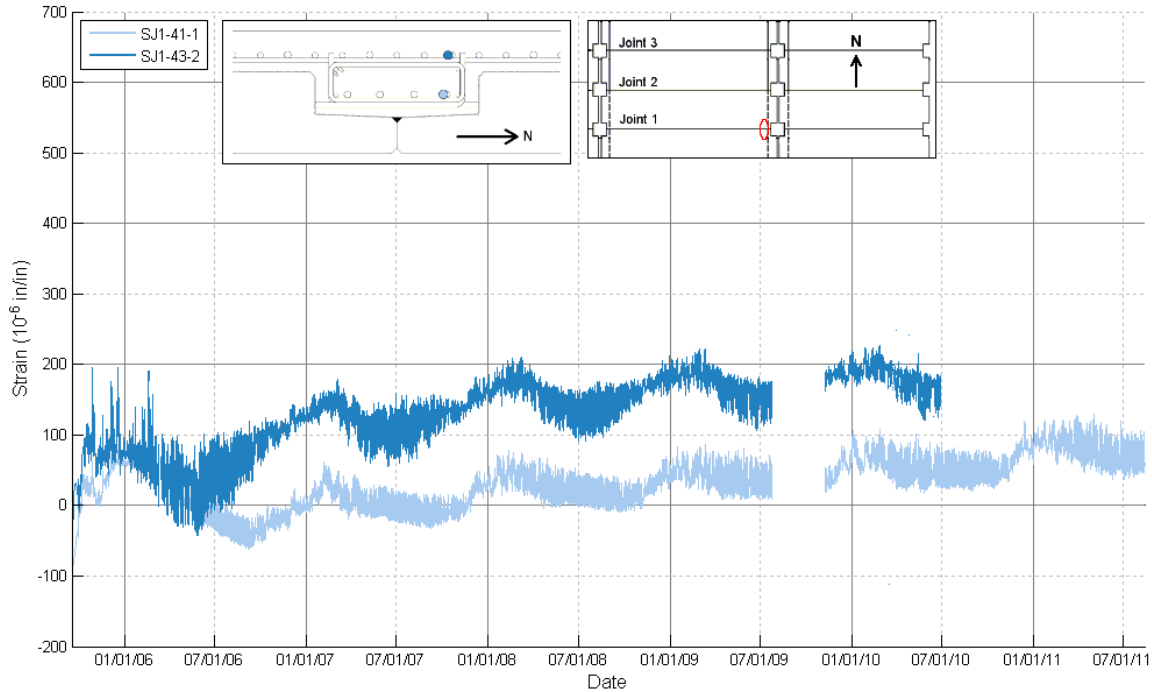


Figure C.14: Longitudinal strain data from spot-weldable gauges on continuity and deck rebar over Joint 1 at the west side of the pier cap

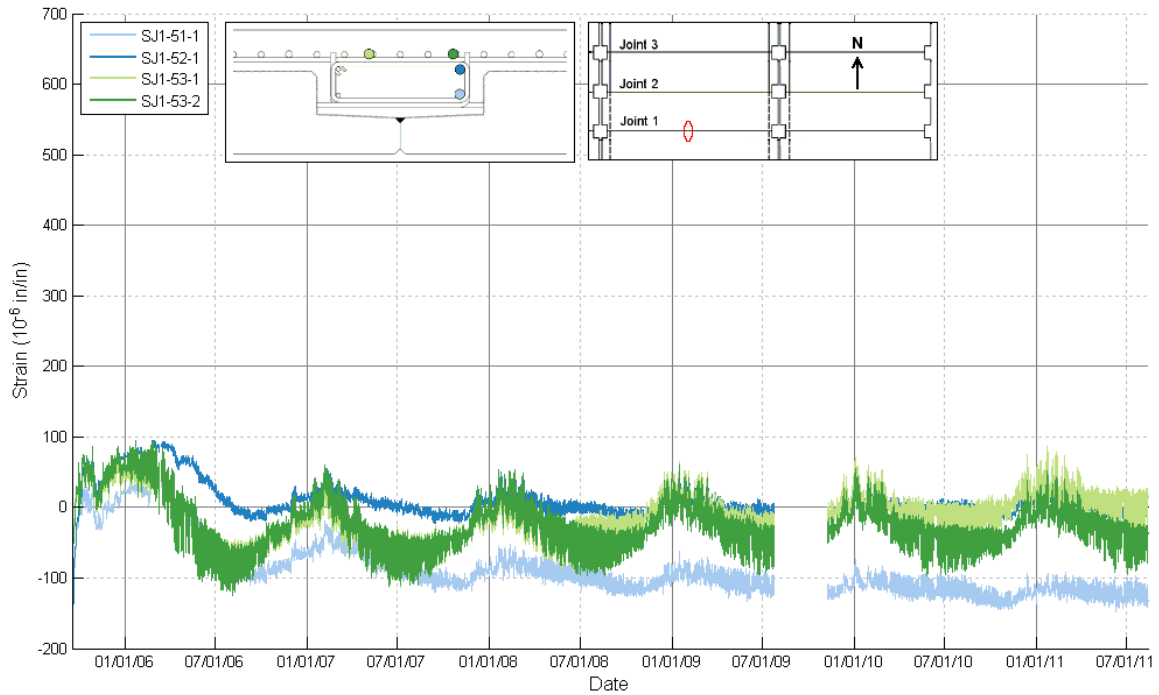


Figure C.15: Longitudinal strain data from spot-weldable gauges on cage and deck rebar over Joint 1 at midspan of the center span

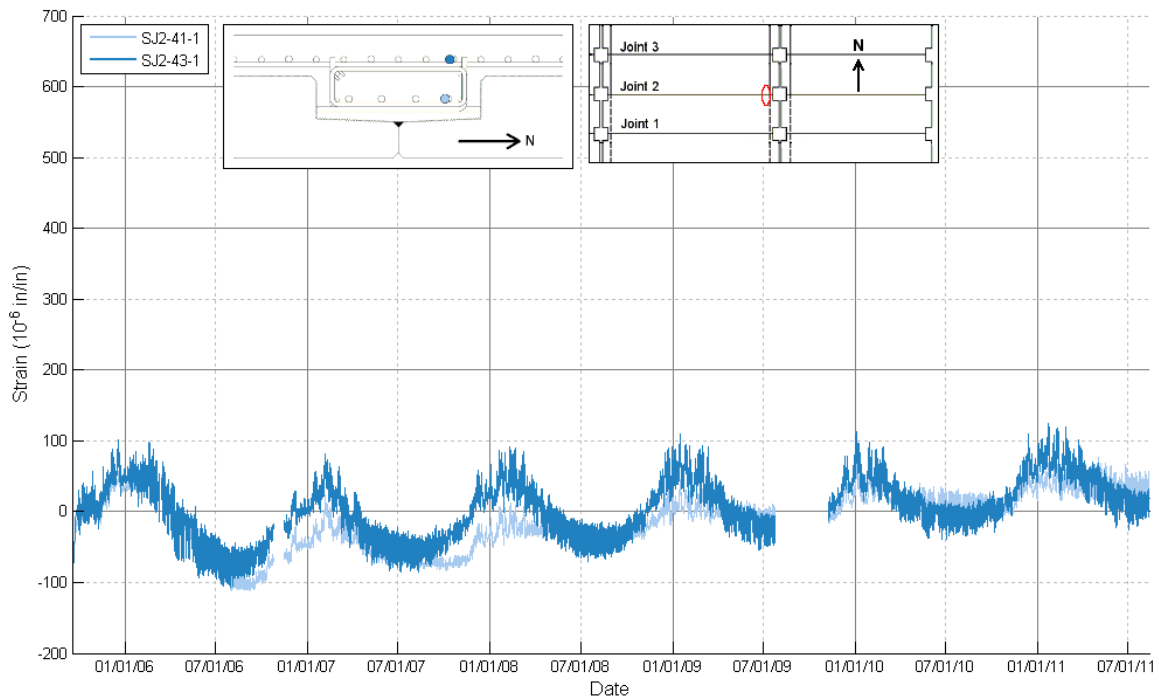


Figure C.16: Longitudinal strain data from spot-weldable gauges on continuity and deck rebar over Joint 2 at the west side of the pier cap

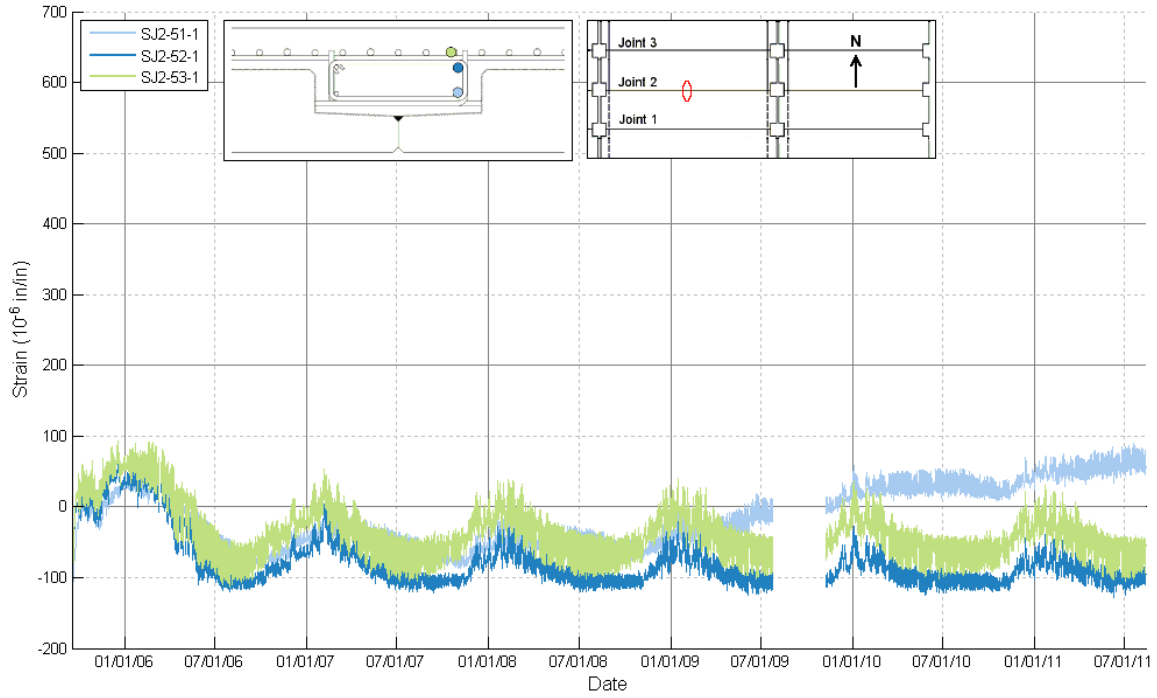


Figure C.17: Longitudinal strain data from spot-weldable gauges on continuity and deck rebar over Joint 2 at midspan of the center span

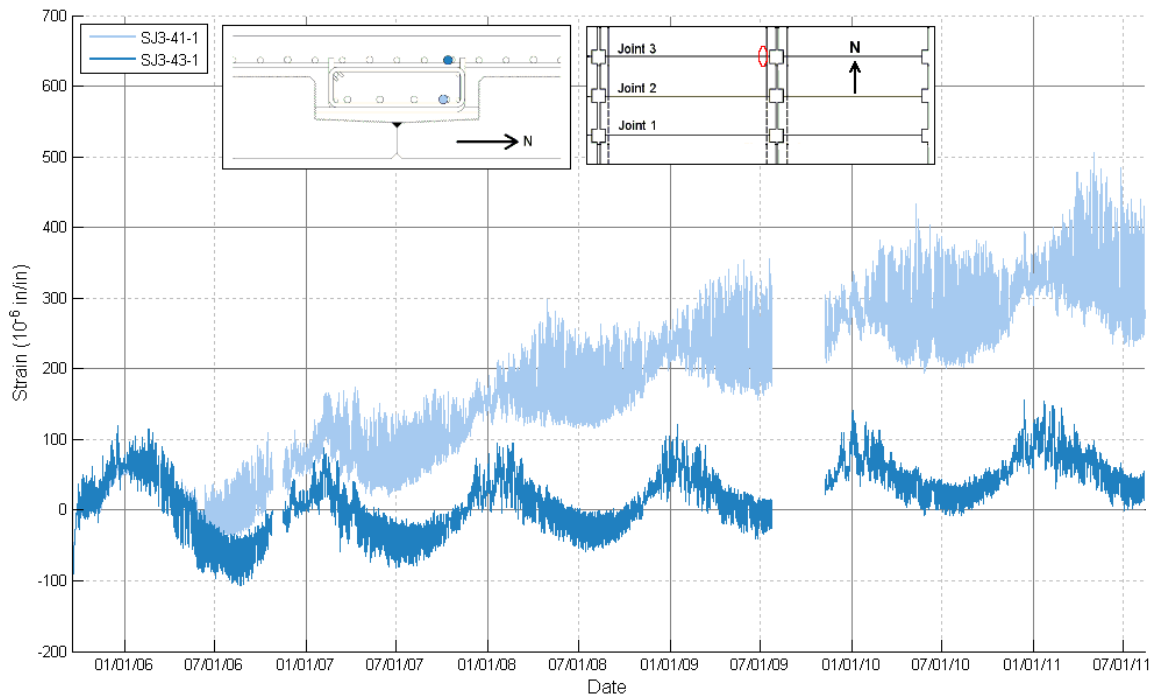


Figure C.18: Longitudinal strain data from spot-weldable gauges on continuity and deck rebar over Joint 3 at the west side of the pier cap

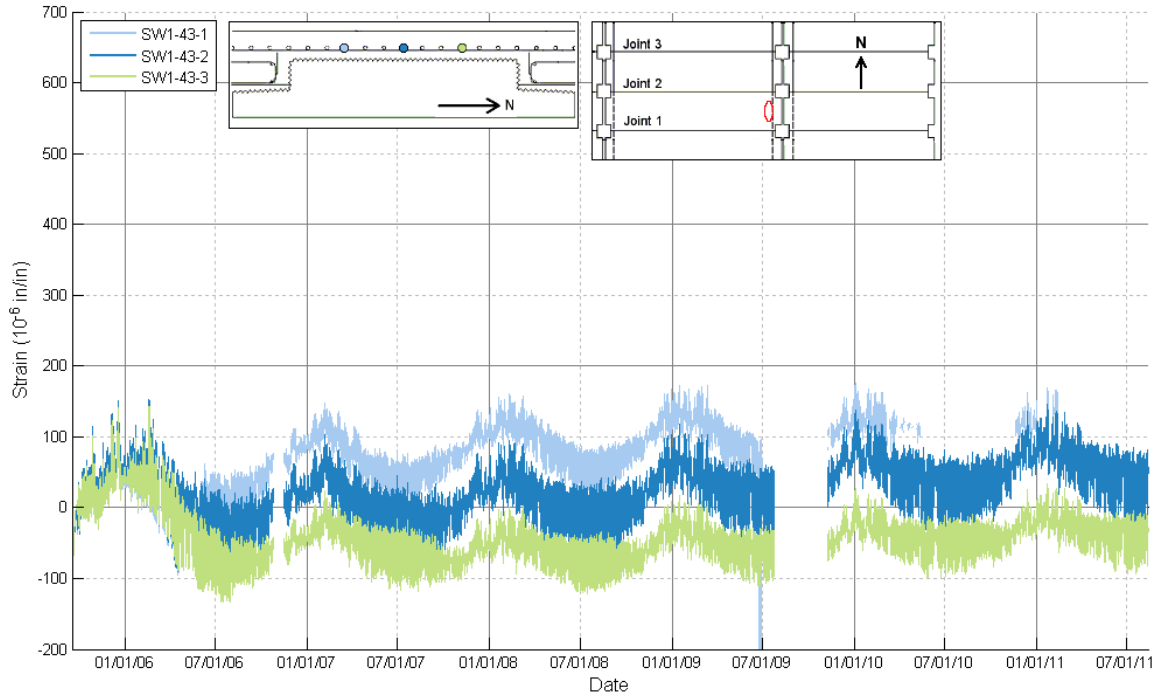


Figure C.19: Longitudinal strain data from spot-weldable gauges on deck rebar over the precast web, between Joints 1 and 2, at the west side of the pier cap

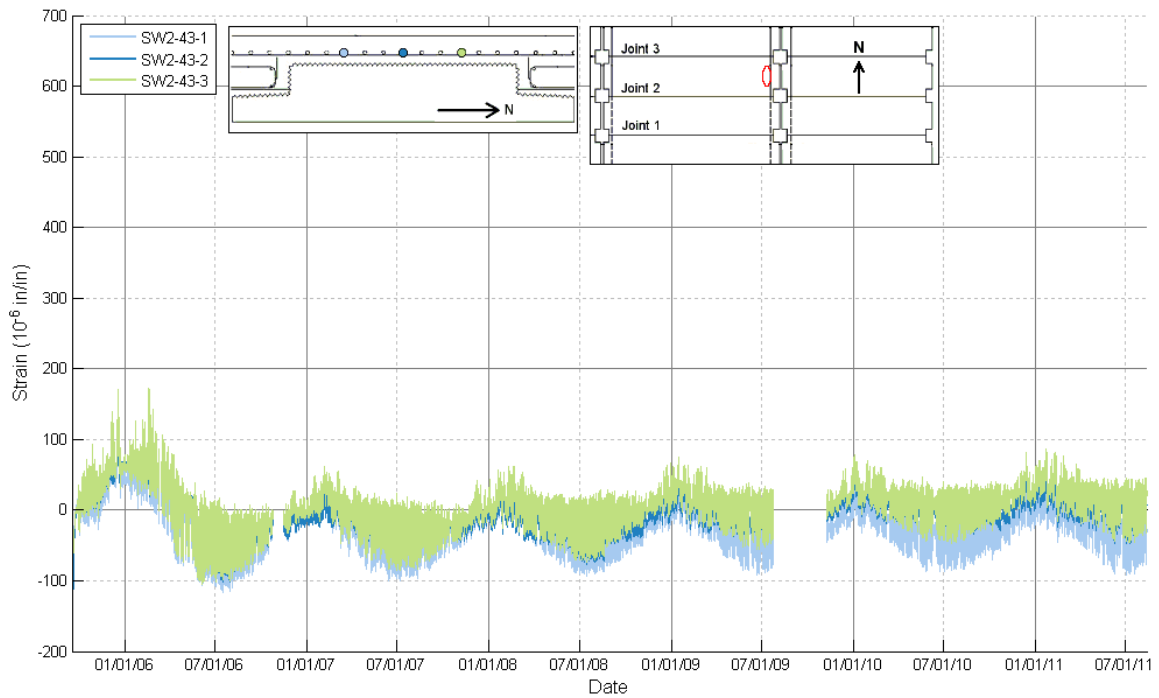


Figure C.20: Longitudinal strain data from spot-weldable gauges on deck rebar over the precast web, between Joints 2 and 3, at the west side of the pier cap

Appendix D: Sample Calculations for PCSSS Design

The sample calculations presented in this appendix are representative of the design calculations used in the parametric study, described in Chapter 6. These calculations are intended to explain the process used for the parametric study and to further illustrate the complexities of calculating restraint moments. PCSSS design for the parametric study was done in accordance with the AASHTO Bridge Design Specification (2010). All equation numbers in this appendix reference the 2010 edition of AASHTO.

The sample calculations are taken from the design of a continuous PCSSS bridge, with three 34 ft spans. The precast beam is 14 in. deep, with a 6 in. CIP concrete deck. In design, these calculations were done for the tenth points of each span. For simplicity, only the sample calculations for the bearing point at the pier end of the end span will be shown. This location is the point of maximum restraint moment, both time-dependent and thermal gradient, and is where the continuity check is critical.

D.1 Creep and Shrinkage

The creep and shrinkage model used in Part 3 of the parametric study was from AASHTO Section 5.4.2.3 (2010). The AASHTO 2004 model used in Part 1 is not illustrated in this appendix.

To determine the creep and shrinkage factors, the following four k factors must be calculated. First, the shape factor, k_s , is calculated as a function of the volume-to-surface ratio, (V/S) (in.). The PCSSS has a relatively large volume to surface ratio, so k_s is always 1.0.

$$\begin{aligned} k_s &= 1.45 - 0.13(V/S) \geq 1.0 && (5.4.2.3.2-2) \\ &= 1.45 - 0.13(4.34 \text{ in.}) = 0.89 \geq 1.0 \end{aligned}$$

$$\mathbf{k_s = 1.0}$$

Next, the humidity factor, k_{hc} , is calculated as a function of the average annual relative humidity, H , given in AASHTO Figure 5.4.2.3.3-1 (2010). The relative humidity is location dependent and was interpolated from the figure to be 73% for Minnesota.

$$k_{hc} = 1.56 - 0.008H = 1.56 - 0.008(73) \quad (5.4.2.3.2-3)$$

$$\mathbf{k_{hc} = 0.976}$$

The strength factor, k_f , is calculated as a function of the concrete strength at prestressing release, f'_{ci} .

$$k_f = \frac{5}{1 + f'_{ci}} = \frac{5}{1 + 4 \text{ ksi}} \quad (5.4.2.3.2-4)$$

$$\mathbf{k_f = 1.0}$$

In this case, k_f is 1.0 because the release strength is 4 ksi. For beams with higher release strengths, k_f is smaller and the creep and shrinkage factors are smaller. Finally, the time-dependent factor, k_{td} , is calculated as a function of the time after loading, t (days), and the release strength, f'_{ci} (ksi).

$$k_{td} = \left(\frac{t}{61 - 4f'_{ci} + t} \right) \quad (5.4.2.4.2-5)$$

The controlling design time, t_f , was taken as 75 years so that the creep and shrinkage factors would be large. In this case, k_{td} was equal to 1.0, reflecting the full development of creep and shrinkage effects.

$$k_{td}(t_f) = \left(\frac{(75 \text{ yr}) \left(365 \frac{\text{days}}{\text{yr}} \right)}{61 - 4(4 \text{ ksi}) + (75 \text{ yr}) \left(365 \frac{\text{days}}{\text{yr}} \right)} \right)$$

$$\mathbf{k_{td}(t_f) = 0.998 \approx 1.0}$$

The creep and shrinkage factors were also needed at the time of deck placement, t_d , for both prestress loss and restraint moment calculations. At deck placement, the loading time was 14 days minus 0.75 days for the assumed curing time before prestress transfer. Therefore, k_{td} was 0.227 for the precast beam at deck placement:

$$k_{td}(t_d) = \left(\frac{(14 \text{ days} - 0.75 \text{ days})}{61 - 4(4 \text{ ksi}) + (14 \text{ days} - 0.75 \text{ days})} \right)$$

$$\mathbf{k_{td}(t_d) = 0.227}$$

For loads applied at the time of deck placement, i.e. the deck self weight, k_{td} is also 1.0 because the total development time is 75 years less 14 days.

With the k factors calculated, the creep and shrinkage factors for various times can be calculated. The creep factor equation given by AASHTO (2010) is as follows,

$$\psi(t, t_i) = 1.9k_s k_{hc} k_f k_{td} t_i^{-0.118} \quad (5.4.2.3.2-1)$$

where t_i is the time of initial loading after casting (days). For prestressing loads, t_i was taken as 0.75 days to reflect the curing time before release.

Total creep factor for the precast beam for loads applied at release:

$$\psi(t_f, t_i) = 1.9(1.0)(0.976)(1.0)(1.0)(0.75 \text{ day})^{-0.118}$$

$$\mathbf{\psi(t_f, t_i) = 1.918}$$

Creep factor at deck placement for loads applied at release:

$$\psi(t_d, t_i) = 1.9(1.0)(0.976)(1.0)(0.227)(0.75 \text{ day})^{-0.118}$$

$$\mathbf{\psi(t_d, t_i) = 0.436}$$

For the deck self-weight load, t_i was taken as $t_d = 14$ days. Total creep factor for the precast beam for loads applied at the time of deck placement:

$$\psi(t_f, t_d) = 1.9(1.0)(0.976)(1.0)(1.0)(14 \text{ day})^{-0.118}$$

$$\psi(t_f, t_d) = \mathbf{1.358}$$

The shrinkage strain equation given by AASHTO (2010) is as follows:

$$\varepsilon_{sh} = k_s k_{hs} k_f k_{td} 0.48 \times 10^{-3} \quad (5.4.2.3.3-1)$$

where the k factors are the same as for the creep factor. For the restraint moment calculations, the shrinkage of the beam after deck placement needs to be calculated. Shrinkage of the precast beam between deck placement and the design time:

$$\varepsilon_{bdf} = \varepsilon_{bif} - \varepsilon_{bid} = (0.976)(1 - 0.227)(0.48 \times 10^{-3})$$

$$\varepsilon_{bdf} = \mathbf{362 \mu\varepsilon}$$

Next the total shrinkage of the deck concrete is calculated. The strength factor, k_f , is 1.19 for the CIP concrete because f'_{ci} is 3.2 ksi.

$$\varepsilon_{ddf} = (0.976)(1.19)(0.48 \times 10^{-3}) \quad (5.4.2.3.3-1)$$

$$\varepsilon_{ddf} = \mathbf{557 \mu\varepsilon}$$

From these calculations it is clear that the CIP concrete will shrink more than the precast concrete after continuity is established. The differential shrinkage, ε_s , is then:

$$\varepsilon_s = \varepsilon_{ddf} - \varepsilon_{bdf} = 557 \mu\varepsilon - 362 \mu\varepsilon \quad (5.4.2.3.3-1)$$

$$\varepsilon_s = \mathbf{195 \mu\varepsilon}$$

D.2 Restraint Moment

Restraint moment analysis was done using the Peterman method (P-method) (Peterman and Ramirez 1998). Restraint moments result from creep caused by long-term prestressing forces and dead loads and differential shrinkage between the precast beams and CIP concrete deck. To calculate restraint moments, the P-method requires the calculation of fixed-end moments due to the prestressing force, dead load from both the precast and CIP concrete, and differential shrinkage. These fixed-end moments are then distributed through the system using the stiffness method with matrix analysis. With the P-method, virtual spans are used over the piers, between the bearing points of adjacent spans, taken as 1.5 ft. for all designs in the parametric study. As stated previously, these calculations are demonstrated in this appendix for the bearing point at the pier for an end span to find the maximum restraint moment.

The prestressing fixed-end moment is the prestressing force, P_{ps} (k), multiplied by the eccentricity of the prestressing strand for the composite section, e_c (in). After determining prestress losses and composite section properties, shown in Figure D.1, the prestressing force and eccentricity are:

$$P_{nc} = (163 \text{ ksi}) \left(0.153 \frac{\text{in}^2}{\text{strand}} \right) (22 \text{ strands}) = \mathbf{549 \text{ k}}$$

$$M_{p1_{FEM}} = 307 \text{ k} \cdot \text{ft}$$

After moment distribution: $M_{p1} = 435 \text{ k} \cdot \text{ft}$

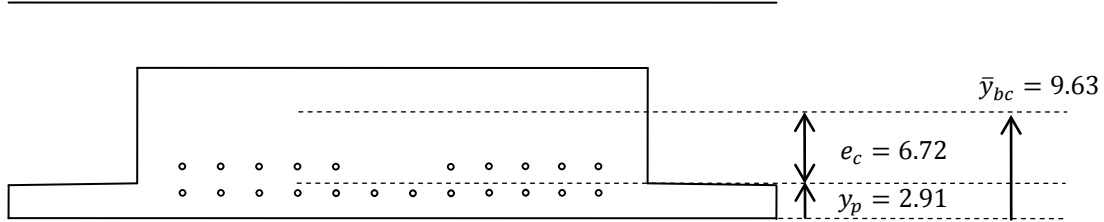


Figure D.1: Composite cross-section of the 14in. deep PCSSS beam showing the eccentricity of prestressing force.

The dead load fixed-end moment due to the precast concrete self-weight is as follows, for a uniform load, w_{pc} (k/ft), and span length between bearing points, l (ft):

$$(M_d)_{precast_{FEM}} = -\frac{w_{pc}l^2}{12} = -\frac{(150 \text{ lb/ft}^3)(747 \text{ in}^2)(33.25 \text{ ft})^2}{12}$$

$$(M_d)_{precast_{FEM}} = -72 \text{ k} \cdot \text{ft}$$

After moment distribution: $(M_d)_{precast} = -101 \text{ k} \cdot \text{ft}$

Similarly, the dead load fixed-end moment due to the CIP concrete self-weight is as follows, for a uniform load, w_{CIP} (k/ft):

$$(M_d)_{CIP_{FEM}} = -\frac{w_{CIP}l^2}{12} = -\frac{(150 \text{ lb/ft}^3)(432 \text{ in}^2)(33.25 \text{ ft})^2}{12}$$

$$(M_d)_{CIP_{FEM}} = -41 \text{ k} \cdot \text{ft}$$

After moment distribution: $(M_d)_{CIP} = -59 \text{ k} \cdot \text{ft}$

The fixed-end moment due to the effect of differential shrinkage is defined in the P-method using the equation from the PCA method with a modifier, η , that accounts for shrinkage restraint from the precast beam and deck reinforcement. The modifier η is calculated as follows, with precast concrete modulus of elasticity and area, E_p (ksi) and A_p (in²) respectively, CIP concrete modulus of elasticity and area, E_d (ksi) and A_d (in²) respectively, and steel modulus of elasticity and area, E_s (ksi) and A_s (in²) respectively. The area of the CIP deck was taken conservatively as only the top 6 in. of the deck, neglecting the concrete in the trough regions. The area of deck reinforcement was taken conservatively as the area of No. 7 bars spaced at 12 in., neglecting reinforcement over the piers that did not extend the full length of the bridge.

$$\eta = \left(\frac{1}{1 + \frac{E_p A_p}{E_d A_d}} \right) \left(\frac{1}{1 + \frac{E_s A_s}{E_d A_d}} \right)$$

$$= \left(\frac{1}{1 + \frac{(4696 \text{ ksi})(747 \text{ in}^2)}{(3834 \text{ ksi})(432 \text{ in}^2)}} \right) \left(\frac{1}{1 + \frac{(29,000 \text{ ksi})(3.60 \text{ in}^2)}{(3834 \text{ ksi})(432 \text{ in}^2)}} \right)$$

$\eta = 0.302$

The differential shrinkage fixed-end moment is calculated as follows, with the thickness of the CIP deck, h (in.):

$$M_{SFEM} = -\varepsilon_s E_d A_d \left(e_c + \frac{h}{2} \right) \eta$$

$$= -(195 \mu\varepsilon)(3834 \text{ ksi})(432 \text{ in}^2) \left(4.37 \text{ in} - \frac{6 \text{ in}}{2} \right) (0.302)$$

$M_{SFEM} = -60 \text{ k} \cdot \text{ft}$

After moment distribution: **$M_s = -85 \text{ k} \cdot \text{ft}$**

The P-method also requires the calculation of several creep coefficients, defined as follows:

$$\Delta(1 - e^{-\phi_1}) = (1 - e^{-\psi(t, t_i)}) - (1 - e^{-\psi(t_d, t_i)})$$

$$= (1 - e^{-1.918}) - (1 - e^{-0.436})$$

$\Delta(1 - e^{-\phi_1}) = 0.499$

$$(1 - e^{-\phi_2}) = (1 - e^{-\psi(t, t_d)})$$

$$= (1 - e^{-1.358})$$

$(1 - e^{-\phi_2}) = 0.743$

$$(1 - e^{-\phi_2})/\phi_2 = (1 - e^{-\psi(t, t_d)})/\psi(t, t_d)$$

$$= (1 - e^{-1.358})/1.3581$$

$(1 - e^{-\phi_2})/\phi_2 = 0.522$

Finally, the time-dependent restraint moment is calculated with the following equation:

$$\begin{aligned}
M_{RM} &= [M_p - (M_d)_{precast}][\Delta(1 - e^{-\phi_1})] - (M_d)_{CIP}(1 - e^{-\phi_2}) - M_s \left(\frac{1 - e^{-\phi_2}}{\phi_2} \right) \\
&= [435 \text{ k} \cdot \text{ft} - 101 \text{ k} \cdot \text{ft}][0.499] - (59 \text{ k} \cdot \text{ft})(0.743) - (85 \text{ k} \cdot \text{ft})(0.547) \\
&\qquad\qquad\qquad \mathbf{M_{RM} = 77 \text{ k} \cdot \text{ft}}
\end{aligned}$$

This is the restraint moment at the bearing point of the end span at the pier, which tapers to 0 at the bearing point at the abutment.

For service limit state checks, the stress due to the restraint moment, f_{RM} (ksi), at the bottom of the section must be calculated. The section modulus is calculated using the composite moment of inertia, I_c (in^4), and the distance from the bottom of the section to the composite neutral axis, y_{bc} (in.). Depth in the cross-section is negative below the neutral axis, so negative stresses indicate tensile stresses at the bottom fiber at the pier.

$$\begin{aligned}
f_{RM}(y_{bc}) &= M_{RM} \frac{y_{bc}}{I_c} \\
&= (77 \text{ k} \cdot \text{ft}) \frac{(-9.63 \text{ in})}{(43,127 \text{ in}^4)} \\
&\qquad\qquad\qquad \mathbf{f_{RM}(y_{bc}) = -0.206 \text{ ksi}}
\end{aligned}$$

D.3 Thermal Gradient

The design thermal gradient is defined in AASHTO Section 3.12.3 (2010) as shown in Figure D.2. Analysis of the thermal gradient is defined in AASHTO Section 4.6.6 (2010). The effect of the thermal gradient is divided into three components: uniform axial expansion, uniform flexural deformation, and internal stress to maintain compatibility.

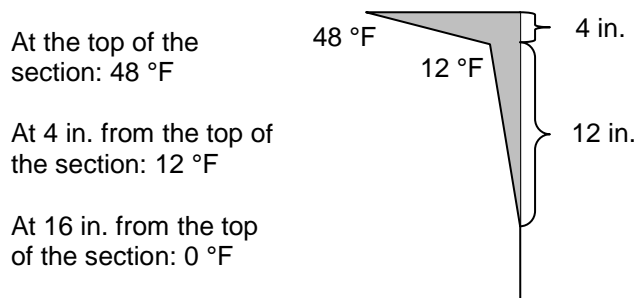


Figure D.2: Definition of the thermal gradient according to AASHTO Section 3.12.3 (2010), Zone 2.

Uniform axial expansion is defined as follows, where A_c is the area of the composite section (in^2), $T_G(z)$ is the thermal gradient defined in Figure D.2 ($^{\circ}\text{F}$), z is the depth measured from the composite neutral axis (in.), and b is the width of the section (in.).

$$T_{UG} = \frac{1}{A_c} \iint T_G \, dw \, dz \qquad\qquad\qquad (\text{C4.6.6-1})$$

$$\begin{aligned}
&= \frac{1}{A_c} b \int T_G(z) dz \\
&= \frac{1}{1313 \text{ in}^2} (72 \text{ in})(160.8 \text{ }^\circ\text{F} \cdot \text{in})
\end{aligned}$$

$$\mathbf{T_{UG} = 8.82 \text{ }^\circ\text{F}}$$

The thermal strain caused by this uniform axial expansion, ε_u ($\mu\varepsilon$), is calculated as follows, with the coefficient of thermal expansion of concrete taken as

$\alpha = 6 \times 10^{-6} \text{ }^\circ\text{F}^{-1}$ as specified in AASHTO Section 5.4.2.2 for design in lieu of specific data (AAHSTO 2010). This value of α is also close to the experimentally determined value for Bridge No. 13004, $\alpha = 5.67 \times 10^{-6} \text{ }^\circ\text{F}^{-1}$ (Smith et al., 2008).

$$\varepsilon_u = \alpha T_{UG} = (6 \times 10^{-6} \text{ }^\circ\text{F}^{-1})(8.82 \text{ }^\circ\text{F})$$

$$\mathbf{\varepsilon_u = 52.9 \mu\varepsilon}$$

Assuming that the system is fully axially restrained, which was the case for the parametric study, the stress caused by uniform axial expansion is calculated as follows, where E_{pc} is the modulus of elasticity of the precast concrete (ksi).

$$\sigma_u = E_{pc} \varepsilon_u = (4696 \text{ ksi})(52.9 \mu\varepsilon)$$

$$\mathbf{\sigma_u = 0.248 \text{ ksi}}$$

The effect of flexural deformation is defined as follows, where ϕ is the uniform induced curvature (in^{-1}), and I_c is the composite moment of inertia (in^4).

$$\phi = \frac{\alpha}{I_c} \iint T_G z dw dz \quad (\text{C4.6.6-3})$$

$$= \frac{\alpha}{I_c} b \int T_G(z) z dz$$

$$= \frac{6 \times 10^{-6} \text{ }^\circ\text{F}^{-1}}{43,127 \text{ in}^4} (72 \text{ in.})(1038 \text{ }^\circ\text{F} \cdot \text{in}^2)$$

$$\mathbf{\phi = 1.04 \times 10^{-5} \text{ in}^{-1}}$$

The thermal strain caused by flexural deformation varies linearly through the section with a slope of ϕ , defined as follows.

$$\varepsilon_f(z) = \phi z = (1.04 \times 10^{-5} \text{ in}^{-1}) z$$

$$\varepsilon_f(y_{bc}) = (1.04 \times 10^{-5} \text{ in}^{-1})(-9.63 \text{ in})$$

$$\mathbf{\varepsilon_f(y_{bc}) = -100.2 \mu\varepsilon}$$

Therefore, flexural deformation causes positive (expanding) strains at the top of the section and negative (contracting) strains at the bottom of the section.

If the system is rotationally restrained, as is the case with the continuous systems from the parametric study, flexural deformation causes restraint moments to develop similarly to time-dependent restraint moments. A fixed-end moment is calculated, and then distributed using the same stiffness method. The fixed-end moment, M_{FEM} (k-ft), produced by the rotational restraint is:

$$M_{FEM} = EI_c \phi \quad (C4.6.6-5)$$

$$= (4696 \text{ ksi})(43,127 \text{ in}^4)(1.04 \times 10^{-5} \text{ in}^{-1})$$

$$M_{FEM} = 175 \text{ k} \cdot \text{ft}$$

After moment distribution: $M_{TG} = 247 \text{ k} \cdot \text{ft}$

The stress caused by the thermal gradient restraint moment, $\sigma_f(z)$ (ksi), is:

$$\sigma_f(z) = M_{TG} \frac{z}{I_c}$$

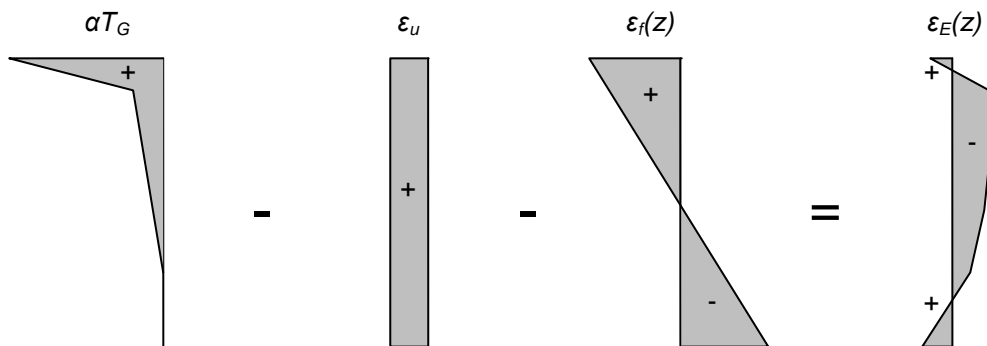
$$\sigma_f(y_{bc}) = (247 \text{ k} \cdot \text{ft}) \frac{-9.63 \text{ in}}{43,127 \text{ in}^4}$$

$$\sigma_f(y_{bc}) = -0.661 \text{ ksi}$$

The internal mechanical strain needed for compatibility is defined as the total, non-linear thermal strain from the thermal gradient, minus the uniform axial expansion strain and the linear flexural deformation strain, illustrated in Figure D.3.

$$\varepsilon_E(z) = \varepsilon_{TG}(z) - \varepsilon_u - \varepsilon_f(z)$$

$$= \alpha T_G(z) - \varepsilon_u - \varepsilon_f(z)$$



Figure

D.3: Illustration of the mechanical strain, ε_E , required for compatibility in the presence of a non-linear thermal gradient

The internal strain is compressive at the top and bottom of the section and tensile inside the section. The strain and stress at the bottom of the section is calculated as follows:

$$\varepsilon_E(y_{bc}) = (6 \times 10^{-6} \text{ } ^\circ\text{F}^{-1})(0 \text{ } ^\circ\text{F}) - 52.9 \mu\varepsilon - (-100.2 \mu\varepsilon)$$

$$\varepsilon_E(y_{bc}) = 47.3 \mu\varepsilon$$

$$\sigma_E(y_{bc}) = E_{pc}\varepsilon_E(y_{bc}) = (4696 \text{ ksi})(47.3 \mu\varepsilon)$$

$$\sigma_E(y_{bc}) = 0.222 \text{ ksi}$$

Finally, the total stress due to thermal gradient effects at the bottom of the section is calculated as a superposition of the three components.

$$f_{TG} = \sigma_u + \sigma_f + \sigma_E$$

$$f_{TG}(y_{bc}) = (0.248 \text{ ksi}) + (-0.661 \text{ ksi}) + (0.222 \text{ ksi})$$

$$f_{TG}(y_{bc}) = -0.191 \text{ ksi}$$

Compared to the time-dependent restraint moment stress, the thermal gradient stress is roughly equal. The contribution of restrained axial expansion made the total thermal gradient stress less tensile, reducing the critical service limit state stress. If axial expansion was not restrained, the total thermal gradient stress would be -0.439 ksi, significantly higher than the time-dependent restraint moment stress.

D.4 Continuity Check

In order to use continuity to reduce the live load envelope, the continuity connection must be fully effective. The continuity check from AASHTO Section 5.14.1.4.5 (2010) requires the following load combination to be compressive at the bottom of the section at the pier for full continuity:

$$f_{DL_2} + 0.5f_{LL} + f_{RM} + f_{TG} \geq 0$$

where f_{DL_2} is stress due to post-continuity dead loads, f_{LL} is stress due to live load, f_{RM} is stress due to the restraint moment, and f_{TG} is stress due to the thermal gradient, all in units of ksi. The live load stress is the stress at the pier caused by the live load configuration with the maximum positive moment, as described in Section 6.1.3. The continuity check is evaluated as follows:

$$0.054 \text{ ksi} + 0.5(0.210 \text{ ksi}) - 0.206 \text{ ksi} - 0.5(0.191 \text{ ksi}) = -0.143 \text{ ksi NG}$$

$$0.054 \text{ ksi} + 1.0(0.210 \text{ ksi}) - 0.206 \text{ ksi} - 0.5(0.191 \text{ ksi}) = -0.038 \text{ ksi NG}$$

In this case, the continuity check fails under the required load combination, so the continuity connection is not fully effective. Furthermore, increasing the live load coefficient to 1.0 still does not pass the continuity check, so partial continuity is not possible. Therefore, no continuity is developed and the simply-supported live load envelope is used in design.

In order to demonstrate the use of partial continuity, the following calculations are taken from the 24-24-24 configuration from the parametric study. In this case, full continuity is not possible, but partial continuity can be used.

$$0.041 \text{ ksi} + 0.5(0.226 \text{ ksi}) - 0.135 \text{ ksi} - 0.5(0.184 \text{ ksi}) = -0.017 \text{ ksi}$$

$$0.041 \text{ ksi} + \mathbf{0.83}(0.226 \text{ ksi}) - 0.135 \text{ ksi} - 0.5(0.184 \text{ ksi}) = 0.0 \text{ ksi}$$

By increasing the live load coefficient to 0.83, effectively 83% of the live load stress is enough to result in no bottom tension at the pier. Therefore, the continuity connection is 17% effective (100% - 83% required to achieve continuity). The design live load envelope is determined by superimposing the simply-supported and continuous system envelopes as follows, where LL_{simple} is the simply-supported envelope and $LL_{continuous}$ is the continuous system envelope:

$$0.83LL_{simple} + 0.17LL_{continuous} = LL$$

This superposition is illustrated in Figure D.4, showing the simply-supported, continuous system, and partial continuity live load envelopes. The partial continuity envelope is less than the simply-supported envelope, but greater than the continuous system envelope.

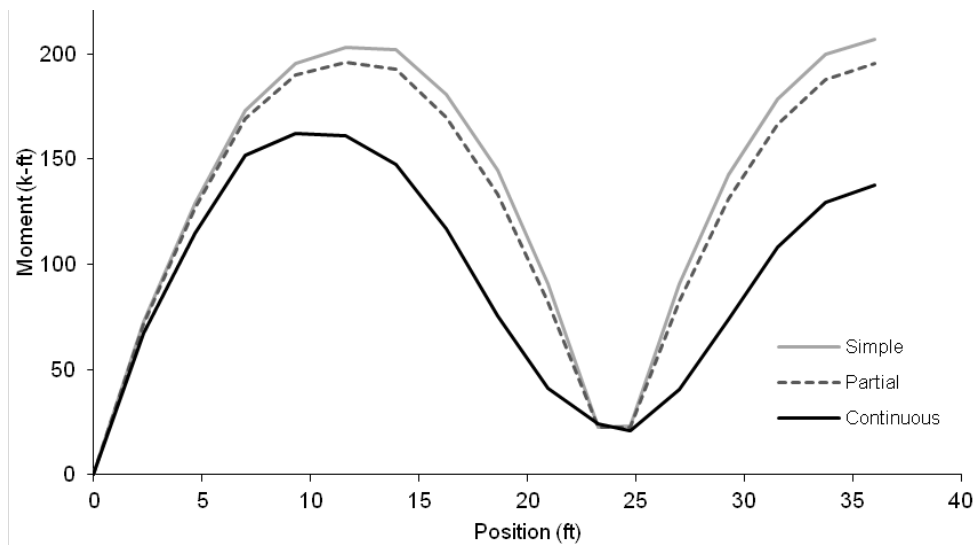


Figure D.4: Superposition of the partially continuous live load envelope for the 24-24-24 bridge. The envelopes are cut off between bearing points of the adjacent spans.